



HAL
open science

Hypothesis of a Non-SNARE-Function of Syntaxin-5

Stefan Rathjen

► **To cite this version:**

Stefan Rathjen. Hypothesis of a Non-SNARE-Function of Syntaxin-5. Molecular biology. Université Paris Saclay (COMUE), 2017. English. NNT : 2017SACLS450 . tel-02408332

HAL Id: tel-02408332

<https://theses.hal.science/tel-02408332v1>

Submitted on 13 Dec 2019

HAL is a multi-disciplinary open access archive for the deposit and dissemination of scientific research documents, whether they are published or not. The documents may come from teaching and research institutions in France or abroad, or from public or private research centers.

L'archive ouverte pluridisciplinaire **HAL**, est destinée au dépôt et à la diffusion de documents scientifiques de niveau recherche, publiés ou non, émanant des établissements d'enseignement et de recherche français ou étrangers, des laboratoires publics ou privés.

Hypothesis on a non-SNARE function of syntaxin-5

Thèse de doctorat de l'Université Paris-Saclay

Préparée à « Institute Curie »

École doctorale n°568

Biosigne – Signalisations et reseaux integratifs en biologie

Aspects moléculaires et cellulaires de la biologie

Sciences de la vie et de la santé

Thèse présentée et soutenue à Paris, le 12/12/2017, par

Stefan Jan-Matthias RATHJEN

Composition du Jury :

- Marc le MAIRE Président
Professeur Émérite, Université Paris-Sud, CEA – UMR 9198
- Thierry GALLI Rapporteur
Directeur d'unité, Center of Psychiatry and Neuroscience – INSERM U894
- Catherine JACKSON Rapporteur
Chef d'équipe, Institut Jaques Monod – UMR 7592 CNRS
- Jost ENNINGA Examineur
Chef d'équipe, Institut Pasteur
- Anne HOUDUSSE Examinatrice
Chef d'équipe, Institute Curie –UMR144 CNRS
- Ludger JOHANNES Directeur de thèse
Directeur d'unité, Institute Curie – UMR3666

Familie und Liebe!

1 FRENCH ABSTRACT

Titre : Hypothèse d'une fonction non-SNARE de la syntaxine-5

Mots clés : Syntaxin-5, GPP130, Retro-2, Sec16A, transport rétrograde, Shiga toxine

Abstract :

L'introduction commence avec la description de toxines d'origines bactérienne et végétale, en particulier la toxine Shiga ainsi que les toxines de la même famille (chapitre 9.1.2). Les petites molécules inhibitrices de ces toxines sont ensuite résumées dans le chapitre 9.1.3, en particulier le composé Retro-2. L'efficacité de ces toxines à atteindre leurs cibles reposant sur le trafic intracellulaire, un aperçu général de l'endocytose et du trafic endosomal sont présentés (chapitre 9.2). Puis, l'entrée de la voie rétrograde est décrite (chapitre 9.2.5), avec un intérêt particulier porté sur la clathrine, le rétromère et GPP130, une protéine qui circule de manière continue entre le Golgi, la membrane plasmique et les endosomes. Les protéines SNARE, en particulier la syntaxine-5 et la syntaxine-16, sont ensuite introduites (chapitre 9.2.6). Après une brève section sur les micro-ARNs de la famille 199 (chapitre 9.3), l'introduction se termine avec la description des techniques clés utilisées au cours de mon travail, tels que la chimie click bio-orthogonale, la synchronisation du trafic antérograde par rétention grâce à des hameçons spécifiques (RUSH), et la ligation par proximité basé sur des anticorps (chapitre 9.4).

Ci-inclus, mon article en cours de soumission ouvre la partie résultats (chapitre 10.1), dans laquelle je présente l'intérêt de la chimie click bio-orthogonale pour identifier les cibles cellulaires de Retro-2. Je décris un des candidats potentiels, Sec16A, et illustre comment grâce à la technique de RUSH, perturber la fonction de Sec16A conduit à la relocalisation partielle de la syntaxin-5 au niveau du reticulum endoplasmique via l'inhibition du transport antérograde de la syntaxine-5. La seconde partie de l'article décrit comment la relocalisation de la syntaxine-5 induit l'inhibition du trafic de la toxine Shiga des endosomes au TGN. Je présente une nouvelle interaction entre la syntaxine-5 et la protéine TGN GPP130, qui ont déjà été caractérisées en relation avec le trafic de la toxine Shiga. Mon travail connecte à la fois les facteurs de trafic avec le trafic rétrograde au niveau de l'interface endosome-TGN. De manière frappante, cette interaction est très probablement basée sur une fonction non-SNARE de la syntaxine-5 car le domaine de fixation sur GPP130 est structurellement non lié à toute fonction SNARE.

En collaboration avec Juan Francisco Aranda et Carlos Fernandez aux Etats-Unis, nous avons placés des micro-ARNs dans un contexte de régulation endogène du trafic rétrograde de la toxine Shiga (chapitre 11.2). Une discussion plus approfondie sera apportée dans le chapitre 12.

Enfin, une vue d'ensemble des projets en cours est apportée dans la section des perspectives (chapitre 12), dans laquelle les collaborations plus approfondies sont mises en lumière.

Mots clés : transport rétrograde, toxine Shiga, toxine de la famille Shiga, STxB, syntaxin-5, Sec16A, GPP130, Retro-2, Retro-2.1, chimie click sans cuivre, identification des cibles de petites molécules, spectrométrie de masse, fonction non-SNARE, inhibition du trafic antérograde, miARN, miR199, rétromère, VPS26

2 ENGLISH ABSTRACT

Title: Hypothesis on a non-SNARE-Function of Syntaxin-5

Keywords: Syntaxin-5, GPP130, Retro-2, Sec16A, retrograde transport, Shiga toxin

Abstract:

The introduction of my PhD manuscript starts with describing plant and bacterial toxins (chapter 9.1), in particular Shiga toxin and Shiga-like toxins (SLTs) (chapter 9.1.2). Small molecule inhibitors of these toxins are summarized afterwards in chapter 9.1.3, notably the Retro-2 compound. Since these toxins rely on intracellular trafficking to reach their molecular targets, a general overview of endocytosis and endosomal trafficking is provided (chapter 9.2). Next, the retrograde route entry is presented (chapter 9.2.5), with focus on clathrin, the retromer and GPP130, a protein that constantly cycles between Golgi, plasma membrane, and endosomes. SNARE proteins, particularly syntaxin-5 and syntaxin-16, are then introduced (chapter 9.2.6). After a brief section of the micro RNA family 199 (chapter 9.3), the introduction finishes with the description of some salient techniques that were used in my work, such as - bio-orthogonal Click-Chemistry, anterograde trafficking synchronization with the retention using selective hooks (RUSH) assay, and the antibody-based proximity ligation assay (chapter 10.6.1, 10.11.1).

Herein, my submitted publication opens the results part (chapter 11.1), in which I present the utility of biorthogonal click chemistry for the search of the cellular targets of Retro-2, a small molecule inhibitor that was previously shown to protect cells and animals against Shiga toxin and ricin. I describe that Sec16A is a likely cellular target candidate, and illustrate using the RUSH approach how interfering with Sec16A functions leads to the partial relocalization of syntaxin-5 to the endoplasmic reticulum (ER) by slowing-down its anterograde transport. The second part of the paper describes how syntaxin-5 relocalization causes the inhibition of Shiga toxin trafficking from endosomes to the TGN. I present a novel interaction between syntaxin-5 and the Golgi protein GPP130, which both have been already described in relation to Shiga toxin trafficking. My work connects both trafficking factors in retrograde trafficking at the endosomes-TGN interface. Strikingly, I demonstrate that this interaction is most probably based on a non-SNARE function of syntaxin-5.

In collaboration with Juan Francisco Aranda and Carlos Fernandez in the US, we put micro RNAs into an endogenous regulation context of Shiga toxin retrograde trafficking (chapter 11.2). An extended discussion will be given in chapter 12.

Last, a general outlook of ongoing projects is given in the perspectives section (chapter 13), in which further collaborations are highlighted.

Keywords: Retrograde transport, Shiga toxin, Shiga-like toxin (SLT), STxB, syntaxin-5, Sec16A, GPP130, Retro-2, Retro-2.1, azide-functionalized Retro-2, copper-free click chemistry, small molecule target identification, mass spectrometry, non-SNARE function, anterograde trafficking inhibition, miRNA, miR199, retromer, VPS26

3 ACKNOWLEDGEMENTS

It is finally done! After 3 years of doing top-notch research at the Institut Curie in Paris, I could assemble this manuscript with the help of many people who deserve to be mentioned here. These words cannot express nearly my gratitude for them. More importantly, I cannot mention everyone by name. Thus, I hope that everyone will find himself between the lines.

First of all, I would like to thank Ludger who gave me the opportunity to work with him on this research project and who guided and formed me professionally through this thesis period. Regarding this project I have to stress the work and passion of Maria Daniela Garcia-Castillo, who taught me a lot and initiated this work. It has been a pleasure working with her. I also want to mention everyone else on related to this project. The current and previous members of the unit: Henri-Francois Renard, Valérie Chambon, Alison Forrester and Raphaël Rodriguez. Our collaborators within the institute and beyond: The Nikon imaging facility of the Institute Curie, the mass spectrometry platform around Damaris Loew, the groups of Christophe Lamaze, Franck Perez, Anne Houdusse, Graça Raposo, Adam Linstedt, Ben Glick, Jean-Christophe Cintrat and Daniel Gillet. We appreciated very much your expertise, kindness and responsiveness.

The UMR3666! All of you! Thanks for the support on a professional but also on a personal level! In no particular order: Marco, Anne (Thanks for all the translation of texts into French), Julio, Raphael, aka Philippe, Siau, Joanna, Lavaniya, Veronica, the other Anne, Thomas, the other Thomas, Estelle, Massi, Dhiraj, Christian, Sebastian, Steve, Bhanu, Bibhuti, Satish, Senthil, Vesela, Tatiana, Antoine, Stephanie, Christine (both), Sylvie, Frederic, Yannick, Barbara, Yoane, Katharina, Daniela, Melissa, Nicolas, Cedric, Ulrike, Haifei, Alena, Cesar and everyone else, I shamefully forgot!

Basically everyone else who crossed my path in the past years, here at the campus! The people of the ADIC. They are such a great bunch of people. I enjoyed involving myself with the many events we organized. I hope to keep as many connection throughout the upcoming years and decades.

All my friends! The ones in Germany and in France! The ones involved in science and also the ones outside academia. If a mention you here, I'll expand the scope of this manuscript. Yes, you are mentioned here, for sure.

Thanks to my family, especially my parents, Bernd and Astrid, my siblings, Melina and Björn! I love you! Thank you for everything. I want to mention also the family that I gained though my beloved Amorcita! I has been a pleasure to get so many lovely people into my live.

Last and by far the most important to me within the past years, my Amorcita, aka Pelusa or Mari! I cannot express my gratitude, appreciation and love. I don't want to know how much harder all the struggles would have been without you! I consider myself blessed and lucky to have "discovered" (found) you within my research period here in Paris. I love you!

I want to thank you all from the bottom of my heart!

Sincerely yours,

Stefan

PS: I also want to thank Bluetooth technology and my headphones for shutting off all the daily noise and distractions! Much appreciated! Hooray to technology!

4 TABLE OF CONTENTS

	Page
1 FRENCH ABSTRACT.....	I
2 ENGLISH ABSTRACT.....	II
3 ACKNOWLEDGEMENTS	1
4 TABLE OF CONTENTS.....	2
5 LIST OF TABLES	6
6 TABLE OF FIGURES	7
7 ABBREVIATIONS.....	19
8 SUMMARY.....	22
9 INTRODUCTION	1
9.1 PLANT AND BACTERIAL RIBOSOMAL INACTIVATING PROTEIN-TOXINS.....	2
9.1.1 <i>Bioterrorism, bio threat agents and biodefense</i>	4
9.1.2 <i>Shiga toxin and its Shiga-like toxins</i>	4
9.1.3 <i>Small molecule inhibitors of the retrograde route</i>	7
9.1.3.1 Retro compounds.....	7
9.1.3.1.1 Structural evolution of Retro-2.....	10
9.1.3.1.2 Retro-2 effect on viral infections.....	11
9.1.3.1.3 Retro-2 effect on intracellular parasites	12
9.1.3.1.4 Retro-2 effect on intracellular bacteria.....	13
9.1.3.1.5 Bio threats that are not affected by Retro-2	13
9.1.3.2 Other small molecules.....	13
9.1.3.2.1 Inhibitors with identified target.....	14
9.1.3.2.1.1 Ilimaquinone (IQ)	15
9.1.3.2.1.2 Brefeldin A (BFA)	15
9.1.3.2.1.3 Exo2 and LG186.....	16

9.1.3.2.1.4	Golgicide A (GCA).....	16
9.1.3.2.2	Compounds with unknown target.....	17
9.2	INTRACELLULAR TRAFFICKING	18
9.2.1	<i>Anterograde trafficking via the biosynthetic/secretory pathway</i>	18
9.2.1.1	ER Exit Sites (ERES).....	21
9.2.1.1.1	Sec16A and the COPII coat	22
9.2.1.1.2	COPII coat dynamics: Two models for Sec16A function	22
9.2.1.1.2.1	Model one: Sec16 as a scaffolding protein	24
9.2.1.1.2.2	Model two: Sec16A as a regulator of COPII vesicle release	26
9.2.2	<i>Endocytosis</i>	27
9.2.2.1	Clathrin-mediated endocytosis (CME).....	28
9.2.2.2	Clathrin-independent Endocytosis (CIE)	30
9.2.3	<i>The recycling pathways</i>	34
9.2.3.1	Fast recycling – direct pathway.....	35
9.2.3.2	Slow recycling – Rab11 mediated.....	35
9.2.4	<i>The lysosomal/degradation pathway</i>	35
9.2.5	<i>Retrograde trafficking</i>	36
9.2.5.1	GPP130: A cycling Golgi protein involved in Shiga toxin trafficking	37
9.2.5.2	Clathrin.....	38
9.2.5.3	Retromer.....	38
9.2.6	<i>SNAREs</i>	40
9.2.6.1	The general mode of vesicle fusion.....	41
9.2.6.2	Syntaxin-5 (STX5).....	43
9.2.6.3	Syntaxin-16.....	43
9.3	MICRO INTERFERING RNA FAMILY MIR199.....	44
10	MATERIAL AND METHODS	46
10.1	CELL LINES	47

10.2	ANTIBODIES AND REAGENTS.....	47
10.3	RNA INTERFERENCE.....	48
10.4	CALCIUM PHOSPHATE–DNA CO-PRECIPIATION.....	48
10.5	RETRO-2 TREATMENTS.....	48
10.6	CLICK CHEMISTRY LABELING	49
10.6.1	<i>METHODOLOGY ASPECTS: Bio-orthogonal Click chemistry</i>	49
10.7	IMMUNOPRECIPIATION.....	51
10.8	SHIGA TOXIN TRAFFICKING	51
10.9	PROXIMITY LIGATION ASSAY (PLA).....	51
10.9.1	<i>METHODOLOGY ASPECTS: Proximity ligation assay</i>	52
10.10	CONFOCAL IMAGING	53
10.11	RETENTION USING SELECTIVE HOOKS (RUSH).....	53
10.11.1	<i>METHODOLOGY ASPECTS: Retention Using Selective Hooks (RUSH)</i>	53
10.12	INTOXICATION ASSAY.....	54
10.13	WESTERN BLOT ANALYSIS.....	55
10.14	STATISTICS	55
11	RESULTS.....	56
11.1	MANUSCRIPT FOR SUBMISSION: SYNTAXIN-5 FUNCTIONALLY INTERACTS WITH GPP130 FOR RETROGRADE SHIGA TOXIN TRAFFICKING.....	57
11.1.1	<i>Abstract</i>	58
11.1.2	<i>Author contributions</i>	58
11.1.3	<i>Introduction</i>	59
11.1.4	<i>Results</i>	61
11.1.4.1	Retro-2 targets the COPII machinery.....	61
11.1.4.2	Depletion of Sec16A phenocopies Retro-2 treatment	63

11.1.4.3	Retro-2 slows the anterograde transport of STX5	66
11.1.4.4	STX5 SNARE complexes remain unchanged upon Retro-2 treatment.....	68
11.1.4.5	STX5 binds to GPP130 in a Retro-2 sensitive manner	71
11.1.4.6	The GPP130-STX5 interaction is required for STxB trafficking to the Golgi	73
11.1.5	<i>Discussion</i>	77
11.2	THE EFFECT OF MiR199 ON RETROGRADE SHIGA TOXIN TRAFFICKING.....	79
11.2.1	<i>Objectives and summary</i>	79
11.2.2	<i>Results</i>	80
11.2.2.1	MiR199 down regulates retromer expression	80
11.2.2.2	MiR199 impairs retrograde transport of STxB	80
11.2.2.3	MiR199 inhibits SLT intoxication.....	82
12	DISCUSSION	83
13	PERSPECTIVES	85
14	REFERENCES	86
15	ANNEX	A
15.1	MANUSCRIPTS.....	B
15.1.1	<i>(published) Retrograde transport is not required for cytosolic translocation of Shiga toxin B-subunit</i>	B
15.1.2	<i>(Revision) MiR-199a-5p attenuates retrograde transport and protects against Shiga toxin cytotoxicity</i>	D
15.2	POWERPOINT PRESENTATION OF THE DEFENSE ON DECEMBER 12 TH 2017	DD

5 LIST OF TABLES

	Page
Table 1: Shiga toxin and isoforms (Johannes and Römer, 2010).....	7
Table 2: Retro-1 and Retro-2 protection factors on HeLa cells against Ricin, Stx1, and Stx2. Protection factors calculated over the indicated number of experiments. Means \pm SEM are shown. (Stechmann et al., 2010)	8
Table 3: supplementary information: Full mass-spectrometry tables of GFP-STX5 pulldown.	76

6 TABLE OF FIGURES

	Page
Figure 1: Structure of ribosome-inactivating proteins (RIP) type 1 and 2 (Barbieri et al., 1993). The number of binding sites per B-subunit of Type 2 RIPs can vary. The B-subunit of Shiga toxin provides in total 15 binding sites (3 binding sites per monomer) (Ling et al., 1998).....	2
Figure 2: Schematic presentation of the biochemical action of ribosome-inactivating proteins (RIPs), such as ricin and Shiga toxin. The A-subunit targets the α -sarcin site on the large (28S) subunit of ribosomes, which results in an inhibition of protein biosynthesis. (Stirpe, 2005).....	3
Figure 3: Shiga toxin structures. (A) Schematic drawing of the Shiga holotoxin, catalytic A-subunit (STxA); five B-fragment monomers that form the homopentameric B-subunit (STxB). (B) A ribbon diagram of Shiga toxin, illustrating the binding sites on STxB for globotriaosylceramide (Gb3). Gb3 is shown in a ball-and-stick representation. (C) A zoom into the furin cleavage (Arg ²⁴⁸ -Val-Ala-Met ²⁵¹) site of STxA; the disulfide bond (between Cys ²⁴² and Cys ²⁶¹) is shown in yellow. (D) A ribbon diagram of a STxB from below, pointing out the three Gb3-binding sites. Gb3 is shown as a ball-and-stick representation. (Johannes and Römer, 2010).....	5
Figure 4: Structures of Retro compounds.....	8
Figure 5: Retro-2 protects mice against ricin challenge. Comparison of survival curves from mice that were treated with single intraperitoneal dose of Retro-2 with indicated concentrations one hour before toxin exposure. Ricin was administered to mice via the nasal route (2 mg/kg). The control group received only the vehicle in prior to ricin exposure. The curves for treated animals are statistically different from control as measured by the log rank test ($p < 0.0001$ for 2 μ g/kg of Retro-2, orange; $p = 0.015$ for 10 mg/kg, brown; $p = 0.031$ for 20 mg/kg, purple; $p = 0.0007$ for 200 mg/kg, red). (Stechmann et al., 2010).....	9

Figure 6: Illustration of the retrograde trafficking of Shiga toxin and site of action of Retro-2 (Gupta et al., 2017). Toxins (e.g. ricin and SLTs) traffic via the retrograde route, starting from the plasma membrane through endosomes and Golgi to the ER (Johannes and Popoff, 2008). Retro-2 inhibits the toxin trafficking step from endosomes to the Golgi9

Figure 7: Structural evolution of Retro-2. Structures A and B show the original hit compound Retro-2 (Stechmann et al., 2010). Structure B illustrates how the spontaneous cyclisation to molecule C (Retro-2_{cyclic}) may take place (Park et al., 2012). Structure D shows the optimized molecule of Retro-2 based on C, called Retro2.1 (Noel et al., 2013). Additional structural groups are highlighted in blue. Molecule E is the azide-functionalized Retro-2.1, called “clickable Retro-2”, due to its potential to be used in a biorthogonal click chemistry approach (see chapter 0). The azide is marked in red.10

Figure 8: Chemical structures of inhibitors of SLTs for which the cellular target is already known.....14

Figure 9: Chemical structures of inhibitors of SLTs for which the cellular target is still unknown, including the Retro compounds.17

Figure 10: Models for intra-Golgi vesicular transport. Cargo synthesized in the ER and transported through the secretory pathway is shown in yellow; Golgi processing enzymes are shown in blue. Arrows indicate the direction of trafficking: From left to right: The model of cisternae maturation – the vesicular transport model – the rapid-partitioning model (Jackson, 2009) – Blue dots are Golgi localized enzymes; yellow dots are cargo; blue areas are glycerophospholipid-enriched membranes; green areas are sphingolipid-enriched membranes; green circles within each Golgi stack are sphingolipid-enriched export domains19

Figure 11: A schematic representation of an ER exit site (ERES) showing the ER cup lacking ribosomes, forming COPII-coated vesicles.....21

Figure 12: Model for assembly of the COPII coat complex, describing Sec16 as a scaffolding protein. The common model for assembly of the COPII coat complex is modified to include the role of Sec16. For simplicity, cargo molecules are omitted. (1) The Sec13–Sec16 tetramer is stably associated with the ER membrane and binds the integral membrane protein Sed4 or its homologue Sec12. Sar1 becomes associated with the membrane, when it is converted from the GDP- to GTP-bound state. Concentration of membrane-associated proteins begins to bend membrane. (2) Sec13–Sec16 and Sar1 collaborate to recruit the cargo adaptor Sec23–Sec24 dimer. (3) A precoat self-associates into higher-order oligomers. (4) Sec13–Sec16 and Sec23–Sec24–Sar1 form independent interactions with Sec13–Sec31, causing it to assemble near and/or in place of Sec16. (5) The forming coat contains progressively more Sec13–Sec31 and less Sec13–Sec16. Hand-off of Sec23–Sec24–Sar1 from Sec16 to Sec31 sets the stage for GTP hydrolysis by Sar1. (6) A final COPII coat is formed, and vesicle budding is complete. Sec13–Sec16 remains mostly associated with the ER. - (Whittle and Schwartz, 2010)..... 25

Figure 13: Structure and assembly of the COPII coat. The guanine nucleotide exchange factor, Sec12 (McMahon et al., 2012) catalyzes GTP loading on Sar1, which switches from a cytosolic GDP-bound form (Huang et al., 2001) to a membrane-associated GTP-bound form (Bi et al., 2002) through exposure of an N-terminal amphipathic α -helix. Membrane-associated Sar1 recruits Sec23/Sec24 (Bi et al., 2002). Sec24 provides cargo-binding function by directly interacting with sorting signals on transmembrane clients. The Sar1/Sec23/Sec24 ‘pre-budding’ complex in turn recruits Sec13/Sec31 (Fath et al., 2007). Sec13/Sec31 self-assembles into a polyhedral cage (Stagg et al., 2006) that at least in part drives membrane curvature and contributes to vesicle scission. Sec23 is the GTPase-activating protein for Sar1, with Sec31 further contributing to hydrolysis via a proline-rich domain that extends across the surface of Sec23/Sar1. Sec16 is a peripheral component that binds to Sec13 (Whittle and Schwartz, 2010), modulates GTPase activity by preventing

Sec31 action and otherwise contributes to vesicle formation in poorly understood ways. - (Miller and Schekman, 2013)26

Figure 14: Pathways of entry into cells. Large particles can be taken up by phagocytosis, whereas fluid uptake occurs by macro-pinocytosis. Both processes appear to be triggered by and are dependent on actin-mediated re-modelling of the plasma membrane at a large scale. Compared with the other endocytic pathways, the size of the vesicles formed by phagocytosis and macro-pinocytosis is much larger. Numerous cargoes can be endocytosed by mechanisms that are independent of the coat protein clathrin and the fission GTPase, dynamin. Some of these clathrin-independent pathways are also dynamin independent. Most internalized cargoes are delivered to the early endosome via vesicular (clathrin- or caveolin-coated vesicles) or tubular intermediates (known as clathrin-independent carriers (CLICs)) that are derived from the plasma membrane. Some pathways may first traffic to intermediate compartments, such as the caveosome or glycosylphosphatidylinositol-anchored protein enriched early endosomal compartments (GEEC), en route to the early endosome. - (Mayor and Pagano, 2007)27

Figure 15: Model for the assembly and disassembly of a clathrin coat. The drawing indicates the direction of the rotational movement (counterclockwise) that is required to lock a relatively rigid clathrin triskelion into the lattice. The reverse process would be required to disassemble the coat. - (Kirchhausen, 2000)28

Figure 16: Clathrin-mediated endocytosis. (a) Stages of clathrin-mediated endocytosis. Step 1: FCHO protein mediated nucleation. Step 2: Cargo recruitment by AP-2. Step 3: Coat assembly. Step 4: Dynamin-mediated scission. Step 5: Un-coating. (b) Network of interacting partners involved in CME. (c) Depletion of FCHO proteins, AP-2, clathrin, and dynamin and their effect on CCP formation (McMahon and Boucrot, 2011).30

Figure 17: (a) STxB-driven membrane invagination in interaction with the GSL Gb3. – adopted from (Johannes et al., 2016). 31

Figure 18: Model of actin-driven scission. After SLT binding on to Gb3, membrane curvature is induced, leading to the clathrin independent formation of PM invaginations. Actin polymerization causes scission through membrane reorganization (Römer et al., 2010) 32

Figure 19: Gal3-driven membrane bending. (Johannes et al., 2015) 33

Figure 20: A schematic representation of the ‘tubular endosomal network’ (TEN). Endocytic vesicles are delivered to clathrin-coated early endosomes, which start to mature involving progressive acidification of their lumen. The TEN contains various domains (labeled in different colors) and the necessary machinery to sort cargoes to their various destinations. - (Bonifacino and Rojas, 2006) 34

Figure 21: The generation of multi-vesicular bodies, leading to lysosomes. The degradation pathway is shown by solid arrows. Membrane invaginations and internal vesicles are shown in red, highlighting multi-vesicular regions in EE and LE. The recycling pathways (slow and fast) are shown by dashed arrows. - (Gruenberg and Stenmark, 2004) 36

Figure 22: Schematic drawing of retrograde trafficking entry points. The retrograde transport step from endosomes to the TGN can originate from several points: recycling (blue), early (green) or late (red) endosomes. - (Johannes and Wunder, 2011b)..... 37

Figure 23: Schematic presentation of a speculative model of the retromer coat on a membrane tubule. SNX dimer in purple. - (Hierro et al., 2007) 39

Figure 24: SNARE proteins form a four-helical bundle complex that drives membrane fusion. (a) VAMP (blue) on the vesicle interacts with syntaxin (red) and SNAP-25 (green) on the plasma membrane to form a four-helix bundle that zips up concomitant with bilayer fusion. (b) The backbone of the SNARE complex is

shown on the left, with the central ionic layer (red) and 15 hydrophobic layers (black) that mediate the core interactions. Top-down views of side-chain interactions are shown on the right, with the four SNARE helices that are represented as ribbons. The ball-and-stick structures represent the indicated amino acids; the dotted lines represent hydrogen bonds or salt bridges that stabilize interactions between SNAREs. Q-SNAREs and R-SNAREs are characterized by a glutamine (Q) or arginine (R) residue, respectively, in the central layer of the SNARE complex. (SNARE; soluble NSF attachment protein receptor, where NSF stands for N-ethyl-maleimide-sensitive fusion protein; SNAP-25, 25 kDa synaptosome-associated protein; VAMP, vesicle-associated membrane protein). - (Chen and Scheller, 2001)40

Figure 25: Model of SNARE-mediated lipid fusion. (a) The two membranes are in the vicinity of each other but the SNAREs are not yet in contact. (b) SNARE complexes start zipping from the amino-terminal end, which draws the two membranes further towards each other. (c) Zipping proceeds, causing increased curvature and lateral tension of the membranes, exposing the bilayer interior. Spontaneous hemi fusion occurs as the separation is sufficiently reduced. (d) The highly unfavorable void space at the membrane junction in (c) causes the establishment of contacts between the distal membrane leaflets. (e) The lateral tension in the trans-bilayer contact area induces membrane breakdown, yielding a fusion pore. (f) The fusion pore expands and the membrane relaxes. - (Chen and Scheller, 2001)41

Figure 26: Schematic summary of known mammalian SNARE complexes and their site(s) of action in the exocytic and/or endocytic pathways. The potential v-SNAREs are indicated in red. - (Hong, 2005)42

Figure 27: Proposed model of regulation of receptor-mediated endocytosis by dynamin and miR-199a/b. Sense strands of the dynamin genes are transcribed and translated to synthesize dynamin proteins that are involved in endosome trafficking. miR-199a- 5p is transcribed in the nucleus from the antisense strand of introns in the DNM2 and DNM3 genes and regulates receptor-

mediated endocytosis and intracellular cholesterol levels by balancing the post-transcriptional levels of genes involved in endocytosis such as LDLR, CLTC, Cav-1, Rab5A and Rab21. - (Aranda et al., 2015) 44

Figure 28: Design and synthesis of Cu-free click chemistry reagents. (A) The copper-catalyzed azide–alkyne cycloaddition. (B) The Cu-free click reaction of azides and DIFOs. (C) Single step synthesis of DIFO. (D) Derivatives of DIFO and a linear alkyne (alk) containing Alexa Fluor 488, Alexa Fluor 568, or biotin. - (Baskin et al., 2007) 50

Figure 29: Detection of protein-protein proximity with the proximity ligation assay (PLA). (a) Schematic presentation of proximity probe-templated DNA circularization and subsequent rolling circle amplification (RCA) and detection. If two proximity probes bind close to each other, such as by binding two proteins present in the same complex, then subsequently added linear connector oligonucleotides are guided to form a circular structure covalently joined by enzymatic DNA ligation. After ligation, RCA is initiated using one of the proximity probes as a primer. The RCA product is detected through hybridization of fluorescence-labeled oligonucleotides complementary to a tag sequence in the RCA product. The green line in the circle that forms the proximity ligation reaction giving rise to multiple copies of complementary sequence in the RCA product (blue). This motif is detected by hybridizing fluorescence-labeled detection oligonucleotides (green).- (Söderberg et al., 2006)..... 52

Figure 30: The RUSH system. (a) A schematic of the principle illustrates that the reporter is retained in the donor compartment via its interaction with the hook. This interaction is mediated by the core streptavidin and the SBP. Release is induced by addition of biotin to allow trafficking of the reporter to its acceptor compartment. A fluorescent protein is fused to the reporter. (b) Schematics of hooks containing STIM1-NN, Ii or KDEL for ER retention, or Golgin-84 for Golgi retention fused to streptavidin, and of reporters containing SBP fusions with Golgi proteins ST, ManII, GalT or Golgin-84, plasma membrane proteins

VSVGwt, E-cadherin, TNF α or EGFP-GPI and secreted protein SBP-ssEGFP. HA, hemagglutinin tag; FP, fluorescent protein. (c) Schematics of genes coding for the hook and the reporter, expressed under the same CMV promoter (pCMV), separated by a synthetic intron (IVS, intervening sequence) and an internal ribosome entry site (IRES). - (Boncompain et al., 2012).....54

Figure 31: Sec16A is involved in Retro-2 binding on cells. (A) Scheme of biorthogonal Click chemistry adapted to Retro-2. The clickable Retro-2 probe, based on Retro-2.1 (Gupta et al., 2014) was coupled via a DIBO moiety to biotin, or a fluorophore. (B) In two independent pull-down experiments with the clickable Retro-2-biotin probe, Sec16A was identified as the top hit. When indicated, non-clickable Retro-2 was used in excess to compete with clickable Retro-2. DMSO without clickable Retro-2 was used as a control condition. (C) anti-Sec16A Western blots of a representative Retro-2 pull-down (with the clickable Retro-2-probe). Shown are bands on the level of the 250 kDa marker. (D) Confocal acquisitions of Click-staining of a Retro-2-fluorophore-probe on mock-siRNA treated cells (=control), or Sec16A-depleted cells (=Sec16A). DNA was stained with DAPI. (E) Quantification (~100 cells per condition) of the fluorescence intensity of the Retro-2-fluorophore-probe (normalized to 100 ± 9.118 %). The intensity of the fluorescence-probe only (=probe) was set to 0 % intensity. The intensity of Retro-2-fluorophore-probe upon Sec16A depletion resulted in 21.5 ± 6.248 % intensity. *** = <0.000162

Figure 32: Depletion of Sec16A affects Shiga toxin trafficking similar to Retro-2 treatment. (A) HeLa cells were transfected for 72 hours with the indicated siRNAs (scrambled or against Sec16A). After 30 min of pre-incubation with Retro-2 (or DMSO for control), cells were incubated for another 45 minutes at 37°C with STxB-Cy3 (green). The Golgi was immuno-labeled with an anti-rabbit-Giantin antibody (red); DNA was marked with DAPI (blue). The scale bar represents 10 μ m. (B) Quantifications (~100 cells per condition of two independent experiments) of STxB-Cy3 intensity in the Golgi in the region indicated conditions. Control = 91.43 ± 0.9767 %, Retro-2 = 71.17 ± 2.289 %, siSec16A = 60.54 ± 2.309 %, siSec16A + Retro-2 = 46.17 ± 1.683 %. P value of T tests = ***

= <0.0001. (C) Intoxication of HeLa cells with STx1 in the indicated conditions. $EC50_{siControl} = 0.06178$ ng/ml, $EC50_{siSec16A} = 0.3733$ ng/ml, protection factor = 6.042-fold. 64

Figure 33: Depletion of Sec16A affects STX5 localization similar to Retro-2 treatment. (A) HeLa cells were incubated for 30 min at 37°C with Retro-2 (or DMSO as control). STX5 was immuno-labeled with a rabbit antibody (green); the Golgi was immuno-labeled with an anti-goat-TGN antibody (red); DNA was marked with DAPI (blue). The scale bar represents 10 µm. (B) Quantifications (~50 cells per condition of two independent experiments) of STX5 intensity in the Golgi. Control = 69.4 ± 1.543 %, Retro-2 = 33.11 ± 0.9788 %, siSec16A = 44.06 ± 2.739 %, siSec16A + Retro-2 = 31.49 ± 1.27 %. P value of T tests = *** = <0.0001. 65

Figure 34: Retro-2 treatment slows the anterograde transport of STX5. (A) Confocal acquisitions of HeLa cells that expressed the STX5-RUSH construct. The cells were pre-treated for 60 min at 37°C with Retro-2, or DMSO as control (steady state). Trafficking was initiated upon addition of biotin, followed by incubation for 20 min at 37°C. STX5-GFP is shown in green; the Golgi (giantin) is shown in red; the scale bar represents 10 µm. (B) Quantification (four independent experiments, 60 cells per experiment) of STX5-GFP intensity in the Golgi area. Steady state: 17.93 ± 2.494 %, 20 min release in control conditions: 100 %, 20 min release in the presence of Retro-2: 68.15 ± 5.298 %, P value of T tests = *** = 0.0010. (C) Trafficking of the ManII-RUSH construct (green) was analyzed as in (B). (D) Quantifications (~50 cells per condition) of ManII-GFP intensity in the Golgi. Steady state: 17.15 ± 1.531 %, 20 min trafficking: 94.12 ± 1.967 %, 20 min trafficking + Retro-2: 91.18 ± 4.609 %, P value of T tests = NS = not significant. 67

Figure 35 (previous page): STX5-SNARE complexes are not affected upon Retro-2 treatment. (A) Representative confocal acquisitions of the cellular distribution of STX5, GS27, and GS28 in either control (DMSO) or Retro-2 treated cells. (B) Quantification (~110 cells per condition) of Golgi-localized fluorescent signal

of STX5, GS27, and GS28. TGN46 immuno-labeling was used as a Golgi mask. STX5: $56 \pm 1 \%$, STX5 + Retro-2: $28.32 \pm 1.0 \%$, P value of T tests = *** = <0.0001 . GS27 = $64.47 \pm 1.0 \%$, GS27 + Retro-2 = $61.18 \pm 1.7 \%$, P value of T tests = NS = 0.09. GS28: $82.58 \pm 0.9 \%$, GS28 + Retro-2: $81.14 \pm 0.9 \%$, P value of T tests = NS = 0.2774. (C) Table for STX5 interacting proteins that are not competed for by Retro-2 treatment of cells. #-cis-Golgi STX5 SNARE complex proteins, *-trans-Golgi STX5 SNARE complex proteins. (D) anti-GFP, GS27 and GS28 Western blots of a representative eGFP-STX5 pull-down via GFP-trap beads. Controls were un-transfected cells or eGFP transfected cells. eGFP-STX5 cells were treated either with DMSO (control) or Retro-2. (D) anti-GFP, GS27 and GS28 Western blots of a representative eGFP-STX5 pull-down via GFP-trap beads. Controls were un-transfected cells or eGFP transfected cells. eGFP-STX5 cells were treated either with DMSO (control) or Retro-2. (E) Representative confocal acquisitions of STX5-PLA with either GS27 or GS28 upon DMSO (control) or Retro-2 treatment. One cell per picture is shown. (F) Quantification of PLA between STX5 and GS27. Number of dots were normalized by μm^2 . P value of T tests = NS = 0.4766 (G) Quantification of PLA between STX5 and GS28. Number of dots were normalized by μm^2 . P value of T tests = NS = 0.9543.70

Figure 36: The cytosolic domain of GPP130 interacts with STX5. (A) Table of Retro-2-competed interacting proteins of STX5. (B) anti-GFP and GPP130 Western blots of a representative eGFP-STX5 pull-down via GFP-trap beads. Controls were un-transfected cells or eGFP transfected cells. eGFP-STX5 cells were treated either with DMSO (control), Retro-2, siRNA against STX5, siRNA against GPP130, or manganese (leading to GPP130 degradation). (C) SDS-Page analysis of purified STX5 (residues 202-355). The indicated amount (Load) of purified STX5 was incubated with GST, GST-GPP130₁₋₁₀₈ (WT), GST- GPP130₁₋₁₀₈ with a substituted cytosolic domain from DPPIV (DGG), or GST- GPP130₁₋₁₀₈ with KR_{11,12}AA alanine substitution in the cytosolic domain. Anti-GST-beads were used to collect the complexes and after washing, recovery of STX5 (Bound)

was determined by Coomassie staining of SDS-PAGE gels and (D) quantified (n=6±SD)..... 72

Figure 37 (previous page): STX5 binding site in GPP130 is required for its Golgi retrieval and Shiga toxin trafficking. (A) Protein neo-biosynthesis was measured via the incorporation of S35-radiolabeled methionine in function of increasing toxin concentration after one hour of STx1 intoxication. Cells were pretreated either with scrambled siRNA or siRNA against GPP130 72 hours before intoxication. EC50siControl = 2.851 ng/ml, EC50siGPP130 = 27.47 ng/ml, protection factor = 9.6352. (B) STxB-Cy3 trafficking. Quantifications (~50 cells per condition of two independent experiments) of STxB-Cy3 intensity in the Golgi region after 45 min. Control = scrambled siRNA: 86.39 ± 1.488 %, siGPP130: 63.23 ± 2.475 %, WT rescue after GPP130 depletion: 83.23 ± 1.796 %, KR-AA mutant retransfection after GPP130 depletion: 57.08 ± 3.95 %. P value of T tests = *** = <0.0001, NS = non-significant. (C) Representative acquisitions of (D). (D) Gene-edited cells lacking GPP130 were transfected with either HA-GPP130 (WT) or an identical construct with the KR_{11,12}AA alanine substitution (KR-AA) that blocks binding to STX5. The cells were then untreated, treated with monensin for 1 hour to redistribute GPP130 to endosomes, or monensin-treated and then subjected to a 3-hour washout incubation. Only the GPP130 staining is shown to localize the GPP130 constructs, but giantin staining of the same cells indicated the position of the Golgi. Quantification of the washout was carried out by counting cells with primarily Golgi-localized, a mix of Golgi- and endosome-localized, or primarily endosome-localized GPP130 (n=9±SEM, about 50 cells counted per experiment).. Shown is the cellular distribution of the re-transfected GPP130 constructs (WT or KR-AA) upon control = untreated (left column), monensin treatment (middle column), or monensin washout (right column). The scale bar represents 10 µm. 75

Figure 38: Western blot against VPS26. Loading from left to right: molecular weight marker (top to bottom in kDa: 100, 75, 55, 35, 25, 15), scrambled miR transfected cells (miRCM), miR199 transfected cells, cell lysate (input). Expected size: 38 kDa.. 80

- Figure 39: Quantification STxB-Cy3 trafficking in mock or miR199-treated cells. Quantifications (~25 cells per condition) of STxB-Cy3 intensity in the Golgi region after 45 min of incubation. miRCM = scrambled miR: 52.46 ± 3.489 , and miR199 treatment: 33.92 ± 2.713 . Shown is the mean and the SD. P value of T tests = *** = <0.000181
- Figure 40: Representative intoxication curves upon STx1 treatment. Points = control = scrambled miR, triangles = miR199, cubes = siRNAVPS26, protection factors are shown in Figure 39.82
- Figure 41: Quantifications of 3 independent STx1 intoxication experiments. Shown are protection factors. Control = scrambled miR: 1-fold protection, miR199: 3.68 ± 0.8648 fold protection and siRNAVPS26 treatment: 4.507 ± 1.329 fold protection. The difference between miR199 and siRNAVPS26 was not significant ($P = 0.6181$)82

7 ABBREVIATIONS

A

AP	Adaptor protein
AP180	Adaptor protein 180
Arf	ADP-ribosylation Factor GTPase

B

BFA	Brefeldin A
-----	-------------

C

CALM	Clathrin assembly lymphoid myeloid leukaemia
CCP	Clathrin-coated pit
CCV	Clathrin-coated vesicle
CDC	Centers for Disease Control and Prevention
CD-MPR	Cation-dependent mannose-6-phosphate receptor
CMV	Human cytomegalovirus
COP I	Coatomer protein complex I
COP II	Coatomer protein complex II
CTx	Cholera toxin
CTxB	B-subunit of cholera toxin

D

E

EC50	50 % effective toxin concentration
EE	Early endosomes
EE-TGN	Early endosomes-Trans Golgi Network interface
EGF	Epidermal growth factor
eGFP	enhanced green fluorescent protein
EGFR	Epidermal growth factor receptor
EpsinR	Epsin related
ER	Endoplasmic reticulum
ERAD	ER-associated protein degradation
ERES	ER exit site(s)
ERGIC	ER-Golgi intermediate compartment
ESCRT	Endosomal sorting complex required for transport

F

G

GAP	GTPase activating factor
GBF1	Golgi-associated Brefeldin A-resistant factor 1

Gb3 Globotriaosyl ceramide
GCA Golgicide A
GEEC GPI-anchored protein enriched early endosomal compartment
GEF Guanine-nucleotide exchange factor
GFP Green fluorescent protein
GP73 Golgi membrane protein GP73 (Golgi membrane protein 1)
GPI-AP Glycosylphosphatidylinositol-anchored proteins
GPP130 Golgi-localized phosphoprotein of 130 kDa (Golgi integral membrane protein 4)
GS15 Golgi SNARE of 15 kDa
GS28 Golgi SNARE of 28 kDa

H

HSC70 Heat shock cognate 70
HTS High throughput screening
HUS Hemolytic uremic syndrome

I

IL2R Interleukin-2 receptor

J

K

L

LDL Low-density lipoprotein
LDLR Low-density lipoprotein receptor

M

MHC Major histocompatibility complex
miR micro interfering RNA
MPR Mannose 6-phosphate receptor
MVB Multivesicular body

N

O

P

PLA Proximity ligation assay
PM Plasma membrane

Q

R

Rab	Ras-like protein in brain
Rho	Ras homologous
RIP	Ribosome inactivating protein
RME	receptor-mediated endocytosis
RME-8	Receptor-mediated endocytosis-8
RNA	Ribonucleic acid
rRNA	Ribosomal RNA
RT	Room temperature
RTx	Ricin holotoxin
RUSH	Retention using selective hooks

S

siRNA	Small interfering RNA
SLT	Shiga-like toxins (Escherichia coli)
SNAP	Soluble N-ethylmaleimid sensitive factor (NSF) attachment protein
SNAP-25	Synaptosome-associated protein of 25 kDa
SNARE	Soluble N-ethylmaleimid sensitive factor attachment protein (SNAP) receptor
SNX	Sorting nexin
SNX-PX	Sorting nexin-phox homology domain
STEC	Shiga-like-toxin producing Escherichia coli
STx	Shiga toxin; holotoxin (Shigella dysenteriae)
STxA	A-subunit of Shiga toxin (Shigella dysenteriae)
STxB	B-subunit of Shiga toxin (Shigella dysenteriae); identical to Stx1B
Stx1	Shiga-like toxin 1; holotoxin (Escherichia coli)
Stx2	Shiga-like toxin 2; holotoxin (Escherichia coli)
STX5	Syntaxin-5
SV40	Simian virus 40

T

TEN	Tubular endosomal network
Tf	Transferrin
TfR	Transferrin receptor
TGN	Trans-Golgi network
TGN46	Trans-Golgi network protein 46
t-SNARE receptor	targetSoluble N-ethylmaleimid sensitive factor attachment protein (SNAP)

U

V

VAMP	Vesicle-associated membrane protein (also called synaptobrevin)
------	---

8 SUMMARY

The introduction of my PhD manuscript starts with describing plant and bacterial toxins (chapter 9.1), in particular Shiga toxin and Shiga-like toxins (SLTs) (chapter 9.1.2). Small molecule inhibitors of these toxins are summarized afterwards in chapter 9.1.3, notably the Retro-2 compound. Since these toxins rely on intracellular trafficking to reach their molecular targets, a general overview of endocytosis and endosomal trafficking is provided (chapter 9.2). Next, the retrograde route entry is presented (chapter 9.2.5), with focus on clathrin, the retromer and GPP130, a protein that constantly cycles between Golgi, plasma membrane, and endosomes. SNARE proteins, particularly syntaxin-5 and syntaxin-16, are then introduced (chapter 9.2.6). After a brief section of the micro RNA family 199 (chapter 9.3), the introduction finishes with the description of some salient techniques that were used in my work, such as - bio-orthogonal Click-Chemistry, anterograde trafficking synchronization with the retention using selective hooks (RUSH) assay, and the antibody-based proximity ligation assay (chapter 10.6.1, 10.11.1).

Herein, my submitted publication opens the results part (chapter 11.1), in which I present the utility of biorthogonal click chemistry for the search of the cellular targets of Retro-2, a small molecule inhibitor that was previously shown to protect cells and animals against Shiga toxin and ricin. I describe that Sec16A is a likely cellular target candidate, and illustrate using the RUSH approach how interfering with Sec16A functions leads to the partial relocalization of syntaxin-5 to the endoplasmic reticulum (ER) by slowing-down its anterograde transport. The second part of the paper describes how syntaxin-5 relocalization causes the inhibition of Shiga toxin trafficking from endosomes to the TGN. I present a novel interaction between syntaxin-5 and the Golgi protein GPP130, which both have been already described in relation to Shiga toxin trafficking. My work connects both trafficking factors in retrograde trafficking at the endosomes-TGN interface. Strikingly, I demonstrate that this interaction is most probably based on a non-SNARE function of syntaxin-5.

In collaboration with Juan Francisco Aranda and Carlos Fernandez in the US, we put micro RNAs into an endogenous regulation context of Shiga toxin retrograde trafficking (chapter 11.2). An extended discussion will be given in chapter 12.

Last, a general outlook of ongoing projects is given in the perspectives section (chapter 13), in which further collaborations are highlighted.

Keywords: Retrograde transport, Shiga toxin, Shiga-like toxin (SLT), STxB, syntaxin-5, Sec16A, GPP130, Retro-2, Retro-2.1, azide-functionalized Retro-2, copper-free click chemistry, small molecule target identification, mass spectrometry, non-SNARE function, anterograde trafficking inhibition, miRNA, miR199, retromer, VPS26

9 INTRODUCTION

9.1 PLANT AND BACTERIAL RIBOSOMAL INACTIVATING PROTEIN-TOXINS

The description of ribosome-inactivating proteins (RIPs) has been applied to plant proteins that enzymatically damage ribosomes in a catalytic manner, thus inhibiting protein biosynthesis (Desmyter et al., 2003; Peumans et al., 2001; Nielsen and Boston, 2001; Barbieri et al., 1993). The first identified RIPs were two potent toxins, known for more than a century: ricin, from the seeds of *Ricinus communis*, and abrin, from the seeds of *Abrus precatorius*.

Later, further RIPs were discovered and classified into 3 types. Type 1 RIPs are single-chain proteins of around 30 kDa. Type 2 RIPs are built of two subunits: an A-subunit of about 30 kDa that provides the enzymatic activity, and a B-subunit with lectin activity, able to bind to oligosaccharides containing galactose. The third type of RIPs has been attributed to a maize b-32 RIP, regrouping RIPs with a proenzyme stage that get activated after cleavage of a short internal peptide, creating two fragments of 16.5 and 8.5 kDa (Walsh et al., 1991). For RIP JIP60, one of the two pieces is analog to a type 1 RIP, whereas the functions of the other part remains unknown (Reinbothe et al., 1994). Arguably, type 1 and 2 RIPs represent the majority of RIPs. Structural schemes of both classes are shown in Figure 1.

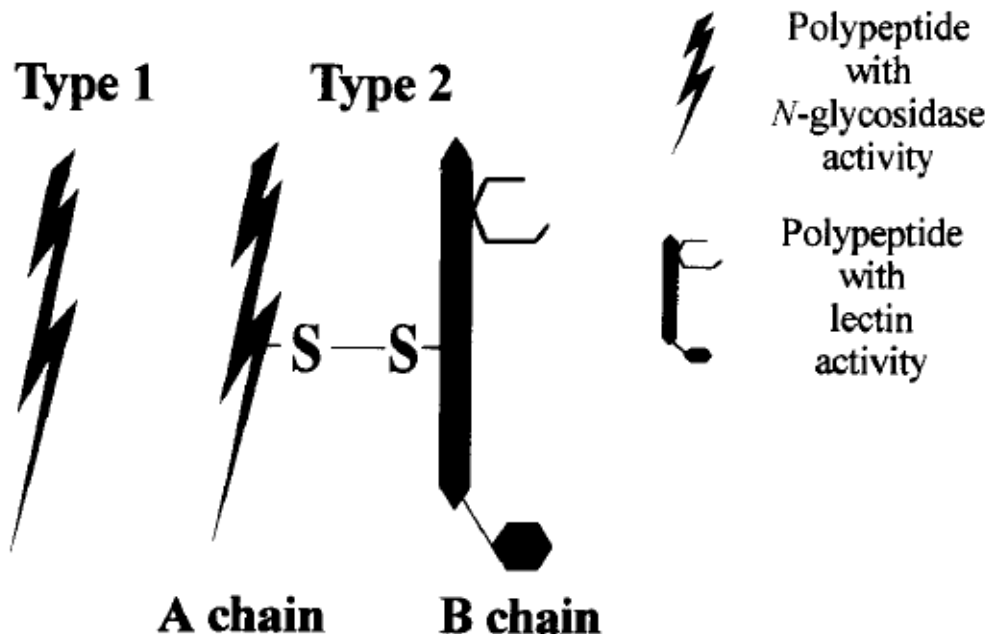
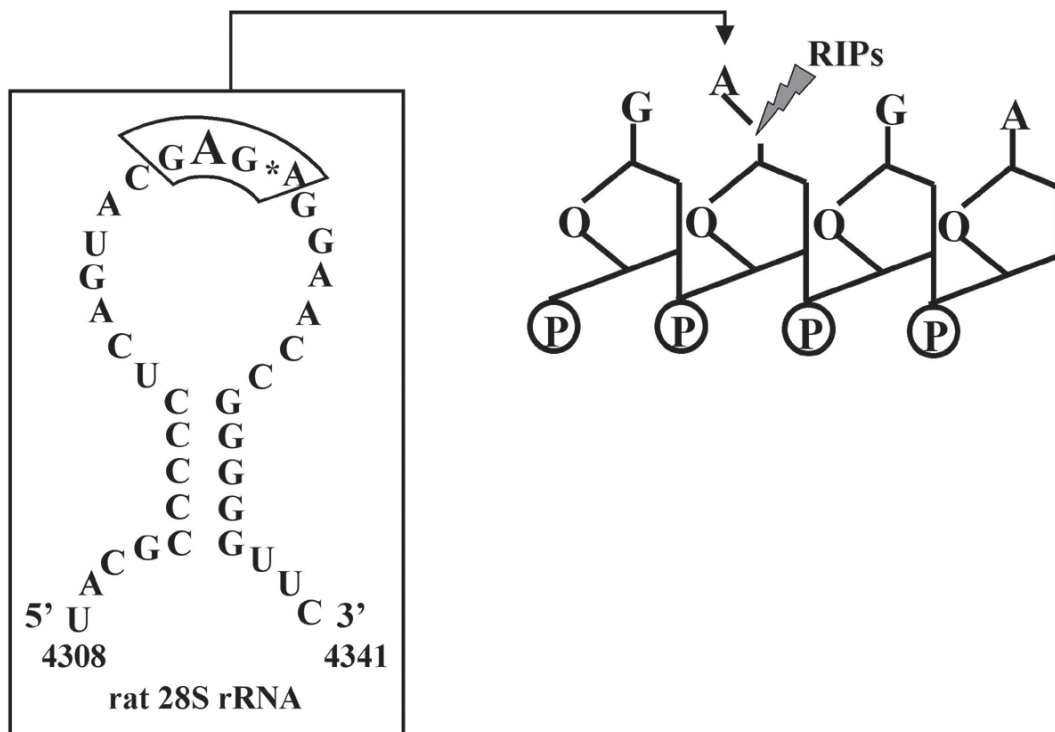


Figure 1: Structure of ribosome-inactivating proteins (RIP) type 1 and 2 (Barbieri et al., 1993). The number of binding sites per B-subunit of Type 2 RIPs can vary. The B-subunit of Shiga toxin provides in total 15 binding sites (3 binding sites per monomer) (Ling et al., 1998).

The unique characteristic of type 2 RIPs is the binding capacity of the B-subunit, which interacts with carbohydrate residues on cell membranes. Moreover, this binding results in the uptake of the toxins. A prominent member of the type 2 RIPs is ricin, which binds to mannose type glycans (Simmons et al., 1986). The endocytosis and intracellular trafficking of type 2 RIPs has been well studied. Characteristically, type 2 RIPs, such as ricin and Shiga toxin, undergo retrograde trafficking. The key step is the arrival to the Golgi and further the endoplasmic reticulum (ER) (Mallard et al., 1998; Sandvig et al., 1992; Sandvig and van Deurs, 2000; Johannes and Goud, 1998), from where their A-subunits are retrotranslocated into the cytosol to reach their molecular targets: the ribosomes. In the cytosol, the A-subunits cleave an adenine base on position 4,324 within the 28S-subunit of ribosomes (Endo et al., 1988; Saxena et al., 1989) (Figure 2). Through the catalytic cleavage, elongation factors are not recruited anymore, disabling ribosomes, inhibiting protein biosynthesis, and leading to cell death.



*** α -Sarcin target**

Figure 2: Schematic presentation of the biochemical action of ribosome-inactivating proteins (RIPs), such as ricin and Shiga toxin. The A-subunit targets the α -sarcin site on the large (28S) subunit of ribosomes, which results in an inhibition of protein biosynthesis. (Stirpe, 2005)

9.1.1 Bioterrorism, bio threat agents and biodefense

For the last decades, health emergencies due to infectious diseases have increased (*E. coli* O104:H4, Ebola virus, H1N1 *influenza* virus, etc.) (Morens et al., 2004; Jones et al., 2008). A recent outbreak that happened back in 2011 in central Europe, mainly Germany, demonstrated the overwhelming potential of toxins as bio-threats (King et al., 2012; Nr et al., 2011). The relative ease with which toxins are produced has enabled bioterroristic assaults (anthrax letters in 2001, or ricin letters to former US president Barak Obama), which kept bioterrorism on the political agenda throughout the years (Bekerman and Einav, 2015; Gottron and Shea, 2010; Gonzales et al., 2006; Council, 2007). As defined by the U.S. Centers for Disease Control and Prevention (CDC), the intended release of toxins, bacteria, viruses or other harmful biological agents to damage or kill people, animals, or plants is considered as a bioterrorist attack (Sciences et al., 2016). Biodefense is defined as the means or methods of preventing, detecting, or managing an attack involving biological weapons.

The discovery of effective and direct medical agents against biological threats is clearly important. In the past decade, high-throughput screenings (HTS) have been performed by the French Commission for Alternative Energies and Atomic Energy (CEA - Commissariat à l'énergie atomique et aux énergies alternatives) and the Curie institute in Paris. This will be discussed in chapter 9.1.3.

9.1.2 Shiga toxin and its Shiga-like toxins

In the following text, I will mainly focus on Shiga toxin and its isoforms. Shiga toxin was characterized by and named after Kiyoshi Shiga (Trofa et al., 1999; Konowalchuk et al., 1977). Shiga toxins are members of a family that includes Shiga toxin, produced by *Shigella dysenteriae* and Shiga-like toxins (SLTs), produced by enterohemorrhagic strains (EHEC) of *Escherichia coli* (or Shiga-like toxin producing (STEC) strains) (

Table 1) (Johannes and Römer, 2010; O'Brien et al., 1984). The production of these toxins by *E. coli* has been directly linked to the development of hemolytic uremic syndrome (HUS), which can have deadly outcome (Karmali et al., 1983). The enterohemorrhagic *E. coli* strains with the serotypes O157:H7 and O104:H4 are most common sources for SLTs. No direct treatments exist against EHEC-induced HUS, and the application of the anti-C5 complement component antibody eculizumab® remains questionable (Karpman, 2012). Furthermore, a treatment with conventional antibiotics seems to increase toxin release from bacteria and worsens the outcome (Agger et al., 2015).

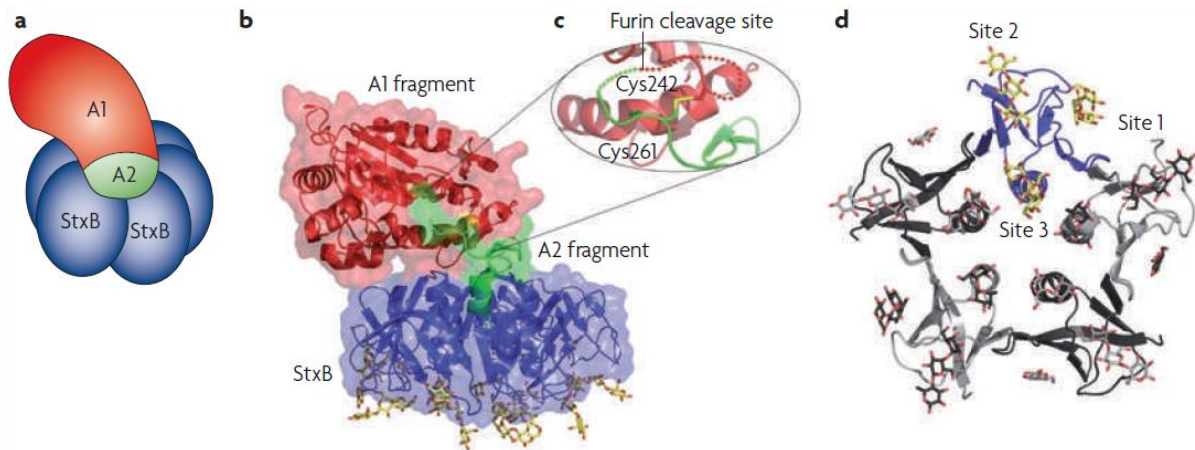


Figure 3: Shiga toxin structures. (A) Schematic drawing of the Shiga holotoxin, catalytic A-subunit (STxA); five B-fragment monomers that form the homopentameric B-subunit (STxB). (B) A ribbon diagram of Shiga toxin, illustrating the binding sites on STxB for globotriaosylceramide (Gb3). Gb3 is shown in a ball-and-stick representation. (C) A zoom into the furin cleavage (Arg²⁴⁸-Val-Ala-Met²⁵¹) site of STxA; the disulfide bond (between Cys²⁴² and Cys²⁶¹) is shown in yellow. (D) A ribbon diagram of a STxB from below, pointing out the three Gb3-binding sites. Gb3 is shown as a ball-and-stick representation. (Johannes and Römer, 2010)

Structurally and functionally, SLTs share many characteristics with other type 2 RIPs. Figure 3 schematically shows the molecular set up of SLTs (Johannes and Römer, 2010). SLTs are built of a catalytic A-subunit (STxA) and a homo-pentameric B-subunit (STxB). STxA inhibits protein biosynthesis through ribosomal RNA N-glycosidase activity, as mentioned above in chapter 9.1.

In the process of cellular trafficking, STxA can be cleaved into two fragments by the *trans*-Golgi-network-(TGN)-localized enzyme furin, which specifically recognizes an Arg-X-X-Arg sequence (Molloy et al., 1992) (Figure 3 C). Specifically, the cleavage occurs in the positions Arg²⁴⁸-Val-Ala-Met²⁵¹ and requires low pH for cell intoxication (Sandvig, 2001; Garred et al., 1995). This leads to the production of the STxA1 (28 kDa) and STxA2 (4 kDa) fragments. Both fragments remain connected via a disulfide bond between Cys242 and Cys261 until they reach the ER.

Table 1: Shiga toxin and isoforms (Johannes and Römer, 2010)

<i>Organism</i>	<i>Toxin</i>	Sequence similarity to Shiga toxin [%]		<i>Characteristics</i>	<i>Synonyms</i>	<i>Cellular receptors</i>
		A-subunit	B-subunit*			
<i>Shigella dysenteriae</i>	Shiga toxin	100	100	N/A	N/A	Gb3
STEC	STx1	97	98	N/A	SLTI & VT1	Gb3
	STx1c	97	98	N/A	SLTIc and VT1c	Gb3
	STx2	53	64	Associated with severe disease in humans	SLTII and VT2	Gb3
	STx2c	53	61	N/A	SLTIIc and VT2c	Gb3
	STx2d	54	61	N/A	SLTIIId and VT2d	Gb3
	STx2e	53	61	Associated with the piglet edema disease	SLTIIe and VT2e	Gb3 & Gb4
	STx2f	54	60	N/A	SLTIIIf and VT2f	Gb3

*Gb3, Globotriaosylceramide; N/A, not applicable; SLT, Shiga-like toxin; STEC, Shigella toxin-producing Escherichia coli; Stx1, Shiga toxin 1; VT: Vero toxin. *This is the sequence similarity for mature B-fragments, without signal sequences.*

Strikingly, STxB (except STxB2e, Table 1) binds specifically the glycosphingolipid globotriaosylceramide (Gb3 or CD77) (Jacewicz et al., 1986; Waddell et al., 1990; Lindberg et al., 1987). Crystal structures revealed three binding sites per monomer, resulting in 15 binding sites per STxB (Ling et al., 1998). After binding to Gb3, SLTs were found in clathrin coated pits (Sandvig et al., 1989). Still, the depletion of clathrin only partially affects the uptake of Shiga toxin (maximally 35 % inhibition), suggesting that these toxins mostly enter cells through clathrin-independent endocytosis (CIE) (Lauvrak, 2004; Saint-Pol et al., 2004; Nichols et al., 2001). After endocytosis, SLTs traffic through the retrograde route, from early endosomes (EE) to the Golgi and the ER (Sandvig et al., 1992) (Figure 6, page 9). Chapter 9.2 is going to introduce this intracellular trafficking in further detail.

9.1.3 Small molecule inhibitors of the retrograde route

One major strategy in developing a direct treatment against plant and bacterial toxins, such as ricin and Shiga toxin is small molecule HTS of chemical libraries. Since the beginning of the 21st century, several inhibitory small molecule compounds have been found that protect cells and animals against toxins through perturbation of their intracellular trafficking (Barbier et al., 2012). A recent review describes the latest development of new compounds that target the intracellular retrograde transport process (Gupta et al., 2017). In the upcoming chapter I am going to dissect their characteristics in further detail.

9.1.3.1 Retro compounds

In prior to 2010, my host laboratory collaborated with the CEA that had screened more than 16,000 small molecules for inhibitory effects against ricin, and found two protecting small molecules, called Retro1 and Retro-2 (structures are shown in Figure 4).

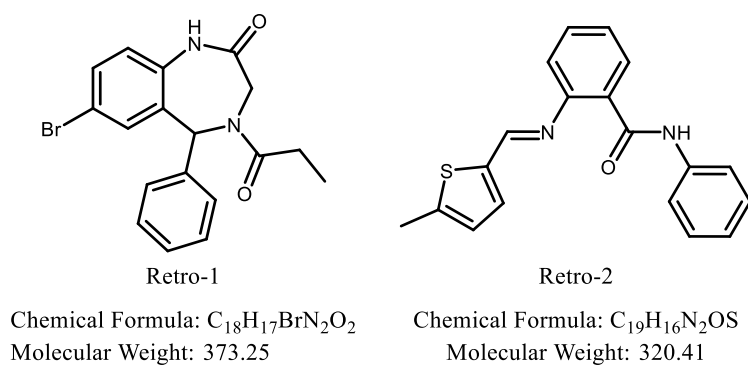


Figure 4: Structures of Retro compounds.

Ricin and SLT share the retrograde trafficking route. Therefore, those two compounds were also tested for their protective effect against intoxication of cells by SLTs, revealing an even higher protection factors (shown in Table 2), Moreover, it seemed that Retro-1 and Retro-2 affected only one out of 26 tested trafficking factors that were known to be involved in endosomes-to-Golgi trafficking: Syntaxin-5 (STX5) was relocalized out of the Golgi without dispersing the Golgi itself (Stechmann et al., 2010), pointing to the possibility that the Retro compounds might be of interest for pharmaceutical developments. A proper introduction into intracellular trafficking is given in chapter 9.2, on page 18.

Table 2: Retro-1 and Retro-2 protection factors on HeLa cells against Ricin, Stx1, and Stx2. Protection factors calculated over the indicated number of experiments. Means \pm SEM are shown. (Stechmann et al., 2010)

Retro-1		Retro-2	
Protection factor		Protection factor	
Ricin, 4 h	3.6 \pm 0.1 (n=2)	Ricin, 4 h	2.7 \pm 0.1 (n=2)
STx1, 1 h	37 \pm 10 (n=6)	STx1, 1 h	42 \pm 9 (n=4)
STx1, 4 h	24 \pm 2 (n=2)	STx1, 4 h	22 \pm 12 (n=3)
STx2, 1 h	75 \pm 25 (n=2)	STx2, 1 h	>100 (n=2)
STx2, 4 h	>100 (n=2)	STx2, 4 h	65 \pm 35 (n=2)

Remarkably, even in mice Retro-2 was effective against ricin, shown in Figure 5. Furthermore, Retro-2 was also effective in a more clinically relevant scenario in mice, an *E. coli* O104:H4 infection (Secher et al., 2015). On the cellular level, the Retro compounds blocked Shiga toxin trafficking in endosomal structures and delayed its entry into the Golgi, as illustrated in Figure 6 (Stechmann et al., 2010)

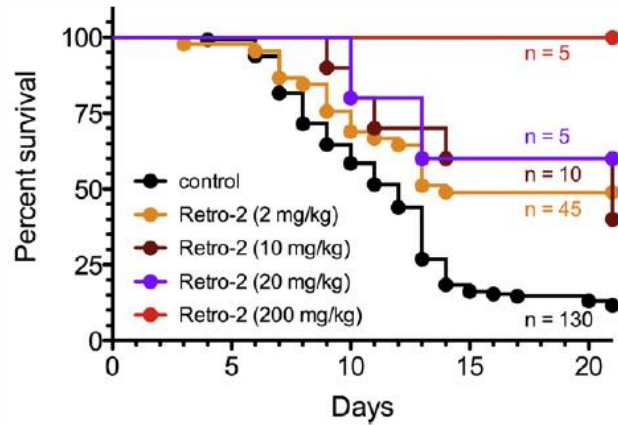


Figure 5: Retro-2 protects mice against ricin challenge. Comparison of survival curves from mice that were treated with single intraperitoneal dose of Retro-2 with indicated concentrations one hour before toxin exposure. Ricin was administered to mice via the nasal route (2 mg/kg). The control group received only the vehicle in prior to ricin exposure. The curves for treated animals are statistically different from control as measured by the log rank test ($p < 0.0001$ for 2 $\mu\text{g}/\text{kg}$ of Retro-2, orange; $p = 0.015$ for 10 mg/kg, brown; $p = 0.031$ for 20 mg/kg, purple; $p = 0.0007$ for 200 mg/kg, red). (Stechmann et al., 2010)

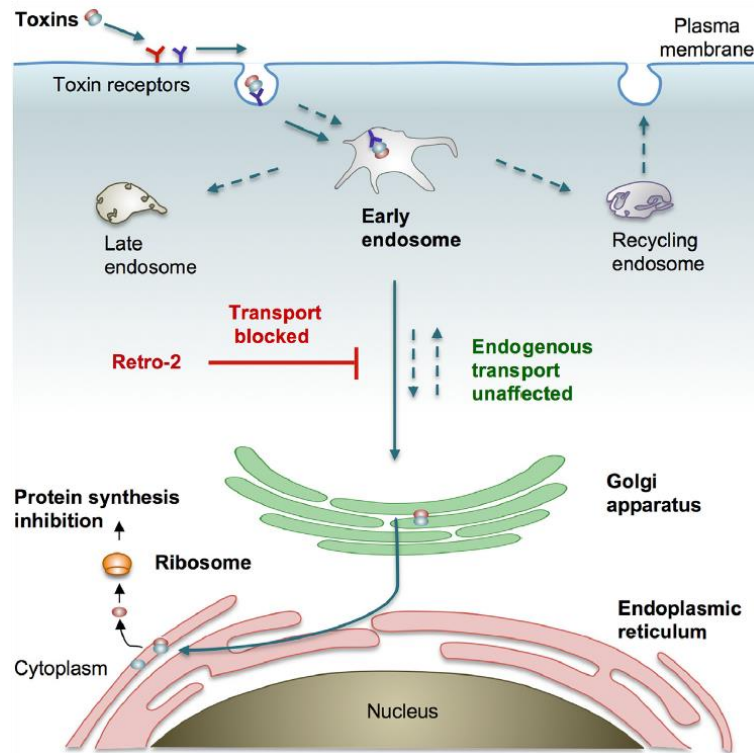


Figure 6: Illustration of the retrograde trafficking of Shiga toxin and site of action of Retro-2 (Gupta et al., 2017). Toxins (e.g. ricin and SLTs) traffic via the retrograde route, starting from the plasma membrane through endosomes and Golgi to the ER (Johannes and Popoff, 2008). Retro-2 inhibits the toxin trafficking step from endosomes to the Golgi

Moreover, very recent studies have shown that Retro-2 protected against *Leishmania*, poxviruses, filoviruses and Chlamydiales (Nonnenmacher et al., 2015; Gupta et al., 2017). Together with ricin and

STEC, poxviruses, filoviruses and Chlamydiales are listed on the NIAID emerging disease list (National Institute of Allergy and Infectious Disease, 2017) and the CDC bioterrorism bio threat agent list (CDC, 2017). While *Leishmania* are not mentioned on those lists, a study from 2009 to 2012 showed that *Leishmania* was reemerging in Madrid, Spain, thus representing an emerging health risk (Arce et al., 2013).

9.1.3.1.1 Structural evolution of Retro-2

The original Retro-2 molecule was found to inhibit toxin trafficking (Stechmann et al., 2010). In 2012, it was shown that the actual active configuration of Retro-2 is a cyclic compound that forms spontaneously (Park et al., 2012). The groups of D. Gillet and J.-C. Cintrat optimized Retro-2 by performing a structure-activity relationship (SAR) study (Noel et al., 2013), which yielded a molecule that was termed Retro-2.1. After thereby improving the protection potency against SLTs by a factor of 500 when compared to the original hit compound (Noel et al., 2013), Retro-2.1 has been chemically functionalized with an azide group, herein referred to as “clickable Retro-2” (Figure 31) with the goal of identifying the cellular target of the molecule. As part of a target pull down strategy, this azide derivate enables biorthogonal click chemistry, which will be introduced in further detail in chapter 10.6.1 on page 49. A summary of the structural evolution of Retro-2 is illustrated in Figure 7.

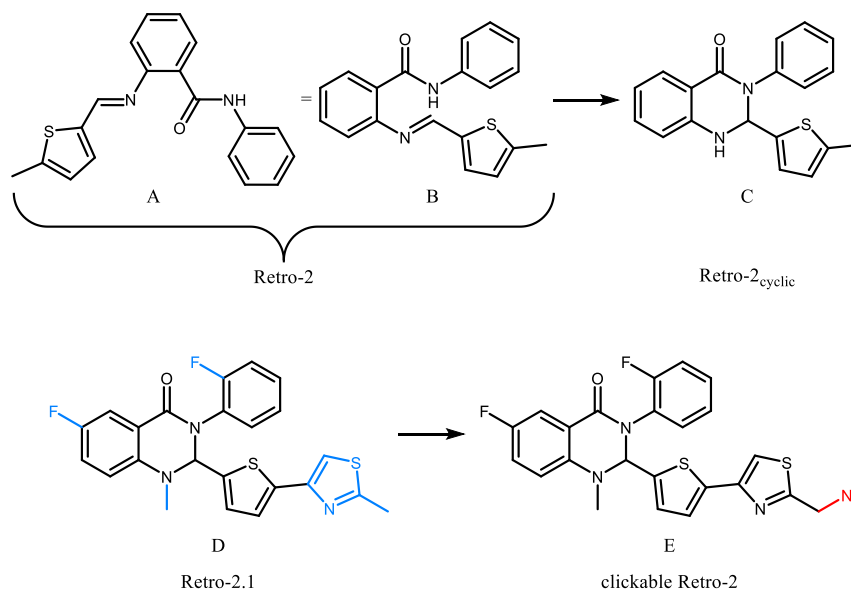


Figure 7: Structural evolution of Retro-2. Structures A and B show the original hit compound Retro-2 (Stechmann et al., 2010). Structure B illustrates how the spontaneous cyclisation to molecule C (Retro-2_{cyclic}) may take place (Park et al., 2012). Structure D shows the optimized molecule of Retro-2 based on C, called Retro2.1 (Noel et al., 2013). Additional structural groups are highlighted in blue. Molecule E is the azide-functionalized Retro-2.1, called “clickable Retro-2”, due to its potential to be used in a biorthogonal click chemistry approach (see chapter 0). The azide is marked in red.

Dihydro-quinazolinone analogs of Retro-2_{cycl} showed a protective effect in monkey and human polyoma- and papillomavirus infection *in vitro* (Carney et al., 2014; Nelson et al., 2013). Hence, the demonstrated protective effects of Retro-2 *in vitro* and *in vivo* turn the optimized derivatives into promising antidotes against many bio threats, including plant and bacterial toxins, viruses, intracellular parasites and bacteria.

9.1.3.1.2 Retro-2 effect on viral infections

Viruses are known to enter their host cells through different routes (Harper et al., 2013). Enveloped viruses dock and fuse directly with the plasma membrane (PM) and translocate their nucleo-capsid directly into the cytosol. Yet, non-enveloped viruses and others have to be taken up first, and then traffic through the host cell before the release into the cytosol. Some viruses even undergo retrograde trafficking (Grove and Marsh, 2011) which led to the idea that Retro-2 might protect against those viruses as well.

Adeno-associated viruses (AAV) have shown promising biomedical potential in gene therapy, and their evaluation for the treatment of various diseases is still ongoing. The retrograde trafficking of AAV is essential to reach the nucleus. Thus, its TGN arrival is a critical step, which has been shown to be syntaxin-5 (STX5) dependent and could be inhibited by Retro-2 (Nonnenmacher et al., 2015). Hence, Retro-2 could be exploited in anti-viral disease treatments.

As members of non-enveloped DNA viruses, polyomaviruses (PyV) (including human papillomaviruses (HPVs)) cause severe diseases in immunocompromised patients. BKPyV is the causative agent of polyomavirus-induced nephropathy and hemorrhagic cystitis, and JCPyV is the causative agent of the fatal demyelinating disease progressive multifocal leukoencephalopathy. Thus far, no vaccine or antiviral therapy for these viruses has been found (De Gascun and Carr, 2013). HPVs have been put in context with cancer development in the uterine cervix and oropharynx. Although vaccination showed success against some types of HPVs, many HPVs infections remain present and still are of public health concern (Carney et al., 2014). It has been shown that Retro-2 (c = 100µM) inhibited JCPyV, BKPyV and simian virus 40 (also a PyV) infections on tissue cells in average by around 30 %. Retro-2 blocked the PyVs' arrival to the ER, which is strictly required for infection (Nelson et al., 2013). These results were confirmed in cell culture for PyVs. Additionally, Retro-2 protected cells also against HPVs (Carney et al., 2014).

As filamentous enveloped viruses, Ebola and Marburg filoviruses (FV) are members of the family Filoviridae, which cause viral hemorrhagic fevers in humans resulting in a high mortality rate of up to

90 % (Bausch et al., 2006; Feldmann and Geisbert, 2011). Thus far, only few drugs (favipiravir) have been tried in animals or humans, without promising results. Furthermore, no vaccination strategy is yet available (Sissoko et al., 2016), resulting in a biosafety level-4 classification for FVs. Recently, the growth of a new Ebola virus variant in West Africa has alerted health authorities. Favipiravir is the only small molecule drug that was tested in mice, showing an IC₅₀ of 67 μ M (Oestereich et al., 2014). Unpublished data of our collaborators at the CEA have shown that Retro-2 protected *in vitro* against an Ebola virus and Marburg virus infection (article in revision).

Two independent high throughput siRNA screens of Vaccinia virus (VACV) identified proteins of the endosomes-to-Golgi retrograde transport step to be pro-viral host factors (Sivan et al., 2013; Beard et al., 2014). Recently, further studies demonstrated that Retro-2 reduced spreading of VACV and Monkey pox viruses in cell cultures by interfering with their replication (Sivan et al., 2016; Harrison et al., 2016). The Retro-2 effect relied on a membrane wrapping process during late stages of virion maturation (Smith et al., 2002). Two viral proteins, involved in the maturation process, rely on retrograde trafficking from endosomes to the TGN. Retro-2 miss-localizes these proteins, and thus, blocks the maturation process.

In summary, Retro-2 shows significant potential in antiviral treatment, relying on its capacity to block retrograde trafficking.

9.1.3.1.3 Retro-2 effect on intracellular parasites

Leishmania is an intracellular parasite and causes leishmaniosis, affecting about twelve million people with two million new cases per year worldwide. Although *Leishmania* is not classified as a bioterrorism agent, the *Leishmania* outbreak from 2009 to 2012 in Madrid, Spain, affected 446 individuals (Arce et al., 2013). Current treatments against *Leishmania* are either toxic or lead to the emergence of drug resistant strains, resulting in a strong need for new treatments against *Leishmania* (No, 2016; Sundar et al., 2014; Mansueto et al., 2014). *Leishmania* are internalized by macrophages into intracellular compartments called *Leishmania* parasitophorous vacuoles (LPVs), similar to phagosomes. Previous studies suggested that STX5 is involved in the creation of those LPVs. Consistently with the effect of Retro-2 on STX5 localization (see chapter 11.1.4.2, page 63), Retro-2 inhibited the development of LPVs in *Leishmania amazonensis* infected cells. Moreover, Retro-2 protected mice from *L. amazonensis* infections, without showing any toxicity by itself (Canton and Kima, 2012). Retro-2 also protected against *L. donovani* *in vitro* and *in vivo*. Thus, Retro-2 affects parasites inside and outside their host.

9.1.3.1.4 Retro-2 effect on intracellular bacteria

Simkania negevensis is an obligate intracellular Gram-negative bacterium that belongs to the family of Chlamydiales. Although its natural host remains unknown, *S. negevensis* is common among humans, where it has been related to infections of the upper respiratory tract. *S. negevensis* grows in membrane-bound vesicular ER contact sites (ERES). In 2016, it has been shown that Retro-2 inhibited bacterial replication in either a primary and consecutive infection (Herweg et al., 2016). Remarkably, Retro-2 treated *S. negevensis* offsprings were significantly less infectious. The morphology of *S. negevensis*-containing vacuoles seemed to be affected, resulting in replication deficiencies of the bacteria (Herweg et al., 2016)

9.1.3.1.5 Bio threats that are not affected by Retro-2

Diphtheria toxin (DT), Clostridium botulinum neurotoxin A (BoNT/A), dengue virus serotype 4 (DENV-4), chikungunya virus (CHIKV) and Venezuelan equine encephalitis virus (VEEV) were not affected upon Retro-2 treatment. Briefly, the missing effect of Retro-2 on DT and BoNT/A could readily be explained, as these toxins do not depend on the retrograde trafficking route. After the internalization of DT into endosomes, the catalytic domain is translocated to the cytosol, exploiting a strong pH decrease that occurs in toxin containing endosomal compartments (Gillet et al., 2015). For BoNT/A, the toxin traffics directly in synaptic vesicles or clathrin-coated vesicles in the nerve terminus, where similar to DT, acidification causes the translocation of the catalytic subunit into the cytosol (Gillet et al., 2015).

In the case of DENV-4, CHIKV and VEEV the available data suggests that the envelop maturation does not rely on the retrograde route. It has been suggested that DENV-4 is translocated from lysosomes, after trafficking through Rab5-positive early endosomes and Rab7-positive late endosomes (Van Der Schaar et al., 2008; Acosta et al., 2012). Alphaviruses, CHIKV and VEEV are most probably taken up through receptor-mediated endocytosis (RME), followed by acidification of endosomes (Li et al., 2010; White and Helenius, 1980). Another hypothesis is direct entry through the plasma membrane (Vancini et al., 2013).

9.1.3.2 Other small molecules

In addition to Retro-2, other small molecule inhibitors have been found that protect cells against plant and bacterial toxins. For some, the cellular targets have been identified (Figure 8), whereas for the others, including Retro-2, this is not yet the case (Figure 9).

9.1.3.2.1 Inhibitors with identified target

1) Inhibitors with known target

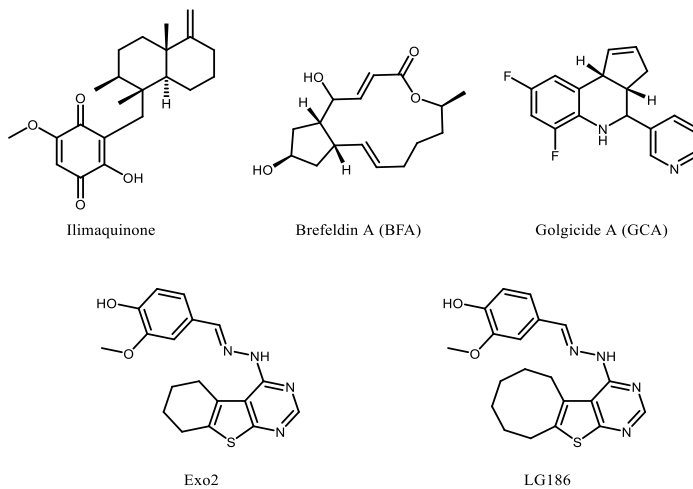


Figure 8: Chemical structures of inhibitors of SLTs for which the cellular target is already known.

9.1.3.2.1.1 Ilimaquinone (IQ)

IQ (Figure 8) is a sesquiterpenoid quinone metabolite isolated from marine sponges, which on Vero cells reversibly protects against ricin, DT and other toxins (Nambiar, 1995). IQ disrupts the Golgi into small vesicles (Takizawa et al., 1993; Lu et al., 2007), due to its interaction with enzymes that are involved in the methyl cycle. It has been suggested that S-adenosyl-methionine synthetase, S-adenosyl-homocysteinase, and methyl transferases communicate with small GTPases (Radeke et al., 1999).

9.1.3.2.1.2 Brefeldin A (BFA)

BFA (Figure 8) is an isoprenoid fungal metabolite that protects cells against ricin and SLTs (Yoshida et al., 1991; Thompson et al., 1995; Donta et al., 1995). Similar to IQ, BFA disrupts the Golgi structure and function, thereby perturbing intracellular protein trafficking and secretion (Klausner et al., 1992). By targeting specifically guanine nucleotide exchange factors (GEFs), BFA inactivates the ADP-ribosylation factor (Arf) family (Donaldson et al., 1992). GEFs regulate Arf GTPases by catalyzing the exchange of GDP (inactive) to GTP (active), abling the interaction with effectors (Peyroche et al., 1999; Mossessova et al., 2003b).

Arf1 has been described to be involved in the regulation of anterograde and retrograde trafficking in eukaryotic cells (Donaldson et al., 2005; Donaldson and Honda, 2005), by recruiting the coatamer complex at the level of the cis-Golgi, which assembles COPI vesicles. On the level of the trans-Golgi and endosomes, Arf1 recruits the clathrin adapter proteins.

The GEFs GBF1 (mainly *cis*-Golgi), Brefeldin A-inhibited GEP 1 (BIG1), and Brefeldin A-inhibited GEP 2 (BIG2), both localized at the *trans*-Golgi, are sensitive to BFA. They share a Sec7 domain, which is needed for guanine nucleotide exchange. By acting as an uncompetitive inhibitor, BFA binds and thus, disables the Arf1-GDP-Sec7 domain GEF complex (Peyroche et al., 1999). GBF1 regulates COPI vesicle formation, which traffic from the Golgi towards the ER (Bonifacino and Glick, 2004). BIG1 and BIG2 are involved in the recruitment of clathrin adaptors (AP-1 and AP-3) and non clathrin dependent adaptor (AP-4) to the Golgi. These adaptors are involved in the trafficking between endosomes and the Golgi (Robinson, 2004; Mattera et al., 2015).

Since its discovery 40 years ago, BFA is arguably one of the best understood small molecule, and its study has led to the general concept of interfacial inhibition. Yet, its high toxicity excludes BFA from being used as a pharmaceutical compound.

9.1.3.2.1.3 *Exo2 and LG186*

Initially, Exo2 (Figure 8) was found in a chemical genetics study as an inhibitor of the anterograde/secretory pathway (Feng et al., 2003; Yarrow et al., 2003). Afterwards, it has been shown that Exo2 inhibits anterograde trafficking from the ER to the Golgi. Hence, it leads to the disruption of the Golgi. Further, Exo2 was used to explore Golgi function and retrograde toxin trafficking (Feng et al., 2004; Spooner et al., 2008). Exo2 had no inhibitory effect on cholera toxin (CT) (Feng et al., 2004). In contrast, Exo2 significantly inhibited SLT trafficking to the ER, by disrupting the TGN, in a similar way as BFA. However, Exo2 did not fuse and tabulate TGN and endosomes (Spooner et al., 2008). Besides, Exo2 dissociated COPI compounds from membranes, without affecting AP-1. It was proposed that this is due to a selective inhibition of GBF1, without affecting BIG1 and BIG2. Still, other phenotypical changes cannot be explained by the inhibition of ArfGEFs (Boal et al., 2010).

LG186, a derivate of Exo2, was found to enhance the selectivity of Exo2 towards GBF (Boal et al., 2010). The cyclohexenyl ring was changed into a cyclooctenyl ring (Figure 8). Due to this molecular change, LG186 became capable of perturbing the Golgi even in MDCK cells by removing COPI from vesicle membranes. The cyclooctenyl ring of LG186 could interact with the M832L residue of GBF1 (Boal et al., 2010). Nonetheless, LG186 seems to inhibit further ArfGEFs. Other Exo2 derivates were designed to lower cytotoxicity, without losing their protective capacities against SLTs (Guetzoyan et al., 2010a; b). Compared to BFA, Exo2 and its derivatives proved to be more selective tools to decode membrane trafficking.

9.1.3.2.1.4 *Golgicide A (GCA)*

GCA (Figure 8) was found in a cell based HTS designed for bacterial toxin inhibition (Saenz et al., 2007). GCA strongly protected Vero cells from SLTs, and was found to be a potent reversible inhibitor GBF1 without affecting BIG1 or BIG2. As other trafficking inhibitors, GCA disperses the Golgi by interfering at the Arf1 and Sec7 domain of GBF1 (Sáenz et al., 2009). As previously mentioned, the inhibition of GBF1 results in the dissociation of COPI vesicles on the level of Golgi to ER trafficking, leading to the disassembly of the Golgi.

9.1.3.2.2 Compounds with unknown target

II) Inhibitors with unknown target

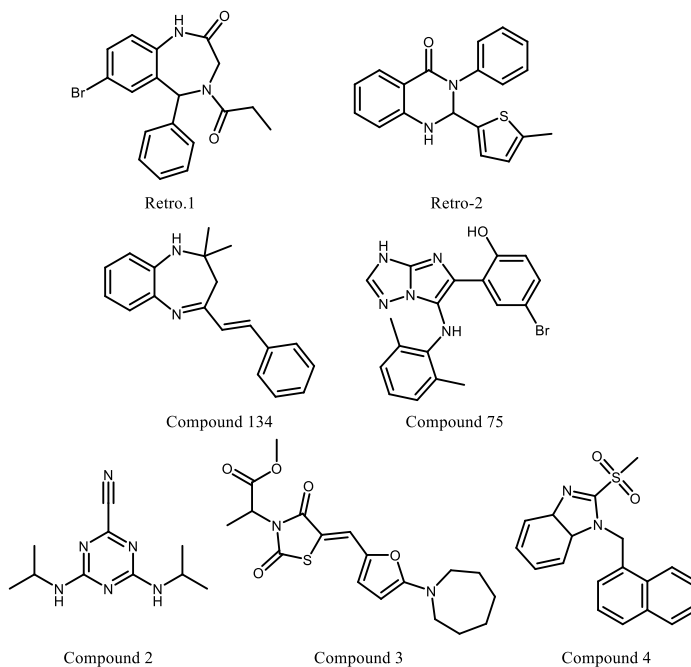


Figure 9: Chemical structures of inhibitors of SLTs for which the cellular target is still unknown, including the Retro compounds.

Figure 9 shows the chemical structures of other small molecules that protect against several bacterial and plant toxins. Retro-1 and Retro-2 were found in HTS on ricin intoxication, and have already been described above (chapter 9.1.3.1) (Stechmann et al., 2010). For Retro-1, no cellular target has been found, and for Retro-2, this matter will be addressed in chapter 11.1.4.1. Remarkably, the Retro compounds protected cells without dispersing the Golgi apparatus (Stechmann et al., 2010).

Similar to the Retro compounds, compounds 75 and 134 protect Vero cells against ricin and SLTs (Saenz et al., 2007), by disrupting their intracellular trafficking along the retrograde route. Compound 75 also inhibits DT, whereas compound 134 remained inactive against DT. Thus, compound 75 most probably acts early at the level of EE, whereas compound 134 might act at a later stage of the retrograde route. Indeed STxB was blocked in EE upon treatment of cells with compound 75 (Saenz et al., 2007), whereas it was found in perinuclear recycling endosomes (RE) upon compound 134 treatment. Moreover, only compound 75 partially blocked secretion from the TGN, confirming that they most likely have different mechanisms of action. Both compounds did not affect toxin binding to cells, toxin endocytosis, or the anterograde pathway. However, both compounds change the morphology of the Golgi in a reversible manner. Sulfation assays (Mallard and Johannes, 2003) showed that the trafficking of toxins to the TGN

was reduced (Saenz et al., 2007). Yet, the cellular targets of these two compounds remain to be identified. Their pharmaceutical value remains questionably due to their interference with the Golgi morphology.

The compounds 2, 3, and 4 (Figure 9) were found in HTS based on ricin intoxication (Wahome et al., 2010). Little is known about these compounds.

All the small molecules that were discussed in this chapter need further characterization. Regardless of whether they are of pharmaceutical value, they remain of high interest for research, helping to understand bio threats better and uncover cellular trafficking processes.

9.2 INTRACELLULAR TRAFFICKING

Intracellular trafficking deals with the movement of vesicular or tubular carriers between membrane-bounded compartments. In this chapter, I will discuss the biosynthetic/secretory or anterograde pathway (chapter 9.2.1), with an emphasis on COPII vesicle formation (chapter 9.2.1.1.1). I will then discuss trafficking processes that lead to the entry of extracellular materials into cells. These endocytic processes (chapter 9.2.2) will be further dissected into clathrin-mediated endocytosis (CME, chapter 9.2.2.1) and clathrin-independent endocytosis (CIE, chapter 9.2.2.2). At the level of endosomes, the recycling (chapter 9.2.3), lysosomal (chapter 9.2.4), and retrograde (chapter 9.2.5) pathways will be addressed. Due to its importance for my PhD work, retrograde trafficking between endosomes and the TGN will be dissected in further detail. The role of clathrin (9.2.5.2), retromer (chapter 9.2.5.3), and SNAREs (chapter 9.2.6) will be discussed, followed by introducing a Golgi protein that cycles via the retrograde route, termed GPP130 (chapter 9.2.5.1).

The basic steps in intracellular membrane transport are (Bonifacino and Glick, 2004):

- carrier formation from a donor compartment
- translocation of transport intermediates to a target compartment
- tethering of transport intermediates with the target compartment
- and, finally, carrier fusion with the target compartment

9.2.1 Anterograde trafficking via the biosynthetic/secretory pathway

Cell growth and survival depends on interaction with their environment, mediated by PM receptors and their ligands. Both, receptors and ligands are synthesized in the ER, and are then transported to the PM. Every third protein of the mammalian proteome is involved in the biosynthetic/secretory

pathway (Sharpe et al., 2010). The vesicular transport hypothesis stated in the 1970s that transport between organelles of the biosynthetic/secretory pathway occurred through vesicular intermediates that bud from a donor compartment and then fuse with an acceptor compartment (Palade, 1975). In the 1980, screening in yeast for genes that were required for protein secretion allowed to identify 23 “Sec” genes (Novick et al., 1980; Spang, 2015). The exit out of the ER and trafficking towards the Golgi are the first steps of the anterograde pathway, which is initiated by the formation of COPII vesicles (chapter 9.2.1.1.1) (Bonifacino and Glick, 2004). In the Golgi, proteins and lipids are modified (e.g. sulfation, glycosylation...).

Three main hypothesis have been proposed to explain how molecules pass through the Golgi (Figure 10):

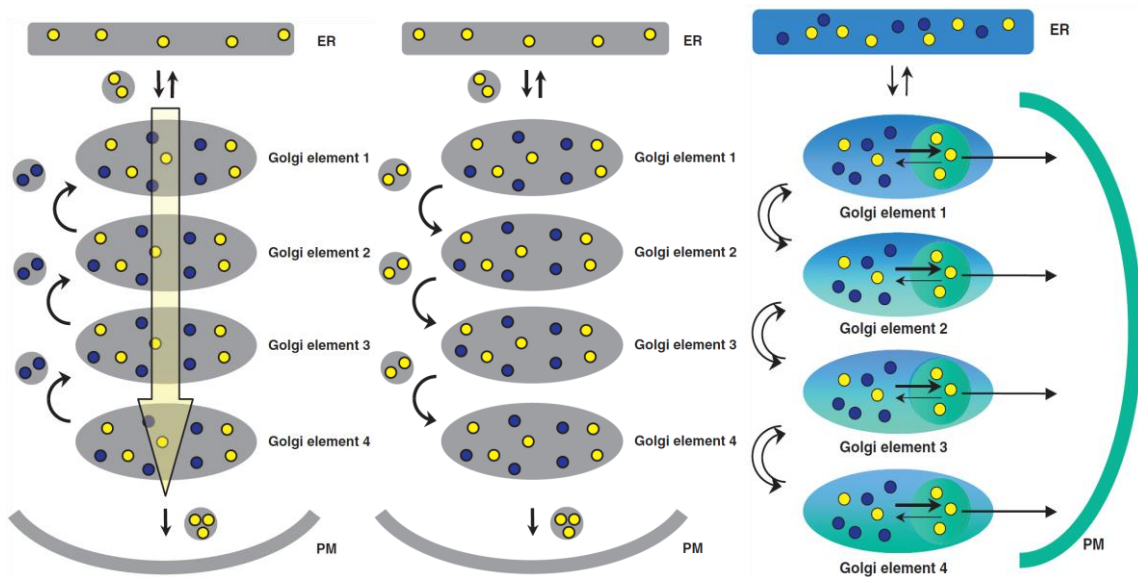


Figure 10: Models for intra-Golgi vesicular transport. Cargo synthesized in the ER and transported through the secretory pathway is shown in yellow; Golgi processing enzymes are shown in blue. Arrows indicate the direction of trafficking: From left to right: The model of cisternae maturation – the vesicular transport model – the rapid-partitioning model (Jackson, 2009) – Blue dots are Golgi localized enzymes; yellow dots are cargo; blue areas are glycerophospholipid-enriched membranes; green areas are sphingolipid-enriched membranes; green circles within each Golgi stack are sphingolipid-enriched export domains

The model of cisternae maturation views the Golgi as a rather dynamic structure, in which the cisternae as such move and mature forward passively (Bonfanti et al., 1998). The vesicular transport model claims that Golgi cisternae are stationary and therefore vesicles move from one cisternae to another (Orci et al., 1997). The latest proposed model, termed the ‘rapid partitioning model’, proposes that cargos

traffic from the ER to the cis-Golgi, where they can move in-between the Golgi-stacks and depart the Golgi from any Golgi stack based on a specific lipid-protein-combination (Patterson et al., 2008).

After leaving the Golgi, secretory vesicles will fuse with the PM, leading to secretion of soluble vesicular components, or to the delivery to the PM of lipids or transmembrane proteins (e.g. receptors, transporters, or enzymes). Post-Golgi trafficking also connects to the endocytic pathway to deliver lipids, enzymes, and other cargoes to late endosomes and lysosomes.

9.2.1.1 ER Exit Sites (ERES)

Newly synthesized proteins that are supposed to leave the ER depart from dedicated sites that are termed ER exit sites (ERESs, or transitional ER sites (tER)). Characteristically, these are ribosome-free regions in the ER (also referred as the ER cup; (Bannykh et al., 1996) with COPII-coated components on buds and vesicles that contain anterograde cargoes (Lee et al., 2004) (Figure 11). COPII vesicles then fuse with the ER–Golgi intermediate compartment (ERGIC), from where proteins are processed and further directed to the Golgi.

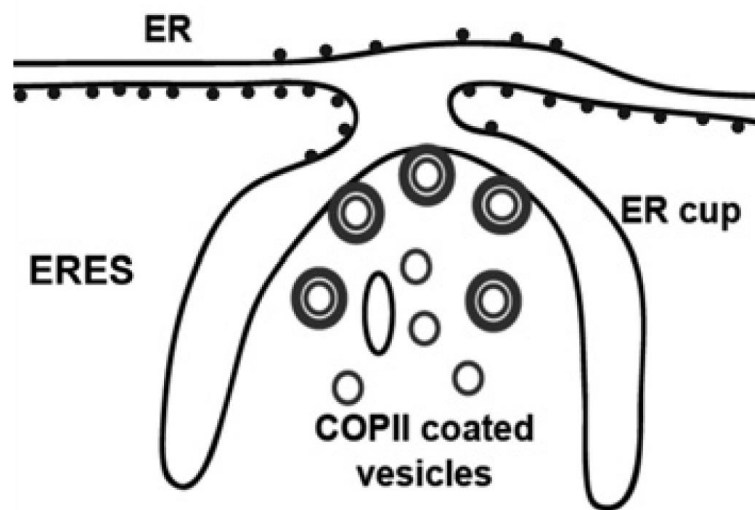


Figure 11: A schematic representation of an ER exit site (ERES) showing the ER cup lacking ribosomes, forming COPII-coated vesicles.

The assembly of the COPII coat requires 6 key factors:

- The transmembrane protein Sec12
- The small GTPase Sar1
- Sec23 and Sec24, which form the inner coat heterodimer
- Sec13 and Sec31, which form the outer coat heterodimer

Sec23 has GAP activity towards Sar1, whereas Sec24 has several binding sites to carry cargoes out of the ER. Their discovery was rewarded with the Nobel Prize in Physiology and Medicine in 2013 to Randy Schekman (Miller and Barlowe, 2010). After their assembly, COPII vesicles bud from the ER and uncoat, by the conversion of Sar1-GTP to its inactive GDP-bound form, mediated by Sec23 (Yoshihisa et al., 1993).

9.2.1.1.1 Sec16A and the COPII coat

In vitro experiments have shown that purified Sec23/24, Sec13/31 and a GTP-locked form of Sar1 are sufficient to coat liposomes and drive the formation of buds and small vesicles (Matsuoka et al., 1998). Nonetheless, at the level of the ERES many more proteins are involved, suggesting that other factors help during this process (Supek et al., 2002; Matsuoka et al., 1998).

Sec16 has been associated with a clear role in COPII coat dynamics. It was found in a screening in *Saccharomyces cerevisiae* where it appeared to be essential for the function of the early secretory pathway (Supek et al., 2002; Matsuoka et al., 1998). Despite the fact that there is a major subgroup of unicellular organisms lacking Sec16A, called Excavata (Neumann et al., 2010), Sec16A is relatively conserved in many species, including *S. cerevisiae*, (Kaiser and Schekman, 1990), *Pichia pastoris* (Connerly et al., 2005), *Caenorhabditis elegans* (Witte et al., 2011), *Trypanosoma brucei* (Sealey-Cardona et al., 2014) and *Drosophila* (Ivan et al., 2008). Sec16A is a rather big hydrophilic protein of approximately 240 kDa, having various isoforms. With Sec16A (large, ~230 kDa) and Sec16B (short, ~115 kDa), mammals have two genes encoding homologous Sec16 proteins. The B homologue was first identified as regucalcin, a gene promoter region-related protein (Bhattacharyya and Glick, 2007; Hughes et al., 2009; Budnik et al., 2011). Sec16 is strongly associated to ER membranes, and Triton X-100 with high salt concentrations or high pH is needed to extract it.

Sec16 interacts with the COPII coat components. The best characterized interactions have been described in *S. cerevisiae* (Shaywitz et al.; Espenshade et al., 1995; Gimeno et al., 1996), many of which then have also been established biochemically.

9.2.1.1.2 COPII coat dynamics: Two models for Sec16A function

Sec16 being an essential factor for proper COPII vesicle formation, a loss of Sec16 function has been shown to result in perturbed ERES organization and protein export (Espenshade et al., 1995; Yorimitsu and Sato, 2012). A temperature sensitive mutation in Sec16 leads to the disappearance of ERES, and the loss of the Sec23-Sec13 interaction (Shindiapina and Barlowe, 2010). In *Drosophila*, Sec16A depletion strongly reduces cell proliferation (Ivan et al., 2008), and in *T. brucei* the size of ERES is dysregulated (Sealey-Cardona et al., 2014). Mammalian Sec16A and B have overlapping (Bhattacharyya and Glick, 2007; Watson et al., 2006) and non-redundant functions (Budnik et al., 2011). For instance, the non-conserved C-terminus of Sec16B is involved in peroxisome biogenesis (Shindiapina and Barlowe, 2010). Generally, Sec16 is involved in both the initiation of COPII budding and in the

uncoating/release of COPII vesicles. Although they seem to be contradictory, these two roles are not mutually exclusive. They lead arguably to two different theories.

9.2.1.1.2.1 Model one: Sec16 as a scaffolding protein

The first model suggests that Sec16 works as a scaffolding protein for COPII assembly (Connerly et al., 2005). A scaffolding protein assembles other proteins (Figure 12) (Whittle and Schwartz, 2010). Hence, according to this model, Sec16 initiates COPII recruitment, coat formation, and ERES biogenesis. For this, Sec16 has to localize properly in an independent manner. This hypothesis was tested in *drosophila* S2 cells, in which the localization of Sec16 was analyzed in the absence of the COPII components Sec23, Sec24 and Sar1. It was found that the protein indeed remained properly localized in budded structures (Ivan et al., 2008). Similar effects were observed in human cells (Hughes et al., 2009; Watson et al., 2006). Overexpression and depleting Sar1 did not cause any miss-localization of Sec16 either.

On the other hand, depletion of Sec16 affected Sar1 localization, suggesting that Sec16 scaffolds Sar1 recruitment (Ivan et al., 2008). An overexpression of Sec16 generates ERES even without Sar1 (Watson et al., 2006). In vitro, it has been shown that liposome-bound Sec16 recruits COPII vesicles to membranes in a Sar1 and nucleotide-independent manner (Supek et al., 2002). These data strongly suggest that Sec16 operates upstream of Sar1 and the other COPII components.

In vitro experiments weaken this model, since Sec16 needs Sar1 to operate on neutral liposomes (Supek et al., 2002) and microsomal membranes (Yonekawa et al., 2011). Moreover, a miss-localization of Sec16 in *P. pastoris* did not lead to the relocalization of other COPII components (Bharucha et al., 2013). Thus, whether the principal role of Sec16 is in scaffolding remains to be proven, at least in yeast.

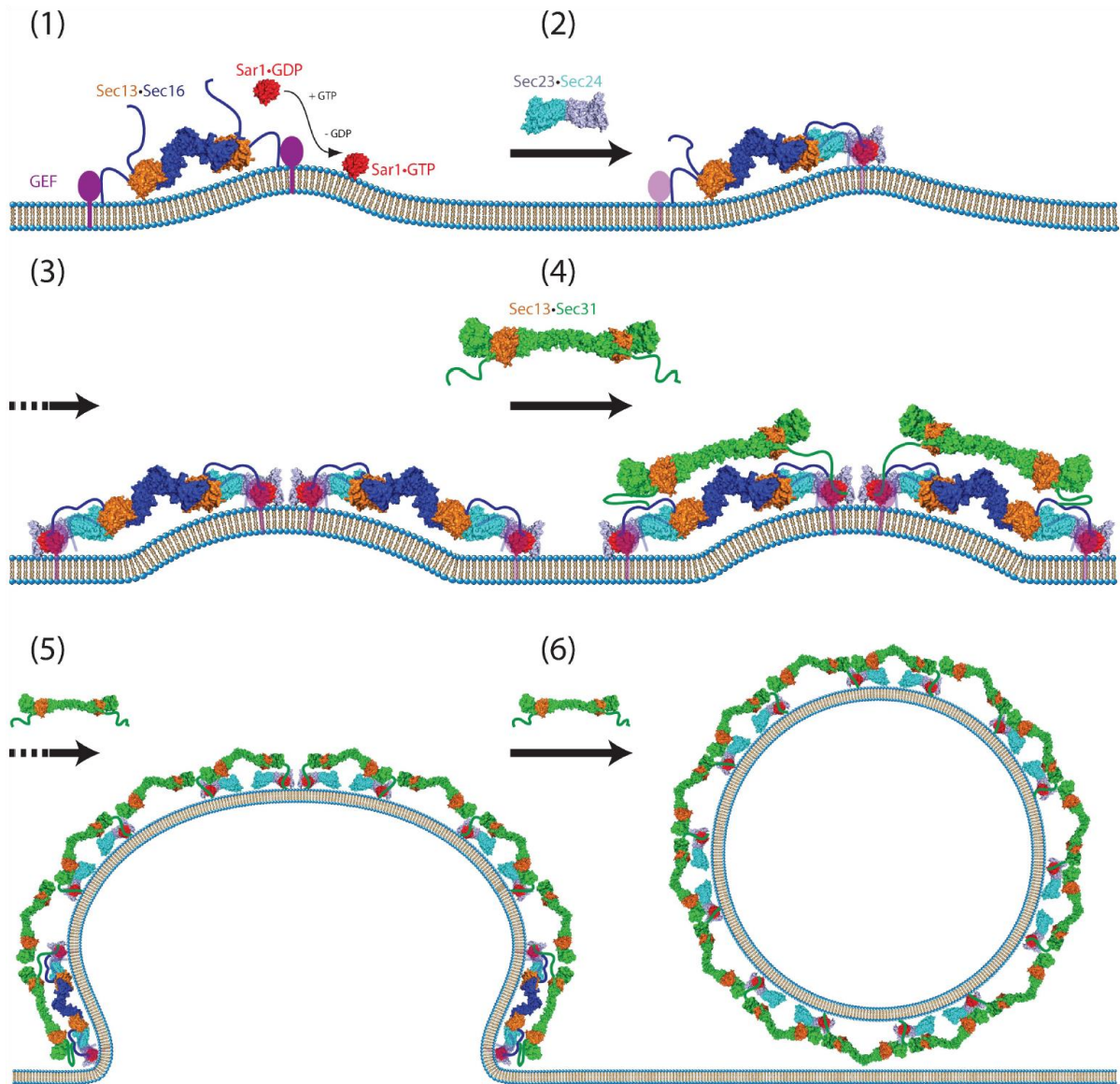
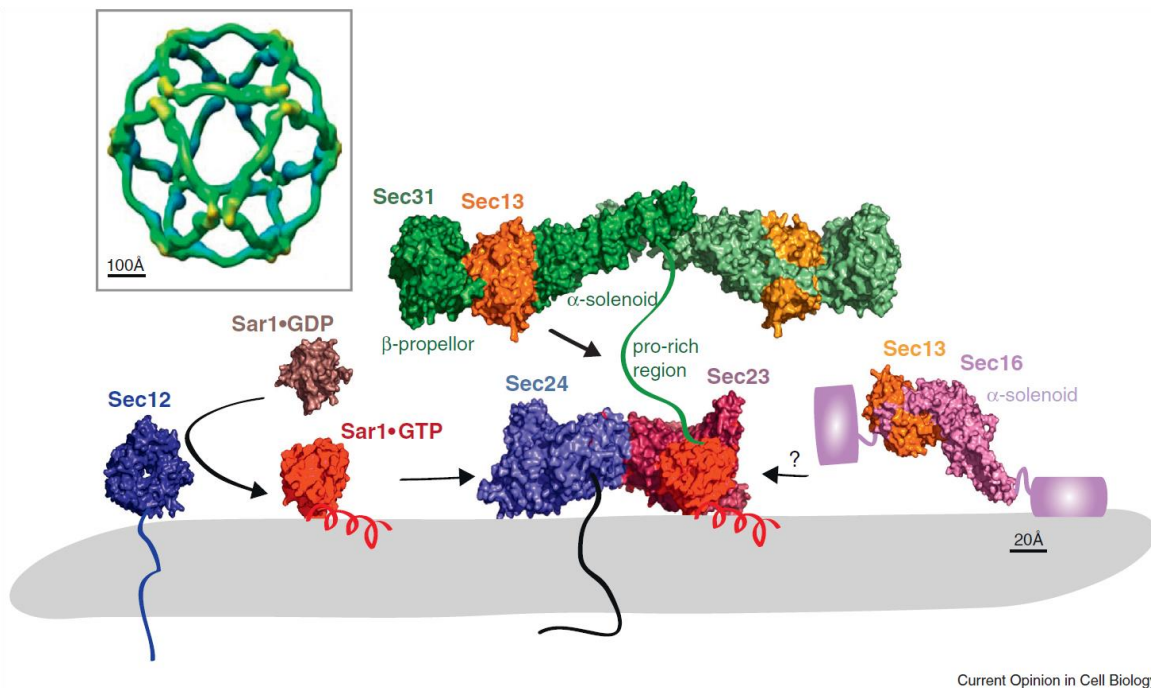


Figure 12: Model for assembly of the COPII coat complex, describing Sec16 as a scaffolding protein. The common model for assembly of the COPII coat complex is modified to include the role of Sec16. For simplicity, cargo molecules are omitted. (1) The Sec13-Sec16 tetramer is stably associated with the ER membrane and binds the integral membrane protein Sed4 or its homologue Sec12. Sar1 becomes associated with the membrane, when it is converted from the GDP- to GTP-bound state. Concentration of membrane-associated proteins begins to bend membrane. (2) Sec13-Sec16 and Sar1 collaborate to recruit the cargo adaptor Sec23-Sec24 dimer. (3) A precoat self-associates into higher-order oligomers. (4) Sec13-Sec16 and Sec23-Sec24-Sar1 form independent interactions with Sec13-Sec31, causing it to assemble near and/or in place of Sec16. (5) The forming coat contains progressively more Sec13-Sec31 and less Sec13-Sec16. Hand-off of Sec23-Sec24-Sar1 from Sec16 to Sec31 sets the stage for GTP hydrolysis by Sar1. (6) A final COPII coat is formed, and vesicle budding is complete. Sec13-Sec16 remains mostly associated with the ER. - (Whittle and Schwartz, 2010)

9.2.1.1.2.2 Model two: Sec16A as a regulator of COPII vesicle release

As opposed to the first model, the second one suggests that Sec16 acts downstream of Sar1 and the assembly of the COPII coat. Here, Sec16 would have a regulatory function in the release of COPII vesicles (Figure 13). Sec16 affects the GTP cycle of Sar1 (Supek et al., 2002). Earlier, it has been demonstrated that Sec23/24 have GAP activity on Sar1 that occurs after Sec13/31 binding (Yoshihisa et al., 1993; Antonny et al., 2001). The regulatory effect of Sec16 is not due to a stabilization of Sar1 (Espenshade et al., 1995). Rather, Sec16 inhibits the stimulatory effect of Sec23 on COPII release (Yorimitsu and Sato, 2012). In the case of *S. cerevisiae*, this Sec16 function seems to be stimulated by Sec24. A perturbation would lead to smaller vesicles, meaning that Sec24 engages Sec16 to inhibit the Sar1 GTPase activity (Bharucha et al., 2013; Kung et al., 2012). Comparing Sec16 in yeast and metazoans, it seems possible that Sar1 regulation is well conserved, and that a further scaffolding function was added during evolution. Further data will be needed to validate this possibility.



Current Opinion in Cell Biology

Figure 13: Structure and assembly of the COPII coat. The guanine nucleotide exchange factor, Sec12 (McMahon et al., 2012) catalyzes GTP loading on Sar1, which switches from a cytosolic GDP-bound form (Huang et al., 2001) to a membrane-associated GTP-bound form (Bi et al., 2002) through exposure of an N-terminal amphipathic α -helix. Membrane-associated Sar1 recruits Sec23/Sec24 (Bi et al., 2002). Sec24 provides cargo-binding function by directly interacting with sorting signals on transmembrane clients. The Sar1/Sec23/Sec24 'pre-budding' complex in turn recruits Sec13/Sec31 (Fath et al., 2007). Sec13/Sec31 self-assembles into a polyhedral cage (Stagg et al., 2006) that at least in part drives membrane curvature and contributes to vesicle scission. Sec23 is the GTPase-activating protein for Sar1, with Sec31 further contributing to hydrolysis via a proline-rich domain that extends across the surface of Sec23/Sar1. Sec16 is a peripheral component that binds to Sec13 (Whittle and Schwartz, 2010), modulates GTPase activity by preventing Sec31 action and otherwise contributes to vesicle formation in poorly understood ways. - (Miller and Schekman, 2013)

9.2.2 Endocytosis

Endocytosis is required for nutrients uptake, signals transduction, and the processing of extracellular molecules. This includes a range of activities from receptor uptake, antigen processing by immune cells, to lipid homeostasis. Several different endocytic processes have been described (Figure 14). These vary in cargoes, protein machinery, and size and morphology of endocytic carriers. Classically, one differentiates between clathrin-mediated and clathrin-independent endocytosis (CME vs CIE). Both are often used by pathogens to enter their host cells. In the next chapters, I describe the differences and similarities between CIE and CME.

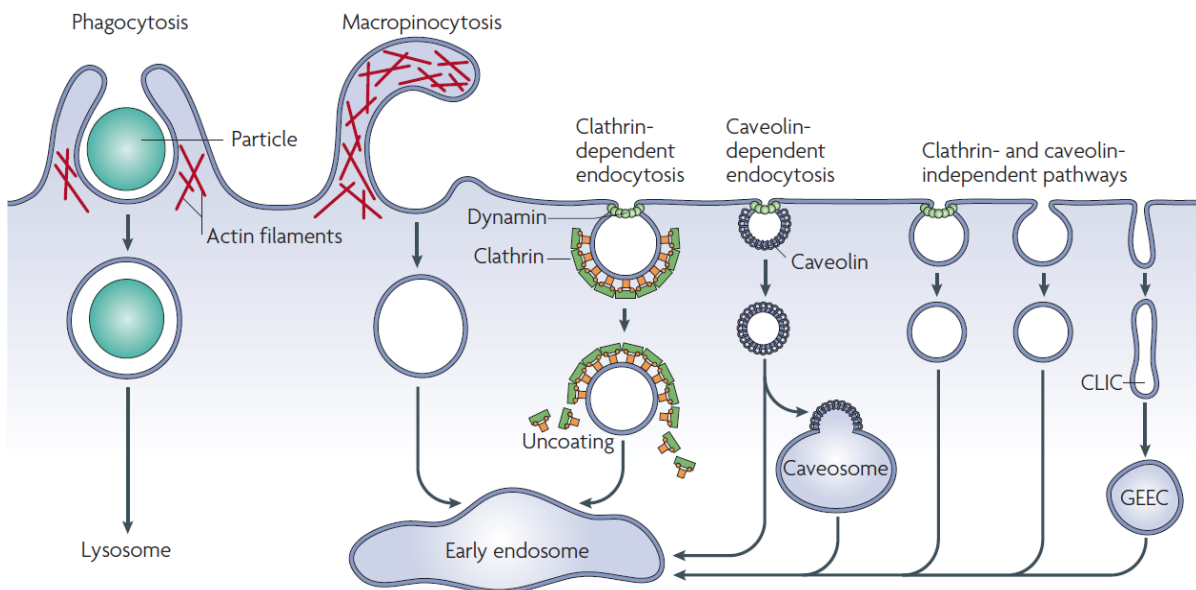


Figure 14: Pathways of entry into cells. Large particles can be taken up by phagocytosis, whereas fluid uptake occurs by macro-pinocytosis. Both processes appear to be triggered by and are dependent on actin-mediated re-modelling of the plasma membrane at a large scale. Compared with the other endocytic pathways, the size of the vesicles formed by phagocytosis and macro-pinocytosis is much larger. Numerous cargoes can be endocytosed by mechanisms that are independent of the coat protein clathrin and the fission GTPase, dynamin. Some of these clathrin-independent pathways are also dynamin independent. Most internalized cargoes are delivered to the early endosome via vesicular (clathrin- or caveolin-coated vesicles) or tubular intermediates (known as clathrin-independent carriers (CLICs)) that are derived from the plasma membrane. Some pathways may first traffic to intermediate compartments, such as the caveosome or glycosylphosphatidylinositol-anchored protein enriched early endosomal compartments (GEEC), en route to the early endosome. - (Mayor and Pagano, 2007)

9.2.2.1 Clathrin-mediated endocytosis (CME)

Clathrin-mediated endocytosis (CME) is arguably the most studied and best understood entry pathway. Many proteins and ligands are endocytosed via clathrin-coated vesicles (CCV). Most prominent members are the transferrin receptor (TfR) and low-density lipoprotein receptor (LDLR). Clathrin-coated pits (CCP) were initially described as bristle-like structures in yolk protein uptake by mosquito oocytes (Roth and Porter, 1964). Later, a large protein of around 180 kDa, named clathrin heavy chain (CHC), was found to be the major component of these vesicles (Pearse, 1976). Clathrin forms 'spider-like triskelion' cages (Figure 15) (Kirchhausen, 2000). Three CHC together with clathrin light chains (CLC) form a three dimensional lattice without needing other components (Kirchhausen and Harrison, 1981).

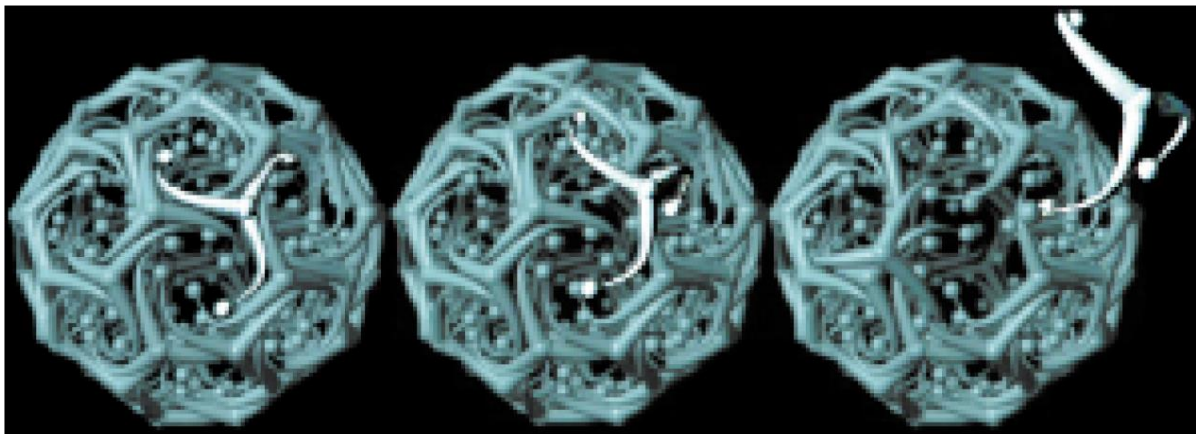


Figure 15: Model for the assembly and disassembly of a clathrin coat. The drawing indicates the direction of the rotational movement (counterclockwise) that is required to lock a relatively rigid clathrin triskelion into the lattice. The reverse process would be required to disassemble the coat. - (Kirchhausen, 2000)

CCV include nonstructural adaptor proteins (AP), which are involved in cargo recruitment, coat assembly, and the recruitment of uncoating machinery (Kirchhausen et al., 2014). CME represents a highly orchestrated process, starting with nucleation, cargo selection, coat assembly, scission, and ending with uncoating (McMahon and Boucrot, 2011). Yet, from the beginning to the end, everything will happen in less than one minute.

More recently, the F-BAR domain-containing Fer/Cip4 homology domain-only proteins 1 and 2 (FCHO1/2) have been put forward as initiators of CCV formation (Henne et al., 2010). Yet, this function is not fully established, and FCHO1/2 may not be CCP initiators in all cell types (Cocucci et al., 2012; Umasankar et al., 2012). FCHO2 binds and recruits directly the epidermal growth factor receptor

pathway substrate 15 (eps15) and intersectin, which will then initiate CCP maturation and AP-2 recruitment. Additionally, CPP could be formed by random nucleation and stabilization in presence of cargo (Ehrlich et al., 2004). Since clathrin does not bind directly to the PM, the APs were described to (A) bind and recruit clathrin for CCP initiation, and (B) to bind short sorting signal regions in the cytosolic tails of PM receptors (Boehm and Bonifacino, 2001; Owen, 2004). AP-2 mainly acts on the level of PM, whereas AP-1, AP-3, and AP-4 mediate sorting-events on the level of endosomes and/or the TGN. All APs are built from two large subunits (for AP-1 and AP-2 these are γ and $\beta 1$ or α and $\beta 2$, respectively), a medium subunit ($\mu 1$ or $\mu 2$), and a small (1σ or 2σ) subunit (Kirchhausen, 1999). The $\mu 2$ chain of AP-2 has been described in internalization events of transferrin (Tf) and epidermal growth factor (EGF) by binding to a Ypp ϕ motif in the cytosolic tails of their respective receptors (Boll et al., 1995; Collawn et al., 1990; Sorkin et al., 1996). The $\beta 2$ chain connects with clathrin and supports the CCV formation (Gallusser and Kirchhausen, 1993). Synaptogamin and the phosphoinositide PtdIns(4,5)P₂ were shown to be needed for AP-2 association at the PM (Zhang et al., 1994). Further players have been described to be involved in the organization of CCPs: β -arrestins, epsin, AP180/CALM (clathrin assembly lymphoid myeloid leukemia), Dab2, and ARH (autosomal assembly lymphoid myeloid leukemia). Epsin and AP180/CALM bind clathrin, AP-2, and PtdIns(4,5)P₂ (Ford, 2001).

AP180/CALM regulates the size of CCVs by binding to AP-2. The GTPase dynamin (DNM) is needed for the scission of CCVs, likely involving its interaction with Src homology 3 domain (SH3)-containing proteins, such as amphiphysin, endophilin, SNX9 (sorting nexin 9), and intersecting (McMahon and Boucrot, 2011). DNM has been described as a 'pinchase' that constricts the opposing sites of the endocytic pit until the CCV is released (Sweitzer and Hinshaw, 1998).

Through their concave structure and an amphipathic helix, amphiphysin, endophilin, SNX9 (members of the BAR (Bin/amphiphysin/Rvs)-domain protein family) are able to sense curved membranes and control pit formations (Peter, 2004).

After scission, the clathrin coat is disassembled for subsequent fusion with the target compartment (McMahon and Boucrot, 2011). The uncoating process is mediated by an ATPase, the heat shock cognate 70 (HSC70) and its cofactor, auxilin (Schlossman et al., 1984; Ungewickell et al., 1995).

One full circle of a CCV formation is shown in Figure 16. The role of clathrin in the process of retrograde transport is introduced in further detail in chapter 9.2.5.2.

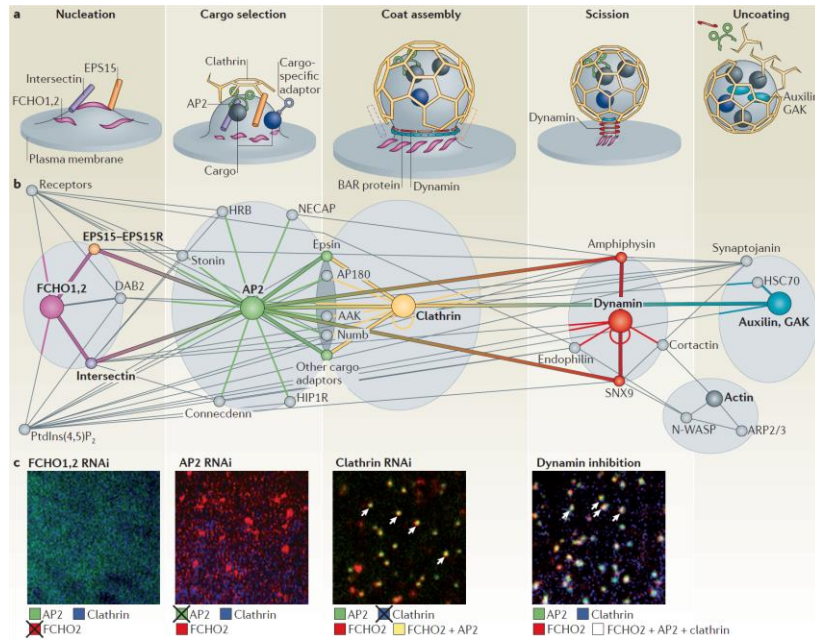


Figure 16: Clathrin-mediated endocytosis. (a) Stages of clathrin-mediated endocytosis. Step 1: FCHO protein mediated nucleation. Step 2: Cargo recruitment by AP-2. Step 3: Coat assembly. Step 4: Dynamin-mediated scission. Step 5: Un-coating. (b) Network of interacting partners involved in CME. (c) Depletion of FCHO proteins, AP-2, clathrin, and dynamin and their effect on CCP formation (McMahon and Boucrot, 2011).

9.2.2.2 Clathrin-independent Endocytosis (CIE)

Clathrin-independent endocytosis (CIE), or non clathrin endocytosis (NCE), was observed in the 1980s when the bacterial cholera toxin (Montesano et al., 1982) and the plant toxin ricin (Moya et al., 1985) were shown to still be able to enter their host cells after inhibiting CME. Further, CIE has been described to act in parallel to CME (Doherty and McMahon, 2009; Johannes et al., 2015; Mayor et al., 2014). CIE mediates uptake related to quicker responses, such as receptor hyper stimulation, stress hormone uptake for fight-or-flight responses, chemotaxis and compensatory endocytosis for membrane hemostasis (Watanabe and Boucrot, 2017). Several viruses, prions, bacteria and their bacterial toxins use CIE to enter their host cells (Yamauchi and Helenius, 2013). Thus, a variety of apparently heterogeneous endocytic events are regrouped under the term of CIE.

For many years, CIE was seen as a single, non-selective, bulk uptake process, which was called either macro- or micro-pinocytosis, regarding the size of the vesicles that were created. Yet, the classification by size and shape, trying to create a morphology-based nomenclature does not seem to be fully satisfactory, since clathrin independent carriers (CLICs) are 50 to 200 nm in size, while macro-pinosomes can reach several microns, due to their creation by membrane ruffles folding back onto the PM (Maldonado-Báez et al., 2013).

Another approach to further dissect CLICs was by their cargo, resulting in a classification that is not fully satisfactory, as some cargos are only expressed by some cell types (interleukin 2 receptor - IL2R). Furthermore, in many cases cargos are not exclusively endocytosed by only one endocytic mechanism. Equally, the effort to find a specific relation to exclusive GTPases (dynamin, Arf6, Cdc42 and Rac1) was not fruitful either, since these have broader functions, and are not limited to only one type of endocytic event. Furthermore, relating trafficking factors to certain endocytic structures is not operational either, as the latter often merge into the same endosomal compartments, which makes it difficult to track down their origin.

My host lab has suggested that one overarching mechanism to explain a number of CIE events is based on the lectin-driven extracellular clustering of glycosylated lipids and cargo proteins, leading to the formation of tubular membrane invagination and the biogenesis of co-called clathrin-independent carriers. This mechanism is termed the GL-Lect-hypothesis (Johannes et al., 2016).

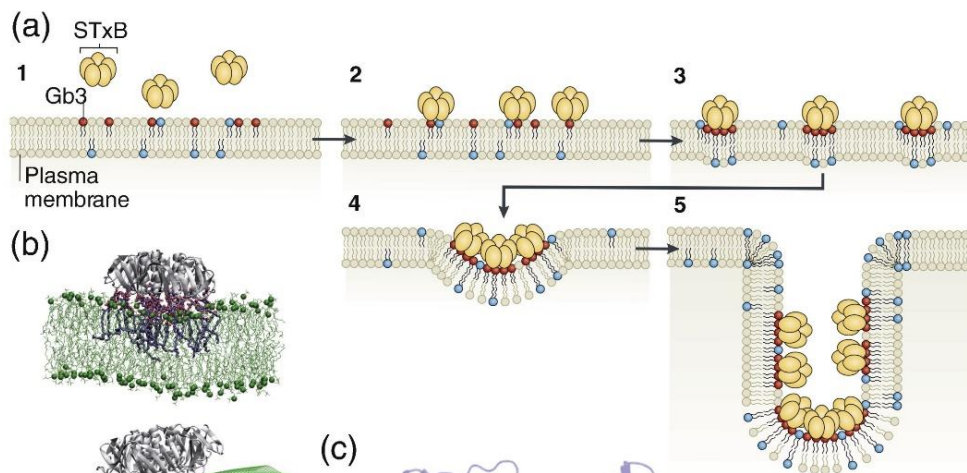


Figure 17: (a) STxB-driven membrane invagination in interaction with the GSL Gb3. – adopted from (Johannes et al., 2016).

For toxins, such as SLTs or CT, for the polyomavirus SV40, and for norovirus, it has been shown that glycosphingolipids (GSL) not only function as cellular receptors. Their binding also results in cargo clustering and the creation of tubular membrane invaginations, as shown on model membranes and cells. For SLTs, their B-subunits (termed STxB) are lectins that bind to the cellular toxin receptor, the GSL Gb3 (Figure 17). The 15 binding sites of each STxB homo-pentamer are arranged in a way such that as to drive spontaneous membrane bending. This orchestrated GSL/lectin-mediated curvatures lead to the formation of narrow membrane invaginations, not depending on the cytosolic clathrin machinery

(Römer et al., 2007; Ewers et al., 2010; Rydell et al., 2013; Pezeshkian et al., 2016). Moreover, this process seems to be temperature and cholesterol dependent (Römer et al., 2010). On the inner side of the membrane, actin was enriched on SLT invaginations illustrating their role in the reorganization and the scission process. Figure 18 illustrates the model of clathrin-independent SLT-driven membrane invagination stressing the role of actin in the scission process (Römer et al., 2010).

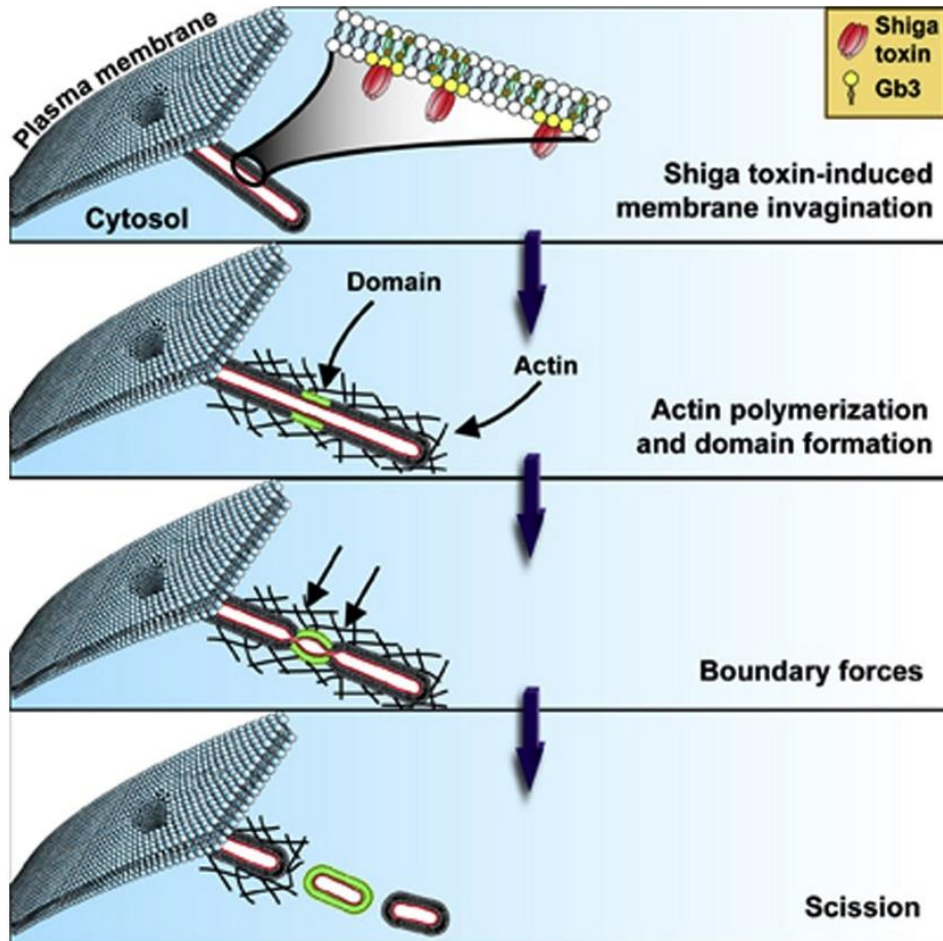


Figure 18: Model of actin-driven scission. After SLT binding on to Gb3, membrane curvature is induced, leading to the clathrin independent formation of PM invaginations. Actin polymerization causes scission through membrane reorganization (Römer et al., 2010)

This hypothesis has been extended to endogenous cargos. The galectin family appears to drive the formation of tubular membrane invagination from which clathrin-independent carriers are formed. This process occurs in interaction with glycosylated cargo proteins such as $\alpha 5 \beta 1$ -integrin and CD44, and glycosphingolipids (Lakshminarayan et al., 2014) (Figure 19).

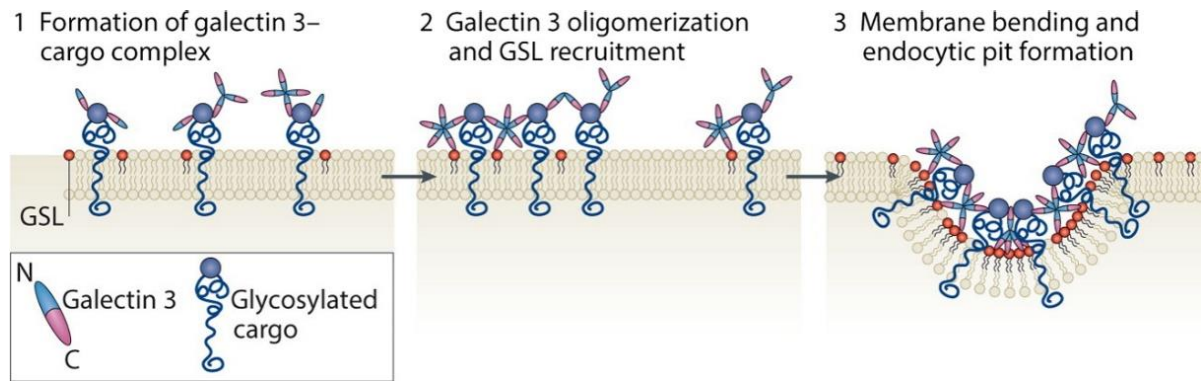


Figure 19: Gal3-driven membrane bending. (Johannes et al., 2015)

Caveolae uptake was often portrayed as one example of dynamin-dependent CIE. Caveolae (Latin for “little caves”) are relatively small (50 to 100 nm) flask-shaped invaginations at the PM (Yamada, 1955) that are rich in caveolins, sphingolipids, and cholesterol. Caveolin-1 and caveolin-2 are expressed in non-muscle cells, and caveolin-3 in muscle cells (Parton and del Pozo, 2013). Caveolae are mostly expressed in cells that are submitted to mechanical stress such as stretching and swelling, including muscle cells, endothelial cells, and adipocytes. Upon mechanical stress, Caveolae flatten out and function as a membrane reservoir to protect cells against mechanical rupture (Sinha et al., 2011). It seems likely that the major function of caveolae is in mechano-protection and mechano-signaling (Nassoy and Lamaze, 2012). In contrast, the endocytic function of caveolae has been called into question. Simian 40 virus (SV40) may be taken as an example to illustrate this point. It was initially put forward that SV40 is internalized by caveolae-mediated endocytosis (Pelkmans et al., 2001). However, it was then found that the SV40 uptake was if anything increased in the absence of caveolae (Damm et al., 2005). Similar observations were made for other presumed cargo proteins of caveolae endocytosis. The IL2R requires dynamin, without needing clathrin or caveolins-1 (Lamaze et al., 2001) and the IL2R uptake is regulated through Rho family GTPases and coractin (Grassart et al., 2008; Lamaze et al., 2001).

9.2.3 The recycling pathways

Recycling between endosomes and the plasma membrane regulates diverse processes such as cytokinesis, cell adhesion, morphogenesis, cell fusion, as well as learning and memory, and is thought to occur either via a rapid (direct) or slow (indirect) pathways (Grant and Donaldson, 2009).

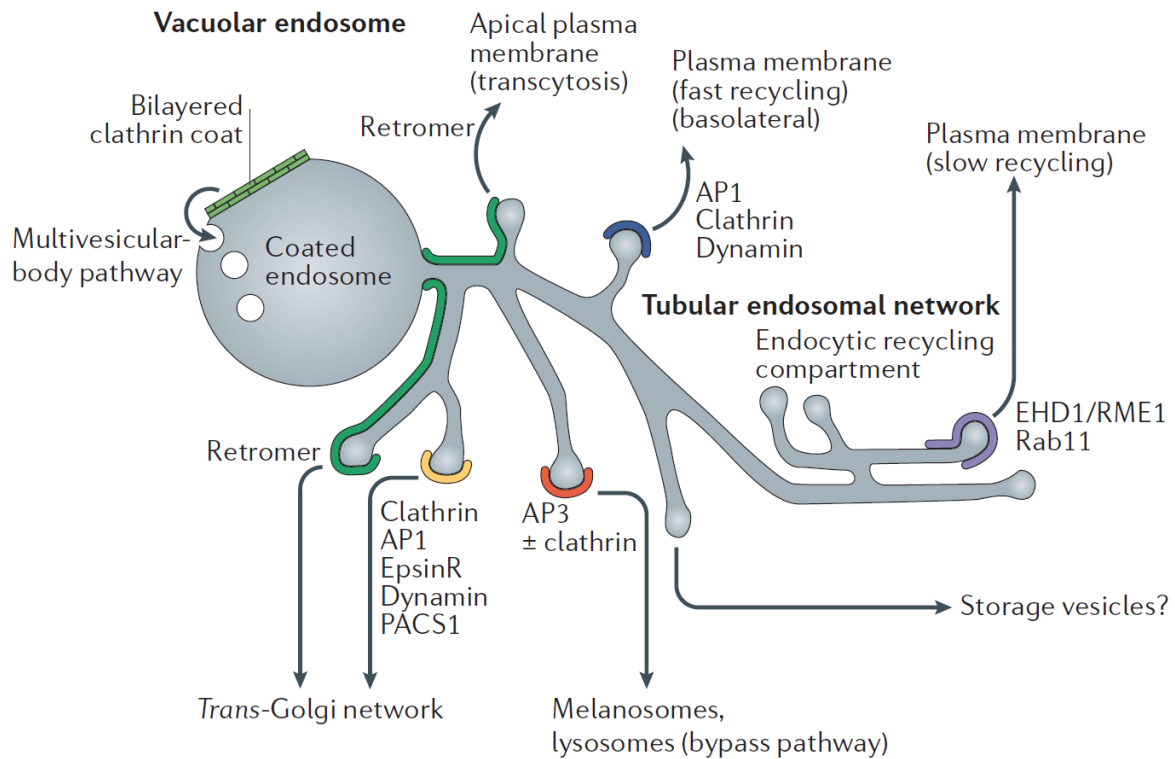


Figure 20: A schematic representation of the ‘tubular endosomal network’ (TEN). Endocytic vesicles are delivered to clathrin-coated early endosomes, which start to mature involving progressive acidification of their lumen. The TEN contains various domains (labeled in different colors) and the necessary machinery to sort cargoes to their various destinations. - (Bonifacino and Rojas, 2006)

9.2.3.1 Fast recycling – direct pathway

The fast recycling pathway (from EE or an earlier endocytic step) initially emerged from Tf studies (Harding et al., 1983) (Figure 20). Tf binds iron and mediates its cellular uptake through binding to the Tf receptor (TfR). After CME, Tf traffics to EE where iron dissociates from Tf due to a decrease in pH. Afterwards the TfR shuttles Tf back to the PM. This process has been suggested to be regulated by the small GTPase Rab4, and may apply to TfR, β -adrenogenic receptor, and class A (fast-recycling) G-protein-coupled receptors (GPCR) (Seachrist, 2000; van der Sluijs et al., 1992). Rab35 was likewise associated with the fast recycling pathway. Upon its inhibition, many endocytic markers accumulate within endosomal structure without cycling back to the PM (Kouranti et al., 2006). Furthermore, the GTPase ADP-ribosylation factor-6 (Arf 6) and the JNK-interacting proteins 3 and 4 (JIP3 and JIP4) have been associated with fast recycling pathway of Tf (Montagnac et al., 2011).

9.2.3.2 Slow recycling – Rab11 mediated

Slow recycling describes the cargo transport from EE through the juxta-nuclear endocytic recycling compartment (ERC) back to the PM (Grant and Donaldson, 2009). The ERC is defined by EHD1, Rab11 and a tubular shape (Sönnichsen et al., 2000). Rab11 is found in RE and the TGN where it regulates the slow recycling process (Figure 20).

9.2.4 The lysosomal/degradation pathway

Cargoes intended to be degraded traffic into multi-vesicular bodies (MVBs) and end up in lysosomes (Gruenberg and Stenmark, 2004) (Figure 21). MVB arise by inward budding of vesicles from endosomal compartments (Piper and Katzmann, 2007). A major degradation signal for cargos is ubiquitination. The endosomal sorting complexes required for transport I, II, and III (ESCRT I-III) recognize ubiquitinated cargos and initiate MVB formation. The degradation of the epidermal growth factor receptor (EGFR) is well-studied. After CME endocytosis, the EGFR is sorted to lysosomes and degraded. This leads to the reduction of the receptor pool at the PM and thus used to modulate the stimulatory signal (Felder et al., 1990; Futter et al., 1996; Haigler et al., 1979). This was confirmed in electron microscopy, in which was shown that the EGFR is found in MVB (Futter et al., 1996). In the process of antigen presentation, MVBs are important for the loading of major histocompatibility complex class II (MHC II) receptors with antigenic peptides (Murk et al., 2002; Kleijmeer et al., 2001).

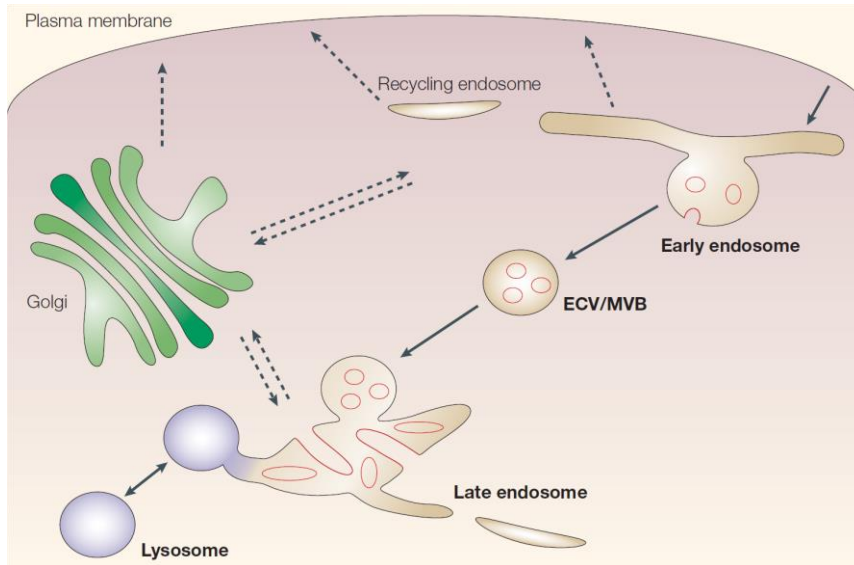


Figure 21: The generation of multi-vesicular bodies, leading to lysosomes. The degradation pathway is shown by solid arrows. Membrane invaginations and internal vesicles are shown in red, highlighting multi-vesicular regions in EE and LE. The recycling pathways (slow and fast) are shown by dashed arrows. - (Gruenberg and Stenmark, 2004)

9.2.5 Retrograde trafficking

Newly synthesized proteins and lipids are transported anterogradely from the ER to the PM (chapter 9.2.1). For membrane homeostasis, the secretory transport is compensated by retrograde trafficking (Johannes and Popoff, 2008; Bonifacino and Rojas, 2006). For this, cargo proteins and lipids can be transported from different endosomal sub-compartments back to the Golgi (Figure 22), and in some cases to the ER, as shown for the first time for Shiga toxin (Sandvig et al., 1992).

Historically, the retrograde transport route was discovered by studying toxins (read more in chapter 9.1) (Gonatas et al., 1975). The TfR was the first endogenous cargo for which retrograde trafficking could be shown (Snider and Rogers, 1985). Later, mannose 6-phosphate receptors (MPRs) were shown to rely on retrograde trafficking as part of their functional cycle (Duncan and Kornfeld, 1988). Lysosomal enzymes shuttle through MPRs from the TGN to endosomes. Afterwards, empty MPRs cycle back to the TGN. Many physiological functions depend on the retrograde trafficking (Burd, 2011). In case of malfunction of retrograde transport, it has also been demonstrated that the amount of amyloid β -peptides is increased (Burgos et al., 2010).

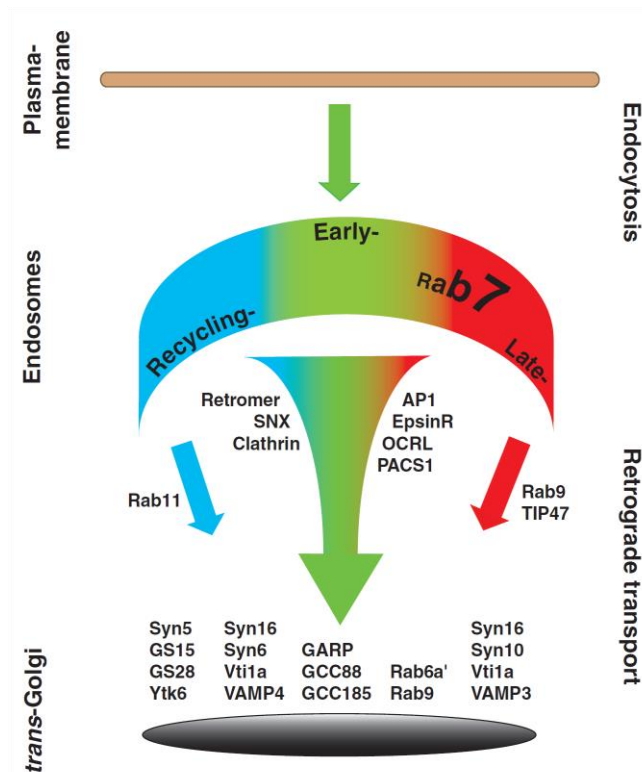


Figure 22: Schematic drawing of retrograde trafficking entry points. The retrograde transport step from endosomes to the TGN can originate from several points: recycling (blue), early (green) or late (red) endosomes. - (Johannes and Wunder, 2011b)

MPRs are a historical example for late endosomes-to-TGN trafficking (Lombardi et al., 1993). The existence of a trafficking interface between EE and the TGN was pioneered with Shiga toxin (Mallard et al., 1998). It was then also suggested that Shiga toxin could traffic from RE to the TGN (Lieu and Gleeson, 2010). Thus, several retrograde trafficking routes may exist in parallel, as summarized in Figure 22 (Johannes and Wunder, 2011b).

9.2.5.1 GPP130: A cycling Golgi protein involved in Shiga toxin trafficking.

GPP130 is a homo-dimeric type II single pass transmembrane protein. The major part of the protein is oriented intra-luminal, and has a predicted coiled-coil domain and an unstructured acidic domain (Linstedt et al., 1997). GPP130 constantly cycles between the cis-Golgi and the PM. Thus, it constitutively undergoes retrograde trafficking. Further, GPP130 cycles through the direct EE to Golgi pathway (Puri et al., 2002). Upon minor increases in intra-Golgi manganese (Mn) concentrations, GPP130 relocates from the Golgi to MVBs and lysosomes for degradation (Mukhopadhyay et al., 2010). This redistribution is Rab5, DNM and microtubule-independent, but Rab7-dependent. Additionally, neither endocytosis nor early endosome trafficking are involved (Mukhopadhyay et al., 2010). Recently,

it has been shown that the redistribution is caused by an oligomerization through Mn (Tewari et al., 2014, 2015). The predicted coiled-coil domain of GPP130 holds distinct Golgi and post-Golgi endosomal targeting regions, enabling its trafficking between cis-Golgi and endosomes (Bachert et al., 2001; Puri et al., 2002) and its Mn induced clustering (Mukhopadhyay et al., 2010). The main function(s) of GPP130 still remain(s) unclear. However, no other Golgi protein has been described to be degraded upon a Mn stimulus (Mukhopadhyay et al., 2010).

GPP130 has been shown to bind Shiga toxin and SLT1s (Mukhopadhyay et al., 2013). Furthermore, Mn-induced depletion of GPP130 protects cells against Shiga toxin (Mukhopadhyay and Linstedt, 2012). Still, how exactly GPP130 is involved in Shiga toxin trafficking to the Golgi has to be further investigated.

9.2.5.2 Clathrin

Clathrin has been found on endosomes (Stoorvogel et al., 1996). Clathrin does not bind directly to membranes and requires adaptor proteins (see chapter 9.2.2.1). Instead of PM-localized AP-2, different studies have provided evidence for a function of AP-1 in retrograde trafficking from endosomes to the TGN (Fölsch et al., 2001; Mallard et al., 1998; Meyer et al., 2000). Further, AP-1 co-localizes with STxB (Mallard et al., 1998; Saint-Pol et al., 2004), and interacts with the adaptor protein EpsinR, which further interacts with clathrin and the phosphatidylinositol lipid PtdIns(4)P (Mills et al., 2003; Hirst et al., 2003; Kalthoff et al., 2002). Strikingly, while the endocytosis of STxB still occurs after clathrin depletion, its Golgi arrival seems to strongly depend on clathrin (Saint-Pol et al., 2004).

9.2.5.3 Retromer

Retromer is a pentameric complex that is localized on endosomes where it sorts cargos for retrograde trafficking. It is composed of two sub-complexes: the vacuolar protein sorting trimer VPS26/VPS29/VPS35 sub-complex, and a sorting nexins dimer (SNX) sub-complex (Rojas et al., 2008; Hierro et al., 2007). Historically, it was proposed that the trimeric VPS-sub-complex recruits cargoes via VPS35 and VPS26 (Seaman, 2004) (Figure 23). The retromer complex interacts with GTP-activated Rab7, and binds to combinations of SNX dimers (out of SNX1, SNX2, SNX5 and/or SNX6), thus leading to membrane bending, tubule formation, and trafficking to the TGN (Rojas et al., 2008; van Weering et al., 2012). The scission mechanism is still unclear. At the level of the TGN, the tethering factors GARP and EARP (Schindler et al., 2015; Perez-Victoria and Bonifacino, 2009), SNARE complexes involving syntaxin-16 (Mallard et al., 2002; Ganley et al., 2008), and the GTPase Rab6 (Mallard et al., 2002) will mediate the fusion. It should be mentioned that various recent studies suggest that SNX proteins may also participate in cargo sorting (reviewed in (Johannes and Wunder, 2011a)).

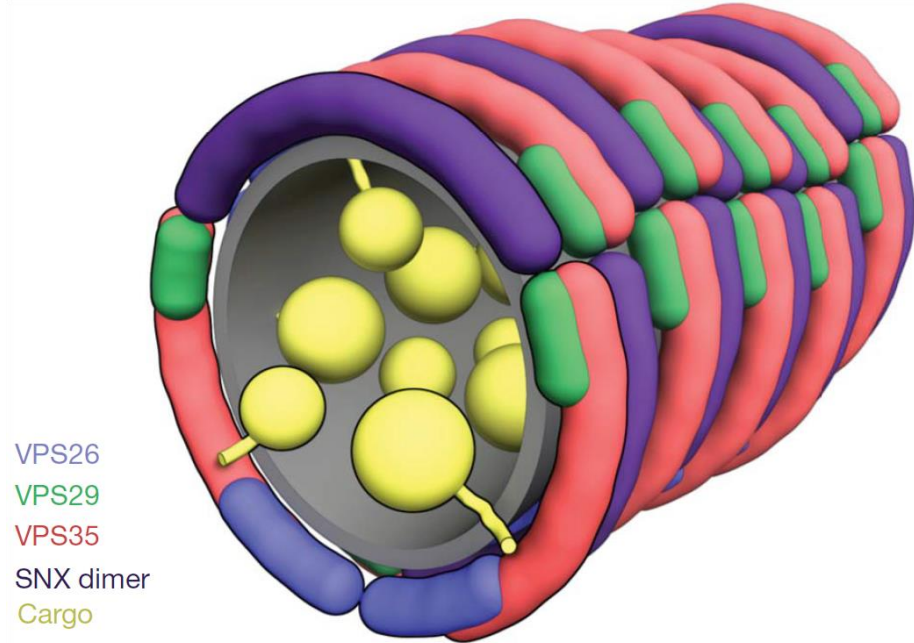


Figure 23: Schematic presentation of a speculative model of the retromer coat on a membrane tubule. SNX dimer in purple. - (Hierro et al., 2007)

The depletion of Vps26 inhibits the TGN arrival of STxB. STxB-containing tubules are likely processed by retromer, even if the exact mechanism remains elusive (Popoff et al., 2007). The actions of clathrin and retromer appear to be interconnected by RME-8 (receptor-mediated endocytosis-8) and Hrs (hepatocyte growth factor-regulated tyrosine kinase substrate), which interacts with SNX1 (Popoff et al., 2009). Moreover, RME-8 binds to the ATPase HSC70 that uncoats clathrin. RME and HSC70 depletions affects retrograde trafficking between EE and the TGN.

9.2.6 SNAREs

SNAREs (soluble N-ethylmaleimide-sensitive factor attachment protein receptors) function in the last step of vesicles fusion with the target compartment (Söllner et al., 1993; McNew et al., 2000; Hu, 2003). Functionally, SNAREs can be classified into vesicle located v-SNAREs and target compartment-located t-SNAREs.

The v-SNARE (or R-SNARE) contributes a single SNARE motif and is localized on carriers, whereas t-SNAREs (or Q-SNAREs) are structurally composed of two or three polypeptides that localize on target compartments (Fukuda et al., 2000). A heterodimeric t-SNARE is built from one member of the syntaxin (STX) family, which contributes with one SNARE motif, and one member of the SNAP-25 family, which contributes two SNARE motifs. A heterotrimeric t-SNARE is made out of 3 STX proteins. Upon v-SNARE-t-SNARE interaction, a trans-SNARE complex is formed, in which four SNARE motifs assemble as a twisted parallel four-helical bundle, leading to the apposition and fusion of the vesicle with the target compartment (Sutton et al., 1998; Antonin et al., 2002; Weber et al., 1998) (Figure 24).

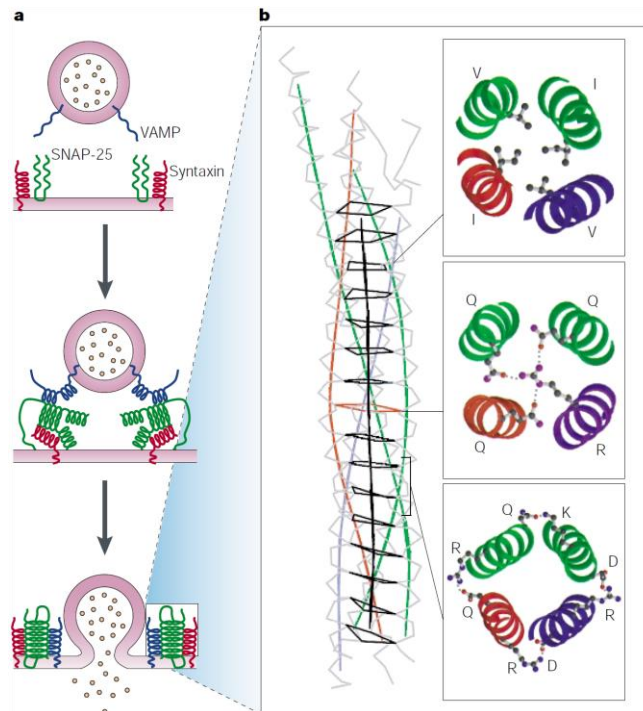


Figure 24: SNARE proteins form a four-helical bundle complex that drives membrane fusion. (a) VAMP (blue) on the vesicle interacts with syntaxin (red) and SNAP-25 (green) on the plasma membrane to form a four-helix bundle that zips up concomitant with bilayer fusion. (b) The backbone of the SNARE complex is shown on the left, with the central ionic layer (red) and 15 hydrophobic layers (black) that mediate the core interactions. Top-down views of side-chain interactions are shown on the right, with the four SNARE helices that are represented as ribbons. The ball-and-stick structures represent the indicated amino acids; the dotted lines represent hydrogen bonds or salt bridges that stabilize interactions between SNAREs. Q-SNAREs and R-SNAREs are characterized by a glutamine (Q) or arginine (R) residue, respectively, in the central layer of the SNARE complex. (SNARE; soluble NSF attachment protein receptor, where NSF stands for N-ethyl-maleimide-sensitive fusion protein; SNAP-25, 25 kDa synaptosome-associated protein; VAMP, vesicle-associated membrane protein). - (Chen and Scheller, 2001)

9.2.6.1 The general mode of vesicle fusion

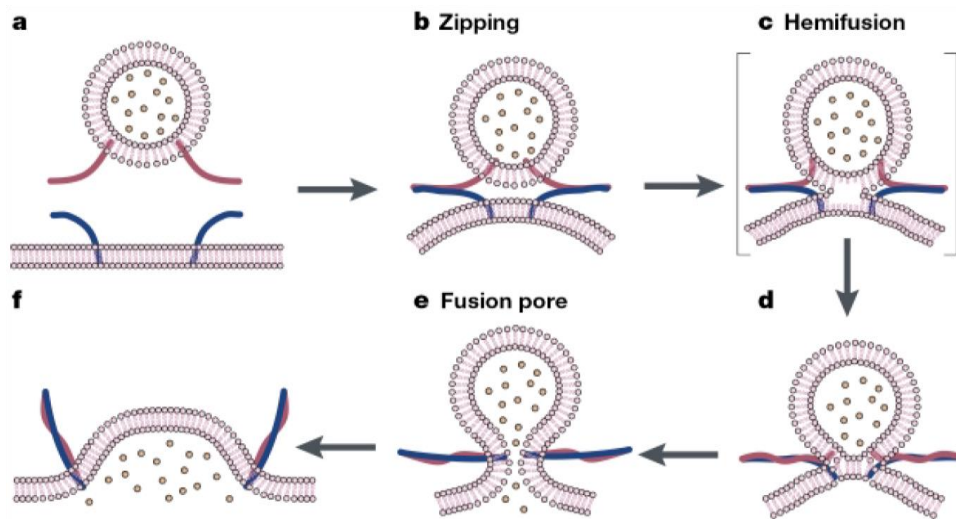


Figure 25: Model of SNARE-mediated lipid fusion. (a) The two membranes are in the vicinity of each other but the SNAREs are not yet in contact. (b) SNARE complexes start zipping from the amino-terminal end, which draws the two membranes further towards each other. (c) Zipping proceeds, causing increased curvature and lateral tension of the membranes, exposing the bilayer interior. Spontaneous hemifusion occurs as the separation is sufficiently reduced. (d) The highly unfavorable void space at the membrane junction in (c) causes the establishment of contacts between the distal membrane leaflets. (e) The lateral tension in the trans-bilayer contact area induces membrane breakdown, yielding a fusion pore. (f) The fusion pore expands and the membrane relaxes. - (Chen and Scheller, 2001)

The general mode of action of SNAREs in carrier-mediated transport is highlighted in Figure 25. First, the v-SNARE is packaged together with other cargo proteins into the budding vesicle so that the resulting transport intermediate is competent to fuse with the target compartment (Figure 25 a). SNAREs also play a role in the formation of carriers via the direct interaction with coat proteins, as shown for COPII formation at the level of the ER (Mossessova et al., 2003a; Miller et al., 2003), for COPI (Rein et al., 2002), and the interaction of Vti1b with EpsinR in endosomes-to-TGN trafficking (Hirst et al., 2004). Next, various tethering factors (Gillingham and Munro, 2003; Whyte and Munro, 2002) position the incoming carriers, preparing them for docking. The tethering factors act over longer distances than pairs of v-SNARE and t-SNAREs (Shorter et al., 2002). Afterwards, the formation of the trans-SNARE complex causes docking, and zipping-up leads to fusion (Chen and Scheller, 2001; Jahn et al., 2003). Indeed, the unstructured SNARE motifs zip and become highly organized into a four-helical bundle (Figure 24, Figure 25 b). The energy released during the SNARE complex assembly (which functions like a zipper; zipping starts from the N-terminal ends, and progresses toward the C-termini) overcomes the energy barrier that opposes the process of bringing the carrier and target compartment

membranes in fusion-compatible distances (Figure 25 b to d). After fusion, the 4 SNARE motifs are now in a cis-SNARE complex in the target compartment. The disassembly of cis-SNARE complexes is mediated by α -SNAP (soluble N-ethylmaleimide-sensitive factor attachment protein) and NSF (N-ethylmaleimide-sensitive factor), the latter of which is an ATPase (Hohl et al., 1998; Brunger and DeLaBarre, 2003; Furst et al., 2003; Wimmer et al., 2001).

Known mammalian SNARE complexes throughout the cell are shown in Figure 26.

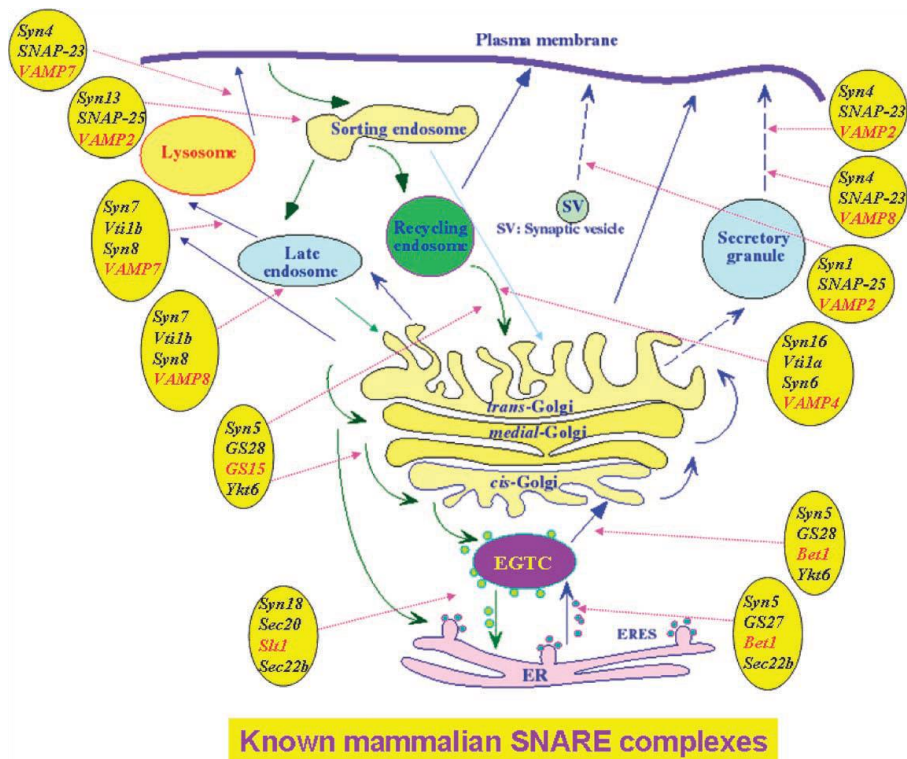


Figure 26: Schematic summary of known mammalian SNARE complexes and their site(s) of action in the exocytic and/or endocytic pathways. The potential v-SNAREs are indicated in red. - (Hong, 2005)

9.2.6.2 Syntaxin-5 (STX5)

Out of the 12 SNARE proteins that are associated with the Golgi, Syntaxin-5 (STX5, Sed5p in yeast, 33 % identity) is one of the best characterized (Nichols and Pelham, 1998). STX5 has been shown in several SNARE complexes, mainly in the trafficking towards the Golgi. STX5 assembles with four other t-SNARE proteins: GS28 (trans-Golgi), GS27 (cis-Golgi), Sec22b (cis-Golgi) and Ykt6 (trans-Golgi). Further, two different v-SNAREs have been proposed: GS15 (Xu, 2002) for retrograde trafficking, and Bet1 (Hay et al., 1998) for anterograde trafficking (Figure 26). The STX5/GS28/Ykt6/GS15 complex has been reported to be involved in STxB trafficking to the Golgi (Tai et al., 2004).

STX5 has two isoforms: a short (35 kDa, Golgi localized) and a long isoform (42 kDa), which has a type-II ER retention signal at its N-terminus. These are translation products from the same mRNA (Hui et al., 1997). The short isoform is involved all reported SNARE complexes, whereas the long isoform has been found only in the cis-Golgi SNAREs (Nichols and Pelham, 1998) (Figure 26).

9.2.6.3 Syntaxin-16

Syntaxin-16 (STX16) is a t-SNARE that functions in endosomes-to-TGN trafficking (Mallard et al., 2002). It forms a SNARE complex with the t-SNAREs Syntaxin-6 (STX6) and Vti1a and the endosomal v-SNARE, VAMP4 (Tang et al., 1998; Hirst et al., 2004). The reason for bringing up STX16 in this manuscript is that this protein has been reported to be involved in retrograde trafficking of STxB, CTxB, ricin, and MPR, similar to STX5 (Amessou et al., 2007; Tai et al., 2004; Mallard et al., 2002). It remains unclear how the functions of these SNARE proteins are articulated in retrograde endosomes-to-Golgi trafficking. Do they have redundant functions? Or have we missed something about the full scope of their activities? The work in my PhD has allowed to address this aspect.

9.3 MICRO INTERFERING RNA FAMILY MIR199

It has been generally established, that short non-coding RNAs, known as microRNAs (miRNAs), regulate many cellular processes (Bushati and Cohen, 2007). miRs bind normally to 3' untranslated regions (3'UTRs) of target mRNAs, promoting their degradation and thus interfering with the translation process (Bartel, 2009; Filipowicz et al., 2008; Ambros, 2004). Around half of the miRNA genes are located in intergenic regions or introns and are usually close to their host gene (Saini et al., 2007) and often get co-transcribed (van Rooij et al., 2009; Rayner et al., 2010; Rodriguez et al., 2004).

Interestingly, the miR199 family members are encoded within introns of the DNM genes in the opposite orientation to the host gene. The family is composed of three members, miR199a1, miR199a2, and miR199b, that are located within the DNM2, DNM3 and DNM1 genes, respectively. miR199 gene sequences are highly conserved across species and potentially target the same group of genes. Through bio-informatics, Rab5A, Rab21, LDLR, and Cav1, all endocytic proteins, have been identified as putative targets of the miR199 family (Aranda et al., 2015). The miR199s have indeed been reported to regulate endocytic processes (Figure 27).

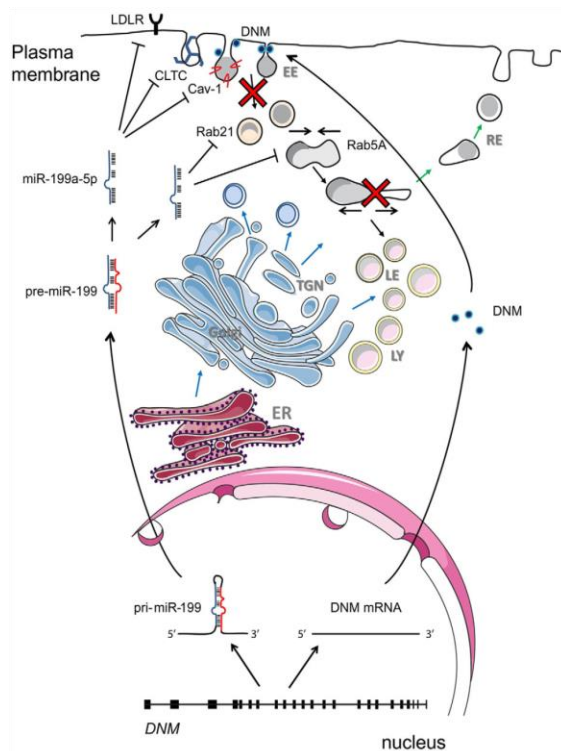


Figure 27: Proposed model of regulation of receptor-mediated endocytosis by dynamin and miR-199a/b. Sense strands of the dynamin genes are transcribed and translated to synthesize dynamin proteins that are involved in endosome trafficking. miR-199a-5p is transcribed in the nucleus from the antisense strand of introns in the DNM2 and DNM3 genes and regulates

receptor-mediated endocytosis and intracellular cholesterol levels by balancing the post-transcriptional levels of genes involved in endocytosis such as LDLR, CLTC, Cav-1, Rab5A and Rab21. - (Aranda et al., 2015)

10 MATERIAL AND METHODS

10.1 CELL LINES

HeLa cells were maintained at 37°C under 5 % CO₂ in DMEM/GlutaMAX[®]/4,5 g l⁻¹ glucose (Invitrogen, Waltham, MA, USA), supplemented with 10 % heat-inactivated fetal bovine serum (Invitrogen, origin: Australia), 0.01 % penicillin-streptomycin (Invitrogen), and 1 mM pyruvate (Invitrogen). For Shiga toxin intoxication, a HeLa cell clones was selected for a homogenous expression of the Gb₃-receptor and cultured as above. A stable cell line expressing KDEL-SNAP-fusion-protein, referred to as “ER-SNAP” cells, was produced from HeLa cells and was cultured as above, including 0,5 mg ml⁻¹ G418. ER-SNAP cells were used for the ELISA assays.

10.2 ANTIBODIES AND REAGENTS

Polyclonal rabbit antibodies against STX5 was obtained from Synaptic Systems (Goettingen, Germany). The TGN46 antibodies and SDS-Page pre-casted gels were purchased from BioRad (Hercules, CA, USA). The CHC, GS27 and GS28 antibodies were purchased from BD Biosciences. The rabbit giantin antibody was purchased from the protein platform of the Curie Institute (Paris, France). The rabbit antibody against Vps26 was obtained from Abcam. The rabbit anti-Sec16A antibody was bought from Proteintech Europe (Manchester, UK). The plasmid encoding STX5-EGFP was a gift from Jeffrey E. Pessin (The University of Iowa, USA). The plasmid encoding Sec16A-GFP was a gift for David Stephens (University of Bristol, England), and the RUSH and the mCherry-KDEL constructs were provided by the group of Franck Perez (Institut Curie, Paris, France). STxB-Cy3 was produced in-house, as described in (Mallard et al., 1998).

10.3 RNA INTERFERENCE

siRNAs against Sec16A, GP73, TGN46 or GPP130 were purchased from Qiagen. siRNA pools were composed of one, two or four different oligonucleotides. Scrambled siRNA was used as a control. 150.000 HeLa cells were plated overnight in 35 mm well dishes (6 well plates), and transfected with 25 pmol siRNA, 7,5 µl Lipofectamine[®] RNAiMAX transfection reagent (Invitrogen). Experiments were performed 72 hours after transfection.

For miR experiments, HeLa cells were transfected with 40 nM miR199 using RNAimax (Invitrogen). All experimental control samples were treated with an equal concentration of a non-targeting control mimic sequence (CM). Verification of miR-199a-5p over-expression and inhibition was determined using Western blotting against Vps26.

10.4 CALCIUM PHOSPHATE–DNA CO-PRECIPIATION

HeLa cells were plated overnight in complete medium supplemented with 25 mM HEPES (pH7,2 - 7,4) to reach a confluency of 50 to 80 %. A solution of 10 µl of 2.5 M CaCl₂ and the optimized amount of plasmid DNA was diluted in 90 µl TE buffer (1 mM Tris–HCl, 0.1 mM EDTA, pH 7.6) to a final volume of 100 µl. The Ca/DNA/TE mix was added dropwise to an equal volume of 2× HeBS solution (160 mM NaCl, 1.5 mM Na₂HPO₄, 50 mM HEPES, pH 7.05 at 23°C). This transfection solution was added dropwise onto cells in a 1:10 dilution (Jordan et al., 1996).

10.5 RETRO-2 TREATMENTS

Retro-2 (2-([(5-methyl-2-thienyl)methylene]amino)-N-phenylbenzamide) was purchased from Sigma Aldrich (St. Louis, MO, USA) and stored at 50 mM in DMSO at -20°C. Cells were pre-treated at 37°C either 30 minutes for Shiga toxin intoxication and STx trafficking, or 60 minutes for the STX5-RUSH assay and STX5-co-immunolabeling experiments with 25 µM Retro-2, diluted in complete growth medium. DMSO at a concentration of 0,05 % in complete growth medium was used as control.

10.6 CLICK CHEMISTRY LABELING

Copper-free click reactions were essentially performed as per the manufacturer's recommendations. Briefly, HeLa cells were treated with the clickable Retro-2 compound ($c = 25 \mu\text{M}$) for 30 minutes at 5 % CO_2 and 37°C . The copper free click-reaction was performed on cells with DIBO-probes (Invitrogen, Click-iT reagents, $c = 10 \mu\text{M}$) for 1 hour at room temperature and covered from light. For fluorescence labeling, cells were fixed for 10 min at room temperature with 4 % paraformaldehyde. For silver gel, Western blot, and mass spectrometry analysis, the cells were lysed for 30 min, at 4°C with a TNE buffer containing 1 % NP-40 and proteinase inhibitor cocktail.

10.6.1 METHODOLOGY ASPECTS: Bio-orthogonal Click chemistry

Azides do not naturally occur in biological systems as functional groups. Therefore, azide groups can be exploited for bio-orthogonal chemistry to covalently modify biomolecules with selected probes. The azide can be specifically reacted with bio-orthogonal alkynes and forms a triazole product. This reaction is also known as click chemistry. Moreover, since its discovery in 1961 (Wittig and Pohlke, 1961; Huisgen, 1961), the 1,3-cyclo-addition has been shown to occur under various conditions: Two groups simultaneously showed that a copper-catalyzed click reaction would happen very efficiently under mild reaction conditions (Figure 28 A) (Rostovtsev et al., 2002; Tornøe et al., 2002). For biological applications, copper is highly toxic (Nutra and Sandstead, 2016). In 2004, further developments showed that by restraining the alkyne chemically, the use of copper could be avoided (Figure 28 B) (Agard et al., 2004). Thus, click chemistry could be performed in biological systems at low temperatures (room temperature, or 37°C), in cellulose (Ning et al., 2008) and in living organisms (Baskin et al., 2007). Further studies optimized the copper-free click chemistry and created other reactive alkynes. In this study, 4-dibenzocyclooctynol-based (DIBO) probes have been used for highly stable conjugations and for shorter reaction times (Ning et al., 2008). We performed a copper-free click chemistry approach coupled to mass spectrometry for the identification of proteins that interact with Retro-2.

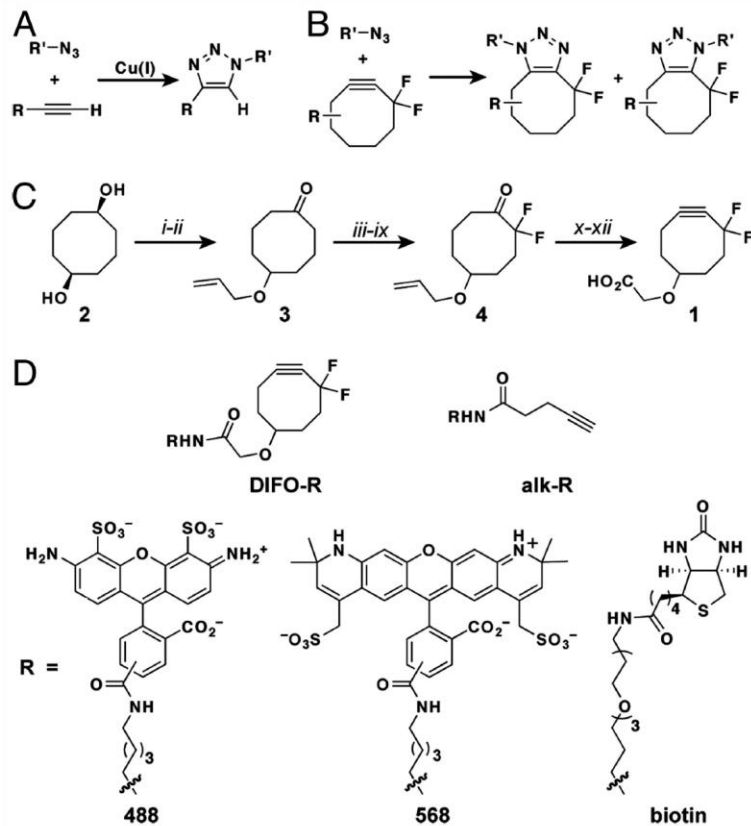


Figure 28: Design and synthesis of Cu-free click chemistry reagents. (A) The copper-catalyzed azide–alkyne cycloaddition. (B) The Cu-free click reaction of azides and DIFOs. (C) Single step synthesis of DIFO. (D) Derivatives of DIFO and a linear alkyne (alk) containing Alexa Fluor 488, Alexa Fluor 568, or biotin. - (Baskin et al., 2007)

10.7 IMMUNOPRECIPITATION

Retro-2 sensitive interacting partners of STX5 were identified in a stable HeLa cell lines expressing a STX5-GFP fusion protein. The clickable Retro-2 pull-down was performed on HeLa cells. Cells were lysed for 30 min on ice in lysis buffer (100 mM PBS, 150 mM NaCl, 1 % NP-40, PIC). NeutrAvidin® beads (for clickable Retro-2 pull-down) or GFP-trap beads (for STX5-GFP pull-down) were equilibrated in lysis buffer. The beads purification was done by centrifugation (5 min, 500 x g) or magnet collection, following the manufacturer's instructions. The respective beads were incubated with cell lysates over night at 4°C on an end-over-end rotation device. Retro-2 treatment was performed to determine binding partners (clickable version), or to detect interactions that are sensitive to this compound (non-clickable version). Vehicle alone (DMSO, w/o Retro-2) was used as control. After three washing steps, interacting proteins were eluted in Laemmli buffer (0.1 % 2-mercaptoethanol, 0.5 % bromophenol blue, 10 % glycerol, 2 % SDS, 63 mM Tris-HCl, pH 6.8) for 10 min at 95°C. The samples were analyzed by SDS-PAGE and either silver stained, Western blotted against indicated proteins, or digested for mass spectrometry analysis.

10.8 SHIGA TOXIN TRAFFICKING

HeLa cells, either DMSO or Retro-2 treated, were incubated with 2 µM (0.85 µg/ml) STxB-Cy3 on ice for 30 minutes. After the removal of unbound STxB-Cy3, its trafficking was initiated and followed for 45 minutes at 37°C in the presence of DMSO, or Retro-2 respectively. Cells were fixed for 10 minutes at RT with 4 % paraformaldehyde (PFA), permeabilized with 0.25 mg/ml saponin, and immune-labeled with the indicated antibodies.

10.9 PROXIMITY LIGATION ASSAY (PLA)

The PLA was adopted from the Landegren group (Söderberg et al., 2006). HeLa cells were incubated for 30 min at 37°C with Retro-2 (c =25µM) in complete medium, fixed with 4 % PFA for 10 min at room temperature, permeabilized with 0.25 mg/ml saponin, and immunostained for 30 min for STX5 and GS28 or GS27, respectively, after which PLA was performed according to the manufacturer's instructions (Duolink In Situ Orange Starter kit Mouse/Rabbit; Sigma-Aldrich). For quantification, at least 25 cells per experiment from two independent ones were quantified in each condition.

10.9.1 METHODOLOGY ASPECTS: Proximity ligation assay

The proximity ligation assay (PLA) is based on traditional immunoassays, detecting proximity between proteins or their post-translational modifications with high specificity and sensitivity, as long as appropriate antibodies are available. Two proteins of interest (or their possible post-translational modifications) are labeled with appropriate primary antibodies that were raised in different species. Matching species-specific secondary antibodies are labeled with PLA probes. PLA probes are composed of unique short DNA strands. If the PLA probes are in close proximity (20 to 40 nm), the DNA strands align and thereby become substrates for rolling circle DNA synthesis, which thereby creating a many-hundredfold amplification of the DNA circle. Fluorescent nucleotides are then attached onto the amplified DNA. The corresponding fluorescent signals are detected by epifluorescence or confocal microscopy (Figure 29) (Söderberg et al., 2006).

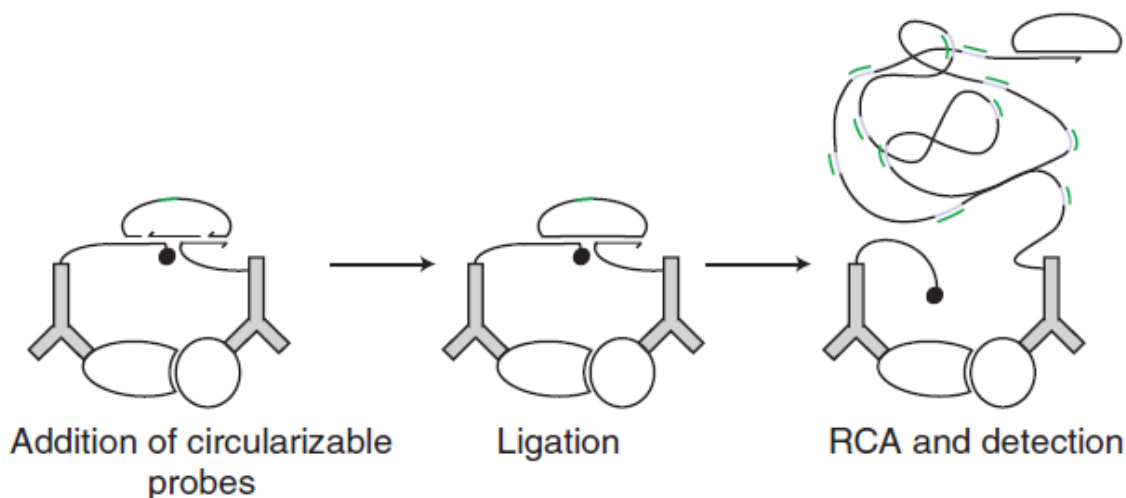


Figure 29: Detection of protein-protein proximity with the proximity ligation assay (PLA). (a) Schematic presentation of proximity probe-templated DNA circularization and subsequent rolling circle amplification (RCA) and detection. If two proximity probes bind close to each other, such as by binding two proteins present in the same complex, then subsequently added linear connector oligonucleotides are guided to form a circular structure covalently joined by enzymatic DNA ligation. After ligation, RCA is initiated using one of the proximity probes as a primer. The RCA product is detected through hybridization of fluorescence-labeled oligonucleotides complementary to a tag sequence in the RCA product. The green line in the circle that forms the proximity ligation reaction giving rise to multiple copies of complementary sequence in the RCA product (blue). This motif is detected by hybridizing fluorescence-labeled detection oligonucleotides (green).- (Söderberg et al., 2006)

10.10 CONFOCAL IMAGING

Samples were imaged on an inverted microscope Nikon Ti-E with motorized XY stage (for Ti-E/Ni-E) fitted with a confocal A1R system, using a 60x oil immersion objective. Nikon NIS software, version 3.2.6 (Minato, Tokyo, Japan), and ImageJ software, version 2.0.0 (National Institutes of Health, Bethesda, MD), were used for image acquisition and processing, respectively. Single stacks of approximately 200 nm thickness were used to analyze co-localization.

I would like to greatly acknowledge the Cell and Tissue Imaging (PICT-IBiSA) and Nikon Imaging Centre, Institut Curie, member of the French National Research Infrastructure France-BioImaging (ANR10-INBS-04).

10.11 RETENTION USING SELECTIVE HOOKS (RUSH)

The RUSH system was invented by the group of Franck Perez (Boncompain et al., 2012). Briefly, the STX5-SBP-eGFP gene was cloned into a RUSH construct with the *Ascl* and *XbaI* restriction sites. After overnight transfection, cells were treated with Retro-2 or DMSO, as described above. Trafficking was initiated with 40 μ M biotin in complete medium. The cells were kept 20 min at 37°C, before being fixed with PFA for 10 min at room temperature with PFA. Immune labeling were performed as indicated.

10.11.1 METHODOLOGY ASPECTS: Retention Using Selective Hooks (RUSH)

To investigate secretory traffic, the retention using selective hooks (RUSH) system was used. RUSH is based on the interaction of an immobile hook protein (here KDEL) in a donor compartment (here the ER), fused to a core streptavidin. A reporter protein of interest (here STX5) is fused to a streptavidin-binding peptide (SBP) and a fluorophore (here eGFP). In the non-induced state, the hook protein prevents cellular trafficking of the reporter (here: STX5 is retained in the ER). Upon biotin treatment (induction), the reporter is released from the hook and synchronously traffics to acceptor compartment(s) (here from the ER to the Golgi) (Figure 30) (Boncompain et al., 2012).

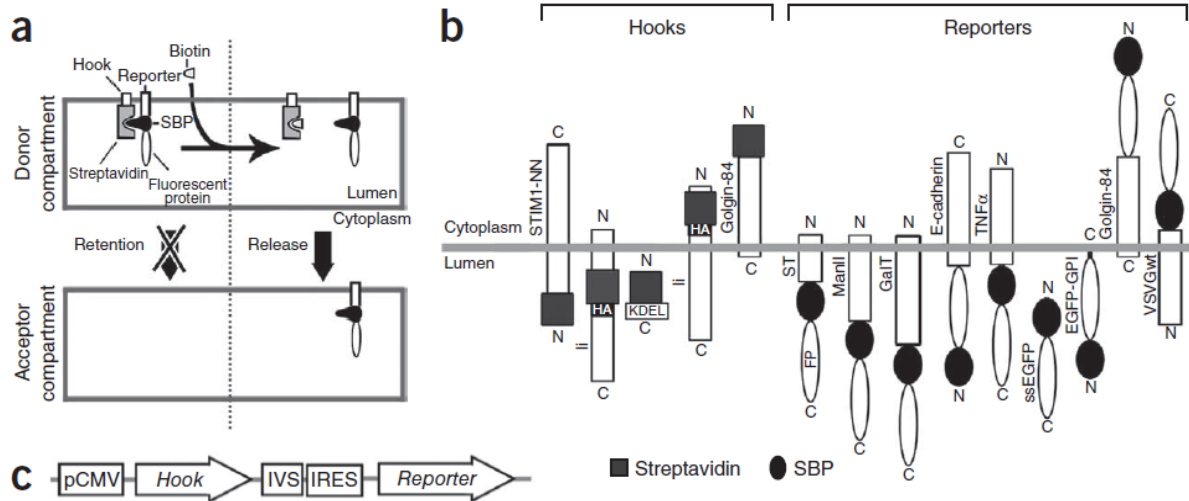


Figure 30: The RUSH system. (a) A schematic of the principle illustrates that the reporter is retained in the donor compartment via its interaction with the hook. This interaction is mediated by the core streptavidin and the SBP. Release is induced by addition of biotin to allow trafficking of the reporter to its acceptor compartment. A fluorescent protein is fused to the reporter. (b) Schematics of hooks containing STIM1-NN, li or KDEL for ER retention, or Golgin-84 for Golgi retention fused to streptavidin, and of reporters containing SBP fusions with Golgi proteins ST, ManII, GalT or Golgin-84, plasma membrane proteins VSVGwt, E-cadherin, TNF α or EGFP-GPI and secreted protein SBP-ssEGFP. HA, hemagglutinin tag; FP, fluorescent protein. (c) Schematics of genes coding for the hook and the reporter, expressed under the same CMV promoter (pCMV), separated by a synthetic intron (IVS, intervening sequence) and an internal ribosome entry site (IRES). - (Boncompain *et al.*, 2012)

10.12 INTOXICATION ASSAY

STx1 intoxication was performed on of specific or scrambled siRNA-transfected HeLa cells (Stechmann *et al.*, 2010). Briefly, 20.000 HeLa cells per well were seeded into flat-bottomed 96-well optical plates (Nunc) and grown overnight at 37°C. After pretreatment with Retro-2 or DMSO, cells were incubated with increasing doses of STx1 from 0,005 to 10 ng/ml for one hour at 37°C. After the washes with PBS, 1 μ Ci [³⁵S]-methionine (Perkin Elmer) was added to each well for 60 min at 37°C. Radiolabeled proteins were precipitated by washing cells three times with 4°C-cold 5 % trichloroacetic acid (TCA). Before liquid scintillation measurements, TCA was removed by three washes with PBS. Normalized duplets were used to determine the mean percentage of protein biosynthesis. The Prism software, version 7 (GraphPad, CA, USA) was used to fit and calculate the 50 % effective toxin concentration (EC50) from sigmoidal dose response fitting. Protection factors are shown as EC_{50drug}, EC_{50siRNA} and EC_{50control}.

10.13 WESTERN BLOT ANALYSIS

Cells on a thermo-shaker were lysed for 10 min at 95°C in Laemmli buffer (see chapter 10.7). Samples were size separated via SDS-Page. Protein were transferred onto nitrocellulose membranes with Pierce™ Power blotter (Thermo Fisher Scientific, Waltham, MA, USA). The following antibody concentrations were used: Vps26A (1:1500), STX5 (1:1000), GS27 (1:1000), GS28 (1:1000), CHC (1:5000) and GFP (1:1000). Corresponding HRP-coupled secondary antibodies (1:5000, Jackson ImmunoResearch Laboratories, West Grove, PA, USA) were used. Protein bands were visualized with SuperSignal (Thermo Scientific), and analyzed on a Fusion S Western blot imager (Vilber Lourmat, Marne-la-Vallée, France). Densitometry analysis of the gels was carried out using ImageJ software from the NIH.

10.14 STATISTICS

All data are presented as mean \pm SD. Unpaired Student's *t* tests were used to determine the statistical significance of possible differences between two data sets. A value of $P \leq 0.05$ was *considered* as significant. GraphPad Prism Software Version 7.03 (GraphPad, San Diego, CA) was used to illustrate the graphs and perform the analysis. * $P \leq 0.05$, ** $P \leq 0.01$, *** $P \leq 0.001$, NS = not significant.

11 RESULTS

11.1 MANUSCRIPT FOR SUBMISSION: SYNTAXIN-5 FUNCTIONALLY INTERACTS WITH GPP130 FOR RETROGRADE SHIGA TOXIN TRAFFICKING

Stefan J. Rathjen^{1#}, Maria Daniela Garcia-Castillo^{1#}, Collin Bachert², Audrey Couhert³, Valerie Chambon¹, Xavier Heiligenstein⁴, Alison Forrester¹, Henri-François Renard¹, Graça Raposo⁴, Raphaël Rodriguez⁵, Jean-Christophe Cintrat³, Julien Barbier³, Adam D. Linstedt², Daniel Gillet³, Ludger Johannes^{1*}

¹ Institut Curie, PSL Research University, Cellular and Chemical Biology unit, U1143 INSERM, UMR3666 CNRS, Endocytic trafficking and intracellular delivery group, 26 rue d'Ulm, 75248 Paris Cedex 05, France

² Department of Biological Sciences, Carnegie Mellon University, Pittsburgh, PA 15213

³ Institute of Biology and Technology of Saclay (IBITECS), CEA, LabEx LERMIT, Université Paris-Saclay, F-91191, Gif Sur Yvette, France

⁴ Institut Curie, PSL Research University, Subcellular structure and cellular dynamics unit, UMR144 CNRS, Biogenesis and functions of lysosome-related organelles group, 26 rue d'Ulm, 75248 Paris Cedex 05, France

⁵ Institut Curie, PSL Research University, Cellular and Chemical Biology unit, U1143 INSERM, UMR3666 CNRS, Chemical biology of cancer group, 26 rue d'Ulm, 75248 Paris Cedex 05, France

* Correspondence to: ludger.johannes@curie.fr

Keywords: Retrograde transport, STxB, Shiga toxin, Retro-2, chemical genetics, syntaxin-5, STX5, Sec16A, GPP130, azide-functionalized Retro-2, copper-free click chemistry, small molecule target identification, mass spectrometry. Non-SNARE function, TGN, trans-Golgi network, COPII vesicle formation, anterograde trafficking, Proximity ligation assay, PLA,

11.1.1 Abstract

The small molecule compound Retro-2 protects cells and mice against bacterial Shiga-like toxins and the plant toxin ricin. The molecular mechanisms by which this protective effect is achieved have remained unknown. Here, we provide evidence that Retro-2 targets the COPII component Sec16A, and reduces the anterograde transport specifically of syntaxin-5, leading to its relocalization from the Golgi to the endoplasmic reticulum. While the formation of SNARE complexes involving syntaxin-5 is not affected in Retro-2-treated cells, the discovery of novel syntaxin-5 binding partners, GPP130, GP73 and TGN46 is described for which it is found that they are displaced under Retro-2 incubations conditions. Strikingly, these proteins have previously been found to cycle between Golgi, plasma membrane and endosomes, and for GPP130, a function in retrograde trafficking of Shiga toxin had been documented. We show here that GPP130 must indeed interact with syntaxin-5 to drive Shiga toxin transport from endosomes to the Golgi. Our findings strongly suggest a non-SNARE function for syntaxin-5 at the endosomes-Golgi interface, in interaction with retrograde cycling proteins.

11.1.2 Author contributions

LJ and DG conceived and designed the study. SJR, HFR, and MDGC performed click chemistry immunofluorescence, and MDGC mass spectrometry experiments with the help of RR. SJN performed SNARE PLA, SNARE re-localization, STX5-RUSH, and GPP130 rescue analysis. Intoxication assays were done by SRN, MDGC, and JB. The purification of STX5 and GPP130 variants, the monensin study and the *in vitro* STX5-pulldown of the GPP130 variants were performed by CB and AL. SJR, VC, AF, and XH performed HPF-CLEM with the help of GR. SJR and MDGC performed Sec16A and syntaxin-5 proteomics analysis, immunofluorescence. AF performed the Sec23 kinetic studies. AC and JCC designed and performed the chemical synthesis of azide-functionalized Retro-2 derivatives. SJR and LJ wrote the paper. JCC, JB, DG, and GR critically revised the manuscript as well as aided in the design and analysis of experiments.

11.1.3 Introduction

Shigella dysenteriae and enterohemorrhagic strains of *Escherichia coli* (EHEC) produce the bacterial Shiga toxin and Shiga-like toxins (SLT), respectively (Johannes and Römer, 2010). Notably, SLTs of *E. coli* strain O157:H7 are responsible for pathological manifestations that can lead to hemolytic-uremic syndrome (HUS), the leading cause for pediatric renal failure in the world. These toxins are also a threat to adults as it became apparent in 2011, when an outbreak with *E. coli* strain O104:H4 in Germany and neighboring countries claimed dozens of adult victims, and thousands of adult patients who were hospitalized with severe symptoms. The most life-threatening extra-intestinal disease manifestations are renal failure and central nervous system complications. To date, no specific treatment options exist, and clinical management of HUS remains purely supportive (Tarr et al., 2005).

Shiga toxin and the SLTs are type 2 ribosome inactivating proteins (RIPII) with an AB₅ type of molecular structure. The catalytic A-subunit is responsible for the cleavage of an adenine base on position 4,324 of 28S ribosomal RNA (rRNA)(Endo et al., 1988; Saxena et al., 1989). It is non-covalently associated with a homopentameric B-subunit (STxB)(Fraser et al., 1994; Stein et al., 1992). STxB binds the cellular toxin receptor, a glycosylated lipid termed globotriaosylceramide (Gb3, or CD77), with 15 binding sites per STxB homopentamer (Ling et al., 1998). After receptor binding and clustering, Shiga toxin is internalized by clathrin-dependent (Sandvig et al., 1989) and independent (Römer et al., 2007) endocytosis. From early and maturing endosomes, the toxin is then transported via the retrograde route to the TGN (Mallard et al., 1998) and the endoplasmic reticulum (ER) (Sandvig et al., 1992), from where the catalytic A-subunit is translocated to the cytosol (Spooner and Lord, 2012).

Retrograde sorting of Shiga toxin on early and maturing endosomes has been extensively studied (Johannes and Popoff, 2008). Key players are clathrin (Lauvrak, 2004; Saint-Pol et al., 2004) and the retromer complex (Bujny et al., 2007; Popoff et al., 2007; Utskarpen et al., 2007). Furthermore, GPP130 was shown to be involved in retrograde transport of Shiga toxin and SLT1 (Mukhopadhyay and Linstedt, 2012), but not that of SLT2 (Mukhopadhyay et al., 2013).

Two Golgi-localized SNARE complexes have been identified to be involved in Shiga toxin trafficking: one composed of syntaxin-16, syntaxin-6 and Vti1, and VAMP4 (Mallard et al., 2002); and a second one composed of syntaxin-5 (STX5), GS28, Ykt6, and GS15 (Tai et al., 2004). How the activities of these SNARE complexes are articulated remains unexplored at this stage. Indeed, while VAMP4 is localized on early endosomes and clearly can function as a vSNARE for fusion of endosomal retrograde transport carriers with TGN membranes, the constituents of the STX5/GS28/Ykt6/GS15 complex are all Golgi-

localized only. STX5 has been described to cycle between the Golgi and the ER (Sengupta et al., 2015; Hui et al., 1997; Miyazaki et al., 2012), involving COPII vesicles for its anterograde transport (Mancias and Goldberg, 2008).

Small molecule inhibitors have been developed against Shiga toxin. The Retro compounds stand out as they have been shown to protect mice against the plant toxin ricin (Stechmann et al., 2010) and against SLT1 (Secher et al., 2015). Furthermore, these compounds have activities against pathogens as diverse as *Leishmania* species, Ebola, Marburg poxviruses, and Chlamydiales (Gupta et al., 2017). Retro-2 variants with improved activity were obtained in structure-activity relationship studies (Noel et al., 2013)(Gupta et al., 2014; Dai et al., 2017; Noel et al., 2013).

At the cellular level, Retro-2 leaves compartment morphology intact, but induces the redistribution of STX5 from the Golgi to the ER, and the accumulation of Shiga toxin in early endosomes (Stechmann et al., 2010). Whether and how these events are linked has remained unexplored.

In this study, we used biorthogonal click chemistry to identify Retro-2 interaction partners. The COPII component Sec16A came up as a prime candidate. Our data show that in agreement with an effect on Sec16A activity, Retro-2 treatment leads to a partial redistribution of STX5 to the ER by reducing the anterograde flow of STX5, and a concomitant loss of STX5 Interaction with GPP130. Furthermore, we demonstrate that interaction of STX5 with GPP130 is required for the latter to foster retrograde endosomes-to-Golgi trafficking of Shiga toxin. Thereby, we build a chain of arguments that link the presumed site of action of Retro-2 in the ER with the site of toxin accumulation in early endosomes of cells that are treated with this compound. Furthermore, we provide evidence for a non-SNAERE function of STX5 in interaction with GPP130.

11.1.4 Results

11.1.4.1 Retro-2 targets the COPII machinery.

The intercellular targets of Retro-2 remain unknown. A clickable version of Retro-2 (Figure 31 A) was incubated with HeLa cells for 30 min at 37°C, then bio-orthogonally reacted on cells with a biotin compound, and pull down with streptavidin-beads was performed after cell lysis. Analysis by mass spectrometry from 2 independent experiments revealed the COPII component Sec16A as the top hit (Figure 31 B). In another configuration of the experiment, the incubation with clickable Retro-2 was performed in the presence of a 5-fold molar excess of non-clickable Retro-2. Under these conditions, the Sec16A signal largely disappeared from the pull down (Figure 31 B), which confirmed the specificity of the finding. The result of a pull down of Sec16A with clickable Retro-2 was also confirmed by Western blotting (Figure 31 C). Interestingly, STX5 was not found amongst the presumed Retro-2 interacting partners, suggesting that its relocalization from the Golgi may be an indirect effect.

The clickable version of Retro-2 was then used for biorthogonal labeling with a fluorophore to document the intracellular distribution of the small molecule compound. Under control conditions (scrambled siRNA transfection), Retro-2 was localized to dotted perinuclear structures (Figure 31 D). Upon depletion of Sec16A, Retro-2-specific labeling was strongly diminished. The quantification of fluorescence intensities showed a highly significant reduction to $21.5 \pm 6.248\%$ on Sec16A-depleted cells (Figure 31 E), demonstrating that Sec16A expression was needed for Retro-2 binding to cells. Whether Retro-2 directly interacts with Sec16A needs to be further investigated.

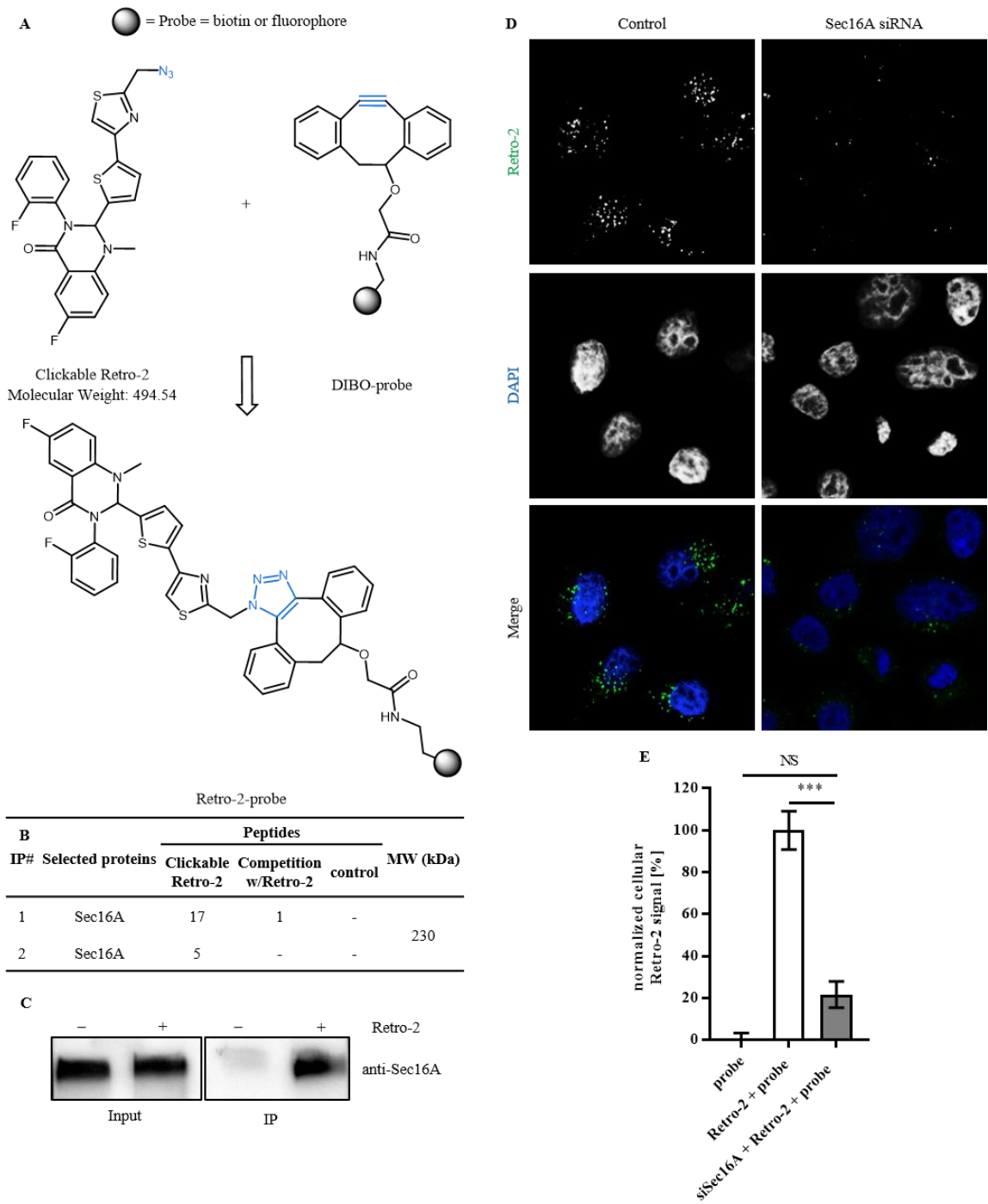


Figure 31: Sec16A is involved in Retro-2 binding on cells. (A) Scheme of biorthogonal Click chemistry adapted to Retro-2. The clickable Retro-2 probe, based on Retro-2.1 (Gupta et al., 2014) was coupled via a DIBO moiety to biotin, or a fluorophore. (B) In two independent pull-down experiments with the clickable Retro-2-biotin probe, Sec16A was identified as the top hit. When indicated, non-clickable Retro-2 was used in excess to compete with clickable Retro-2. DMSO without clickable Retro-2 was used as a control condition. (C) anti-Sec16A Western blots of a representative Retro-2 pull-down (with the clickable Retro-2-probe). Shown are bands on the level of the 250 kDa marker. (D) Confocal acquisitions of Click-staining of a Retro-2-fluorophore-probe on mock-siRNA treated cells (=control), or Sec16A-depleted cells (=Sec16A). DNA was stained with DAPI. (E) Quantification (~100 cells per condition) of the fluorescence intensity of the Retro-2-fluorophore-probe (normalized to 100 ± 9.118 %). The intensity of the fluorescence-probe only (=probe) was set to 0 % intensity. The intensity of Retro-2-fluorophore-probe upon Sec16A depletion resulted in 21.5 ± 6.248 % intensity. *** = <0.0001 .

11.1.4.2 Depletion of Sec16A phenocopies Retro-2 treatment

One of the salient phenotypes of Retro-2 treatment is the inhibition of retrograde transport of STxB between early endosomes and the TGN (Stechmann et al., 2010). We found here that the depletion of Sec16A also led to a retention of STxB in early endosomes of cells that were incubated with STxB for 45 min at 37°C (Figure 32 A). The effect was quantified by measuring the fluorescence signal of STxB within the Golgi region, as marked by anti-giantin immunolabeling, over total cellular STxB signal. This fraction was reduced to 71.17 ± 2.289 % upon Retro-2 treatment, to 60.54 ± 2.309 % upon Sec16A depletion and to 46.17 ± 1.683 % upon concomitant Retro-2 treatment and Sec16A depletion (Figure 32 B). After measuring Sec16A expression by Western blot, we could detect a significant but not complete depletion of the protein (reduction to $7\% \pm 2$). The apparently additive effects between Retro-2 treatment and Sec16A depletion might have originated from the fact that both inhibitions were partial. Alternatively, Sec16A depletion may affect additional intracellular functions that are not targeted when Sec16A activity is inhibited by Retro-2.

Retro-2 treatment also protects cells from intoxication by Shiga toxin (Stechmann et al., 2010), which is measured via the incorporation of radiolabeled methionine into neosynthesized proteins. Similar to Retro-2 treatment, depletion of Sec16A resulted in a 6.042-fold protection of cells (Figure 32 C), which indicated that the toxin reached membranes of the ER from where the catalytic A-subunit in translocated to the cytosol less efficiently.

Retro-2 finally induces the redistribution of STX5 to the ER (Stechmann et al., 2010). Here again, we found that this phenotype was reproduced upon Sec16A depletion. The fraction of STX5 in the Golgi area was determined as described above for STxB. When compared to control conditions, the fraction of Golgi localized STX5 was reduced to 33.11 ± 0.9788 % in Retro-2 treated cells, to 44.06 ± 2.739 % in Sec16A depleted cells, and to 31.49 ± 1.27 % under combined treatment conditions (Figure 33 A and B). The fact that Sec16A depletion did not increase the amplitude of redistribution of the Retro-2 treatment condition indicates that for STX5 localization, the small molecule inhibitor affects the full scope of Sec16A activities that are required for this phenotype.

Taken together, these findings support the idea that Sec16A is the direct or indirect target of Retro-2.

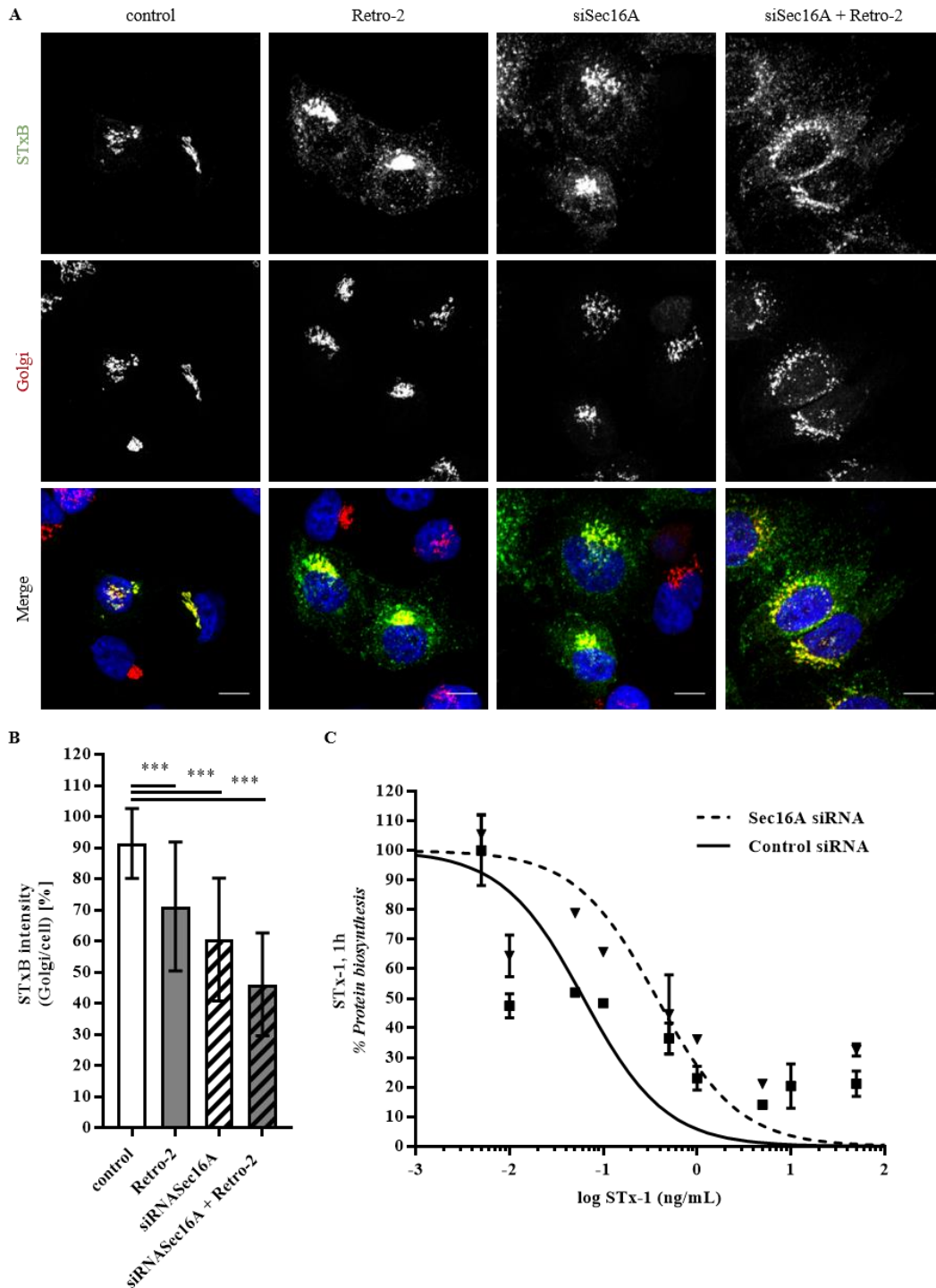
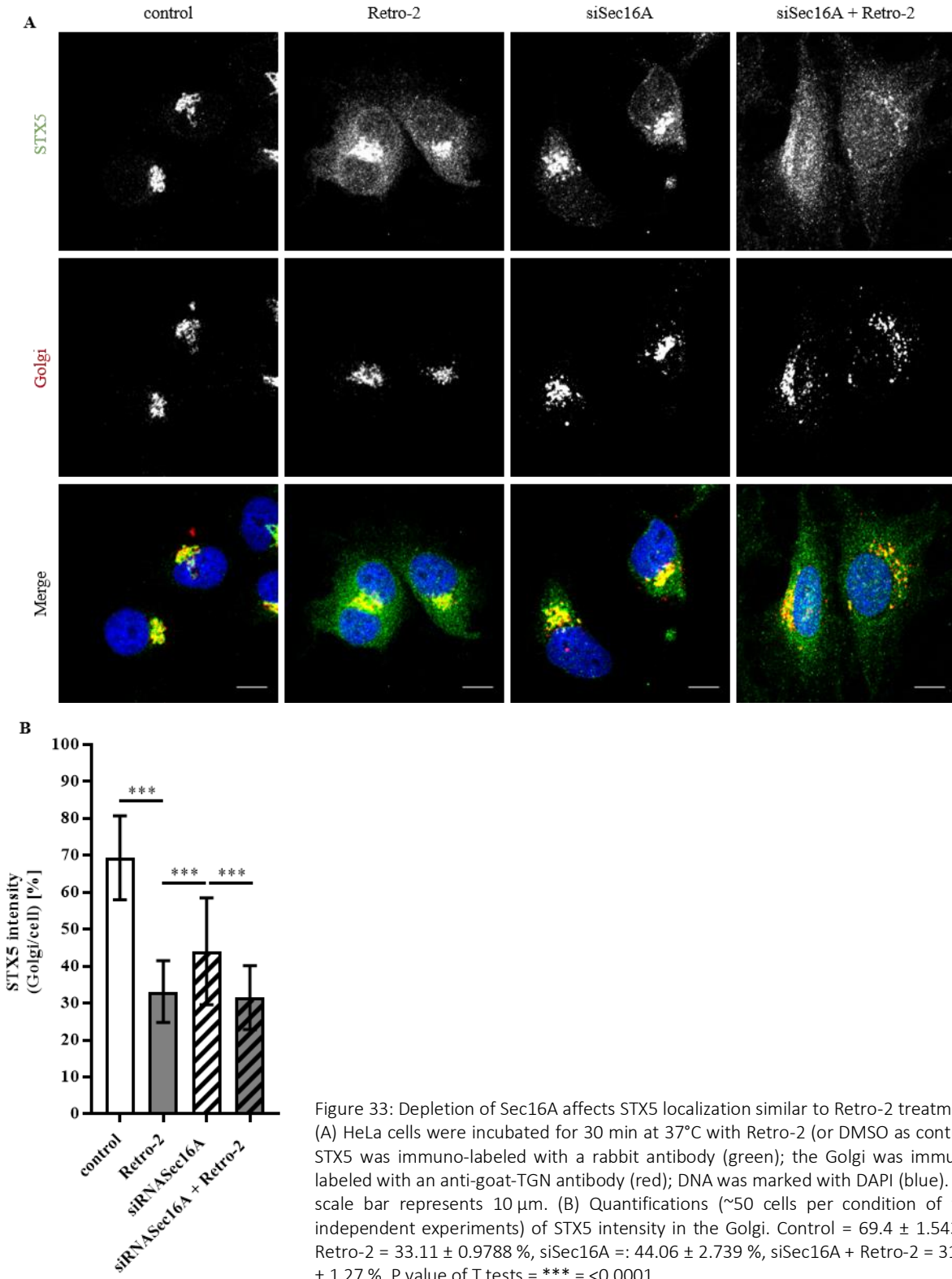


Figure 32: Depletion of Sec16A affects Shiga toxin trafficking similar to Retro-2 treatment. (A) HeLa cells were transfected for 72 hours with the indicated siRNAs (scrambled or against Sec16A). After 30 min of pre-incubation with Retro-2 (or DMSO for control), cells were incubated for another 45 minutes at 37°C with STxB-Cy3 (green). The Golgi was immuno-labeled with an anti-rabbit-Giantin antibody (red); DNA was marked with DAPI (blue). The scale bar represents 10 μ m. (B) Quantifications (~100 cells per condition of two independent experiments) of STxB-Cy3 intensity in the Golgi in the region indicated conditions. Control = 91.43 \pm 0.9767 %, Retro-2 = 71.17 \pm 2.289 %, siSec16A = 60.54 \pm 2.309 %, siSec16A + Retro-2 = 46.17 \pm 1.683 %. P

value of T tests = *** = <0.0001. (C) Intoxication of HeLa cells with STX1 in the indicated conditions. $EC50_{siControl} = 0.06178$ ng/ml, $EC50_{siSec16A} = 0.3733$ ng/ml, protection factor = 6.042-fold.



11.1.4.3 Retro-2 slows the anterograde transport of STX5

As part of the COPII machinery, Sec16A has functions in the biosynthetic/secretory transport of proteins out of the ER. To test whether Retro-2 affects the anterograde transport of STX5, we adapted the Retention Using Selective Hook (RUSH) approach (Boncompain et al., 2012) to this SNARE protein. For this, we fused STX5 to the streptavidin-binding peptide (SBP) and eGFP, and co-expressed a KDEL-core-streptavidin fusion protein, which operates the retention of STX5 in the ER. After addition of biotin, STX5 is released and resumes trafficking. TGN46 was used to define the Golgi in immunofluorescence experiments, and the fraction of STX5 (and other cargoes) in the Golgi was determined as described above. Following release in control conditions, more than 90 % of STX5 was found in the Golgi within 20 min of incubation at 37°C (Figure 34 A). Upon Retro-2 treatment, the amount of STX5 within the Golgi was reduced to 68.15 ± 5.298 % (Figure 34 B). In contrast, the anterograde trafficking of mannosidase II (ManII) (Figure 34 C and D), sialyltransferase (ST), and galactose-1-phosphate uridylyltransferase (GalT) (data not shown) was not affected by Retro-2 treatment.

These findings suggested that the redistribution of STX5 to the ER that is observed upon incubation of cells with Retro-2 results from a reduced rate of anterograde ER-to-Golgi transport. This effect appears to be specific for STX5, as 3 other endogenous cargoes (this study) and one heterologous (Stechmann et al., 2010) were not affected. The molecular reasons for this specificity remain unexplored at this stage. This specificity may explain, however, why Retro-2 is little toxic for cells and animals.

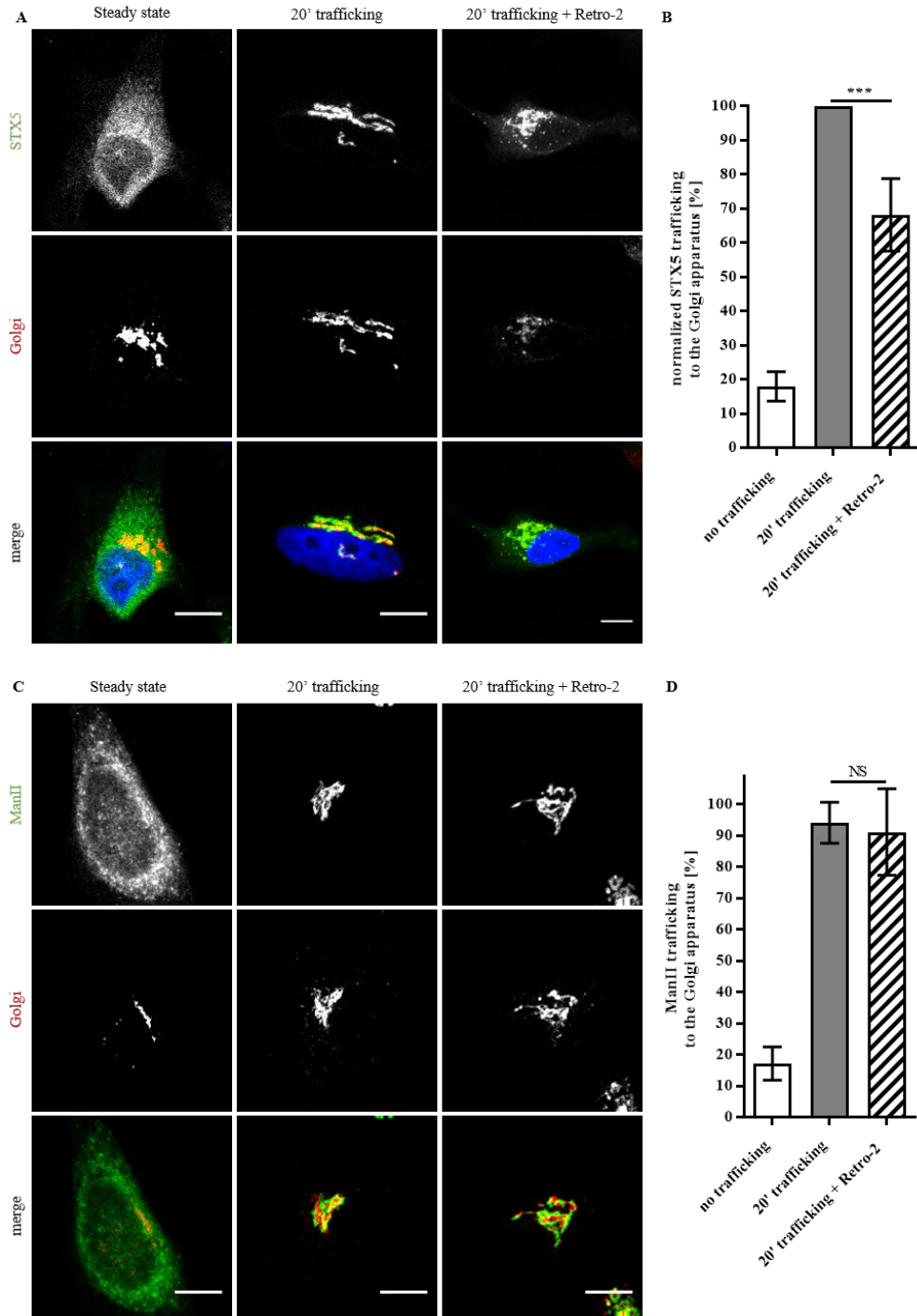


Figure 34: Retro-2 treatment slows the anterograde transport of STX5. (A) Confocal acquisitions of HeLa cells that expressed the STX5-RUSH construct. The cells were pre-treated for 60 min at 37°C with Retro-2, or DMSO as control (steady state). Trafficking was initiated upon addition of biotin, followed by incubation for 20 min at 37°C. STX5-GFP is shown in green; the Golgi (giantin) is shown in red; the scale bar represents 10 μ m. (B) Quantification (four independent experiments, 60 cells per experiment) of STX5-GFP intensity in the Golgi area. Steady state: 17.93 ± 2.494 %, 20 min release in control conditions: 100 %, 20 min release in the presence of Retro-2: 68.15 ± 5.298 %, P value of T tests = *** = 0.0010. (C) Trafficking of the ManII-RUSH construct (green) was analyzed as in (B). (D) Quantifications (\sim 50 cells per condition) of ManII-GFP intensity in the Golgi. Steady state: 17.15 ± 1.531 %, 20 min trafficking: 94.12 ± 1.967 %, 20 min trafficking + Retro-2: 91.18 ± 4.609 %, P value of T tests = NS = not significant.

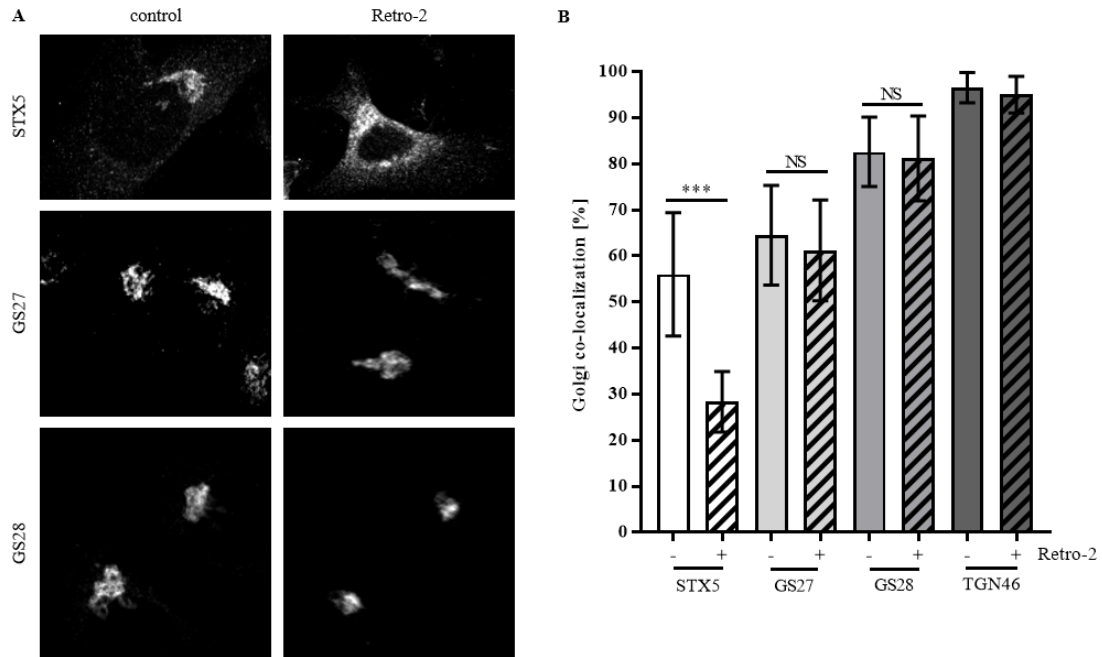
11.1.4.4 STX5 SNARE complexes remain unchanged upon Retro-2 treatment

STX5 forms two Golgi-localized SNARE complexes: STX5/GS27/Bet1/Sec22b at the cis-Golgi, and STX5/GS15/GS28/Ykt6 at medial-to-trans-Golgi (Xu, 2002; Chen and Scheller, 2001; Hong, 2005; Amessou et al., 2007). A function of the latter in endosomes-to-Golgi trafficking of Shiga toxin has been hypothesized (Tai et al., 2004). We therefore analyzed whether the SNARE partners of STX5 were relocalized upon Retro-2 treatment, as observed for STX5 itself. For this, immunolabeling of STX5, GS27, and GS28 in the Golgi area was determined, as described above. Remarkably, the Golgi fraction of GS27 and GS28 remained unaltered upon Retro-2 treatment, whereas the Golgi labeling of STX5 was reduced to half (Figure 35 A and B). Very clearly, the Retro-2 effect was limited to STX5.

We next analyzed the stability of the SNARE complexes involving STX5 in Retro-2 treated cells. HeLa cells were transfected with GFP-tagged STX5, and co-immunoprecipitated proteins were analyzed by mass spectrometry. The SNARE partners of STX5 were readily detected (Figure 35 C; SNARE partners are indicated by # and *). The treatment of cells with Retro-2 prior to immunoprecipitation did not affect the pull down of the SNARE partners (Figure 35 C), despite the redistribution of STX5 under these conditions (see above). This surprising result was confirmed by Western blotting for co-immunoprecipitated GS27 and GS28 (Figure 35 D). This surprising result was confirmed by Western blotting for co-immunoprecipitated GS27 and GS28 (Figure 35 D).

The Proximity Ligation Assays (PLA) was used as a further approach to sample for possible changes upon Retro-2 treatment in the proximity between STX5 and its SNARE partners GS27 or GS28. The number of dots per μm^2 was not affected by the small molecule drug (Figure 35 E-G), which provided another strong argument in favor of an unaltered formation of STX5 SNARE complexes under Retro-2 incubation conditions.

Several convergent lines of evidence thus suggested that despite the partial relocalization of STX5 to the ER, the formation of its SNARE complexes was not affected. It therefore appeared unlikely that the inhibition of retrograde transport of Shiga toxin from endosomes to the Golgi was due to an altered SNARE function.



C

Selected proteins	Peptides		MW [kDa]	Description
	Control	+Retro-2		
STX5 [#]	18	28	39,7	Syntaxin-5
GOSR1 [*]	5	8	28,6	GS28 (Golgi SNAP receptor complex member 1)
VTI1B	4	3	26,7	Vesicle transport through interaction with t-SNAREs homolog 1B
LG3BP	3	3	65,3	Galectin-3-binding protein
GOSR2	3	2	24,8	GS27 (Golgi SNAP receptor complex member 2)
BET1 [#]	2	2	13,3	BET1 homolog
VTI1A [#]	2	2	25,2	Vesicle transport through interaction with t-SNAREs homolog 1A
SC24A	1	1	119,8	Protein transport protein Sec24A
STX6	1	1	29,2	Syntaxin-6
YKT6 [*]	1	1	22,4	Synaptobrevin homolog YKT6
VAMP8	1	3	11,4	Vesicle-associated membrane protein 8

– STX5/GS27/Bet1/Sec22B – cis-Golgi SNARE * – STX5/GS15/GS28/Ykt6 – trans-Golgi SNARE

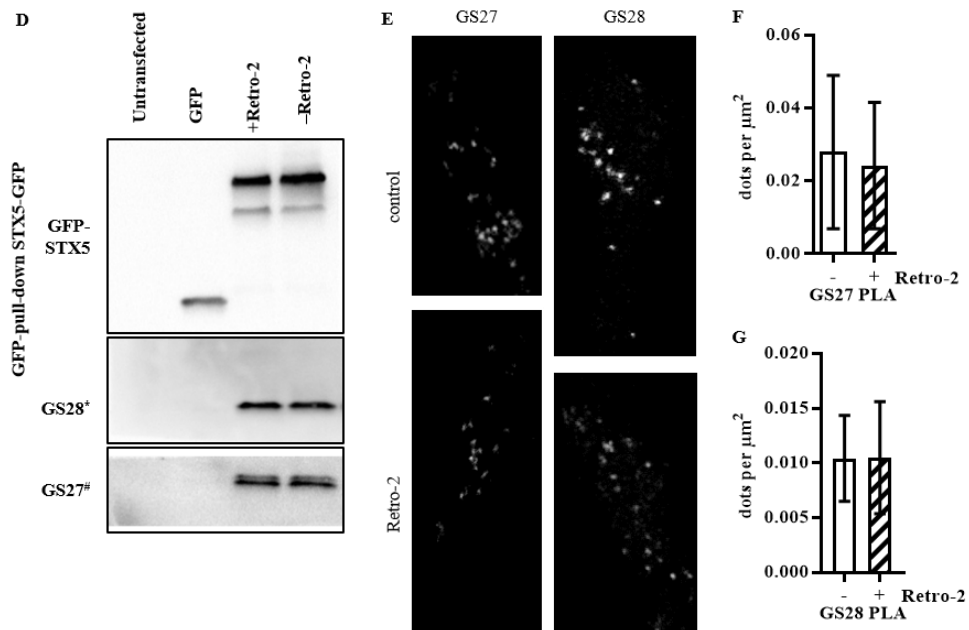


Figure 35 (previous page): STX5-SNARE complexes are not affected upon Retro-2 treatment. (A) Representative confocal acquisitions of the cellular distribution of STX5, GS27, and GS28 in either control (DMSO) or Retro-2 treated cells. (B) Quantification (~110 cells per condition) of Golgi-localized fluorescent signal of STX5, GS27, and GS28. TGN46 immunolabeling was used as a Golgi mask. STX5: 56 ± 1 %, STX5 + Retro-2: 28.32 ± 1.0 %, P value of T tests = *** = <0.0001 . GS27 = 64.47 ± 1.0 %, GS27 + Retro-2 = 61.18 ± 1.7 %, P value of T tests = NS = 0.09. GS28: 82.58 ± 0.9 %, GS28 + Retro-2: 81.14 ± 0.9 %, P value of T tests = NS = 0.2774. (C) Table for STX5 interacting proteins that are not competed for by Retro-2 treatment of cells. #-cis-Golgi STX5 SNARE complex proteins, *-trans-Golgi STX5 SNARE complex proteins. (D) anti-GFP, GS27 and GS28 Western blots of a representative eGFP-STX5 pull-down via GFP-trap beads. Controls were un-transfected cells or eGFP transfected cells. eGFP-STX5 cells were treated either with DMSO (control) or Retro-2. (D) anti-GFP, GS27 and GS28 Western blots of a representative eGFP-STX5 pull-down via GFP-trap beads. Controls were un-transfected cells or eGFP transfected cells. eGFP-STX5 cells were treated either with DMSO (control) or Retro-2. (E) Representative confocal acquisitions of STX5-PLA with either GS27 or GS28 upon DMSO (control) or Retro-2 treatment. One cell per picture is shown. (F) Quantification of PLA between STX5 and GS27. Number of dots were normalized by μm^2 . P value of T tests = NS = 0.4766 (G) Quantification of PLA between STX5 and GS28. Number of dots were normalized by μm^2 . P value of T tests = NS = 0.9543.

11.1.4.5 STX5 binds to GPP130 in a Retro-2 sensitive manner

Several proteins were identified that were lost from the list of STX5 interacting partners upon incubation of cells with Retro-2 (Figure 36 A). Three of these, TGN46, GP73 and GPP130, are proteins that have previously been shown to cycle between TGN, PM and endosomes (Reaves et al., 1993; Puri et al., 2002), and for GPP130, a function in Shiga toxin trafficking between endosomes and the TGN has been demonstrated (Mukhopadhyay and Linstedt, 2012; Natarajan and Linstedt, 2004). For GPP130, the interaction results obtained by mass spectrometry were confirmed by Western blotting, in which incubation with manganese that was shown previously to lead to GPP130 degradation in lysosomes (Mukhopadhyay and Linstedt, 2012), siRNA-mediated depletion of GPP130, or Retro-2 treatment led to the loss of GPP130 from immunoprecipitates with GFP-tagged STX5 (Figure 36 B).

STX5 has a luminal domain of only one amino acid. It therefore seemed likely that the interaction of STX5 with GPP130 occurred via the cytosolic domains of both proteins, which for GPP130 is of only 12 amino acids. To test this hypothesis, the GST-tagged cytosolic domain of GPP130 and the non-tagged cytosolic domain of STX5 (residues 202 to 355) were purified, and pull down assays were performed on glutathione beads. Proteins of the pull downs were quantified by Coomassie blue staining of SDS-PAGE gels (Figure 36 C). For GPP130, the KR_{11,12}AA mutant, an unrelated sequence from the cytosolic domain of the dipeptidyl peptidase-4 (DPPIV, also known as adenosine deaminase complexing protein 2, or CD26), and GST were included in this analysis. The dipeptidyl peptidase-4 domain is referred to as DGG. Wild-type GST-tagged cytosolic domain of GPP130 bound 30.5 ± 7.9 % of STX5 cytosolic domain that was present in the incubation, whereas only 2.6 ± 1.4 % of STX5 was pulled down on pure GST (negative control) (Figure 36 D). The pull down of STX5 cytosolic domain was equally inefficient on GST-tagged KR_{11,12}AA or DGG (DGG: 5.4 ± 1.2 % and KR_{11,12}AA: 4.8 ± 1.2 %, respectively).

It could be concluded that the interaction between GPP130 and STX5 is direct, efficient, and that it can be prevented by the KR_{11,12}AA mutation on GPP130. It was then tested whether this interaction was functionally required for Shiga toxin trafficking.

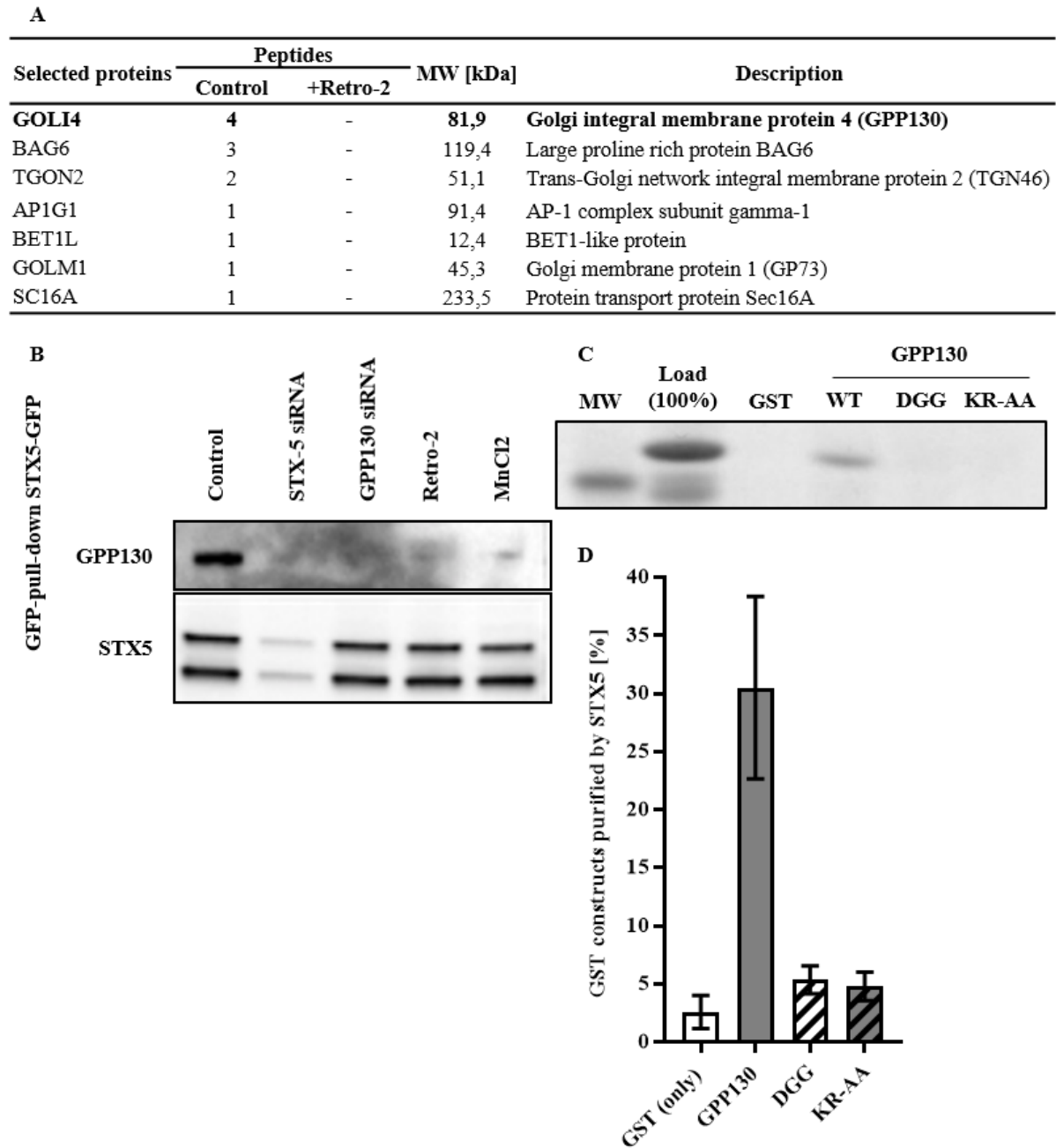


Figure 36: The cytosolic domain of GPP130 interacts with STX5. (A) Table of Retro-2-competed interacting proteins of STX5. (B) anti-GFP and GPP130 Western blots of a representative eGFP-STX5 pull-down via GFP-trap beads. Controls were untransfected cells or eGFP transfected cells. eGFP-STX5 cells were treated either with DMSO (control), Retro-2, siRNA against STX5, siRNA against GPP130, or manganese (leading to GPP130 degradation). (C) SDS-Page analysis of purified STX5 (residues 202-355). The indicated amount (Load) of purified STX5 was incubated with GST, GST-GPP130₁₋₁₀₈ (WT), GST- GPP130₁₋₁₀₈ with a substituted cytosolic domain from DPPIV (DGG), or GST- GPP130₁₋₁₀₈ with KR_{11,12}AA alanine substitution in the cytosolic domain. Anti-GST-beads were used to collect the complexes and after washing, recovery of STX5 (Bound) was determined by Coomassie staining of SDS-PAGE gels and (D) quantified (n=6±SD).

11.1.4.6 The GPP130-STX5 interaction is required for STxB trafficking to the Golgi

As described before (Natarajan and Linstedt, 2004), GPP130 expression is required for efficient intoxication of cells (Figure 37 A) and retrograde transport of STxB to the Golgi (Figure 37 B). To test for the importance of the interaction between GPP130 with STX5 for the retrograde transport function, GPP130 depleted cells were re-transfected with wild-type GPP130 or the KR_{11,12}AA mutant. Upon an incubation for 45 min at 37°C with HeLa cells, 86,4 ± 1,5 % of STxB reached the Golgi area under control conditions. GPP130 depletion reduced the presence of STxB in the Golgi area to 63.23 ± 2.475 % (Figure 37 B). Upon re-transfection of wild-type GPP130, this value went up to 83.23 ± 1.796 % again, indicating that GPP130 activity was efficiently rescued. In contrast, when the KR_{11,12}AA construct was expressed, only 57.08 ± 3.95 % of STxB was found in the Golgi area, which is similar to the GCC130 depletion condition. The KR_{11,12}AA thus failed to rescue GPP130 function in retrograde trafficking of STxB, indicating that the interaction with STX5 was important for this activity.

Monensin has been described to disperse trans-Golgi network determinants (Ledger et al., 1980) due to its ionophoric properties (Bergen and Bates, 1984; Mollenhauer et al., 1990). Upon monensin treatment, wild-type GPP130 and the KR_{11,12}AA mutant relocalized out of the Golgi into endosomal structures (Figure 37 C and D, middle panel). Upon washout of monensin, GPP130 is retrieved back to the Golgi. After three hours, wild-type GPP130 was mainly localized back in the Golgi, whereas the majority of the KR_{11,12}AA mutant population was still in endosomal or intermediate structures, showing that the retrieval was strongly delayed and that the cytosolic domain was physiologically involved in the proper distribution of GPP130 due to its binding capacities to STX5 (Figure 37 C and D, right panel). The STxB transport assay and the Golgi retrieval assay strongly implied the physiological importance of the GPP130-STX5 interaction for efficient retrograde STxB trafficking between endosomes and the Golgi, and for proper GPP130-distribution.

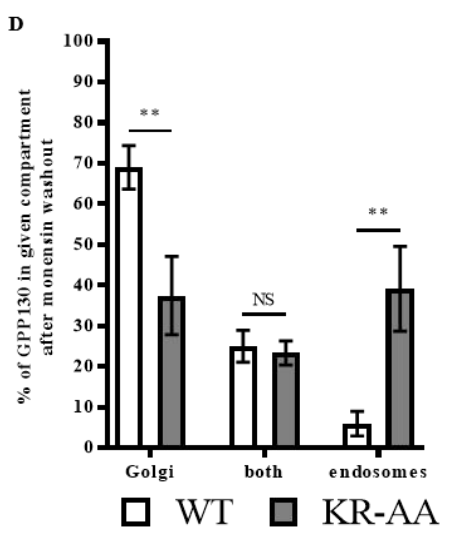
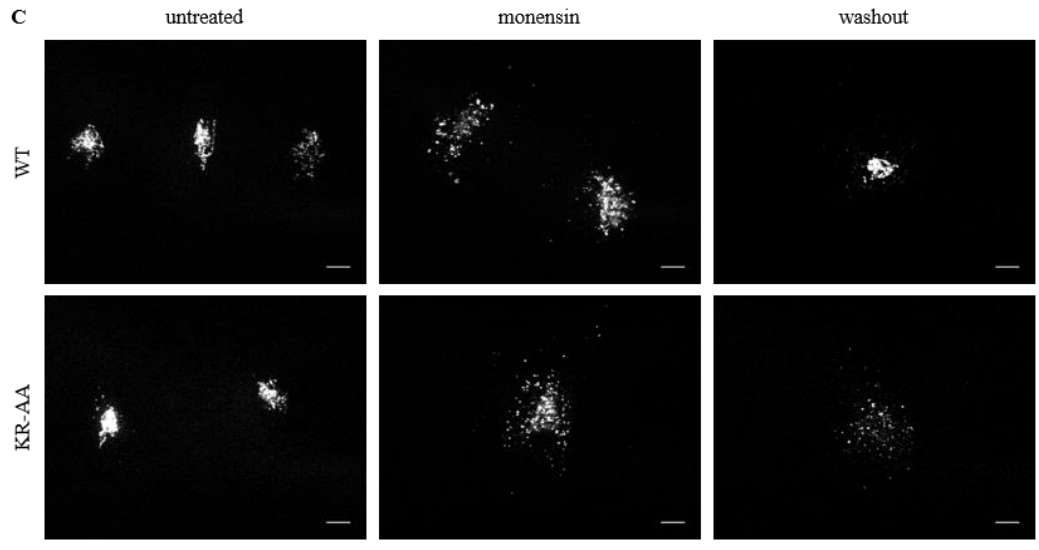
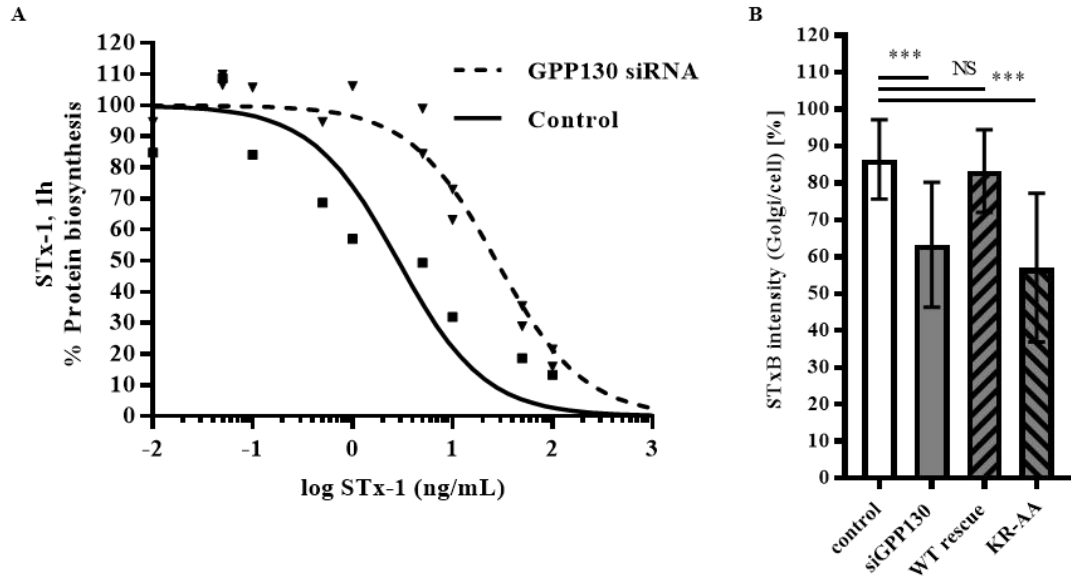


Figure 37 (previous page): STX5 binding site in GPP130 is required for its Golgi retrieval and Shiga toxin trafficking. (A) Protein neo-biosynthesis was measured via the incorporation of ³⁵S-radiolabeled methionine in function of increasing toxin concentration after one hour of STX1 intoxication. Cells were pretreated either with scrambled siRNA or siRNA against GPP130 72 hours before intoxication. EC50siControl = 2.851 ng/ml, EC50siGPP130 = 27.47 ng/ml, protection factor = 9.6352. (B) STxB-Cy3 trafficking. Quantifications (~50 cells per condition of two independent experiments) of STxB-Cy3 intensity in the Golgi region after 45 min. Control = scrambled siRNA: 86.39 ± 1.488 %, siGPP130: 63.23 ± 2.475 %, WT rescue after GPP130 depletion: 83.23 ± 1.796 %, KR-AA mutant retransfection after GPP130 depletion: 57.08 ± 3.95 %. P value of T tests = *** = <0.0001, NS = non-significant. (C) Representative acquisitions of (D). (D) Gene-edited cells lacking GPP130 were transfected with either HA-GPP130 (WT) or an identical construct with the KR_{11,12}AA alanine substitution (KR-AA) that blocks binding to STX5. The cells were then untreated, treated with monensin for 1 hour to redistribute GPP130 to endosomes, or monensin-treated and then subjected to a 3-hour washout incubation. Only the GPP130 staining is shown to localize the GPP130 constructs, but giantin staining of the same cells indicated the position of the Golgi. Quantification of the washout was carried out by counting cells with primarily Golgi-localized, a mix of Golgi- and endosome-localized, or primarily endosome-localized GPP130 (n=9±SEM, about 50 cells counted per experiment).. Shown is the cellular distribution of the re-transfected GPP130 constructs (WT or KR-AA) upon control = untreated (left column), monensin treatment (middle column), or monensin washout (right column). The scale bar represents 10 µm.

Table 3: supplementary information: Full mass-spectrometry tables of GFP-STX5 pulldown.

Selected proteins	PEPTIDES		MW (kDa)	Description
	CONTROL	+RETRO-2		
SCFD1_HUMAN	19	36	72.4	Sec1 family domain-containing protein 1
STX5_HUMAN	18	28	39.7	Syntaxin-5
SNP29_HUMAN	5	8	29.0	Synaptosomal-associated protein 29
VT11B_HUMAN	4	3	26.7	Vesicle transport through interaction with t-SNAREs homolog 1E
LG3BP_HUMAN	3	3	65.3	Galectin-3-binding protein
GOSR2_HUMAN	3	2	24.8	Golgi SNAP receptor complex member 2
BET1_HUMAN	2	2	13.3	BET1 homolog
VT11A_HUMAN	2	2	25.2	Vesicle transport through interaction with t-SNAREs homolog 1A
CLCB_HUMAN	1	1	25.2	Clathrin light chain B
LEG7_HUMAN	1	1	15.1	Galectin-7
MUCL1_HUMAN	1	1	9.0	Mucin-like protein 1
SC24A_HUMAN	1	1	119.8	Protein transport protein Sec24A
STX6_HUMAN	1	1	29.2	Syntaxin-6
STX8_HUMAN	1	1	26.9	Syntaxin-8
YKT6_HUMAN	1	1	22.4	Synaptobrevin homolog YKT6
VAMP8_HUMAN	1	3	11.4	Vesicle-associated membrane protein 8

Selected proteins	PEPTIDES		MW (kDa)	Description
	CONTROL	+RETRO-2		
GOLI4_HUMAN	4	-	81.9	Golgi integral membrane protein 4 (GPP130)
ARFG2_HUMAN	2	-	56.7	ADP-ribosylation factor GTPase-activating protein 2
FAK1_HUMAN	2	-	119.2	Focal adhesion kinase 1
TGON2_HUMAN	2	-	51.1	Trans-Golgi network integral membrane protein 2 (TGN46)
AP1G1_HUMAN	1	-	91.4	AP-1 complex subunit gamma-1
ARFG1_HUMAN	1	-	44.7	ADP-ribosylation factor GTPase-activating protein 1
BET1L_HUMAN	1	-	12.4	BET1-like protein
GOLM1_HUMAN	1	-	45.3	Golgi membrane protein 1 (GP73)
SC16A_HUMAN	1	-	233.5	Protein transport protein Sec16A

Selected proteins	PEPTIDES		MW (kDa)	Description
	CONTROL	+RETRO-2		
AKAP1_HUMAN	-	4	97.3	A-kinase anchor protein 1, mitochondrial
ATLA3_HUMAN	-	2	60.5	Atlastin-3
COG5_HUMAN	-	2	92.7	Conserved oligomeric Golgi complex subunit 5
AP3S2_HUMAN	-	1	22.0	AP-3 complex subunit sigma-2
ARF6_HUMAN	-	1	20.1	ADP-ribosylation factor 6
BIG1_HUMAN	-	1	208.8	Brefeldin A-inhibited guanine nucleotide-exchange protein 1
COG1_HUMAN	-	1	109.0	Conserved oligomeric Golgi complex subunit 1
COPG2_HUMAN	-	1	97.6	Coatomer subunit gamma-2
EPN4_HUMAN	-	1	68.3	Clathrin interactor 1
ERGI1_HUMAN	-	1	32.6	Endoplasmic reticulum-Golgi intermediate compartment protein 1
ERGI2_HUMAN	-	1	42.5	Endoplasmic reticulum-Golgi intermediate compartment protein 2
GOGA7_HUMAN	-	1	15.8	Golgin subfamily A member 7
HIP1R_HUMAN	-	1	119.4	Huntingtin-interacting protein 1-related protein
P4K2A_HUMAN	-	1	54.0	Phosphatidylinositol 4-kinase type 2-alpha
RAB12_HUMAN	-	1	27.2	Ras-related protein Rab-12
RAB32_HUMAN	-	1	25.0	Ras-related protein Rab-32
RAB35_HUMAN	-	1	23.0	Ras-related protein Rab-35
SC61G_HUMAN	-	1	7.7	Protein transport protein Sec61 subunit gamma
SHLB2_HUMAN	-	1	44.0	Endophilin-B2
SNX3_HUMAN	-	1	18.8	Sorting nexin-3
STX12_HUMAN	-	1	31.6	Syntaxin-12
STX3_HUMAN	-	1	33.2	Syntaxin-3
STXB1_HUMAN	-	1	67.6	Syntaxin-binding protein 1

11.1.5 Discussion

Studies in mice have shown that the small molecule inhibitor Retro-2 protects against the plant toxin ricin (Stechmann et al., 2010) and the bacterial Shiga-like toxins (Secher et al., 2015). The molecular mechanism of action of the compound had remained unknown. Here we provide evidence for the COPII component Sec16A as a likely target of Retro-2. Sec16A function in the anterograde transport of the Golgi SNARE protein syntaxin 5 (STX5) appears to be disturbed by Retro-2, thereby leading to partial relocalization of the SNARE to the ER. Concomitantly with this relocalization, the interaction of STX5 with the endosomal cycling protein GPP130 is lost. Our functional interaction data strongly suggest that this STX5-GPP130 interaction is required for efficient Shiga toxin trafficking from endosomes to the Golgi. This chain of events provides a solid model on how Retro-2 causes a toxin trafficking block at the levels of endosomes, and provides a fresh perspective on a possible non-SNARE function of STX5 in interaction with GPP130.

Based on structural arguments, it has been predicted that STX5 binds the COPII component Sec24 (Mossessova et al., 2003a). Since the Sec23/Sec24 dimer interacts with Sec16A in the progress of COPII vesicle formation (Whittle and Schwartz, 2010), it might be speculated that Retro-2 interferes with COPII vesicle formation. The fact that from the different anterograde cargoes that we have analyzed, only STX5 was affected points to the possibility that such interfering effect would be cargo specific. The multi-domain nature of Sec16A might be compatible with the hypothesis of cargo-specific functions (Campbell and Schekman, 1997).

Our initial hypothesis was that STX5 itself would be the target of Retro-2, and that Retro-2's effect on Shiga toxin trafficking would come from the perturbation of the SNARE function of this molecule. It was therefore a surprise when several convergent lines of evidence demonstrated that the integrity of STX5 SNARE complexes was not affected. At first sight, these findings on unperturbed SNARE complex formation appear to be in contradiction with the 50 % reduction of STX5 labeling to the Golgi area of Retro-2-treated cells. However, some STX5 still remains present in the Golgi, and these remaining levels are likely sufficient to maintain SNARE activity.

The interaction between STX5 and the Golgi-plasma membrane-endosomes cycling proteins TGN46, GPP130, and GP73 represents another discovery of our study. For GPP130, a function in Shiga toxin trafficking has clearly been established (Natarajan and Linstedt, 2004; Mukhopadhyay and Linstedt, 2012), which is quite exciting in the context of the current study. Whether also TGN46 and GP73 are

trafficking chaperons remains to be tested directly. For TGN46, a function in anterograde trafficking of $\alpha 5\beta 1$ integrin from the Golgi to the plasma membrane has been suggested (Wang and Howell, 2000).

At this stage, by which mechanism(s) the interaction between STX5 and GPP130 translates into function remains unknown. Since binding occurs at the level of the cytosolic domains, one might invoke some type of trans-interaction. Yet, a role as tethering factors appears unlikely when one considers the short length of GPP130's cytosolic domain. More work needs to be done to elucidate this aspect. It is not clear either why Retro-2-induced STX5 relocalization leads to a loss of the SNARE's interaction with GPP130. Most likely, STX5 is depleted from the trans-most cisternae of the Golgi upon Retro-2 treatment, where TGN46, GPP130, and GP73 are trafficking back and forth between plasma membrane and endosomes.

In conclusion, the current study breaks new ground for the investigation of the Retro-2 effect on cells, and suggests a non-SNARE function for STX5 in interaction with GPP130. Further mechanistic details will need to be worked out in future studies.

11.2 THE EFFECT OF miR199 ON RETROGRADE SHIGA TOXIN TRAFFICKING

11.2.1 Objectives and summary.

The data that are presented below contributed to a study in collaboration with Juan F. Aranda in the group of Carlos Fernández-Hernando at Yale University School of Medicine in New Haven, Connecticut, USA. My work addressed the role of the miR199 in the retrograde trafficking of STxB upon miR199 treatment. A manuscript is currently in revision at Molecular and Cell Biology (MCB).

Retrograde transport allows the retrieval of receptors and other cellular cargoes to the Golgi contributing to the maintenance of cellular homeostasis. This transport route is also commonly used by several bacterial toxins to exert their deleterious actions on eukaryotic cells. While the retrograde transport process has been well characterized, the contribution of microRNAs (miRNAs) in regulating this cellular transport mechanism remains poorly explored. Here, we found that the intronic miRNA family, miR199, coordinate genes regulating retrograde transport and endosome trafficking. In particular, we demonstrate that miR199 attenuates the expression of the retromer component VPS26, the GTPase Rab9B and the shuttling receptor M6PR, thereby controlling retrograde transport from endosomes to Trans Golgi network (TGN). Importantly, we found that overexpression of a VPS26 construct that is resistant to the miRNA action abolish the effect of miR199 on retrograde trafficking. Finally, we demonstrate that miR199 transfection attenuates STxB-mediated inhibition of protein biosynthesis. In summary, our work identifies the first non-coding RNA that influences retrograde trafficking and suppresses the cytotoxicity caused by bacterial toxins.

11.2.2 Results

11.2.2.1 MiR199 down regulates retromer expression

In the submitted paper, our collaborator showed that the miR199 family targets the expression of VPS26, Rab9B and M6PR. For reproduction of the results obtained by our collaborators and as a surrogate control for the fact that my experimental observations were due to the miR199 treatment, I measured by Western blotting the expression of the retromer compartment VPS26. Indeed, miR199 successfully downregulated VPS26, as shown in Figure 38.

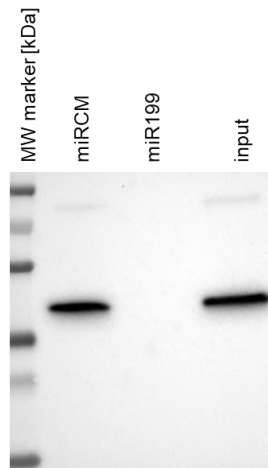


Figure 38: Western blot against VPS26. Loading from left to right: molecular weight marker (top to bottom in kDa: 100, 75, 55, 35, 25, 15), scrambled miR transfected cells (miRCM), miR199 transfected cells, cell lysate (input). Expected size: 38 kDa.

11.2.2.2 MiR199 impairs retrograde transport of STxB

As part of the retromer, VPS26 has been previously reported to be involved in retrograde trafficking of Shiga toxin (Popoff et al., 2007) (read more in chapter 9.2.5.3). To test whether miR199 regulates the retrograde transport route, STxB-Cy3 trafficking was measured for 45 min at 37°C in scrambled and miR199 transfected HeLa cells by determining the fraction of STxB in the Golgi area over the total cell-associated STxB signal (see section 10.8 for the method).

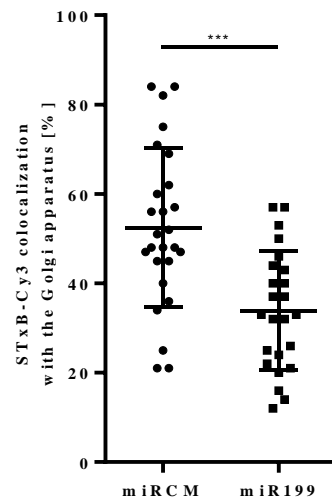


Figure 39: Quantification STxB-Cy3 trafficking in mock or miR199-treated cells. Quantifications (~25 cells per condition) of STxB-Cy3 intensity in the Golgi region after 45 min of incubation. miRCM = scrambled miR: 52.46 ± 3.489 , and miR199 treatment: 33.92 ± 2.713 . Shown is the mean and the SD. P value of T tests = *** = <0.0001 .

As shown in Figure 39, STxB was efficiently internalized after 45 min at 37°C of incubation under control conditions. However, its accumulation in the Golgi was significantly reduced by 1.56-fold in miR199 treated cells. By co-labeling with EEA1, our collaborator has shown that STxB remained in EE under these conditions (see (Aranda et al., 2017), Annex chapter 15.1.2, from page D).

11.2.2.3 MiR199 inhibits SLT intoxication.

Given that miR199 inhibited STxB trafficking to the Golgi, I further tested whether miR199 protected cells against SLT intoxication. Protein biosynthesis was measured as described in Section 10.12 via the incorporation of [³⁵S]-labeled methionine into neosynthesized proteins. In miR199-transfected cells, significant more toxin was needed to obtain the same level of protein biosynthesis inhibition, which indicated that the cells were partially protected (Figure 40). The protection factors observed on miR199-transfected or VPS26-depleted cells were similar (Figure 41), in agreement with the effect of miR199 on VPS26 expression. These results clearly are consistent with the hypothesis that miR199 regulates retrograde transport.

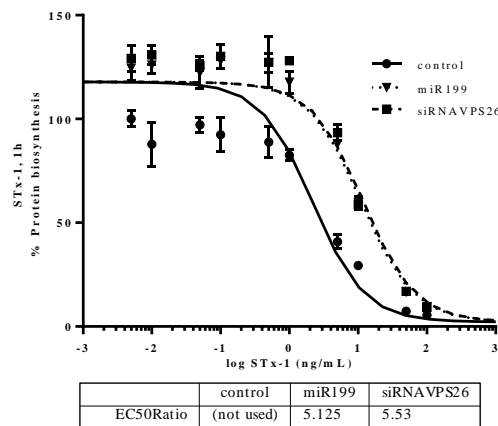


Figure 40: Representative intoxication curves upon STx1 treatment. Points = control = scrambled miR, triangles = miR199, cubes = siRNAVPS26, protection factors are shown in Figure 39.

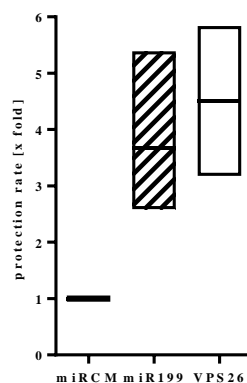


Figure 41: Quantifications of 3 independent STx1 intoxication experiments. Shown are protection factors. Control = scrambled miR: 1-fold protection, miR199: 3.68 ± 0.8648 fold protection and siRNAVPS26 treatment: 4.507 ± 1.329 fold protection. The difference between miR199 and siRNAVPS26 was not significant ($P = 0.6181$)

12 DISCUSSION

After identifying Sec16A as the likely cellular target of Retro-2 (chapter 11.1.4.1), we showed that cells lacking Sec16A exhibited similar phenotypes than Retro-2-treated cells, such as STX5 relocalization out of the Golgi, and inhibition of retrograde STxB-Cy3 trafficking to the Golgi and intoxication of cells by STX1 (chapter 11.1.4.2). In a chemical biology approach, we used biorthogonal click chemistry in combination with optimized small molecules to determine drug targets and localization, similar to previously studies (Rodriguez and Miller, 2014; Bagert et al., 2014; Mai et al., 2017).

By targeting Sec16A, Retro-2 slows down STX5 anterograde trafficking to the Golgi (chapter 11.1.4.3), explaining its delocalization out of the Golgi, likely due to dis-equilibrated anterograde and retrograde trafficking rates (Miles et al., 2001; Ward et al., 2001; Sengupta et al., 2015). Unexpectedly, Retro-2 specifically affects the anterograde transport of only STX5, and not of ManII, ST, or GalT. This stresses the need for further examination of the mechanism by which Retro-2 affects the activity of Sec16A. Since STX5 has a putative binding sequence for Sec24 (Mossessova et al., 2003a), and Sce23/Sec24 interacts with Sec16A, Retro-2 might interfere with either COPII vesicle formation or prevent COPII vesicle release (Sprangers and Rabouille, 2015). How cargo specificity is achieved in this context remains to be determined.

Several novel STX5 interacting proteins were found in our experiments: TGN38/46 (Luzio et al., 1990; Puri et al., 2002; Reaves et al., 1992), GP73 (Puri et al., 2002; Bachert et al., 2007) and GPP130 (Linstedt et al., 1997; Natarajan and Linstedt, 2004). These have all been shown to cycle between Golgi, PM, and endosomes. GPP130 has been already described in SLT trafficking and has been suggested as a intracellular receptor of Shiga toxin (Mukhopadhyay et al., 2013). Here, we provide direct evidence that STX5 and GPP130 directly interact with each other via their cytosolic domains (chapter 11.1.4.5). Whether this mechanism extends the number of retrograde trafficking routes between endosomes and the Golgi, or whether the GPP130-STX5 interaction is part of the various described routes (Johannes and Wunder, 2011b), remains to be further analyzed.

Regarding the miR199 study, our data confirm the importance of retromer in the retrograde transport of SLTs. Our collaborators' findings identified miR199 as a novel regulator of retrograde trafficking. miR199 regulates the expression of proteins that are involved in retrograde transport, such as VPS26 and Rab9, and cargoes such as M6PR. Mechanistically, we demonstrate that miR199 influences SLT trafficking by downregulating Vps26. These findings might point at an endogenous protection

mechanism against bacterial, viral and/or other pathogens that use the retrograde route to enter into cells. Future studies will clarify whether miR199 also acts against other pathogens (McGourty et al., 2012). Whether miR199 interferes with the trafficking of GPP130 to the Golgi not been addressed yet.

While our study establishes miR199 as a novel regulator of the retrograde route, further experiments will be important to elucidate the molecular mechanism that controls the endogenous expression of miR199.

13 PERSPECTIVES

Together with the Raposo team in UMR144, we are addressing the question to which compartment(s) STX5 exactly relocates upon Retro-2 treatment (ER, cis/medial/trans-Golgi...). High pressure freezing (HPF) correlative light and electron microscopy (CLEM) is used to address this question on eGFP-STX5 expressing cells. The comparison of mock and Retro-2-treated cells should reveal changes in the localization of STX5, and possible changes in compartment structures, as previously published for other experimental systems (Delevoe et al., 2016).

Furthermore, we are in the process of studying COPII dynamics. Together with Alison Forrester (post-doc in our team, previously at the TIGEM, Italy) and the Nikon imaging facility at the Curie Institute, live cell imaging of GFP-Sec23 recruitment and release within living cells shall allow us to test whether Retro-2 perturbs COPII kinetics.

With the group of Daniel Gillet (CEA, France), we follow up on the purification of fragments of Sec16A. A crystal structure would help in proving Retro-2 binding to Sec16A, and would allow to further improve the chemical development of next generation inhibitors based on structure guided design. Thus far, Sec16A has not been purified from mammalian sources. A co-crystal has been published of Sec13 with a Sec16 fragment from yeast (Whittle and Schwartz, 2010).

Until now, only Shiga toxin has been identified as a cargo of GPP130. In collaboration with Adam Linstedt's group (Pittsburgh, USA), we are exploring the possible existence of endogenous Sec16A interacting partner, and their dependency on the GPP130-STX5 interaction for retrograde trafficking.

14 REFERENCES

- Acosta, E.G., V. Castilla, and E.B. Damonte. 2012. Differential Requirements in Endocytic Trafficking for Penetration of Dengue Virus. *PLoS One*. 7. doi:10.1371/journal.pone.0044835.
- Agard, N.J., J.A. Prescher, and C.R. Bertozzi. 2004. A strain-promoted [3 + 2] azide-alkyne cycloaddition for covalent modification of biomolecules in living systems. *J. Am. Chem. Soc.* 126:15046–15047. doi:10.1021/ja044996f.
- Agger, M., F. Scheutz, S. Villumsen, K. Mølbak, and A.M. Petersen. 2015. Antibiotic treatment of verocytotoxin-producing *Escherichia coli* (VTEC) infection: a systematic review and a proposal. *J. Antimicrob. Chemother.* 70:2440–2446. doi:10.1093/jac/dkv162.
- Ambros, V. 2004. The functions of animal microRNAs. *Nature*. 431:350–355. doi:10.1038/nature02871.
- Amessou, M., A. Fradagrada, T. Falguieres, J.M. Lord, D.C. Smith, L.M. Roberts, C. Lamaze, and L. Johannes. 2007. Syntaxin 16 and syntaxin 5 are required for efficient retrograde transport of several exogenous and endogenous cargo proteins. *J. Cell Sci.* 120:1457–1468. doi:10.1242/jcs.03436.
- Antonin, W., D. Fasshauer, S. Becker, R. Jahn, and T.R. Schneider. 2002. Crystal structure of the endosomal SNARE complex reveals common structural principles of all SNAREs. *Nat. Struct. Biol.* 9:107–111. doi:10.1038/nsb746.
- Antonny, B., D. Madden, S. Hamamoto, L. Orci, and R. Schekman. 2001. Dynamics of the COPII coat with GTP and stable analogues. *Nat Cell Biol.* 3:531–537. doi:10.1038/35078500.
- Aranda, J.F., A. Canfran-Duque, L. Goedeke, Y. Suarez, and C. Fernandez-Hernando. 2015. The miR-199-dynamin regulatory axis controls receptor-mediated endocytosis. *J. Cell Sci.* 128:3197–3209. doi:10.1242/jcs.165233.
- Aranda, J.F., S.J. Rathjen, L. Johannes, and C. Fernández-Hernando. 2017. MiR-199a-5p attenuates retrograde transport and protects against Shiga toxin cytotoxicity. *EMBO*.
- Arce, A., A. Estirado, M. Ordobas, S. Sevilla, N. García, L. Moratilla, S. de la Fuente, A.M. Martínez, A.M. Pérez, E. Aránguez, A. Iriso, O. Sevillano, J. Bernal, and F. Vilas. 2013. Re-emergence of Leishmaniasis in Spain: Community outbreak in Madrid, Spain, 2009 TO 2012. *Eurosurveillance*. 18:20546. doi:10.2807/1560-7917.ES2013.18.30.20546.
- Bachert, C., C. Fimmel, and A.D. Linstedt. 2007. Endosomal trafficking and proprotein convertase cleavage of cis Golgi protein GP73 produces marker for hepatocellular carcinoma. *Traffic*. 8:1415–1423. doi:10.1111/j.1600-0854.2007.00621.x.
- Bachert, C., T.H. Lee, and A.D. Linstedt. 2001. Lumenal endosomal and Golgi-retrieval determinants involved in pH-sensitive targeting of an early Golgi protein. *Mol. Biol. Cell*. 12:3152–60.
- Bagert, J.D., Y.J. Xie, M.J. Sweredoski, Y. Qi, S. Hess, E.M. Schuman, and D.A. Tirrell. 2014. Quantitative, Time-Resolved Proteomic Analysis by Combining Bioorthogonal Noncanonical Amino Acid Tagging and Pulsed Stable Isotope Labeling by Amino Acids in Cell Culture. *Mol. Cell. Proteomics*. 13:1352–1358. doi:10.1074/mcp.M113.031914.
- Bannykh, S.I., T. Rowe, and W.E. Balch. 1996. The organization of endoplasmic reticulum export complexes. *J. Cell Biol.* 135:19–35. doi:10.1083/jcb.135.1.19.
- Barbier, J., C. Bouclier, L. Johannes, and D. Gillet. 2012. Inhibitors of the cellular trafficking of ricin. *Toxins (Basel)*. 4:15–27. doi:10.3390/toxins4010015.
- Barbieri, L., M.G. Battelli, and F. Stirpe. 1993. Ribosome-inactivating proteins from plants. *BBA - Rev. Biomembr.* 1154:237–282. doi:10.1016/0304-4157(93)90002-6.
- Bartel, D.P. 2009. MicroRNAs: Target Recognition and Regulatory Functions. *Cell*. 136:215–233. doi:10.1016/j.cell.2009.01.002.

- Baskin, J.M., J.A. Prescher, S.T. Laughlin, N.J. Agard, P. V. Chang, I.A. Miller, A. Lo, J.A. Codelli, and C.R. Bertozzi. 2007. Copper-free click chemistry for dynamic in vivo imaging. *Proc. Natl. Acad. Sci.* 104:16793–16797. doi:10.1073/pnas.0707090104.
- Bausch, D.G., S.T. Nichol, J.J. Muyembe-Tamfum, M. Borchert, P.E. Rollin, H. Sleurs, P. Campbell, F.K. Tshioko, C. Roth, R. Colebunders, P. Pirard, S. Mardel, L. a Olinda, H. Zeller, A. Tshomba, A. Kulidri, M.L. Libande, S. Mulangu, P. Formenty, T. Grein, H. Leirs, L. Braack, T. Ksiazek, S. Zaki, M.D. Bowen, S.B. Smit, P. a Leman, F.J. Burt, A. Kemp, and R. Swanepoel. 2006. Marburg Hemorrhagic Fever Associated with Multiple Genetic Lineages of Virus. *N. Engl. J. Med.* 355:909–919. doi:10.1056/NEJMoa051465.
- Beard, P.M., S.J. Griffiths, O. Gonzalez, I.R. Haga, T.P. Jowers, D.K. Reynolds, J. Wildenhain, H. Tekotte, M. Auer, M. Tyers, P. Ghazal, R. Zimmer, and J. Haas. 2014. A loss of function analysis of host factors influencing Vaccinia virus replication by RNA interference. *PLoS One.* 9. doi:10.1371/journal.pone.0098431.
- Bekerman, E., and S. Einav. 2015. Combating emerging viral threats. *Science (80-.).* 348:282–283. doi:10.1126/science.aaa3778.
- Bergen, W.G., and D.B. Bates. 1984. Ionophores: their effect on production efficiency and mode of action. *J. Anim. Sci.* 58:1465–1483.
- Bharucha, N., Y. Liu, E. Papanikou, C. McMahon, M. Esaki, P.D. Jeffrey, F.M. Hughson, and B.S. Glick. 2013. Sec16 influences transitional ER sites by regulating rather than organizing COPII. *Mol. Biol. Cell.* 24:3406–3419. doi:10.1091/mbc.E13-04-0185.
- Bhattacharyya, D., and B.S. Glick. 2007. Two Mammalian Sec16 Homologues Have Nonredundant Functions in Endoplasmic Reticulum (ER) Export and Transitional ER Organization. *Mol. Biol. Cell.* 18:839–849. doi:10.1091/mbc.E06-08-0707.
- Bi, X., R.A. Corpina, and J. Goldberg. 2002. Structure of the Sec23/24–Sar1 pre-budding complex of the COPII vesicle coat. *Nature.* 419:271–277. doi:10.1038/nature01040.
- Boal, F., L. Guetzoyan, R.B. Sessions, M. Zeghouf, R.A. Spooner, J.M. Lord, J. Cherfils, G.J. Clarkson, L.M. Roberts, and D.J. Stephens. 2010. LG186: An Inhibitor of GBF1 Function that Causes Golgi Disassembly in Human and Canine Cells. *Traffic.* 11:1537–1551. doi:10.1111/j.1600-0854.2010.01122.x.
- Boehm, M., and J.S. Bonifacino. 2001. Adaptins: the final recount. *Mol. Biol. Cell.* 12:2907–2920. doi:10.1091/mbc.12.10.2907.
- Boll, W., A. Gallusser, and T. Kirchhausen. 1995. Role of the regulatory domain of the EGF-receptor cytoplasmic tail in selective binding of the clathrin-associated complex AP-2. *Curr. Biol.* 5:1168–1178. doi:10.1016/S0960-9822(95)00233-8.
- Boncompain, G., S. Divoux, N. Gareil, H. de Forges, A. Lescure, L. Latreche, V. Mercanti, F. Jollivet, G. Raposo, and F. Perez. 2012. Synchronization of secretory protein traffic in populations of cells. *Nat. Methods.* 9:493–498. doi:10.1038/nmeth.1928.
- Bonfanti, L., A.A. Mironov, J.A. Martínez-Menárguez, O. Martella, A. Fusella, M. Baldassarre, R. Buccione, H.J. Geuze, A.A. Mironov, and A. Luini. 1998. Procollagen traverses the Golgi stack without leaving the lumen of cisternae: Evidence for cisternal maturation. *Cell.* 95:993–1003. doi:10.1016/S0092-8674(00)81723-7.
- Bonifacino, J.S., and B.S. Glick. 2004. The Mechanisms of Vesicle Budding and Fusion. *Cell.* 116:153–166. doi:10.1016/S0092-8674(03)01079-1.
- Bonifacino, J.S., and R. Rojas. 2006. Retrograde transport from endosomes to the trans-Golgi network. *Nat. Rev. Mol. Cell Biol.* 7:568–579. doi:10.1038/nrm1985.
- Brunger, A.T., and B. DeLaBarre. 2003. NSF and p97/VCP: Similar at first, different at last. *FEBS Lett.* 555:126–133. doi:10.1016/S0014-5793(03)01107-4.
- Budnik, A., K.J. Heesom, and D.J. Stephens. 2011. Characterization of human Sec16B: indications of specialized, non-redundant functions. *Sci. Rep.* 1:77. doi:10.1038/srep00077.
- Bujny, M. V., V. Popoff, L. Johannes, and P.J. Cullen. 2007. The retromer component sorting nexin-1 is required for efficient retrograde

- transport of Shiga toxin from early endosome to the trans Golgi network. *J. Cell Sci.* 120:2010–2021. doi:10.1242/jcs.003111.
- Burd, C.G. 2011. Physiology and pathology of endosome-to-Golgi retrograde sorting. *Traffic.* 12:948–955. doi:10.1111/j.1600-0854.2011.01188.x.
- Burgos, P. V., G.A. Mardones, A.L. Rojas, L.L.P. daSilva, Y. Prabhu, J.H. Hurley, and J.S. Bonifacino. 2010. Sorting of the Alzheimer's Disease Amyloid Precursor Protein Mediated by the AP-4 Complex. *Dev. Cell.* 18:425–436. doi:10.1016/j.devcel.2010.01.015.
- Bushati, N., and S.M. Cohen. 2007. microRNA Functions. *Annu. Rev. Cell Dev. Biol.* 23:175–205. doi:10.1146/annurev.cellbio.23.090506.123406.
- Campbell, J.L., and R. Schekman. 1997. Selective packaging of cargo molecules into endoplasmic reticulum-derived COPII vesicles (Sar1pSec16psecretory proteinsSNARE proteins). *Biochemistry.* 94:837–842. doi:10.1073/pnas.94.3.837.
- Canton, J., and P.E. Kima. 2012. Targeting host syntaxin-5 preferentially blocks leishmania parasitophorous vacuole development in infected cells and limits experimental leishmania infections. *Am. J. Pathol.* 181:1348–1355. doi:10.1016/j.ajpath.2012.06.041.
- Carney, D.W., C.D.S. Nelson, B.D. Ferris, J.P. Stevens, A. Lipovsky, T. Kazakov, D. Dimaio, W.J. Atwood, and J.K. Sello. 2014. Structural optimization of a retrograde trafficking inhibitor that protects cells from infections by human polyoma- and papillomaviruses. *Bioorganic Med. Chem.* 22:4836–4847. doi:10.1016/j.bmc.2014.06.053.
- CDC. 2017. CDC | Bioterrorism Agents/Diseases | Emergency Preparedness & Response.
- Chen, Y.A., and R.H. Scheller. 2001. SNARE-mediated membrane fusion. *Nat. Rev. Mol. Cell Biol.* 2:98–106. doi:10.1038/35052017.
- Cocucci, E., F. Aguet, S. Boulant, and T. Kirchhausen. 2012. The first five seconds in the life of a clathrin-coated pit. *Cell.* 150:495–507. doi:10.1016/j.cell.2012.05.047.
- Collawn, J.F., M. Stangel, L.A. Kuhn, V. Esekogwu, S. Jing, I.S. Trowbridge, and J.A. Tainer. 1990. Transferrin receptor internalization sequence YXRF implicates a tight turn as the structural recognition motif for endocytosis. *Cell.* 63:1061–1072. doi:10.1016/0092-8674(90)90509-D.
- Connerly, P.L., M. Esaki, E.A. Montegna, D.E. Strongin, S. Levi, J. Soderholm, and B.S. Glick. 2005. Sec16 is a determinant of transitional ER organization. *Curr. Biol.* 15:1439–1447. doi:10.1016/j.cub.2005.06.065.
- Council, N.R. 2007. Improving the Nation's Water Security: Opportunities for Research. National Academies Press, Washington, D.C. p. 170 pp.
- Dai, W., Y. Wu, J. Bi, X. Lu, A. Hou, Y. Zhou, B. Sun, W. Kong, J. Barbier, J.C. Cintrat, F. Gao, D. Gillet, W. Su, and C. Jiang. 2017. Antiviral effects of Retro-2cycl and Retro-2.1 against Enterovirus 71 in vitro and in vivo. *Antiviral Res.* 144:311–321. doi:10.1016/j.antiviral.2017.07.001.
- Damm, E.M., L. Pelkmans, J. Kartenbeck, A. Mezzacasa, T. Kurzchalia, and A. Helenius. 2005. Clathrin- and caveolin-1-independent endocytosis: Entry of simian virus 40 into cells devoid of caveolae. *J. Cell Biol.* 168:477–488. doi:10.1083/jcb.200407113.
- Delevoye, C., X. Heiligenstein, L. Ripoll, F. Gilles-Marsens, M.K. Dennis, R.A. Linares, L. Derman, A. Gokhale, E. Morel, V. Faundez, M.S. Marks, and G. Raposo. 2016. BLOC-1 Brings Together the Actin and Microtubule Cytoskeletons to Generate Recycling Endosomes. *Curr. Biol.* 26:1–13. doi:10.1016/j.cub.2015.11.020.
- Desmyter, S., F. Vandenbussche, Q. Hao, P. Proost, W.J. Peumans, and E.J.M. Van Damme. 2003. Type-1 ribosome-inactivating protein from iris bulbs: A useful agronomic tool to engineer virus resistance? *Plant Mol. Biol.* 51:567–576. doi:10.1023/A:1022389205295.
- Doherty, G.J., and H.T. McMahon. 2009. Mechanisms of Endocytosis. *Annu. Rev. Biochem.* 78:857–902. doi:10.1146/annurev.biochem.78.081307.110540.
- Donaldson, J.G., D. Finazzi, and R.D. Klausner. 1992. Brefeldin A inhibits Golgi membrane-catalysed exchange of guanine nucleotide onto ARF

- protein. *Nature*. 360:350–352. doi:10.1038/360350a0.
- Donaldson, J.G., and A. Honda. 2005. Localization and function of Arf family GTPases. *Biochem. Soc. Trans.* 33:639–642. doi:10.1042/BST0330639.
- Donaldson, J.G., A. Honda, and R. Weigert. 2005. Multiple activities for Arf1 at the Golgi complex. *Biochim. Biophys. Acta - Mol. Cell Res.* 1744:364–373. doi:10.1016/j.bbamcr.2005.03.001.
- Donta, S.T., T.K. Tomicic, and A. Donohue-Rolfe. 1995. Inhibition of shiga-like toxins by brefeldin a. *J. Infect. Dis.* 171:721–754. doi:10.1093/infdis/171.3.721.
- Duncan, J.R., and S. Kornfeld. 1988. Intracellular movement of two mannose 6-phosphate receptors: Return to the Golgi apparatus. *J. Cell Biol.* 106:617–628. doi:10.1083/jcb.106.3.617.
- Ehrlich, M., W. Boll, A. Van Oijen, R. Hariharan, K. Chandran, M.L. Nibert, and T. Kirchhausen. 2004. Endocytosis by random initiation and stabilization of clathrin-coated pits. *Cell*. 118:591–605. doi:10.1016/j.cell.2004.08.017.
- Endo, Y., K. Tsurugi, T. Yutsude, Y. Takeda, T. Ogasawara, and K. Igarashi. 1988. Site of action of a Vero toxin (VT2) from Escherichia coli O157 : H7 and of Shiga toxin on eukaryotic ribosomes. *Eur. J. Biochem.* 171:45–50. doi:10.1111/j.1432-1033.1988.tb13756.x.
- Espenshade, P., R.E. Gimeno, E. Holzmacher, P. Teung, and C.A. Kaiser. 1995. Yeast SEC16 gene encodes a multidomain vesicle coat protein that interacts with Sec23p. *J. Cell Biol.* 131:311–324. doi:10.1083/jcb.131.2.311.
- Ewers, H., W. Römer, A.E. Smith, K. Bacia, S. Dmitrieff, W. Chai, R. Mancini, J. Kartenbeck, V. Chambon, L. Berland, A. Oppenheim, G. Schwarzmann, T. Feizi, P. Schwille, P. Sens, A. Helenius, and L. Johannes. 2010. GM1 structure determines SV40-induced membrane invagination and infection. *Nat. Cell Biol.* 12:11–18. doi:10.1038/ncb1999.
- Fath, S., J.D. Mancias, X. Bi, and J. Goldberg. 2007. Structure and Organization of Coat Proteins in the COPII Cage. *Cell*. 129:1325–1336. doi:10.1016/j.cell.2007.05.036.
- Felder, S., K. Miller, G. Moehren, A. Ullrich, J. Schlessinger, and C.R. Hopkins. 1990. Kinase activity controls the sorting of the epidermal growth factor receptor within the multivesicular body. *Cell*. 61:623–634. doi:10.1016/0092-8674(90)90474-5.
- Feldmann, H., and T.W. Geisbert. 2011. Ebola haemorrhagic fever. *Lancet*. 377:849–862. doi:10.1016/S0140-6736(10)60667-8.
- Feng, Y., A.P. Jadhav, C. Rodighiero, Y. Fujinaga, T. Kirchhausen, and W.I. Lencer. 2004. Retrograde transport of cholera toxin from the plasma membrane to the endoplasmic reticulum requires the trans-Golgi network but not the Golgi apparatus in Exo2-treated cells. *EMBO Rep.* 5:596–601. doi:10.1038/sj.embor.7400152.
- Feng, Y., S. Yu, T.K.R. Lasell, A.P. Jadhav, E. Macia, P. Chardin, P. Melancon, M. Roth, T. Mitchison, and T. Kirchhausen. 2003. Exo1: a new chemical inhibitor of the exocytic pathway. *Proc. Natl. Acad. Sci. U. S. A.* 100:6469–74. doi:10.1073/pnas.0631766100.
- Filipowicz, W., S.N. Bhattacharyya, and N. Sonenberg. 2008. Mechanisms of post-transcriptional regulation by microRNAs: are the answers in sight? *Nat. Rev. Genet.* 2008:102–114. doi:10.1038/nrg2290.
- Fölsch, H., M. Pypaert, P. Schu, and I. Mellman. 2001. Distribution and function of AP-1 clathrin adaptor complexes in polarized epithelial cells. *J. Cell Biol.* 153:595–606. doi:10.1083/jcb.152.3.595.
- Ford, M.G.J. 2001. Simultaneous Binding of PtdIns(4,5)P2 and Clathrin by AP180 in the Nucleation of Clathrin Lattices on Membranes. *Science (80-)*. 291:1051–1055. doi:10.1126/science.291.5506.1051.
- Fraser, M.E., M.M. Chernaia, Y. V. Kozlov, and M.N.G. James. 1994. Crystal structure of the holotoxin from Shigella dysenteriae at 2.5 Å resolution. *Nat. Struct. Biol.* 1:59–64. doi:10.1038/nsb0194-59.
- Fukuda, R., J.A. McNew, T. Weber, F. Parlati, T. Engel, W. Nickel, J.E. Rothman, and T.H. Söllner. 2000. Functional architecture of an intracellular

- membrane t-SNARE. *Nature*. 407:198–202. doi:10.1038/35025084.
- Furst, J., R.B. Sutton, J. Chen, A.T. Brunger, and N. Grigorieff. 2003. Electron cryomicroscopy structure of N-ethyl maleimide sensitive factor at 11 Å resolution. *EMBO J.* 22:4365–4374. doi:10.1093/emboj/cdg420.
- Futter, C.E., A. Pearse, L.J. Hewlett, and C.R. Hopkins. 1996. Multivesicular endosomes containing internalized EGF-EGF receptor complexes mature and then fuse directly with lysosomes. *J. Cell Biol.* 132:1011–1023. doi:10.1083/jcb.132.6.1011.
- Gallusser, a, and T. Kirchhausen. 1993. The beta 1 and beta 2 subunits of the AP complexes are the clathrin coat assembly components. *EMBO J.* 12:5237–44.
- Ganley, I.G., E. Espinosa, and S.R. Pfeffer. 2008. A syntaxin 10-SNARE complex distinguishes two distinct transport routes from endosomes to the trans-Golgi in human cells. *J. Cell Biol.* 180:159–172. doi:10.1083/jcb.200707136.
- Garred, O., B. Van Deurs, and K. Sandvig. 1995. Furin-induced cleavage and activation of shiga toxin. *J. Biol. Chem.* 270:10817–10821. doi:10.1074/jbc.270.18.10817.
- De Gascun, C.F., and M.J. Carr. 2013. Human polyomavirus reactivation: Disease pathogenesis and treatment approaches. *Clin. Dev. Immunol.* 2013. doi:10.1155/2013/373579.
- Gillet, D., J. Barbier, M.R. Popoff, D. Gillet, and J. Barbier. 2015. Diphtheria toxin. In *The Comprehensive Sourcebook of Bacterial Protein Toxins*. Elsevier. 111–132.
- Gillingham, A.K., and S. Munro. 2003. Long coiled-coil proteins and membrane traffic. *Biochim. Biophys. Acta - Mol. Cell Res.* 1641:71–85. doi:10.1016/S0167-4889(03)00088-0.
- Gimeno, R.E., P. Espenshade, and C. a Kaiser. 1996. COPII Coat Subunit Interactions: Sec24p and Sec23p Bind to Adjacent Regions of Sec16p. *Mol Biol Cell.* 7:1815–1823.
- Gonatas, N.K., A. Steiber, S.U. Kim, D.I. Graham, and S. Avrameas. 1975. Internalization of neuronal plasma membrane ricin receptors into the Golgi apparatus. *Exp. Cell Res.* 94:426–431. doi:10.1016/0014-4827(75)90508-X.
- Gonzales, A.R., R.B. Schofield, and G.R. Schmitt. 2006. Policy Agroterrorism — Why We ’ re Not Ready : A Look at the Role of Law Enforcement.
- Gottron, F., and D.A. Shea. 2010. Federal Efforts to Address the Threat of Bioterrorism : Selected Issues for Congress.
- Grant, B.D., and J.G. Donaldson. 2009. Pathways and mechanisms of endocytic recycling. *Nat. Rev. Mol. Cell Biol.* 10:597–608. doi:10.1038/nrm2755.
- Grassart, A., A. Dujeancourt, P.B. Lazarow, A. Dautry-Varsat, and N. Sauvonnnet. 2008. Clathrin-independent endocytosis used by the IL-2 receptor is regulated by Rac1, Pak1 and Pak2. *EMBO Rep.* 9:356–62. doi:10.1038/embor.2008.28.
- Grove, J., and M. Marsh. 2011. The cell biology of receptor-mediated virus entry. *J. Cell Biol.* 195:1071–1082. doi:10.1083/jcb.201108131.
- Gruenberg, J., and H. Stenmark. 2004. The biogenesis of multivesicular endosomes. *Nat. Rev. Mol. Cell Biol.* 5:317–323. doi:10.1038/nrm1360.
- Guetzoyan, L.J., R.A. Spooner, F. Boal, D.J. Stephens, J.M. Lord, L.M. Roberts, and G.J. Clarkson. 2010a. Fine tuning Exo2, a small molecule inhibitor of secretion and retrograde trafficking pathways in mammalian cells. *Mol. Biosyst.* 6:2030. doi:10.1039/c0mb00035c.
- Guetzoyan, L.J., R.A. Spooner, J.M. Lord, L.M. Roberts, and G.J. Clarkson. 2010b. Simple oxidation of pyrimidinylhydrazones to triazolopyrimidines and their inhibition of Shiga toxin trafficking. *Eur. J. Med. Chem.* 45:275–283. doi:10.1016/j.ejmech.2009.10.007.
- Gupta, N., R. No??l, A. Goudet, K. Hinsinger, A. Michau, V. Pons, H. Abdelkafi, T. Secher, A. Shima, O. Shtanko, Y. Sakurai, S. Cojean, S. Pomel, V. Li??vin-Le Moal, V. Leignel, J.A. Herweg, A. Fischer, L. Johannes, K. Harrison, P.M. Beard, P. Clayette, R. Le Grand, J.O. Rayner, T. Rudel, J. Vacus, P.M. Loiseau, R.A. Davey, E. Oswald, J.C. Cintrat, J. Barbier, and D. Gillet. 2017. Inhibitors of retrograde trafficking

- active against ricin and Shiga toxins also protect cells from several viruses, Leishmania and Chlamydiales. *Chem. Biol. Interact.* 267:96–103. doi:10.1016/j.cbi.2016.10.005.
- Gupta, N., V. Pons, R. Noël, D.A. Buisson, A. Michau, L. Johannes, D. Gillet, J. Barbier, and J.C. Cintrat. 2014. (S)-N-methyldihydroquinazolinones are the active enantiomers of retro-2 derived compounds against toxins. *ACS Med. Chem. Lett.* 5:94–97. doi:10.1021/ml400457j.
- Haigler, H.T., J.A. McKanna, and S. Cohen. 1979. Direct visualization of the binding and internalization of a ferritin conjugate of epidermal growth factor in human carcinoma cells A-431. *J. Cell Biol.* 81:382–395. doi:10.1083/jcb.81.2.382.
- Harding, C., J. Heuser, and P. Stahl. 1983. Receptor-mediated endocytosis of transferrin and recycling of the transferrin receptor in rat reticulocytes. *J. Cell Biol.* 97:329–339. doi:10.1083/jcb.97.2.329.
- Harper, C.B., M.R. Popoff, A. McCluskey, P.J. Robinson, and F.A. Meunier. 2013. Targeting membrane trafficking in infection prophylaxis: Dynamin inhibitors. *Trends Cell Biol.* 23:90–101. doi:10.1016/j.tcb.2012.10.007.
- Harrison, K., I.R. Haga, T. Pechenick Jowers, S. Jasim, J.-C. Cintrat, D. Gillet, T. Schmitt-John, P. Digard, and P.M. Beard. 2016. Vaccinia Virus Uses Retromer-Independent Cellular Retrograde Transport Pathways To Facilitate the Wrapping of Intracellular Mature Virions during Virus Morphogenesis. *J. Virol.* 90:10120–10132. doi:10.1128/JVI.01464-16.
- Hay, J.C., J. Klumperman, V. Oorschot, M. Steegmaier, C.S. Kuo, and R.H. Scheller. 1998. Localization, dynamics, and protein interactions reveal distinct roles for ER and Golgi SNAREs. *J. Cell Biol.* 141:1489–1502. doi:10.1083/jcb.141.7.1489.
- Henne, W.M., E. Boucrot, M. Meinecke, E. Evergren, Y. Vallis, R. Mittal, and H.T. McMahon. 2010. FCHO Proteins Are Nucleators of Clathrin-Mediated Endocytosis. *Science (80-.)*. 328:1281–1284. doi:10.1126/science.1188462.
- Herweg, J.A., V. Pons, D. Becher, M. Hecker, G. Krohne, J. Barbier, H. Berger, T. Rudel, and A. Mehlitz. 2016. Proteomic analysis of the Simkania-containing vacuole: The central role of retrograde transport. *Mol. Microbiol.* 99:151–171. doi:10.1111/mmi.13222.
- Hierro, A., A.L. Rojas, R. Rojas, N. Murthy, G. Effantin, A. V. Kajava, A.C. Steven, J.S. Bonifacio, and J.H. Hurley. 2007. Functional architecture of the retromer cargo-recognition complex. *Nature.* 449:1063–1067. doi:10.1038/nature06216.
- Hirst, J., S.E. Miller, M.J. Taylor, G.F. von Mollard, and M.S. Robinson. 2004. EpsinR Is an Adaptor for the SNARE Protein Vti1b. *Mol. Biol. Cell.* 15:5593–5602.
- Hirst, J., A. Motley, K. Harasaki, S.Y.P. Chew, and M.S. Robinson. 2003. EpsinR: an ENTH Domain-containing Protein that Interacts with AP-1. *Mol. Biol. Cell.* 14:2559–2569. doi:10.1091/mbc.E02.
- Hohl, T.M., F. Parlati, C. Wimmer, J.E. Rothman, T.H. Söllner, and H. Engelhardt. 1998. Arrangement of subunits in 20 S particles consisting of NSF, SNAPs, and SNARE complexes. *Mol. Cell.* 2:539–548. doi:10.1016/S1097-2765(00)80153-7.
- Hong, W. 2005. SNAREs and traffic. *Biochim. Biophys. Acta - Mol. Cell Res.* 1744:120–144. doi:10.1016/j.bbamcr.2005.03.014.
- Hu, C. 2003. Fusion of Cells by Flipped SNAREs. *Science (80-.)*. 300:1745–1749. doi:10.1126/science.1084909.
- Huang, M., J.T. Weissman, S. Béraud-Dufour, P. Luan, C. Wang, W. Chen, M. Aridor, I.A. Wilson, and W.E. Balch. 2001. Crystal structure of Sar1-GDP at 1.7 Å resolution and the role of the NH2 terminus in ER export. *J. Cell Biol.* 155:937–948. doi:10.1083/jcb.200106039.
- Hueisgen, R. 1961. Proceedings of the Chemical Society. October 1961. *Proc. Chem. Soc.* 357. doi:10.1039/ps9610000357.
- Hughes, H., A. Budnik, K. Schmidt, K.J. Palmer, J. Mantell, C. Noakes, A. Johnson, D.A. Carter, P. Verkade, P. Watson, and D.J. Stephens. 2009. Organisation of human ER-exit sites: requirements for the localisation of Sec16 to transitional ER. *J. Cell Sci.* 122:2924–2934. doi:10.1242/jcs.044032.
- Hui, N., N. Nakamura, B. Sönnichsen, D.T. Shima, T. Nilsson, and G. Warren. 1997. An isoform of the Golgi t-SNARE, syntaxin 5, with an endoplasmic reticulum retrieval signal. *Mol. Biol. Cell.* 8:1777–87.

- Ivan, V., G. De Voer, D. Xanthakis, K.M. Spoorendonk, V. Kondylis, and C. Rabouille. 2008. Drosophila Sec16 Mediates the Biogenesis of tER Sites Upstream of Sar1 through an Arginine-Rich Motif. *Mol. Biol. Cell.* 19:4352–4365. doi:10.1091/mbc.E08.
- Jacewicz, M., H. Clausen, E. Nudelman, a Donohue-Rolfe, and G.T. Keusch. 1986. Pathogenesis of shigella diarrhea. XI. Isolation of a shigella toxin-binding glycolipid from rabbit jejunum and HeLa cells and its identification as globotriaosylceramide. *J. Exp. Med.* 163:1391–1404. doi:10.1084/jem.163.6.1391.
- Jackson, C.L. 2009. Mechanisms of transport through the Golgi complex. *J. Cell Sci.* 122:443–452. doi:10.1242/jcs.032581.
- Jahn, R., T. Lang, and T.C. Südhof. 2003. Membrane fusion. *Cell.* 112:519–533. doi:10.1016/S0092-8674(03)00112-0.
- Johannes, L., and B. Goud. 1998. Surfing on a retrograde wave: How does Shiga toxin reach the endoplasmic reticulum? *Trends Cell Biol.* 8:158–162. doi:10.1016/S0962-8924(97)01209-9.
- Johannes, L., R.G. Parton, P. Bassereau, and S. Mayor. 2015. Building endocytic pits without clathrin. *Nat. Rev. Mol. Cell Biol.* 16:311–321. doi:10.1038/nrm3968.
- Johannes, L., and V. Popoff. 2008. Tracing the Retrograde Route in Protein Trafficking. *Cell.* 135:1175–1187. doi:10.1016/j.cell.2008.12.009.
- Johannes, L., and W. Römer. 2010. Shiga toxins — from cell biology to biomedical applications. *Nat. Rev. Microbiol.* 8:105–16. doi:10.1038/nrmicro2279.
- Johannes, L., and C. Wunder. 2011a. The SNXy flavours of endosomal sorting. *Nat. Cell Biol.* 13:884–886. doi:10.1038/ncb2300.
- Johannes, L., and C. Wunder. 2011b. Retrograde transport: Two (or more) roads diverged in an endosomal tree? *Traffic.* 12:956–962. doi:10.1111/j.1600-0854.2011.01200.x.
- Johannes, L., C. Wunder, and M. Shafaq-Zadah. 2016. Glycolipids and Lectins in Endocytic Uptake Processes. *J. Mol. Biol.* 428:4792–4818. doi:10.1016/j.jmb.2016.10.027.
- Jones, K.E., N.G. Patel, M.A. Levy, A. Storeygard, D. Balk, J.L. Gittleman, and P. Daszak. 2008. Global trends in emerging infectious diseases. *Nature.* 451:990–993. doi:10.1038/nature06536.
- Jordan, M., A. Schallhorn, and F.M. Wurm. 1996. Transfecting mammalian cells: Optimization of critical parameters affecting calcium-phosphate precipitate formation. *Nucleic Acids Res.* 24:596–601. doi:10.1093/nar/24.4.596.
- Kaiser, C.A., and R. Schekman. 1990. Distinct sets of SEC genes govern transport vesicle formation and fusion early in the secretory pathway. *Cell.* 61:723–733. doi:10.1016/0092-8674(90)90483-U.
- Kalthoff, C., S. Groos, R. Kohl, S. Mahrhold, and E. Ungewickell. 2002. Clint: A Novel Clathrin-binding ENTH-Domain Protein at the Golgi. *Mol. Biol. Cell.* 13:4060–4073. doi:10.1091/mbc.E02-03-0171.
- Karmali, M.A., M. Petric, B.T. Steele, and C. Lim. 1983. Sporadic Cases of Haemolytic-Uraemic Syndrome Associated With FaecalCytotoxin and Cytotoxin-Producing Escherichia coli In Stools. *Lancet.* i:619–620. doi:10.1111/j.1472-765X.2004.01628.x.
- Karpman, D. 2012. Management of Shiga toxin-associated Escherichia coli-induced haemolytic uraemic syndrome: Randomized clinical trials are needed. *Nephrol. Dial. Transplant.* 27:3669–3674. doi:10.1093/ndt/gfs456.
- King, L.A., F. Nogareda, F.X. Weill, P. Mariani-Kurkdjian, E. Loukiadis, G. Gault, N. Jourdan-Dasilva, E. Bingen, M. MacÉ, D. Thevenot, N. Ong, C. Castor, H. Noël, D. Van Cauteren, M. Charron, V. Vaillant, B. Aldabe, V. Goulet, G. Delmas, E. Couturier, Y. Le Strat, C. Combe, Y. Delmas, F. Terrier, B. Vendrely, P. Rolland, and H. De Valk. 2012. Outbreak of shiga toxin-producing escherichia coli O104:H4 Associated with organic fenugreek sprouts, France, June 2011. *Clin. Infect. Dis.* 54:1588–1594. doi:10.1093/cid/cis255.
- Kirchhausen, T. 1999. Adaptors for Clathrin-Mediated Traffic. *Annu. Rev. Cell Dev. Biol.* 15:705–732. doi:10.1146/annurev.cellbio.15.1.705.

- Kirchhausen, T. 2000. Clathrin. *Annu. Rev. Biochem.*
- Kirchhausen, T., and S.C. Harrison. 1981. Protein organization in clathrin trimers. *Cell.* 23:755–761. doi:10.1016/0092-8674(81)90439-6.
- Kirchhausen, T., D. Owen, and S.C. Harrison. 2014. Molecular structure, function, and dynamics of clathrin-mediated membrane traffic. *Cold Spring Harb. Perspect. Biol.* 6. doi:10.1101/cshperspect.a016725.
- Klausner, R.D., J.G. Donaldson, and J. Lippincott-Schwartz. 1992. Brefeldin A: Insights into the control of membrane traffic and organelle structure. *J. Cell Biol.* 116:1071–1080. doi:10.1083/jcb.116.5.1071.
- Kleijmeer, M., G. Ramm, D. Schuurhuis, J. Griffith, M. Rescigno, P. Ricciardi-Castagnoli, A.Y. Rudensky, F. Ossendorp, C.J.M. Melief, W. Stoorvogel, and H.J. Geuze. 2001. Reorganization of multivesicular bodies regulates MHC class II 11 antigen presentation by dendritic cells. *J. Cell Biol.* 155:53–63. doi:10.1083/jcb.200103071.
- Konowalchuk, J., J.I. Speirs, and S. Stavric. 1977. Vero response to a cytotoxin of Escherichia coli. *Infect. Immun.* 18:775–779.
- Kouranti, I., M. Sachse, N. Arouche, B. Goud, and A. Echard. 2006. Rab35 Regulates an Endocytic Recycling Pathway Essential for the Terminal Steps of Cytokinesis. *Curr. Biol.* 16:1719–1725. doi:10.1016/j.cub.2006.07.020.
- Kung, L.F., S. Pagant, E. Futai, J.G. D'Arcangelo, R. Buchanan, J.C. Dittmar, R.J.D. Reid, R. Rothstein, S. Hamamoto, E.L. Snapp, R. Schekman, and E.A. Miller. 2012. Sec24p and Sec16p cooperate to regulate the GTP cycle of the COPII coat. *EMBO J.* 31:1014–1027. doi:10.1038/emboj.2011.444.
- Lakshminarayan, R., C. Wunder, U. Becken, M.T. Howes, C. Benzing, S. Arumugam, S. Sales, N. Ariotti, V. Chambon, C. Lamaze, D. Loew, A. Shevchenko, K. Gaus, R.G. Parton, and L. Johannes. 2014. Galectin-3 drives glycosphingolipid-dependent biogenesis of clathrin-independent carriers. *Nat. Cell Biol.* 16:595–606. doi:10.1038/ncb2970.
- Lamaze, C., A. Dujeancourt, T. Baba, C.G. Lo, A. Benmerah, and A. Dautry-Varsat. 2001. Interleukin 2 receptors and detergent-resistant membrane domains define a clathrin-independent endocytic pathway. *Mol. Cell.* 7:661–671. doi:10.1016/S1097-2765(01)00212-X.
- Lauvrak, S.U. 2004. Efficient endosome-to-Golgi transport of Shiga toxin is dependent on dynamin and clathrin. *J. Cell Sci.* 117:2321–2331. doi:10.1242/jcs.01081.
- Ledger, P.W., N. Uchida, and M.L. Tanzer. 1980. Immunocytochemical localization of procollagen and fibronectin in human fibroblasts: Effects of the monovalent ionophore, monensin. *J. Cell Biol.* 87:663–671. doi:10.1083/jcb.87.3.663.
- Lee, M.C.S., E.A. Miller, J. Goldberg, L. Orci, and R. Schekman. 2004. Bi-Directional Protein Transport Between the Er and Golgi. *Annu. Rev. Cell Dev. Biol.* 20:87–123. doi:10.1146/annurev.cellbio.20.010403.105307.
- Li, L., J. Jose, Y. Xiang, R.J. Kuhn, and M.G. Rossmann. 2010. Structural changes of envelope proteins during alphavirus fusion. *Nature.* 468:705–708. doi:10.1038/nature09546.
- Lieu, Z.Z., and P.A. Gleeson. 2010. Identification of different itineraries and retromer components for endosome-to-Golgi transport of TGN38 and Shiga toxin. *Eur. J. Cell Biol.* 89:379–393. doi:10.1016/j.ejcb.2009.10.021.
- Lindberg, A., J.E. Brown, N. Strömberg, M. Westling-Ryd, J.E. Schultz, and K. a Karlsson. 1987. Identification of the carbohydrate receptor for Shiga toxin produced by *Shigella dysenteriae* type 1. *J. Biol. Chem.* 262:1779–85.
- Ling, H., A. Boodhoo, B. Hazes, M.D. Cummings, G.D. Armstrong, J.L. Brunton, and R.J. Read. 1998. Structure of the Shiga-like toxin I B-pentamer complexed with an analogue of its receptor Gb3. *Biochemistry.* 37:1777–1788. doi:10.1021/bi971806n.
- Linstedt, A.D., A. Mehta, J. Suhan, H. Reggio, and H.-P. Hauri. 1997. Sequence and Overexpression of GPP130/GIMPc: Evidence for Saturable pH-sensitive Targeting of a Type II Early Golgi Membrane Protein. *Mol. Biol. Cell.* 8:1073–1087.
- Lombardi, D., T. Soldati, M.A. Riederer, Y. Goda, M. Zerial, and S.R. Pfeffer. 1993. Rab9 functions in transport between late endosomes and

- the trans Golgi network. *EMBO J.* 12:677–82.
- Lu, P.H., S.C. Chueh, F.L. Kung, S.L. Pan, Y.C. Shen, and J.H. Guh. 2007. Ilimaquinone, a marine sponge metabolite, displays anticancer activity via GADD153-mediated pathway. *Eur. J. Pharmacol.* 556:45–54. doi:10.1016/j.ejphar.2006.10.061.
- Luzio, J.P., B. Brake, G. Banting, K.E. Howell, P. Braghetta, and K.K. Stanley. 1990. Identification, sequencing and expression of an integral membrane protein of the trans-Golgi network (TGN38). *Biochem. J.* 270:97–102.
- Mai, T.T., A. Hamaï, A. Hienzsch, T. Cañeque, S. Müller, J. Wicinski, O. Cabaud, C. Leroy, A. David, V. Acevedo, A. Ryo, C. Ginestier, D. Birnbaum, E. Charafe-Jauffret, P. Codogno, M. Mehrpour, and R. Rodriguez. 2017. Salinomycin kills cancer stem cells by sequestering iron in lysosomes. *Nat. Chem.* 1–9. doi:10.1038/nchem.2778.
- Maldonado-Báez, L., C. Williamson, and J.G. Donaldson. 2013. Clathrin-independent endocytosis: A cargo-centric view. *Exp. Cell Res.* 319:2759–2769. doi:10.1016/j.yexcr.2013.08.008.
- Mallard, F., C. Antony, D. Tenza, J. Salamero, B. Goud, and L. Johannes. 1998. Direct pathway from early/recycling endosomes to the Golgi apparatus revealed through the study of Shiga toxin B-fragment transport. *J. Cell Biol.* 143:973–990. doi:10.1083/jcb.143.4.973.
- Mallard, F., and L. Johannes. 2003. Shiga toxin B-subunit as a tool to study retrograde transport. *Methods Mol Med.* 73:209–20. doi:10.1385/1-59259-316-X:209.
- Mallard, F., B.L. Tang, T. Galli, D. Tenza, A. Saint-Pol, X. Yue, C. Antony, W. Hong, B. Goud, and L. Johannes. 2002. Early/recycling endosomes-to-TGN transport involves two SNARE complexes and a Rab6 isoform. *J. Cell Biol.* 156:653–664. doi:10.1083/jcb.200110081.
- Mancias, J.D., and J. Goldberg. 2008. Structural basis of cargo membrane protein discrimination by the human COPII coat machinery. *EMBO J.* 27:2918–2928. doi:10.1038/emboj.2008.208.
- Mansueto, P., A. Seidita, G. Vitale, and A. Cascio. 2014. Leishmaniasis in travelers: A literature review. *Travel Med. Infect. Dis.* 12:563–581. doi:10.1016/j.tmaid.2014.09.007.
- Matsuoka, K., L. Orci, M. Amherdt, S.Y. Bednarek, S. Hamamoto, R. Schekman, and T. Yeung. 1998. COPII-coated vesicle formation reconstituted with purified coat proteins and chemically defined liposomes. *Cell.* 93:263–275. doi:10.1016/S0092-8674(00)81577-9.
- Mattera, R., C.M. Guardia, S.S. Sidhu, and J.S. Bonifacino. 2015. Bivalent motif-ear interactions mediate the association of the accessory protein tepsin with the AP-4 adaptor complex. *J. Biol. Chem.* 290:30736–30749. doi:10.1074/jbc.M115.683409.
- Mayor, S., and R.E. Pagano. 2007. Pathways of clathrin-independent endocytosis. *Nat. Rev. Mol. Cell Biol.* 8:603–612. doi:10.1038/nrm2216.
- Mayor, S., R.G. Parton, and J.G. Donaldson. 2014. Clathrin-independent pathways of endocytosis. *Cold Spring Harb. Perspect. Biol.* 6. doi:10.1101/cshperspect.a016758.
- McGourty, K., T.L. Thurston, S.A. Matthews, L. Pinaud, L.J. Mota, and D.W. Holden. 2012. Salmonella inhibits retrograde trafficking of mannose-6-phosphate receptors and lysosome function. *Science.* 338:963–7. doi:10.1126/science.1227037.
- McMahon, C., S.M. Studer, C. Clendinen, G.P. Dann, P.D. Jeffrey, and F.M. Hughson. 2012. The structure of Sec12 implicates potassium ion coordination in Sar1 activation. *J. Biol. Chem.* 287:43599–43606. doi:10.1074/jbc.M112.420141.
- McMahon, H.T., and E. Boucrot. 2011. Molecular mechanism and physiological functions of clathrin-mediated endocytosis. *Nat. Rev. Mol. Cell Biol.* 12:517–533. doi:10.1038/nrm3151.
- McNew, J.A., F. Parlati, R. Fukuda, R.J. Johnston, K. Paz, F. Paumet, T.H. Sollner, and J.E. Rothman. 2000. Compartmental specificity of cellular membrane fusion encoded in SNARE proteins. *Nature.* 407:153–159. doi:10.1038/35025000.
- Meyer, C., D. Zizioli, S. Lausmann, E.L. Eskelinen, J. Hamann, P. Saftig, K. von Figura, and P. Schu. 2000. mu1A-adaptin-deficient mice: lethality, loss of AP-1 binding and rerouting of mannose 6-phosphate receptors. *EMBO J.* 19:2193–2203. doi:10.1093/emboj/19.10.2193.

- Miles, S., H. McManus, K.E. Forsten, and B. Storrie. 2001. Evidence that the entire Golgi apparatus cycles in interphase HeLa cells: Sensitivity of Golgi matrix proteins to an ER exit block. *J. Cell Biol.* 155:543–555. doi:10.1083/jcb.200103104.
- Miller, E.A., and C. Barlowe. 2010. Regulation of coat assembly-sorting things out at the ER. *Curr. Opin. Cell Biol.* 22:447–453. doi:10.1016/j.ceb.2010.04.003.
- Miller, E.A., T.H. Beilharz, P.N. Malkus, M.C.S. Lee, S. Hamamoto, L. Orci, and R. Schekman. 2003. Multiple cargo binding sites on the COPII subunit Sec24p ensure capture of diverse membrane proteins into transport vesicles. *Cell.* 114:497–509. doi:10.1016/S0092-8674(03)00609-3.
- Miller, E.A., and R. Schekman. 2013. COPII - a flexible vesicle formation system. *Curr. Opin. Cell Biol.* 25:420–427. doi:10.1016/j.ceb.2013.04.005.
- Mills, I.G., G.J.K. Praefcke, Y. Vallis, B.J. Peter, L.E. Olesen, J.L. Gallop, P.J.G. Butler, P.R. Evans, and H.T. McMahon. 2003. Epsinr: An AP1/clathrin interacting protein involved in vesicle trafficking. *J. Cell Biol.* 160:213–222. doi:10.1083/jcb.200208023.
- Miyazaki, K., Y. Wakana, C. Noda, K. Arasaki, A. Furuno, and M. Tagaya. 2012. Contribution of the long form of syntaxin 5 to the organization of the endoplasmic reticulum. *J. Cell Sci.* 125:5658–5666. doi:10.1242/jcs.105304.
- Mollenhauer, H.H., D. James Morr e, and L.D. Rowe. 1990. Alteration of intracellular traffic by monensin; mechanism, specificity and relationship to toxicity. *BBA - Rev. Biomembr.* 1031:225–246. doi:10.1016/0304-4157(90)90008-Z.
- Molloy, S.S., P.A. Bresnahan, S.H. Leppla, K.R. Klimpel, and G. Thomas. 1992. Human furin is a calcium-dependent serine endoprotease that recognizes the sequence Arg-X-X-Arg and efficiently cleaves anthrax toxin protective antigen. *J. Biol. Chem.* 267:16396–16402.
- Montagnac, G., H. De Forges, E. Smythe, C. Gueudry, M. Romao, J. Salamero, and P. Chavrier. 2011. Decoupling of activation and effector binding underlies ARF6 priming of fast endocytic recycling. *Curr. Biol.* 21:574–579. doi:10.1016/j.cub.2011.02.034.
- Montesano, R., J. Roth, A. Robert, and L. Orci. 1982. Non-coated membrane invaginations are involved in binding and internalization of cholera and tetanus toxins. *Nature.* 296:651–653. doi:10.1038/296651a0.
- Morens, D.M., G.K. Folkers, and A.S. Fauci. 2004. The challenge of emerging and re-emerging infectious diseases. *Nature.* 430:242–249. doi:10.1038/nature02759.
- Mossessova, E., L.C. Bickford, and J. Goldberg. 2003a. SNARE selectivity of the COPII coat. *Cell.* 114:483–495. doi:10.1016/S0092-8674(03)00608-1.
- Mossessova, E., R.A. Corpina, and J. Goldberg. 2003b. Crystal Structure of ARF1•Sec7 Complexed with Brefeldin A and Its Implications for the Guanine Nucleotide Exchange Mechanism. *Mol. Cell.* 12:1403–1411. doi:10.1016/S1097-2765(03)00475-1.
- Moya, M., A. Dautry-Varsat, B. Goud, D. Louvard, and P. Boquet. 1985. Inhibition of Coated Pit Formation in Hep2 Cells Blocks the Cytotoxicity of Diphtheria Toxin But Not That of Ricin Toxin. *J. Cell Biol.*
- Mukhopadhyay, S., C. Bachert, D.R. Smith, and A.D. Linstedt. 2010. Manganese-induced Trafficking and Turnover of the cis -Golgi Glycoprotein GPP130. *Mol. Biol. Cell.* 21:1282–1292.
- Mukhopadhyay, S., and A.D. Linstedt. 2012. Manganese Blocks Intracellular Trafficking of Shiga Toxin and Protects Against Shiga Toxicosis. *Science (80-.).* 335:332–335. doi:10.1126/science.1215930.
- Mukhopadhyay, S., B. Redler, and A.D. Linstedt. 2013. Shiga toxin-binding site for host cell receptor GPP130 reveals unexpected divergence in toxin-trafficking mechanisms. *Mol. Biol. Cell.* 24:2311–2318. doi:10.1091/mbc.E13-01-0057.
- Murk, J.L., W. Stoorvogel, M.J. Kleijmeer, and H.J. Geuze. 2002. The plasticity of multivesicular bodies and the regulation of antigen presentation. *Semin. Cell Dev. Biol.* 13:303–311. doi:10.1016/S1084952102000605.

- Nambiar, M. 1995. Ilimaquinone Inhibits the Cytotoxicities of Ricin, Diphtheria Toxin, and Other Protein Toxins in Vero Cells. *Exp. Cell Res.* 219:671–678. doi:10.1006/EXCR.1995.1278.
- Nassoy, P., and C. Lamaze. 2012. Stressing caveolae new role in cell mechanics. *Trends Cell Biol.* 22:381–389. doi:10.1016/j.tcb.2012.04.007.
- Natarajan, R., and A.D. Linstedt. 2004. A cycling cis-Golgi protein mediates endosome-to-Golgi traffic. *Mol. Biol. Cell.* 15:4798–806. doi:10.1091/mbc.E04-05-0366.
- National Institute of Allergy and Infectious Disease. 2017. NIAID Emerging Infectious Diseases/Pathogens | NIH: National Institute of Allergy and Infectious Diseases.
- Nelson, C.D.S., D.W. Carney, A. Derdowski, A. Lipovsky, G. V. Gee, B. O’Hara, P. Williard, D. Dimaio, J.K. Sello, and W.J. Atwood. 2013. A retrograde trafficking inhibitor of ricin and Shiga-like toxins inhibits infection of cells by human and monkey polyomaviruses. *MBio.* 4. doi:10.1128/mBio.00729-13.
- Neumann, N., D. Lundin, and A.M. Poole. 2010. Comparative genomic evidence for a complete nuclear pore complex in the last eukaryotic common ancestor. *PLoS One.* 5. doi:10.1371/journal.pone.0013241.
- Nichols, B.J., A.K. Kenworthy, R.S. Polishchuk, R. Lodge, T.H. Roberts, K. Hirschberg, R.D. Phair, and J. Lippincott-Schwartz. 2001. Rapid cycling of lipid raft markers between the cell surface and golgi complex. *J. Cell Biol.* 152:529–541. doi:10.1083/jcb.153.3.529.
- Nichols, B.J., and H.R.B. Pelham. 1998. SNAREs and membrane fusion in the Golgi apparatus. *Biochim. Biophys. Acta - Mol. Cell Res.* 1404:9–31. doi:10.1016/S0167-4889(98)00044-5.
- Nielsen, K., and R.S. Boston. 2001. RIBOSOME-INACTIVATING PROTEINS: A Plant Perspective. *Annu. Rev. Plant Physiol. Plant Mol. Biol.* 52:785–816. doi:10.1146/annurev.arplant.52.1.785.
- Ning, X., J. Guo, M.A. Wolfert, and G.J. Boons. 2008. Visualizing metabolically labeled glycoconjugates of living cells by copper-free and fast huisgen cycloadditions. *Angew. Chemie - Int. Ed.* 47:2253–2255. doi:10.1002/anie.200705456.
- No, J.H. 2016. Visceral leishmaniasis: Revisiting current treatments and approaches for future discoveries. *Acta Trop.* 155:113–123. doi:10.1016/j.actatropica.2015.12.016.
- Noel, R., N. Gupta, V. Pons, A. Goudet, M.D. Garcia-Castillo, A. Michau, J. Martinez, D.A. Buisson, L. Johannes, D. Gillet, J. Barbier, and J.C. Cintrat. 2013. N -Methyldihydroquinazolinone derivatives of retro-2 with enhanced efficacy against shiga toxin. *J. Med. Chem.* 56:3404–3413. doi:10.1021/jm4002346.
- Nonnenmacher, M.E., J.-C. Cintrat, D. Gillet, and T. Weber. 2015. Syntaxin 5-Dependent Retrograde Transport to the *trans* -Golgi Network Is Required for Adeno-Associated Virus Transduction. *J. Virol.* 89:1673–1687. doi:10.1128/JVI.02520-14.
- Novick, P., C. Field, and R. Schekman. 1980. Identification of 23 complementation groups required for post-translational events in the yeast secretory pathway. *Cell.* 21:205–215. doi:10.1016/0092-8674(80)90128-2.
- Nr, S., T. Force, N. Angaben, E.- Sa, D. Bfr, W. Ursache, Z. Schutz, and A. Ehec. 2011. Samen von Bockshornklee mit hoher Wahrscheinlichkeit für EHEC O104 : H4 Ausbruch verantwortlich. 22–24.
- Nutr, J.C., and H. Sandstead. 2016. Sandstead HH : Requirements and toxicity of essential trace elements , illustrated by zinc and illustrated by zinc and copper1 ' 2. 61:5–9.
- O’Brien, A.D., J.W. Newland, S.F. Miller, R.K. Holmes, H.W. Smith, and S.B. Formal. 1984. Shiga-like toxin-converting phages from Escherichia coli strains that cause hemorrhagic colitis or infantile diarrhea. *Science.* 226:694–6. doi:10.1126/science.6387911.
- Oestereich, L., A. Lüdtke, S. Wurr, T. Rieger, C. Muñoz-Fontela, and S. Günther. 2014. Successful treatment of advanced Ebola virus infection with T-705 (favipiravir) in a small animal model. *Antiviral Res.* 105:17–21. doi:10.1016/j.antiviral.2014.02.014.

- Orci, L., M. Stames, M. Ravazzola, M. Amherdt, A. Perrelet, T.H. Söllner, and J.E. Rothman. 1997. Bidirectional transport by distinct populations of COPI-coated vesicles. *Cell*. 90:335–349. doi:10.1016/S0092-8674(00)80341-4.
- Owen, D.J. 2004. Linking endocytic cargo to clathrin: structural and functional insights into coated vesicle formation. *Biochem. Soc. Trans.* 32:1–14. doi:10.1042/BST0320001.
- Palade, G. 1975. Intracellular Aspects of the Process of Protein Synthesis. *Science (80-)*. 189:867–867. doi:10.1126/science.189.4206.867-b.
- Park, J.G., J.N. Kahn, N.E. Tumer, and Y.-P. Pang. 2012. Chemical Structure of Retro-2, a Compound That Protects Cells against Ribosome-Inactivating Proteins. *Sci. Rep.* 2:631. doi:10.1038/srep00631.
- Parton, R.G., and M.A. del Pozo. 2013. Caveolae as plasma membrane sensors, protectors and organizers. *Nat. Rev. Mol. Cell Biol.* 14:98–112. doi:10.1038/nrm3512.
- Patterson, G.H., K. Hirschberg, R.S. Polishchuk, D. Gerlich, R.D. Phair, and J. Lippincott-Schwartz. 2008. Transport through the Golgi Apparatus by Rapid Partitioning within a Two-Phase Membrane System. *Cell*. 133:1055–1067. doi:10.1016/j.cell.2008.04.044.
- Pearse, B.M.F. 1976. Clathrin: A unique protein associated with intracellular transfer of membrane by coated vesicles. *Proc Natl Acad Sci U S A*. 73:1255–1259. doi:10.1073/pnas.73.4.1255.
- Pelkmans, L., J. Kartenbeck, and a Helenius. 2001. Caveolar endocytosis of simian virus 40 reveals a new two-step vesicular-transport pathway to the ER. *Nat. Cell Biol.* 3:473–483. doi:10.1038/35074539.
- Perez-Victoria, F.J., and J.S. Bonifacino. 2009. Dual Roles of the Mammalian GARP Complex in Tethering and SNARE Complex Assembly at the trans-Golgi Network. *Mol. Cell. Biol.* 29:5251–5263. doi:10.1128/MCB.00495-09.
- Peter, B.J. 2004. BAR Domains as Sensors of Membrane Curvature: The Amphiphysin BAR Structure. *Science (80-)*. 303:495–499. doi:10.1126/science.1092586.
- Peumans, W.J., Q. Hao, and E.L.S.J.M. Van Damme. 2001. Ribosome-inactivating proteins from plants: more than RNA N-glycosidases? *FASEB J*. 15:1493–1506. doi:10.1096/fj.00-0751rev.
- Peyroche, A., B. Antony, S. Robineau, J. Acker, J. Cherfils, and C.L. Jackson. 1999. Brefeldin A acts to stabilize an abortive ARF-GDP-Sec7 domain protein complex: Involvement of specific residues of the Sec7 domain. *Mol. Cell*. 3:275–285. doi:10.1016/S1097-2765(00)80455-4.
- Pezeshkian, W., A.G. Hansen, L. Johannes, H. Khandelia, J.C. Shillcock, P.B.S. Kumar, and J.H. Ipsen. 2016. Membrane invagination induced by Shiga toxin B-subunit: from molecular structure to tube formation. *Soft Matter*. 12:5164–5171. doi:10.1039/C6SM00464D.
- Piper, R.C., and D.J. Katzmann. 2007. Biogenesis and Function of Multivesicular Bodies. *Annu. Rev. Cell Dev. Biol.* 23:519–547. doi:10.1146/annurev.cellbio.23.090506.123319.
- Popoff, V., G.A. Mardones, S.K. Bai, V. Chambon, D. Tenza, P. V. Burgos, A. Shi, P. Benaroch, S. Urbé, C. Lamaze, B.D. Grant, G. Raposo, and L. Johannes. 2009. Analysis of articulation between clathrin and retromer in retrograde sorting on early endosomes. *Traffic*. 10:1868–1880. doi:10.1111/j.1600-0854.2009.00993.x.
- Popoff, V., G.A. Mardones, D. Tenza, R. Rojas, C. Lamaze, J.S. Bonifacino, G. Raposo, and L. Johannes. 2007. The retromer complex and clathrin define an early endosomal retrograde exit site. *J. Cell Sci.* 120:2022–2031. doi:10.1242/jcs.003020.
- Puri, S., C. Bachert, C.J. Fimmel, and A.D. Linstedt. 2002. Cycling of Early Golgi Proteins Via the Cell Surface and Endosomes Upon Luminal pH Disruption. *Traffic*. 3:641–653. doi:10.1034/j.1600-0854.2002.30906.x.
- Radeke, H.S., C.A. Digits, R.L. Casaubon, and M.L. Snapper. 1999. Interactions of (-)-ilimaquinone with methylation enzymes: Implications for vesicular-mediated secretion. *Chem. Biol.* 6:639–647. doi:10.1016/S1074-5521(99)80115-X.

- Rayner, K.J., Y. Suarez, A. Davalos, S. Parathath, M.L. Fitzgerald, N. Tamehiro, E.A. Fisher, K.J. Moore, and C. Fernandez-Hernando. 2010. MiR-33 Contributes to the Regulation of Cholesterol Homeostasis. *Science* (80-.). 328:1570–1573. doi:10.1126/science.1189862.
- Reaves, B., M. Horn, and G. Banting. 1993. TGN38/41 recycles between the cell surface and the TGN: brefeldin A affects its rate of return to the TGN. *Mol Biol Cell*. 4:93–105.
- Reaves, B., a Wilde, and G. Banting. 1992. Identification, molecular characterization and immunolocalization of an isoform of the trans-Golgi-network (TGN)-specific integral membrane protein TGN38. *Biochem. J.* 283 (Pt 2:313–316.
- Rein, U., U. Andag, R. Duden, H.D. Schmitt, and A. Spang. 2002. ARF-GAP-mediated interaction between the ER-Golgi v-SNAREs and the COPI coat. *J. Cell Biol.* 157:395–404. doi:10.1083/jcb.200112092.
- Reinbothe, S., C. Reinbothe, J. Lehmann, W. Becker, K. Apel, and B. Parthier. 1994. JIP60, a methyl jasmonate-induced ribosome-inactivating protein involved in plant stress reactions. *Proc. Natl. Acad. Sci. U. S. A.* 91:7012–6. doi:10.1073/pnas.91.15.7012.
- Robinson, M.S. 2004. Adaptable adaptors for coated vesicles. *Trends Cell Biol.* 14:167–174. doi:10.1016/j.tcb.2004.02.002.
- Rodriguez, A., S. Griffiths-Jones, J.L. Ashurst, and A. Bradley. 2004. Identification of mammalian microRNA host genes and transcription units. *Genome Res.* 14:1902–1910. doi:10.1101/gr.2722704.
- Rodriguez, R., and K.M. Miller. 2014. Unravelling the genomic targets of small molecules using high-throughput sequencing. *Nat. Rev. Genet.* 15:783–796. doi:10.1038/nrg3796.
- Rojas, R., T. Van Vlijmen, G.A. Mardones, Y. Prabhu, A.L. Rojas, S. Mohammed, A.J.R. Heck, G. Raposo, P. Van Der Sluijs, and J.S. Bonifacino. 2008. Regulation of retromer recruitment to endosomes by sequential action of Rab5 and Rab7. *J. Cell Biol.* 183:513–526. doi:10.1083/jcb.200804048.
- Römer, W., L. Berland, V. Chambon, K. Gaus, B. Windschiegel, D. Tenza, M.R.E. Aly, V. Fraissier, J.-C. Florent, D. Perrais, C. Lamaze, G. Raposo, C. Steinem, P. Sens, P. Bassereau, and L. Johannes. 2007. Shiga toxin induces tubular membrane invaginations for its uptake into cells. *Nature.* 450:670–675. doi:10.1038/nature05996.
- Römer, W., L.L. Pontani, B. Sorre, C. Rentero, L. Berland, V. Chambon, C. Lamaze, P. Bassereau, C. Sykes, K. Gaus, and L. Johannes. 2010. Actin Dynamics Drive Membrane Reorganization and Scission in Clathrin-Independent Endocytosis. *Cell.* 140:540–553. doi:10.1016/j.cell.2010.01.010.
- van Rooij, E., D. Quiat, B.A. Johnson, L.B. Sutherland, X. Qi, J.A. Richardson, R.J. Kelm, and E.N. Olson. 2009. A Family of microRNAs Encoded by Myosin Genes Governs Myosin Expression and Muscle Performance. *Dev. Cell.* 17:662–673. doi:10.1016/j.devcel.2009.10.013.
- Rostovtsev, V. V., L.G. Green, V. V. Fokin, and K.B. Sharpless. 2002. A stepwise Huisgen cycloaddition process: Copper(I)-catalyzed regioselective “ligation” of azides and terminal alkynes. *Angew. Chemie - Int. Ed.* 41:2596–2599. doi:10.1002/1521-3773(20020715)41:14<2596::AID-ANIE2596>3.0.CO;2-4.
- Roth, T., and K. Porter. 1964. Yolk Protein Uptake in the Oocyte of the Mosquito *Aedes Aegypti*. L. *J. Cell Biol.* 20:313–332. doi:10.1083/jcb.20.2.313.
- Rydell, G.E., L. Svensson, G. Larson, L. Johannes, and W. Römer. 2013. Human GII.4 norovirus VLP induces membrane invaginations on giant unilamellar vesicles containing secretor gene dependent α 1,2-fucosylated glycosphingolipids. *Biochim. Biophys. Acta - Biomembr.* 1828:1840–1845. doi:10.1016/j.bbamem.2013.03.016.
- Saenz, J.B., T.A. Doggett, and D.B. Haslam. 2007. Identification and characterization of small molecules that inhibit intracellular toxin transport. *Infect. Immun.* 75:4552–4561. doi:10.1128/IAI.00442-07.
- Sáenz, J.B., W.J. Sun, J.W. Chang, J. Li, B. Bursulaya, N.S. Gray, and D.B. Haslam. 2009. Golgicide A reveals essential roles for GBF1 in Golgi assembly and function. *Nat. Chem. Biol.* 5:157–165. doi:10.1038/nchembio.144.

- Saini, H.K., S. Griffiths-Jones, and A.J. Enright. 2007. Genomic analysis of human microRNA transcripts. *Proc. Natl. Acad. Sci. U. S. A.* 104:17719–24. doi:10.1073/pnas.0703890104.
- Saint-Pol, A., B. Yélamos, M. Amessou, I.G. Mills, M. Dugast, D. Tenza, P. Schu, C. Antony, H.T. McMahon, C. Lamaze, and L. Johannes. 2004. Clathrin adaptor epsinR is required for retrograde sorting on early endosomal membranes. *Dev. Cell.* 6:525–538. doi:10.1016/S1534-5807(04)00100-5.
- Sandvig, K. 2001. Shiga toxins. *Toxicon.* 39:1629–1635. doi:10.1016/S0041-0101(01)00150-7.
- Sandvig, K., and B. van Deurs. 2000. Entry of ricin and Shiga toxin into cells: molecular mechanisms and medical perspectives. *Embo J.* 19:5943–5950. doi:10.1093/emboj/19.22.5943.
- Sandvig, K., O. Garred, K. Prydz, J. V Kozlov, S.H. Hansen, and B. van Deurs. 1992. Retrograde transport of endocytosed Shiga toxin to the endoplasmic reticulum. *Nature.* 358:510–512. doi:10.1038/358510a0.
- Sandvig, K., S. Olsnes, J.E. Brown, O.W. Petersen, and B. Van Deurs. 1989. Endocytosis from coated pits of Shiga toxin: A glycolipid-binding protein from *Shigella dysenteriae* 1. *J. Cell Biol.* 108:1331–1343. doi:10.1083/jcb.108.4.1331.
- Saxena, S.K., A.D. O'Brien, and E.J. Ackerman. 1989. Shiga toxin, Shiga-like toxin II variant, and ricin are all single-site RNA N-glycosidases of 28 S RNA when microinjected into *Xenopus* oocytes. *J. Biol. Chem.* 264:596–601.
- Van Der Schaar, H.M., M.J. Rust, Chen, H. Van Der Ende-Metselaar, J. Wilschut, X. Zhuang, and J.M. Smit. 2008. Dissecting the cell entry pathway of dengue virus by single-particle tracking in living cells. *PLoS Pathog.* 4. doi:10.1371/journal.ppat.1000244.
- Schindler, C., Y. Chen, J. Pu, X. Guo, and J.S. Bonifacino. 2015. EARP is a multisubunit tethering complex involved in endocytic recycling. *Nat. Cell Biol.* 17:639–650. doi:10.1038/ncb3129.
- Schlossman, D.M., S.L. Schmid, W.A. Braell, and J.E. Rothman. 1984. An enzyme that removes clathrin coats: Purification of an uncoating ATPase. *J. Cell Biol.* 99:723–733. doi:10.1083/jcb.99.2.723.
- Sciences, A., G.-P. Nikoleli, S. Karapetis, S. Bratakou, D.P. Nikolelis, N. Tzamtzis, V.N. Psychoyios, N. Psaroudakis, and G.-P. Nikoleli. 2016. Biosensors for Security and Bioterrorism Applications. Springer, Cham. 1-13 pp.
- Seachrist, J.L. 2000. beta sub2 -Adrenergic receptor internalization, endosomal sorting and plasma membrane recycling are regulated by Rab GTPases. *J. Biol. Chem.* 14.
- Sealey-Cardona, M., K. Schmidt, L. Demmel, T. Hirschmugl, T. Gesell, G. Dong, and G. Warren. 2014. Sec16 Determines the Size and Functioning of the Golgi in the Protist Parasite, *Trypanosoma brucei*. *Traffic.* 15:613–629. doi:10.1111/tra.12170.
- Seaman, M.N.J. 2004. Cargo-selective endosomal sorting for retrieval to the Golgi requires retromer. *J. Cell Biol.* 165:111–122. doi:10.1083/jcb.200312034.
- Secher, T., A. Shima, K. Hinsinger, J.C. Cintrat, L. Johannes, J. Barbier, D. Gillet, and E. Oswald. 2015. Retrograde trafficking inhibitor of Shiga toxins reduces morbidity and mortality of mice infected with enterohemorrhagic *Escherichia coli*. *Antimicrob. Agents Chemother.* 59:5010–5013. doi:10.1128/AAC.00455-15.
- Sengupta, P., P. Satpute-Krishnan, A.Y. Seo, D.T. Burnette, G.H. Patterson, and J. Lippincott-Schwartz. 2015. ER trapping reveals Golgi enzymes continually revisit the ER through a recycling pathway that controls Golgi organization. *Proc. Natl. Acad. Sci.* 112:E6752–E6761. doi:10.1073/pnas.1520957112.
- Sharpe, H.J., T.J. Stevens, and S. Munro. 2010. A Comprehensive Comparison of Transmembrane Domains Reveals Organelle-Specific Properties. *Cell.* 142:158–169. doi:10.1016/j.cell.2010.05.037.
- Shaywitz, D.A., P.J. Espenshade, R.E. Gimeno, and C.A. Kaiser. COPII Subunit Interactions in the Assembly of the Vesicle Coat*.

- Shindiapina, P., and C. Barlowe. 2010. Requirements for transitional endoplasmic reticulum site structure and function in *Saccharomyces cerevisiae*. *Mol Biol Cell*. 21:1530–1545. doi:10.1091/mbc.E09-07-0605.
- Shorter, J., M.B. Beard, J. Seemann, A. Barbara Dirac-Svejstrup, and G. Warren. 2002. Sequential tethering of Golgins and catalysis of SNAREpin assembly by the vesicle-tethering protein p115. *J. Cell Biol.* 157:45–62. doi:10.1083/jcb.200112127.
- Simmons, B.M., P.D. Stahl, and J.H. Russell. 1986. Mannose receptor-mediated uptake of ricin toxin and ricin A chain by macrophages. Multiple intracellular pathways for a chain translocation. *J. Biol. Chem.* 261:7912–7920.
- Sinha, B., D. Köster, R. Ruez, P. Gonnord, M. Bastiani, D. Abankwa, R. V. Stan, G. Butler-Browne, B. Védie, L. Johannes, N. Morone, R.G. Parton, G. Raposo, P. Sens, C. Lamaze, and P. Nassoy. 2011. Cells respond to mechanical stress by rapid disassembly of caveolae. *Cell*. 144:402–413. doi:10.1016/j.cell.2010.12.031.
- Sissoko, D., C. Laouenan, E. Folkesson, A.B. M'Lebing, A.H. Beavogui, S. Baize, A.M. Camara, P. Maes, S. Shepherd, C. Danel, S. Carazo, M.N. Conde, J.L. Gala, G. Colin, H. Savini, J.A. Bore, F. Le Marcis, F.R. Koundouno, F. Petitjean, M.C. Lamah, S. Diederich, A. Tounkara, G. Poelart, E. Berbain, J.M. Dindart, S. Duraffour, A. Lefevre, T. Leno, O. Peyrouset, L. Irengé, N. Bangoura, R. Palich, J. Hinzmann, A. Kraus, T.S. Barry, S. Berette, A. Bongono, M.S. Camara, V. Chanfreau Munoz, L. Doumbouya, Souley Harouna, P.M. Kighoma, F.R. Koundouno, René Lolamou, C.M. Loua, V. Massala, K. Moumouni, C. Provost, N. Samake, C. Sekou, A. Soumah, I. Arnould, M.S. Komano, L. Gustin, C. Berutto, D. Camara, F.S. Camara, J. Colpaert, L. Delamou, L. Jansson, E. Kourouma, M. Loua, K. Malme, E. Manfrin, A. Maomou, A. Milinouno, S. Ombelet, A.Y. Sidiboun, I. Verreckt, P. Yombouno, A. Bocquin, C. Carbonnelle, T. Carmoi, P. Frange, S. Mely, V.K. Nguyen, D. Pannetier, A.M. Taburet, J.M. Treluyer, J. Kolie, R. Moh, M.C. Gonzalez, E. Kuisma, B. Liedigk, D. Ngabo, M. Rudolf, R. Thom, R. Kerber, M. Gabriel, A. Di Caro, R. Wölfel, J. Badir, M. Bentahir, Y. Deccache, C. Dumont, J.F. Durant, K. El Bakkouri, M. Gasasira Uwamahoro, et al. 2016. Experimental Treatment with Favipiravir for Ebola Virus Disease (the JIKI Trial): A Historically Controlled, Single-Arm Proof-of-Concept Trial in Guinea. *PLoS Med.* 13:1–36. doi:10.1371/journal.pmed.1001967.
- Sivan, G., S.E. Martin, T.G. Myers, E. Buehler, K.H. Szymczyk, P. Ormanoglu, and B. Moss. 2013. Human genome-wide RNAi screen reveals a role for nuclear pore proteins in poxvirus morphogenesis. *Proc. Natl. Acad. Sci.* 110:3519–3524. doi:10.1073/pnas.1300708110.
- Sivan, G., A.S. Weisberg, J.L. Americo, and B. Moss. 2016. Retrograde Transport from Early Endosomes to the *trans*-Golgi Network Enables Membrane Wrapping and Egress of Vaccinia Virus Virions. *J. Virol.* 90:8891–8905. doi:10.1128/JVI.01114-16.
- van der Sluijs, P., M. Hull, P. Webster, P. Mâle, B. Goud, and I. Mellman. 1992. The small GTP-binding protein rab4 controls an early sorting event on the endocytic pathway. *Cell*. 70:729–740. doi:10.1016/0092-8674(92)90307-X.
- Smith, G.L., A. Vanderplassen, and M. Law. 2002. The formation and function of extracellular enveloped vaccinia virus. *J. Gen. Virol.* 83:2915–2931. doi:10.1099/0022-1317-83-12-2915.
- Snider, M.D., and O.C. Rogers. 1985. Intracellular movement of cell surface receptors after endocytosis: Resialylation of asialo-transferrin receptor in human erythroleukemia cells. *J. Cell Biol.* 100:826–834. doi:10.1083/jcb.100.3.826.
- Söderberg, O., M. Gullberg, M. Jarvius, K. Ridderstråle, K.-J. Leuchowius, J. Jarvius, K. Wester, P. Hydbring, F. Bahram, L.-G. Larsson, and U. Landegren. 2006. Direct observation of individual endogenous protein complexes in situ by proximity ligation. *Nat. Methods*. 3:995–1000. doi:10.1038/nmeth947.
- Söllner, T., S.W. Whiteheart, M. Brunner, H. Erdjument-Bromage, S. Geromanos, P. Tempst, and J.E. Rothman. 1993. SNAP receptors implicated in vesicle targeting and fusion. *Nature*. 362:318–324. doi:10.1038/362318a0.
- Sönnichsen, B., S. De Renzis, E. Nielsen, J. Rietdorf, and M. Zerial. 2000. Distinct membrane domains on endosomes in the recycling pathway visualized by multicolor imaging of Rab4, Rab5, and Rab11. *J. Cell Biol.* 149:901–913. doi:10.1083/jcb.149.4.901.
- Sorkin, A., M. Mazzotti, T. Sorkina, L. Scotto, and L. Beguinot. 1996. Epidermal Growth Factor Receptor Interaction with Clathrin Adaptors Is Mediated by the Tyr 974 -containing Internalization Motif *. *J. Biol. Chem.* 271:13377–13384.

- Spang, A. 2015. Anniversary of the discovery of sec mutants by Novick and Schekman. *Mol. Biol. Cell.* 26:1783–1785. doi:10.1091/mbc.E14-11-1511.
- Spooner, R.A., and J.M. Lord. 2012. How ricin and Shiga toxin reach the cytosol of target cells: Retrotranslocation from the endoplasmic reticulum. *Curr. Top. Microbiol. Immunol.* 357:19–40. doi:10.1007/82_2011_154.
- Spooner, R.A., P. Watson, D.C. Smith, F. Boal, M. Amessou, L. Johannes, G.J. Clarkson, J.M. Lord, D.J. Stephens, and L.M. Roberts. 2008. The secretion inhibitor Exo2 perturbs trafficking of Shiga toxin between endosomes and the *trans*-Golgi network. *Biochem. J.* 414:471–484. doi:10.1042/BJ20080149.
- Sprangers, J., and C. Rabouille. 2015. SEC16 in COPII coat dynamics at ER exit sites. *Biochem. Soc. Trans.* 43:97–103. doi:10.1042/BST20140283.
- Stagg, S.M., C. Gürkan, D.M. Fowler, P. LaPointe, T.R. Foss, C.S. Potter, B. Carragher, and W.E. Balch. 2006. Structure of the Sec13/31 COPII coat cage. *Nature.* 439:234–238. doi:10.1038/nature04339.
- Stechmann, B., S.K. Bai, E. Gobbo, R. Lopez, G. Merer, S. Pinchard, L. Panigai, D. Tenza, G. Raposo, B. Beaumelle, D. Sauvaire, D. Gillet, L. Johannes, and J. Barbier. 2010. Inhibition of retrograde transport protects mice from lethal ricin challenge. *Cell.* 141:231–242. doi:10.1016/j.cell.2010.01.043.
- Stein, P.E., a Boodhoo, G.J. Tyrrell, J.L. Brunton, and R.J. Read. 1992. Crystal structure of the cell-binding B oligomer of verotoxin-1 from *E. coli*. *Nature.* 355:748–750. doi:10.1038/355748a0.
- Stirpe, F. 2005. Ribosome-inactivating proteins. In *Molecular Neurosurgery With Targeted Toxins*. R.G. Wiley and D.A. Lappi, editors. Springer.
- Stoorvogel, W., V. Oorschot, and H.J. Geuze. 1996. A novel class of clathrin-coated vesicles budding from endosomes. *J. Cell Biol.* 132:21–33. doi:10.1083/jcb.132.1.21.
- Sundar, S., A. Singh, and O.P. Singh. 2014. Strategies to overcome antileishmanial drugs unresponsiveness. *J. Trop. Med.* 2014. doi:10.1155/2014/646932.
- Supek, F., D.T. Madden, S. Hamamoto, L. Orci, and R. Schekman. 2002. Sec16p potentiates the action of COPII proteins to bud transport vesicles. *J. Cell Biol.* 158:1029–1038. doi:10.1083/jcb.200207053.
- Sutton, R.B., D. Fasshauer, R. Jahn, and A.T. Brunger. 1998. Crystal structure of a SNARE complex involved in synaptic exocytosis at 2.4 Å resolution. *Nature.* 395:347–353. doi:10.1038/26412.
- Sweitzer, S.M., and J.E. Hinshaw. 1998. Dynamin undergoes a GTP-dependent conformational change causing vesiculation. *Cell.* 93:1021–1029. doi:10.1016/S0092-8674(00)81207-6.
- Tai, G., L. Lu, T.L. Wang, B.L. Tang, B. Goud, L. Johannes, and W. Hong. 2004. Participation of the Syntaxin 5/Ykt6/GS28/GS15 SNARE Complex in Transport from the Early/Recycling Endosome to the Trans-Golgi Network □ D. *Mol. Biol. Cell.* 15:4011–4022. doi:10.1091/mbc.E03-12.
- Takizawa, P.A., J.K. Yucel, B. Veit, D.J. Faulkner, T. Deerinck, G. Soto, M. Ellisman, and V. Malhotra. 1993. Complete vesiculation of Golgi membranes and inhibition of protein transport by a novel sea sponge metabolite, ilimaquinone. *Cell.* 73:1079–1090. doi:10.1016/0092-8674(93)90638-7.
- Tang, B.L., D.Y. Low, S.S. Lee, A.E. Tan, and W. Hong. 1998. Molecular cloning and localization of human syntaxin 16, a member of the syntaxin family of SNARE proteins. *Biochem. Commun.* 242:673–679. doi:10.1006/bbrc.1997.8029.
- Tarr, P.I., C.A. Gordon, and W.L. Chandler. 2005. Shiga-toxin-producing *Escherichia coli* and haemolytic uraemic syndrome. *Lancet.* 365:1073–1086. doi:10.1016/S0140-6736(05)71144-2.

- Tewari, R., C. Bachert, and A.D. Linstedt. 2015. Induced oligomerization targets Golgi proteins for degradation in lysosomes. *Mol. Biol. Cell.* 26:4427–4437. doi:10.1091/mbc.E15-04-0207.
- Tewari, R., T. Jarvela, and A.D. Linstedt. 2014. Manganese induces oligomerization to promote down-regulation of the intracellular trafficking receptor used by Shiga toxin. *Mol. Biol. Cell.* 25:3049–3058. doi:10.1091/mbc.E14-05-1003.
- Thompson, W.L., J.P. Scovill, and J.G. Pace. 1995. Drugs that show protective effects from ricin toxicity in in vitro protein synthesis assays. *Nat. Toxins.* 3:369–377. doi:10.1002/nt.2620030508.
- Tornøe, C.W., C. Christensen, and M. Meldal. 2002. Peptidotriazoles on solid phase: [1,2,3]-Triazoles by regioselective copper(I)-catalyzed 1,3-dipolar cycloadditions of terminal alkynes to azides. *J. Org. Chem.* 67:3057–3064. doi:10.1021/jo011148j.
- Trofa, A.F., H. Ueno-Olsen, R. Oiwa, and M. Yoshikawa. 1999. Dr. Kiyoshi Shiga: Discoverer of the Dysentery Bacillus. *Clin. Infect. Dis.* 29:1303–1306. doi:10.1086/313437.
- Umasankar, P.K., S. Sanker, J.R. Thieman, S. Chakraborty, B. Wendland, M. Tsang, and L.M. Traub. 2012. Distinct and separable activities of the endocytic clathrin-coat components Fcho1/2 and AP-2 in developmental patterning. *Nat. Cell Biol.* 14:488–501. doi:10.1038/ncb2473.
- Ungewickell, E., H. Ungewickell, S.E.H. Holstein, R. Lindner, K. Prasad, W. Barouch, B. Martini, L.E. Greene, and E. Eisenberg. 1995. Role of auxilin in uncoating clathrin-coated vesicles. *Nature.* 378:632–635. doi:10.1038/378632a0.
- Utskarpen, A., H.H. Slagsvold, A.B. Dyve, S.S. Skånland, and K. Sandvig. 2007. SNX1 and SNX2 mediate retrograde transport of Shiga toxin. *Biochem. Biophys. Res. Commun.* 358:566–570. doi:10.1016/j.bbrc.2007.04.159.
- Vancini, R., G. Wang, D. Ferreira, R. Hernandez, and D.T. Brown. 2013. Alphavirus Genome Delivery Occurs Directly at the Plasma Membrane in a Time- and Temperature-Dependent Process. *J. Virol.* 87:4352–4359. doi:10.1128/JVI.03412-12.
- Waddell, T., A. COHENt, and C.A. Lingwood. 1990. Induction of verotoxin sensitivity in receptor-deficient cell lines using the receptor glycolipid globotriosylceramide. *Cell Biol.* 87:7898–7901. doi:10.1073/pnas.87.20.7898.
- Wahome, P.G., Y. Bai, L.M. Neal, J.D. Robertus, and N.J. Mantis. 2010. Identification of small-molecule inhibitors of ricin and shiga toxin using a cell-based high-throughput screen. *Toxicon.* 56:313–323. doi:10.1016/j.toxicon.2010.03.016.
- Walsh, T.A., A.E. Morgan, and T.D. Hey. 1991. Characterization and molecular cloning of a proenzyme form of a ribosome-inactivating protein from maize: Novel mechanism of proenzyme activation by proteolytic removal of a 2.8-kilodalton internal peptide segment. *J. Biol. Chem.* 266:23422–23427.
- Wang, J., and K.E. Howell. 2000. The luminal domain of TGN38 interacts with integrin beta 1 and is involved in its trafficking. *Traffic.* 1:713–723. doi:tra010904 [pii].
- Ward, T.H., R.S. Polishchuk, S. Caplan, K. Hirschberg, and J. Lippincott-Schwartz. 2001. Maintenance of Golgi structure and function depends on the integrity of ER export. *J. Cell Biol.* 155:557–570. doi:10.1083/jcb.200107045.
- Watanabe, S., and E. Boucrot. 2017. Fast and ultrafast endocytosis. *Curr. Opin. Cell Biol.* 47:64–71. doi:10.1016/j.ceb.2017.02.013.
- Watson, P., A.K. Townley, P. Koka, K.J. Palmer, and D.J. Stephens. 2006. Sec16 defines endoplasmic reticulum exit sites and is required for secretory cargo export in mammalian cells. *Traffic.* 7:1678–1687. doi:10.1111/j.1600-0854.2006.00493.x.
- Weber, T., B. V. Zemelman, J.A. McNew, B. Westermann, M. Gmachl, F. Parlati, T.H. S?plner, and J.E. Rothman. 1998. SNAREpins: Minimal machinery for membrane fusion. *Cell.* 92:759–772. doi:10.1016/S0092-8674(00)81404-X.
- van Weering, J.R.T., R.B. Sessions, C.J. Traer, D.P. Kloer, V.K. Bhatia, D. Stamou, S.R. Carlsson, J.H. Hurley, and P.J. Cullen. 2012. Molecular basis for SNX-BAR-mediated assembly of distinct endosomal sorting tubules. *EMBO J.* 31:4466–4480. doi:10.1038/emboj.2012.283.

- White, J., and A. Helenius. 1980. pH-dependent fusion between the Semliki Forest virus membrane and liposomes. *Proc. Natl. Acad. Sci.* 77:3273–3277. doi:10.1073/pnas.77.6.3273.
- Whittle, J.R.R., and T.U. Schwartz. 2010. Structure of the Sec13-Sec16 edge element, a template for assembly of the COPII vesicle coat. *J. Cell Biol.* 190:347–361. doi:10.1083/jcb.201003092.
- Whyte, J.R.C., and S. Munro. 2002. Vesicle tethering complexes in membrane traffic. *J. Cell Sci.* 115:2627–2637. doi:10.1242/jcs.01596.
- Wimmer, C., T.M. Hohl, C.A. Hughes, S.A. Müller, T.H. Söllner, A. Engel, and J.E. Rothman. 2001. Molecular Mass, Stoichiometry, and Assembly of 20 S Particles. *J. Biol. Chem.* 276:29091–29097. doi:10.1074/jbc.M011292200.
- Witte, K., A.L. Schuh, J. Hegermann, A. Sarkeshik, J.R. Mayers, K. Schwarze, J.R. Yates III, S. Eimer, and A. Audhya. 2011. TFG-1 function in protein secretion and oncogenesis. *Nat. Cell Biol.* 13:550–558. doi:10.1038/ncb2225.
- Wittig, G., and R. Pohlke. 1961. Zur Existenz niedergliedriger Cycloalkine, II. *Chem. Ber.* 94:3276–3286. doi:10.1002/cber.19610941214.
- Xu, Y. 2002. GS15 Forms a SNARE Complex with Syntaxin 5, GS28, and Ykt6 and Is Implicated in Traffic in the Early Cisternae of the Golgi Apparatus. *Mol. Biol. Cell.* 13:3493–3507. doi:10.1091/mbc.E02-01-0004.
- Yamada, E. 1955. the Fine Structure of the Gall Bladder Epithelium of the Mouse. *J. Cell Biol.* 1:445–458. doi:10.1083/jcb.1.5.445.
- Yamauchi, Y., and A. Helenius. 2013. Virus entry at a glance. *J. Cell Sci.* 126:1289–1295. doi:10.1242/jcs.119685.
- Yarrow, J.C., Y. Feng, Z.E. Perlman, T. Kirchhausen, and T.J. Mitchison. 2003. Phenotypic screening of small molecule libraries by high throughput cell imaging. *Comb. Chem. High Throughput Screen.* 6:279–286. doi:10.2174/138620703106298527.
- Yonekawa, S., A. Furuno, T. Baba, Y. Fujiki, Y. Ogasawara, A. Yamamoto, M. Tagaya, and K. Tani. 2011. Sec16B is involved in the endoplasmic reticulum export of the peroxisomal membrane biogenesis factor peroxin 16 (Pex16) in mammalian cells. *Proc. Natl. Acad. Sci. U. S. A.* 108:12746–51. doi:10.1073/pnas.1103283108.
- Yorimitsu, T., and K. Sato. 2012. Insights into structural and regulatory roles of Sec16 in COPII vesicle formation at ER exit sites. *Mol. Biol. Cell.* 23:2930–2942. doi:10.1091/mbc.E12-05-0356.
- Yoshida, T., C. Chen, M. Zhang, and H.C. Wu. 1991. Disruption of the Golgi apparatus by brefeldin A inhibits the cytotoxicity of ricin, modeccin, and Pseudomonas toxin. *Exp. Cell Res.* 192:389–395. doi:10.1016/0014-4827(91)90056-Z.
- Yoshihisa, T., C. Barlowe, and R. Schekman. 1993. Requirement for a GTPase-activating protein in vesicle budding from the endoplasmic reticulum. *Science (80-).* 259:1466–1468. doi:10.1126/science.8451644.
- Zhang, J.Z., B.A. Davletov, T.C. Südhof, and R.G.W. Anderson. 1994. Synaptotagmin I is a high affinity receptor for clathrin AP-2: Implications for membrane recycling. *Cell.* 78:751–760. doi:10.1016/S0092-8674(94)90442-1.

15 ANNEX

15.1 MANUSCRIPTS

15.1.1 (published) Retrograde transport is not required for cytosolic translocation of Shiga toxin B-subunit

Maria Daniela Garcia-Castillo^{1,2,3}, Thi Tran^{4,5}, Alexandre Bobard⁶, Henri-François Renard^{1,2,3}, Stefan J. Rathjen^{1,2,3}, Estelle Dransart^{1,2,3}, Bahne Stechmann^{1,2,3}, Christophe Lamaze^{2,3,7}, Mike Lord⁸, Jean-Christophe Cintrat⁹, Jost Enninga⁶, Eric Tartour^{4,5} and Ludger Johannes^{1,2,3,*}

1. Institut Curie, PSL Research University, Endocytic Trafficking and Therapeutic Delivery Group, 26 rue d'Ulm, Paris Cedex 05 75248, France.
2. CNRS UMR3666, Paris 75005, France.
3. INSERM U1143, Paris 75005, France.
4. INSERM U970, PARCC Université Paris Descartes Sorbonne Paris Cité, Paris 75006, France.
5. Hôpital Européen Georges-Pompidou, AP-HP, Service d'Immunologie Biologique, Paris Cedex 15 75908, France.
6. Dynamique des Interactions Hôte Pathogène, Institut Pasteur, Paris Cedex 15 75724, France.
7. Institut Curie – Centre de Recherche, Membrane Dynamics and Mechanics of Intracellular Signaling Group, 26 rue d'Ulm, Paris Cedex 05 75248, France.
8. Department of Biological Sciences, University of Warwick, Coventry CV4 7AL, UK.
9. CEA, iBiTec-S/SCBM, CEA-Saclay, LabEx LERMIT, Gif-sur-Yvette F-91191, France.
- * Author for correspondence (ludger.johannes@curie.fr)

Keywords: Shiga toxin, Rab6, Rab5, Rab7, Sec22B, lactamase, endoplasmic reticulum, Golgi, endosome, Retro compound, PPMP, brefeldin-A, bafilomycin A1, methyl-beta- cyclodextrin, cholesterol, nanodomain, microdomain, raft, cytotoxic T-lymphocyte, dendritic cell, antigen cross-presentation, endosomal escape, immunotherapy, cancer, infectious disease

ABSTRACT

Antigen presenting cells have the remarkable capacity to transfer exogenous antigens to the cytosol for processing by proteasomes and subsequent presentation on MHC-I molecules, a process termed cross-presentation. It is the target of biomedical approaches that aim to trigger a therapeutic immune response. The receptor-binding B-subunit of Shiga toxin (STxB) is developed as an antigen delivery tool for such immunotherapy applications. In this study, we have analyzed pathways and trafficking factors that are involved in this process. A covalent conjugate between STxB and saporin was generated to quantitatively sample the membrane translocation step to the cytosol in differentiated monocyte-derived THP-1 cells. We have found that retrograde trafficking to the Golgi apparatus was not required for STxB-saporin translocation to the cytosol or for STxB-dependent antigen cross-presentation. Depletion of endosomal Rab7 inhibited, and lowering membrane cholesterol levels favored STxB-saporin translocation. Interestingly, experiments with reducible and non-reducible linker arm STxB conjugates led to the conclusion that after translocation, STxB remained associated with the cytosolic membrane leaflet. In summary, we report novel facets of the endosomal escape process bearing relevance to antigen cross-presentation.

15.1.2 (Revision) MiR-199a-5p attenuates retrograde transport and protects against Shiga toxin cytotoxicity

Juan F. Aranda^{1,2,#}, Stefan Rathjen³, Ludger Johannes³ and Carlos Fernández-Hernando^{1,2,#}

¹ Vascular Biology and Therapeutics Program, Yale University School of Medicine, New Haven, Connecticut, USA.

² Integrative Cell Signaling and Neurobiology of Metabolism Program, Section of Comparative Medicine, Yale University School of Medicine, New Haven, Connecticut, USA.

³ Institut Curie, PSL Research University, Chemical Biology of Membranes and Therapeutic Delivery unit, INSERM, U 1143, CNRS, UMR 3666, 26 rue d'Ulm, 75248 Paris Cedex 05, France.

Corresponding authors: Carlos Fernández-Hernando PhD and Juan Francisco Aranda PhD

10 Amistad Street, Amistad Research Building, Room 337C, New Haven, CT 06510

Yale University School of Medicine

Tel: (203) 737-4615

Fax: (203) 737-2290

Emails: carlos.fernandez-hernando@yale.edu and juan.arandagomez@nyumc.org

Running Title: MiR-199a-5p and retrograde transport

ABSTRACT

Retrograde transport allows cells the retrieval of receptors and other cellular cargoes to the Golgi contributing to the maintenance of cellular homeostasis. This transport route is also commonly used by several bacterial toxins to exert their deleterious actions on eukaryotic cells. While the retrograde transport process has been well characterized, the contribution of microRNAs (miRNAs) in regulating this cellular transport mechanism remains unknown. Here, we identified that the intronic miRNA family, miR-199a/b, coordinate genes regulating retrograde transport (RT) and endosome trafficking. In particular, we demonstrate that miR-199a-5p attenuates the expression Vps26A, Rab9B and M6PR, thereby controlling RT from endosomes to Trans Golgi network (TGN). Importantly, we found that overexpression of Vps26A construct resistant to the miRNA action abolish the effect of miR-199a-5p on RT. Finally, we demonstrate that miR-199-5p transfection attenuates shiga toxin (STxB)-mediated inhibition of protein biosynthesis. In summary, our work identifies the first non-coding RNA that influences RT and suppresses the cytotoxicity caused by bacterial toxins.

INTRODUCTION

The endosomal system homeostasis is crucial for intracellular functions such as development, metabolism and signaling. Endocytic internalization and recycling routes have been studied mechanistically in some detail. For maintenance of proper protein and cargo sorting cells need to coordinate intracellular trafficking through functioning of endosomes. To do so, retrograde transport (RT) route allows trafficking of proteins and lipids cargo from endosomes to trans-Golgi network and plasma membrane (Amessou et al., 2008; Bonifacino and Rojas, 2006; Johannes and Popoff, 2008). It thus regulates the abundance and intracellular distribution of its cargo within cells. Using this pathway, intracellular resident proteins such TGN46, furin or cation-independent mannose-6-phosphate receptor (CI-M6PR) (Arighi et al., 2004; Chia et al., 2011; Shiba et al., 2010) evade degradative trafficking by being retrieved from endosomes to the trans- Golgi Network (TGN). Also, numerous viruses and bacterial toxins utilize RT to enter the cell and reach the endoplasmic reticulum (ER). RT route converges with the forward biosynthetic pathway (exit route) at the Trans-Golgi network (TGN). Retrograde trafficking can be initiated at different levels of the endosome (early, late and recycling endosomes) in a process that is termed retrograde sorting (Liu et al., 2012; Popoff et al., 2007). Exit of cargo molecules is mediated by different retrograde sorting

proteins to reach the TGN and Golgi where a diverse set of tethering factors are acting on acceptor membranes (Chia and Gleeson, 2011; Hierro et al., 2015).

A number of proteins with previously reported roles in endocytosis and intracellular trafficking have been shown to participate in retrograde transport (RT) including Clathrin, AP-1, OCRL, etc, (Popoff et al., 2007; Shiba et al., 2013; van Rahden et al., 2012). Interestingly, there are a set of proteins that have specific roles in RT, among them the evolutionary conserved Retromer complex that mediates sorting from endosomes to the TGN. This protein complex is highly selective and involves two protein subcomplexes. The mammalian retromer is a pentameric complex that consists in the vacuolar protein sorting trimer VPS26/VPS29/VPS35 subcomplex and the less-defined sorting nexins dimer (SNX) in the other subcomplex (Hierro et al., 2007; Rojas et al., 2007). Retrograde transport is initiated by the core trimer responsible of cargo recognition, binding and selection through binding of cytosolic domains of cargo molecules to VPS35 and VPS26 (Seaman, 2004). The resulting nucleation complex also interacts with GTP-activated Rab7. Several SNX (SNX1, SNX2, SNX5 and SNX6) can associate in dimers to this nascent nucleation retromer complex facilitating endosomal membrane curvature to produce tubules/vesicles (Rojas et al., 2008; van Weering et al., 2012). Once the cargo carriers are matured, Dynamin-2 (DNM2) catalyzed the excision of vesicles. Finally the fusion of RT intermediates with the TGN requires tethering factors such as Golgin-97, SNARE complexes and Rab GTPases (Laufman et al., 2011; Lieu et al., 2007; Sohda et al., 2010).

Many proteins are known to traffic between endosomes and the TGN including the acid hydrolase sorting receptor Mannose 6 phosphate receptor (M6PR). In the biosynthetic/secretory pathway, newly synthesized acid hydrolase precursor proteins binds to M6PR in TGN membranes and are transferred to endocytic pathways. At endosome compartment, the low acidic pH in late endosome-lysosome results in the uncoupling of receptor-ligand complexes. M6PR are then recycled back to TGN by means of RT in which the retromer is acting to initiate a new round of delivery (Perez-Victoria et al., 2008). CI-M6PR may follow a more complex route to traffic from plasma membrane to TGN. Alternatively, retrieval of CI-M6PR from late endosomes appears to progress through a TIP/Rab9 dependent pathway that is independent of Retromer (Chia et al., 2011; Dong et al., 2013). In addition to endogenous proteins, several pathogens such as *Shigella dysenteriae* secrete extracellular toxins such as Shiga toxin (STxB) and cholera toxin that exploit the

intracellular RT to enter ER of host cells and be delivered to cytosol by retrotranslocation where they exert their toxic effects (Sandvig et al., 1992).

MicroRNAs (miRNAs) are short non-coding RNAs that regulate gene expression at posttranscriptional level. A single miRNA can control the expression of numerous genes associated to the same physiological pathway. They have been implicated in regulating multiple physiological processes ranging from development, senescence, tumor biology and metabolism amongst others. miRNAs. The membrane fission GTPase DNM is a key regulator during intracellular trafficking having a critical role in endocytosis from plasma membrane. DNMs are encoded by three separate genes in mammalian genomes, and interestingly miR-199 family of miRNAs reside within intronic regions of DNM genes (Aranda et al., 2015). Interestingly, we identified here an important role for miR-199-5p in regulating RT. miR-199-5p overexpression markedly inhibits the expression of genes associated to RT including Vps26A, Rab9B and M6PR and protects against STxB-induced protein biosynthesis inhibition. Most importantly, we elucidate a novel molecular mechanism by which a miRNA family (miR-199-5p) and the host genes where they are encoded (DNM), jointly regulates different genes/proteins involved in the RT intracellular trafficking pathway.

RESULTS

MiR-199a-5p regulates the expression of genes associated to retrograde transport.

We and others have previously shown the intriguing genomic localization of miR-199 miRNA family within intronic sequences of DNM genes (Aranda et al., 2015) (Fig. 1a). Since intronic miRNAs are known to regulate similar cellular functions of the gene where they are encoded, we performed a number of bioinformatics analysis searching for potential mRNA target genes [Targetscan (<http://www.targetscan.org>) and miRanda (<http://www.microrna.org>)]. Interestingly, we found among the highest scored miR-199-5p target genes several key regulators of RT pathway such as Vps26A, SNX6, Rab9B and Rab7A, but also cargo proteins including M6PR, which mediates the transport of hydrolases to the lysosomes (Fig. 1b). Vps26A, SNX6, Rab9B and Rab7A 3'UTR have predicted binding sites for miR-199-5p that are highly conserved across species (Data not shown). To determine whether miR-199a-5p binds directly Vps26A, SNX6, Rab9B and Rab7A 3'UTR, we generated reporter constructs with the luciferase coding sequence fused to the 3'UTR of these genes. The results show that miR-199a-5p markedly repressed Vps26A, SNX6 and Rab9B 3'UTR luciferase activity, demonstrating that the expression of these genes is directly regulated by miR-

199a-5p (Fig. 1c). Importantly, mutations in the miRNA seed sequence binding sites (Fig. 1c-d), release the repression of Vps26A and Rab9B 3'UTR activity, consistent with a direct interaction of miR-199a-5p with these sites. Surprisingly, miR-199a-5p did not repress Rab7A 3'UTR activity despite the presence of a putative specific binding site and the decreased mRNA levels upon miR-199a-5p mimics transfection (Fig. 1c). We next determined whether miR-199-5p levels influence Vps26A, Rab9B and Rab7A mRNA and protein expression levels. To this end, we transfected HeLa cells with miR-199a-5p mimics or scramble control mimic (CM) and assessed Vps26A, Rab9B and Rab7A mRNA and protein expression by qRT-PCR and Western blotting respectively. As expected by the inhibitory effect of miR-199-5p on 3'UTR luciferase activity, miR-199a-5p overexpression significantly attenuated Vps26A and Rab9B mRNA and protein expression (Fig. 1e and Fig. 1f). In addition to Vps26 and Rab9B, we observed that miR-199b-5p overexpression also decreases Rab7A mRNA and protein expression, suggesting that miR-199a-5p might influence Rab7A expression by an indirect mechanism. We further assessed whether miR-199-5p inhibition enhances Vps26A, Rab9B, Rab7A and SNX6 mRNA expression. Importantly, we found that miR-199a-5p antagonism in vitro increase the expression of these genes, suggesting that the endogenous expression of miR-199b-5p influences Vps26A, Rab9B, Rab7A and SNX6 expression (Fig. 1g). Taken together, these results suggest that miR-199a-5p might regulate retrograde transport by controlling directly the expression of Vps26A, Rab9B, Rab7A and SNX6.

MiR-199a-5p impairs intracellular retrograde transport.

Vps26A and SNX6 as part of the retromer (Popoff et al., 2007; Wassmer et al., 2007) and Rab9B and Rab7 in regulating endosome trafficking have been previously reported to have a role in RT (Deinhardt et al., 2006). A number of bacterial toxins including Shiga toxin B (STxB) use RT to enter into the cell (Sandvig et al., 1994). STxB binds to the glycolipid globotriaosylceramide (Gb3), its cellular receptor, and it is further internalized from endosomes to TGN, Golgi and finally locating at Endoplasmic Reticulum (ER). To assess whether miR-199a-5p controls retrograde transport pathway, we transfected HeLa cells with either miR-199a-5p or CM and assessed the internalization of fluorophore-tagged STxB (Cy3-STxB). As seen in Fig. 2a upper panel, STxB appears to be efficiently internalized after 30 min at 37°C of incubation with HeLa cells transfected with CM or miR-199a-5p. However, its accumulation in the TGN-Golgi region was markedly reduced in miR-199a-5p transfected cells, and the protein remained associated with peripheral structures, even

after 60 min of incubation (Fig. 2a lower panel, and fig. 2c). We next characterize the intracellular localization of STxB in cells transfected with miR-199a-5p mimics and found that miR-199a-5p enhances the co-localization of Cy3-STxB with EEA1, an early endosome marker, suggesting that miR-199a-5p impairs the transport from early endosomes to the Golgi (Fig. 2b and d). Interestingly, when we analyzed the Golgi structure in miR-199a-5p transfected cells, we observed an increased Golgi fragmentation compared with CM treated cells (Fig. 2a, arrowheads). This effect was quantified by measuring the number of independent GM130 stained structures in each condition (Fig. 2e). Since miRNAs might inhibit expression of many genes, we measured endogenous levels of EEA1 and the Golgi protein, GM130. As shown in fig. 2f, miR-199a-5p impaired trafficking of STxB is not due to changes of EEA1 and GM130 protein levels.

MiR-199a-5p overexpression markedly attenuates STxB-mediated inhibition of protein biosynthesis.

Given that miR-199a-5p impairs trafficking of STxB via retrograde route, we next tested whether miR-199a-5p might attenuate the inhibitory effect of STxB on protein biosynthesis. To this end, we transfected HeLa cells with CM or miR-199a-5p, then treated with increasing concentrations of STxB and assessed protein biosynthesis by measuring radiolabeled methionine into neosynthesized polypeptides. As seen in Fig. 2g, miR-199a-5p overexpression protects against the inhibitory effect of STxB on protein synthesis as early as 1 hr after toxin exposure. At this time, miR-199a-5p protects cells against Stx1 compared with CM treated cells with an observed protection factor of 3. This value is in close proximity to the observed when we treated HeLa cells with Vps26A siRNA (Fig. 2h). Together with our previous observations, these results strongly demonstrate that miR-199a-5p impairs retrograde transport.

Vps26A expression rescues retrograde transport and Golgi structure maintenance in miR-199a-5p overexpressing HeLa cells.

Vps26A plays a role in the organization of the retromer (Lieu and Gleeson, 2010) therefore, to gain insights into the molecular mechanism by which miR-199a-5p controls RT, we assessed whether Vps26A overexpression could rescue the effect of miR-199a-5p on RT. To this end, we transfected HeLa cells with vector-GFP (control) or Vps26A-GFP that lacked the 3' UTR sequence, thus resistant

to miR-199a-5p inhibitory action. The results showed that both GFP and Vps26A-GFP expressing cells transfected with CM internalized Cy3-STxB and accumulated in perinuclear membranes that were labeled by GM130 (Fig. 3a, upper panels). As seen before (fig. 2a), STxB accumulation in the Golgi area was also reduced in miR-199a-5p transfected cells that only expressed GFP. In contrast, expression of Vps26A-GFP rescued the inhibitory effect on RT in cells transfected with miR-199a-5p (Fig. 3a, lower panels and fig.3b). We also noticed that miR-199a-5p transfected cells that expressed Vps26A-GFP showed a compacted Golgi structure similar to CM transfected cells suggesting that restoration with ectopic Vps26A leads to a proper Golgi architecture maintenance (fig. 3c). These results suggest that Vps26A expression is a major determinant in the effect of miR-199a-5p in regulating RT.

Vps26A regulates subcellular localization and glycosylation state of TGN46

Next, we wondered whether miR-199a-5p might also influence the RT of an endogenous protein. Therefore, we tested whether miR-199a-5p influences the intracellular trafficking of TGN46, a transmembrane glycosylated protein that is localized to the TGN and cycles between the TGN and the plasma membrane (Ganley et al., 2008). In CM transfected cells, TGN46 is predominantly localized in the perinuclear Golgi as co-labeled with GM130 (Fig 4a, panel 1). We also observed that steady-state localization of ectopic Vps26A-GFP is perinuclear but also in endosomes (Fig 4a, panel 2). In contrast to cells transfected with CM, miR-199a-5p overexpression results in TGN46 and GM130 dispersion in the cell periphery, confirming Golgi fragmentation (Fig. 4a, panel 3). Because Vps26A was able to partially restore Golgi location of resident proteins such as GM130 and bacterial STxB retrograde cargo, we assessed whether Vps26A could also rescue the trafficking of endogenous cargoes such as TGN46. Of note, we found that transfection of Vps26A-GFP in miR-199a-5p overexpressing cells restored TGN46 perinuclear localization and Golgi architecture compared with Vps26-GFP non-transfected cells (Fig. 4a, panel 3 and 4).

We next studied the glycosylation pattern of TGN46. TGN46 has a molecular mass of 46 kDa, but as a result of various glycosylation processes occurring at the ER and the Golgi complex (Prescott et al., 1997), the mature protein has an apparent molecular mass of ~110 kDa (Fig. 4b). Interestingly, we found that miR-199a-5p overexpression results in a significant reduction of TGN46 molecular weight (~80 kDa), suggesting that miR-199a-5p impairs TGN46 transport between ER to Golgi, and leading to a reduced glycosylation (Fig. 4b, second line and 4d). More important, the

effect of miR-199a-5p overexpression on TGN46 glycosylation was partially restored when we transfected HeLa cells with a Vps26A construct resistant to miR-199a-5p inhibitory action (Fig. 4b, right line and 4d). Taken together, these results demonstrate that miR-199a-5p controls retrograde transport and Golgi homeostasis mainly by regulating the expression of Vps26A, an essential component of the retromer complex.

MiR-199a-5p controls the expression of M6PR and the lysosome function.

M6PR cycles between the plasma membrane, lysosomes and TGN/Golgi, in the latter M6PR binds to newly synthesized hydrolases that will be transported all the way to lysosomes (Kuliawat et al., 1997; Ludwig et al., 1993). It has been well established that this receptor uses RT to return from late endosomes/lysosomes to TGN and initiates a new cycle of delivery (Medigeshi and Schu, 2003). Interestingly, we found that M6PR is a predicted target for miR-199a-5p in our previous bioinformatic analysis (Fig. 1c). To directly demonstrate that M6PR is a bona fide miR-199a-5p target gene, we cloned the 3' UTR of M6PR in a luciferase reporter construct and measure luciferase activity in HeLa cells transfected with miR-199a-5p or CM. The results showed that miR-199a-5p markedly reduces luciferase activity (Fig. 5a). Most importantly, mutation in the two miR-199a-5p predicted binding sites within the 3' UTR of M6PR abolished the miR-199a-5p inhibitory action, thus confirming the direct binding of miR-199a-5p to the M6PR 3' UTR (Fig. 5a). We next evaluated the effect of miR-199a-5p overexpression on M6PR expression and functionality in HeLa cells. As seen in Fig. 5b and c, overexpression of miR-199a-5p significantly downregulated M6PR mRNA and protein expression compared to CM transfected cells. Moreover, miR-199a-5p largely decreased CI-M6PR internalization and intracellular distribution in live HeLa cells, suggesting that M6PR was not properly transported to lysosomes for degradation but accumulated in TGN (Fig. 5d).

M6PR dissociates from its ligands upstream of lysosomes allowing them to move to lysosomes, and M6PR is recycled back to the TGN. To assess the potential effect of miR-199a-5p on lysosome function, we assessed the colocalization of CD63, a lysosomal protein, with LysoTracker, a red fluorescence probe used for labeling acidic organelles in live cells. Interestingly, the results showed that miR-199a-5p attenuate the colocalization between CD63 and LysoTracker compared to CM cells (Fig. 6a). In addition to an impaired localization of LysoTracker in lysosomes, we also analyzed the internalization of LysoTracker Red fluorescence in control and transfected miR-199a-5p HeLa cells during 30 and 60 min. As shown in fig. 6b lower levels of LysoTracker Red in miR-199a-5p cells

suggest the inhibition in the lysosome acidification. We further analyzed the endolysosomal trafficking by assessing DQ red BSA (DQ-BSA), a fluorogenic probe that traffics through the endosomal pathway that undergoes quenching following proteolytic cleavage in the lysosome. As seen in Fig. 6c, HeLa cells treated with miR-199a-5p mimics had decreased lysosomal DQ-BSA degradation compared with CM cells, suggesting that the endolysosomal trafficking is also affected by miR-199a-5p. Because retromer functions in the RT of the M6PR from endosomes to the TGN, we wondered whether interfering of RT by overexpressing miR-199a-5p in HeLa cells would alter the trafficking of the receptors, leading to missorting of newly synthesized acid hydrolases. To test this hypothesis, we examined the expression of the precursors and mature form of cathepsin D by Western blotting. We found that in control mimic (CM) transfected cells most of the cathepsin D occurred as the 31-kDa mature form with small amounts of the 53-kDa precursor and 47-kDa intermediate forms (Fig. 6d). We also observed a reduced amount of the precursor forms in the conditional media isolated from CM transfected cells (Fig. 6d). This efficient processing and intracellular retention of mature cathepsin D form reflects the integrity of the normal mechanism for trafficking of the enzyme from the TGN to lysosomes. In contrast to the results obtained in CM transfected cells, miR-199a-5p overexpression increased the amount of intracellular cathepsin D precursors and intermediate forms (Fig. 6d). Moreover, the precursor form of cathepsin D was markedly increased in the conditional media of HeLa cells overexpressing miR-199a-5p (Fig. 6d, quantified in lower panel), suggesting that miR-199a-5p impairs the transport of cathepsin D to lysosomes. We also examined the degradation kinetics of epidermal growth factor receptor (EGFR), as the receptor-ligand complex is internalized from the cell surface into endosomes, which ultimately fuse with lysosomes for degradation (Ceresa and Bahr, 2006). The results showed that the total levels of EGFR protein were unaffected in cells with augmented miR-199a-5p levels (Fig. 6e, quantified in right panel). However, the degradation of EGFR was markedly delayed in miR-199a-5p transfected HeLa cells compared with CM transfected cells when examining the EGF-stimulation-mediated endocytic transport of EGFR to lysosomes (Fig. 6g, quantified in right panel). Collectively these results are consistent with the role of miR-199a-5p in regulating retromer function and CI-MPR sorting to lysosomes.

Because autophagic and endocytic pathways converge at the endosome prior to lysosome-mediated degradation (Huotari and Helenius, 2011), we finally asked whether miR-199a-5p plays a role in the autophagy pathway by means of regulation of endolysosomal transport. Upon autophagy induction, soluble microtubule-associated protein light chain 3 (LC3-I) is converted to a

lipidated form (LC3-II) that preferentially associates with the growing autophagosome membrane in puncta formations (Kabeya et al., 2000). Interestingly, we found that the expression of LC3-II and p62/SQSTM1, an autophagic substrate, were increased in miR-199a-5p overexpressing cells compared to CM transfected cells (Fig. 6e, quantified in right panel and fig.6f). These results collectively indicate that autophagosomes are substantially accumulated upon the increased expression of miR-199a-5p.

DISCUSSION

MiR-199a-5p has been shown to be involved in a wide variety of cellular processes such as various cancer development and progression, cardiomyocytes protection or skeletal formation. In particular, many genes associated with these biological processes have been identified as predicted targets of miR-199a-5p and only a few have been functionally validated and mechanistically characterized. The results of this work identify the first microRNA, miR-199a-5p, that collectively exerts its action in a complete set of mRNAs that are related with intracellular RT, thus regulating the abundance of RT protein machinery, specifically Vps26A and Rab9B, but also cargoes such as M6PR. MiR-199a-5p controls RT in HeLa cells at different levels. Firstly, miR-199a-5p is acting at the retromer functioning through diminishing levels of one of its component, Vps26A. Secondly, miR-199a-5p also inhibits the expression of Rab9b, a small GTPase involved in the RT from late endosomes/lysosomes to TGN that is independent of retromer complex. As a consequence of the miR-199a-5p impaired retrograde transport, the entry of bacterial toxins, such as STxB that follow classically the retromer route, is severely impaired. In fact, we demonstrated that miR-199a5p expression was able to protect cells against STxB intoxication. siRNA-mediated knockdown of Vps26A phenocopied the effect of miR-199a-5p during the STxB intoxication, strongly suggesting that miR-199a-5p may exert its protective function via this target. So we hypothesized that miR-199a-5p expression could trigger a first defense against virus and/or other pathogens preventing entry and consequently limiting infection.

Given the inhibitory role of miR-199a-5p over intracellular transport, future studies will clarify whether or not miR-199a-5p could also regulate the internalization of other pathogens such as Salmonella that utilizes RT to enter intracellular compartments (McGourty et al., 2012), but new investigations to address this point need to be done. miRNAs mainly function by translational repression and/ or mRNA degradation (Baek et al, 2008; Guo et al, 2010) MicroRNAs can exert their

actions due to perfect match within the small binding sequence in their targets mainly in the 3' UTR of mRNA, but we cannot exclude unexpected effects in other binding regions in the mRNAs, such as 5' UTR and coding sequences (Lytle et al., 2007), nor viral RNAs, like the case of miR-122 that is able to promote degradation of HBV through 5' UTR binding of (Thibault et al., 2015)

One important finding of this work is the fact of Vps26A expression was able to restore several defects upon miR-199a-5p overexpression in HeLa cells. Despite of microRNA can exert multiple effects by their ability to bind to hundreds of targets mRNA in several pathways, we tested the hypothesis of whether Vps26A was able to restore the different miR-199a-5p trafficking defects in the cell. By using a Vps26A-GFP form in a rescue of function experiment we demonstrated that STxB is efficiently transported to Golgi in cells regardless the elevated levels of miR-199a-5p, highlighting a key role of the retromer Vps26A component in the binding of of cargoes and subsequent transport to TGN. Given the overall effect of miR-199a-5p in intracellular trafficking we expect that miR-199a-5p has direct and indirect effects in RT. As an example, we can speculate that the observed disassembly of Golgi structure in miR-199a-5p cells occurs because of impaired traffic to TGN from endosomes. More importantly, we noticed that some defects in Golgi structure caused by miR-199a-5p expression was also partially restored using the rescue of function strategy, although we cannot exclude the possibility of direct effect of miR-199a-5p in the expression of multiple Golgi resident proteins, involved in both maintenance of Golgi structure, but also in glycosylation. In fact, our bioinformatics analysis showed a group of mRNA candidates coding for several glycosylation enzymes located in the Golgi with highly miR-199a-5p conserved binding sites (data not shown). And not only had that, the miR-199a-5p overexpression in HeLa cells caused de-glycosylation of endogenous RT cargoes such as TGN46. Although we have not explore the mechanism behind this effect, either for direct inhibition of any glycosylase/s or by indirect effect through disorganization of Golgi and hence glycosylation malfunctioning, we observed that Vps26A expression is sufficient to partially restore glycosylation levels in TGN46 probably due to improved RT to TGN.

Other interesting finding is that miR-199a-5p not only regulates RT protein machinery, but also target directly to natural RT cargo such as M6PR mRNA, thus it suggests that miR-199a-5p controls the entire endolysosomal functioning. Our results demonstrated that HeLa cells with elevated levels of miR-199a-5p showed reduced internalization of M6PR from plasma membrane and therefore affecting the normal function of lysosomes as shown by impaired trafficking of

Lysotracker and protein cleavage. Overexpression of miR-199a-5p caused missorting of hydrolase cathepsin D as similar extent that depletion of both Rab7 (Rojas et al., 2008) or Vps26A (Seaman, 2004). Other proof that Lysosomal function is compromised is the fact of EGFR degradation is delayed when high expression of miR-199a-5p remains in the cell. The effects of miR-199a-5p in lysosome functioning might be due not only to direct targeting to M6PR, but also to inhibition of RT and endocytosis as has been described previously (Aranda et al., 2015). In fact, it cannot be ruled out as in the case of other microRNAs, that miR-199a-5p regulates both processes together to coordinate a joint response. Lastly, because lysosomes are the final destination for degradation of endocytic cargoes, such as intracellular components delivered for macroautophagy, our results also showed a blockage of autophagosomal degradation as seen by increased levels of LC3 and p62 in miR-199a-5p overexpressed HeLa cells. This effect in autophagy is mediated most likely because of impaired endocytic trafficking through inhibition of Rab5, Rab7 and Rab9 GTPases, all of them has been reported to have a role in the regulation of autophagy (Jager et al., 2004; Nishida et al., 2009) (Ravikumar et al., 2008). In fact, it has been described recently a role of miR-199a-5p by direct targeting of autophagic regulators such as ATG7, ATGL14 and Beclin-1 (Xu et al., 2012; Yi et al., 2013). The latter could explain the observed indirect effect of miR-199a-5p over Rab5 and Rab7 downregulated expression. In addition to this perturbed endosomal trafficking, miR-199a-5p expression lead to a defective retrograde transport that also may account the lysosome malfunction and ultimately autophagy blockage.

In conclusion, the current study has identified miR-199a-5p as a new regulator of RT pathway mainly through Vps26A and has ascribed functions to this protein in the context of enhanced miR-199a-5p expression. Future studies should be done to determine which physiological and/or pathological conditions trigger changes in miR-199a-5p expression and therefore may influence endosomal trafficking.

EXPERIMENTAL PROCEDURES

Materials

Chemicals were obtained from Sigma-Aldrich unless otherwise noted. EGF was obtained from EMD/Calbiochem (Gibbstown, NJ, USA). Mouse monoclonal antibodies against HSP90, GM130 and EEA1 were purchased from BD Bioscience. The Rabbit antibodies against Vps26A, EGFR and TGN46 were from Abcam. The rabbit polyclonal antibodies to Rab9, LC3-II and p62 were purchased from

Cell Signaling Technology. M6PR monoclonal antibody was purchase from Calbiochem. A rabbit antibody to Cathepsin D was from Epitomics. The monoclonal anti-actin antibody was from Sigma. Red-Lysotracker, Red-DQ-BSA and Secondary fluorescently labeled antibodies were from Molecular Probes (Invitrogen). MiRNA mimics and inhibitors were obtained from Dharmacon. The Vps26A-GFP plasmid was kindly provided by Prof. Juan Bonifacino (Bethesda, NIH). Cy3-STxB was obtained as described in (Mallard et al., 1998).

Cell culture

Cervix carcinoma (HeLa) and monkey kidney fibroblast (COS7) cells were obtained from American Type Tissue Collection (ATCC) and were maintained in Dulbecco's Modified Eagle Medium (DMEM) containing 10 % fetal bovine serum (FBS) and 2 % penicillin-streptomycin in 10 cm² dishes at 37°C and 5 % CO₂. For EGFR degradation assay, subconfluent cultures of HeLa cells transfected with CM or miR-199a-5p were switched to serum-free medium and cultured for approximately 12 h. For EGF stimulation, recombinant EGF (EMD) was added to the medium at a final concentration of 100 ng/ml, and cells were cultured further for the indicated lengths of time.

Bioinformatic analysis of miRNA target genes.

Target mRNA for hsa-miR-199a/b were identified and compared using the online target prediction algorithm, miRWalk (<http://www.umm.uni-heidelberg.de/apps/zmf/mirwalk/>), which provides target interaction information from eight different prediction algorithms. Specifically, the programs miRanda, miRWalk and TargetScan were used. The putative targets produced by all three of these algorithms for miR-199a-5p were uploaded into the gene classification system, PANTHER v8.0 (<http://www.pantherdb.org>) to identify gene targets that were mapped to the transport process (GO:0006810). The functional interactions of these predicted mRNA targets for miR-199a/b-5p described in STRING v9.05 (<http://string-db.org>) were then combined with the functional annotation groups described in DAVID. Matlab and Cytoscape v2.8.3 were used to create the visualization networks, as previously described (Huang da et al., 2009). STRING interactions with a confidence score of 0.4 or higher were added and highlighted in bold. Smaller annotation clusters and unconnected genes were left out of the visualization due to space constraints.

miRNA mimic/inhibitor transfections

HeLa cells were transfected with 40 nM miRIDIAN miRNA mimics (miR-199a-5p) or with 60 nM miRIDIAN miRNA inhibitors (Inh-199a-5p) (Dharmacon) using RNAimax (Invitrogen) or Lipofectamine 2000 (Invitrogen) for co-transfection experiments with the Vps26A-GFP plasmid. All experimental control samples were treated with an equal concentration of a non-targeting control mimic sequence (CM) or inhibitor negative control sequence (CI). Verification of miR-199a-5p over-expression and inhibition was determined using qRT-PCR, as described below.

RNA isolation and quantitative real-Time PCR

Total RNA was isolated using TRIzol reagent (Invitrogen) according to the manufacturer's protocol. For mRNA quantification, cDNA was synthesized using iScript RT Supermix (Bio-Rad), following the manufacturer's protocol. Quantitative real-time PCR (qRT-PCR) analysis was performed in triplicate using iQ SYBR green Supermix (BioRad) on an iCycler Real-Time Detection System (Eppendorf). The mRNA level was normalized to GAPDH (glyceraldehyde-3-phosphate dehydrogenase) as a house keeping gene. The human primer sequences used were: GAPDH, 5'-TTGATTTGGAGGGATCTCG-3' and 5'-CAATGACCCCTTCATTGACC-3'; SNX6, 5'- GAAGCCCCATGCCGCCTGTC -3' and 5'-GGTGCCTGTCTGAGCACGGG -3'; M6PR 5'- GTGTGCCGGAAGCTGGCAA -3' and 5'-CCACGCTCCTCAGACACAGGGT -3'; Rab9B 5'- AGCCAGAAGTGGGACCCACA -3' and 5'-AGGCCCCAGGTCTCATGCACT -3'; Vps26A 5'- TGCTTGTTGATGAGGAAGACCGGAG -3' and 5'-GCCTTTTCCGCCCTCCA -3'; Rab7A 5'- GGGGCTGCTTTCTAACCCA -3' and 5'-TTTGCTAGGTCGGCCTTGTT -3'.

Western blot analysis

Western blot analysis was performed as we previously described (Aranda et al., 2015), briefly, cells were lysed in ice-cold buffer containing 50 mM Tris-HCl, pH 7.5, 125 mM NaCl, 1 % NP-40, 5.3 mM NaF, 1.5 mM NaP, 1 mM orthovanadate and 1 mg/ml of protease inhibitor cocktail (Roche) and 0.25 mg/ml AEBSF (Roche). Then, cell lysates were rotated at 4°C for 1 h before the insoluble material was removed by centrifugation at 12000 x g for 10 min. After normalizing for equal protein concentration, cell lysates were resuspended in SDS sample buffer before separation by SDS-PAGE. Following overnight transfer of the proteins onto nitrocellulose membranes, the membranes were

probed with the following antibodies: Vps26A (1:1000), Rab7 (1:500), Rab9 (1:1000), EEA-1 (1:1000), GM130 (1:1000), TGN46 (1:1000), actin (1:1000) and HSP90 (1:1000). Protein bands were visualized using the Odyssey Infrared Imaging System (LI-COR Biotechnology). Densitometry analysis of the gels was carried out using ImageJ software from the NIH (<http://rsbweb.nih.gov/ij/>).

Fluorescence microscopy

For M6PR-Ab internalization HeLa cells were grown on coverslips and transfected with a miR-199a-5p mimic and a negative control mimic (CM) in DMEM containing 10 % FBS. 48h post transfection, cells were cooled to 4°C for 20 min to stop membrane internalization. Cells were then incubated with M6PR mAb (2G11) (Calbiochem) for 40 min at 4°C. Following incubation, cells were gently washed twice with cold medium and shifted to 37°C to allow for internalization of both M6PR-Ab complexes for the indicated times and fixed with 4 % PFA. After 5 min of Triton X-100 0.2 % permeabilization and 15 min of blocking (PBS-BSA 3 %), cells were stained with anti-mouse Alexa 488 (Molecular Probes) Alexa-594-Phalloidin and TO-PRO 3 (Life Technologies) for 1h at room temperature. After this, cells were washed twice with 1x PBS and mounted on glass slides with Prolong-Gold (Life Technologies).

For Vps26A-GFP rescue experiments, HeLa cells were grown on coverslips and co-transfected with 1 µg Vps26A-GFP and 40 nM of a control mimic CM or miR-199a-5p mimic. 48h post transfection cells were incubated or not with StxB-Cy3 as described. Then, cells were washed twice with 1x PBS, fixed with 4 % PFA, and blocked (3 % BSA in 1x PBS) for 15 min. Following this, cells were washed twice and mounted on glass slides with Prolong-Gold (Life Technologies). All images were analyzed using confocal microscopy (Leica SP5 II) equipped with a 63X Plan Apo Lenses. All gains for the acquisition of comparable images were maintained constant. Analysis of different images was performed using ImageJ (NIH) and Adobe Photoshop CS5.

Image Analysis and Quantification

MacBiophotonics ImageJ was used for image quantification and analysis. To quantify the morphology of the Golgi apparatus, the immunofluorescence of GM130 was recorded as a digital, 8-bit gray-scale, 1024x1024 resolution images. The Golgi labeling image threshold was set at 90 on a 0–255 black to white scale (all pixels with a value under 90 are excluded from the quantification)

to remove background pixels from measurement. A region of interest was defined for each cell, and the number of individual Golgi fragments with a minimum area of three pixels was measured. To quantify colocalization between STxB-Cy3 and GM130 or EEA1 we used the intensity correlation analysis plug in developed for the ImageJ 1.36b software (National Institutes of Health). After image thresholding, the extent of colocalization was obtained by calculating the Pearson coefficients (R1) and the corresponding standard deviation (Bolte and Cordelieres, 2006).

3'UTR luciferase reporter assays

cDNA fragments corresponding to the entire 3'UTR of human Vps26A, Rab9B, SNX6, Rab7A and M6PR were amplified by RT-PCR from total RNA extracted from Huh7 cells with XhoI and NotI linkers. The PCR product was directionally cloned downstream of the Renilla luciferase open reading frame of the psiCHECK2™ vector (Promega) that also contains a constitutively expressed firefly luciferase gene, which is used to normalize transfections. Point mutations in the seed region of the predicted miR-199a binding sites within all the above 3'UTR were generated using the Multisite-Quickchange Kit (Stratagene), according to the manufacturer's protocol. All constructs were confirmed by sequencing. COS7 cells were plated into 12-well plates (Costar) and co-transfected with 1 µg of the indicated 3'UTR luciferase reporter vectors and miR-199a-5p mimics, or control mimics (CM) (Dharmacon) utilizing Lipofectamine 2000 (Invitrogen). Luciferase activity was measured using the Dual-Glo Luciferase Assay System (Promega). Renilla luciferase activity was normalized to the corresponding firefly luciferase activity and plotted as a percentage of the control (cells co-transfected with the corresponding concentration of control mimic). Experiments were performed in triplicate wells of a 12-well plate and repeated at least three times.

Lysotracker internalization assay

For analysis of Red Lysotracker internalization cells were incubated for 30 and 60 min at 37°C in serum-free DMEM. Firstly, cells were first incubated on serum-free media for 30 min. Cells were washed to remove non-internalized Lysotracker and analyzed by FACS experiments or fixed in 4 % PFA 15 min for fluorescence microscopy analysis.

DQ-BSA-green degradation assay

To measure the lysosomal degradation of soluble proteins we used a DQ-BSA-green degradation assay. DQ-BSA-green is a BSA labeled with a self-quenching fluorescent dye. The hydrolysis of the DQ-BSA-green into single dye-labeled peptides by lysosomal proteases relieves self-quenching, thus allowing us to measure the lysosomal DQBSA-green transport. The assay was done according to the manufacturer's protocol (Molecular Probes/Invitrogen, Eugene, OR). Briefly, mock- or siRNA-treated HeLa cells were loaded with 200 $\mu\text{g/ml}$ DQ-BSA-green for 1 h at 37°C. Cells were then washed to remove extracellular DQ-BSA-green and incubated at 37°C for 2 h. The fluorescence of DQ-BSA-green was then monitored by flow cytometry

Statistics

All data are expressed as mean \pm SEM. Statistical differences were measured using an unpaired Student's t test. A value of $P \leq 0.05$ was considered statistically significant. Data analysis was performed using GraphPad Prism Software Version 6.03 (GraphPad, San Diego, CA). * $P \leq 0.05$.

ACKNOWLEDGMENTS

We thank Dr. Juan Bonifacino for generously providing the Vps26A-GFP plasmid. We also thank Carlos Estella for critical discussions and comments about this work. This work was supported by grants from the National Institutes of Health, R01HL107953 and R01HL106063 to CF-H, the Foundation Leducq (MIRVAD network) to CF-H and an Established Investigator Award (16EIA27550004) to CF-H.

FIGURE LEGENDS

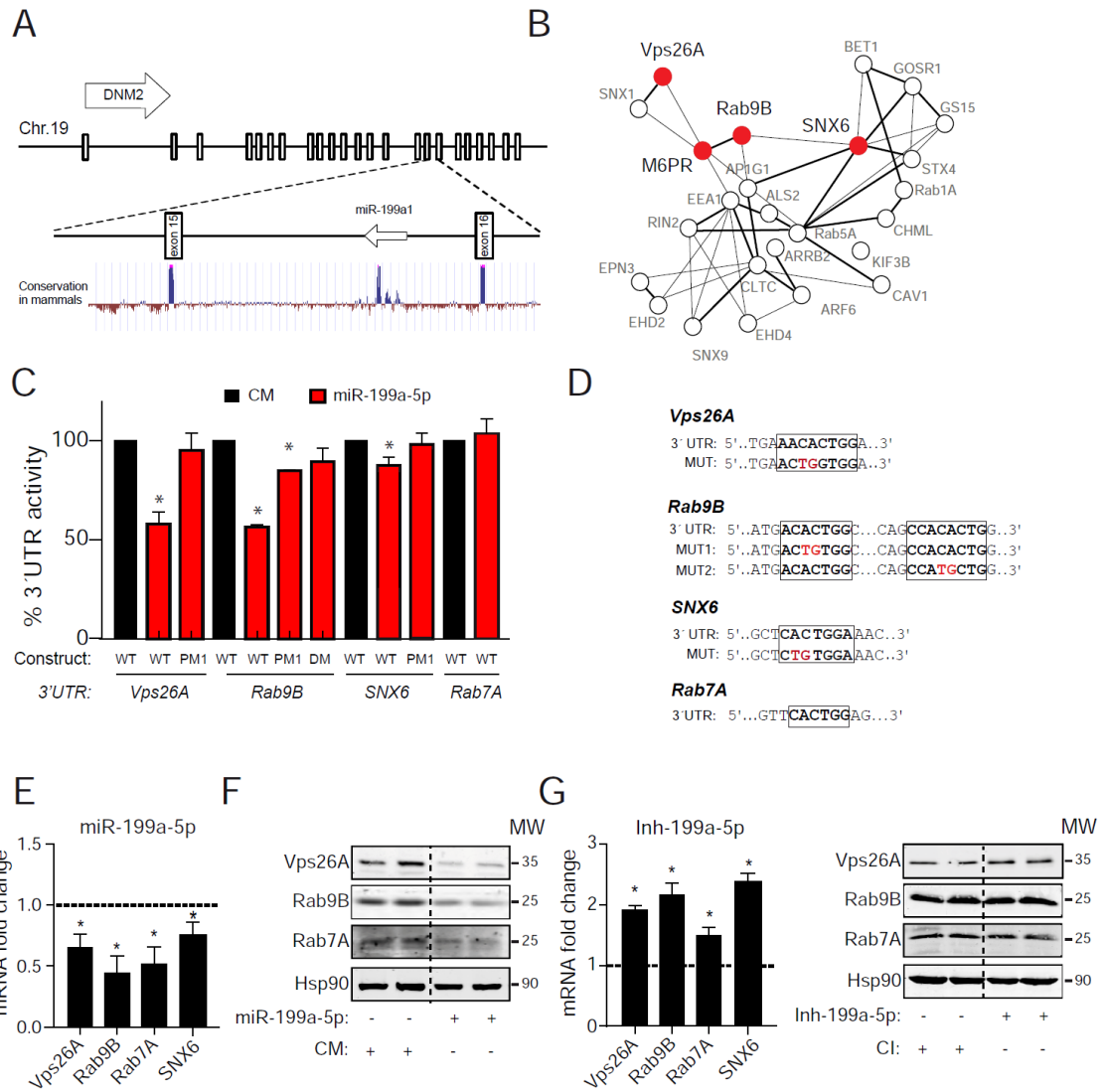


Figure 1. MiR-199a is encoded in DNM loci genomic location regulates the expression of genes associated to the retrograde transport. (A) Schematic representation of genomic location of DNM2 gene and intronic miR-199a1. (B) Gene ontology analysis of the predicted miR-199a/b target genes using Panther software. A protein–protein interaction analysis scheme of selected predicted miR-199a-5p target genes using String 9.1 software and Navigator 2.2. is shown. Retrograde transport protein coding genes are highlighted in red (C-D) Luciferase reporter activity in COS7 cells transfected with control mimic or miR-199a-5p mimic and the indicated human 3' UTR containing or not (wild-type, WT) the indicated point mutation in the target miR-199a-5p-binding sites. (E) Gene expression analyses (qRT-PCR) of Vps26A, Rab9B, Rab7A and SNX6 expression in HeLa cells transfected with non-targeting control mimic (CM) and miR-199a-5p mimic (F). Western blot analysis of Vps26A, Rab9B and Rab7A in HeLa cells transfected with control mimic or miR-199a-5p mimic (left panel). Hsp90 was used as a loading control. (G) Gene expression analyses (qRT-PCR) of Vps26A, Rab9B, Rab7A and SNX6 expression in HeLa cells transfected with control inhibitor (CI) or miR-199a-5p inhibitor. Results are mean±SEM for three experiments. In C, data are expressed as percentage of 3'UTR activity of control mimic (±SEM) and are representative of ≥3 experiments performed in triplicate. In E, data are expressed as a mean±SEM, and representative of ≥3 experiments in triplicate. *P≤0.05.

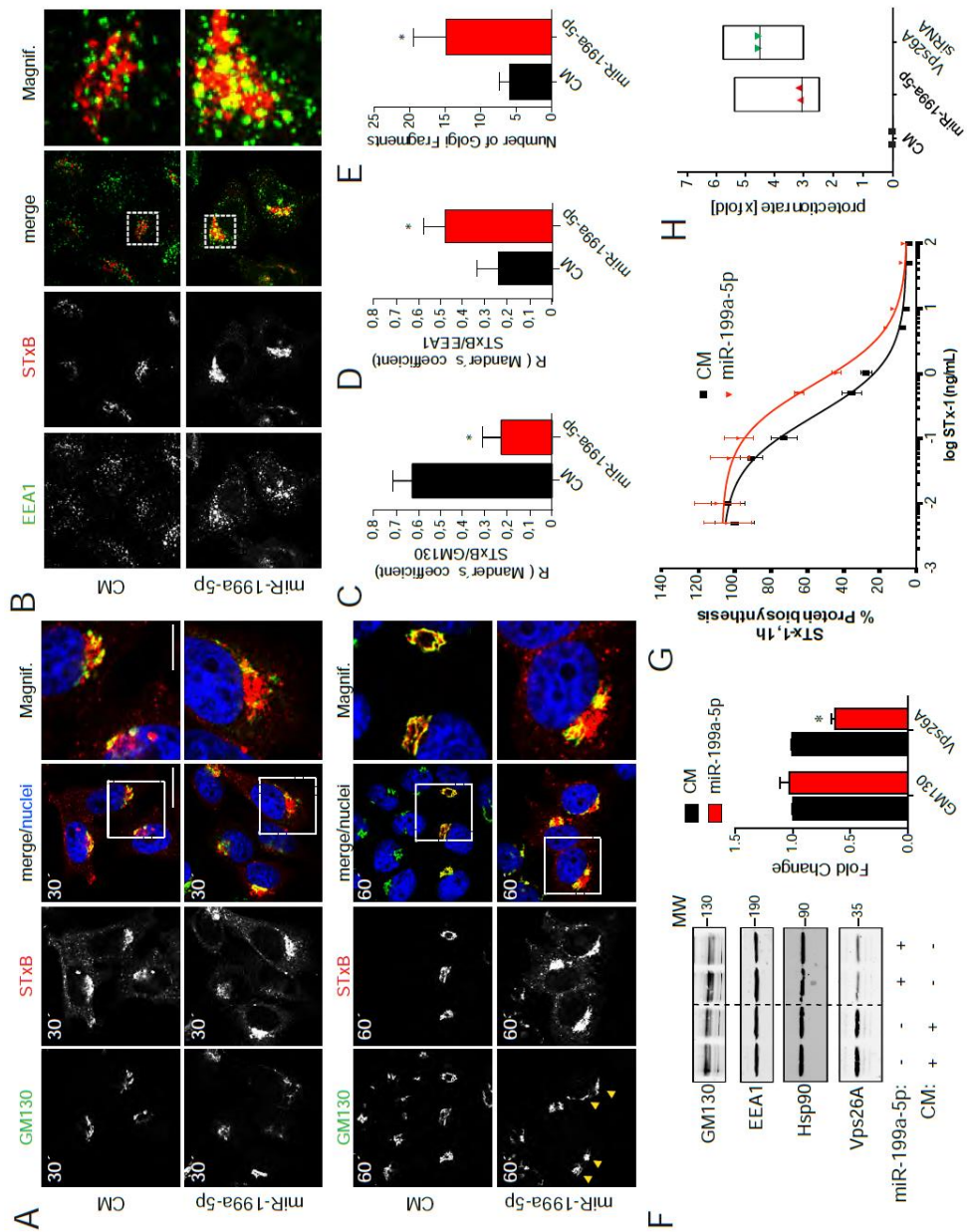


Figure 2. miR-199a-5p regulates Shiga toxin internalization and protect against intoxication in HeLa cells. (A) CM and miR-199a-5p transfected cells during 48 h were incubated with Cy3-STxB (5 μ g/mL) on ice, which were then shifted to 37°C for 30 min (upper panel) and 60 min (lower panel). (B) HeLa cells treated as (A) and incubated with Cy3-STxB (5 μ g/mL) on ice, which were then shifted to 37°C for 30 min. In A and B cells were fixed and labeled for GM130 (A), EEA1 (B) and DAPI (A-B) and Z-projections of confocal stacks are shown. Note that in miR-199a-5p overexpressing cells, increased accumulation of STxB in peripheral membranes was observed. Magnification inset are shown in right panels. (C-D) Quantification of the colocalization manders coefficients of Cy3-STxB localized in the Golgi (GM130) or early endosomes (EEA1) in experiments as shown in (A) and (B) respectively. (E) Quantification of Golgi fragments in CM and miR-199a-5p transfected cells showed in A. Arrowheads show Golgi dispersed structures (F). Western blot analysis of GM130, EEA1 and Vps26A in cells transfected with CM and miR-199a-5p. Quantification of the relative amounts of proteins on experiments is shown in right panel. The means \pm SEM of three independent experiments are shown. (G) HeLa cells were transfected 48 h with CM (black data points) and miR-199a-5p (red data points) before addition of Shiga toxin 1h. Intoxication of HeLa cells is shown. Each point corresponds to the mean \pm SEM of a representative experiment out of two to three determinations. (H) Protection factors calculated over the indicated number of experiments. Means \pm SEM are shown. The p-Value was calculated using the t-test. *P \leq 0.05 Scale bars=15 μ M

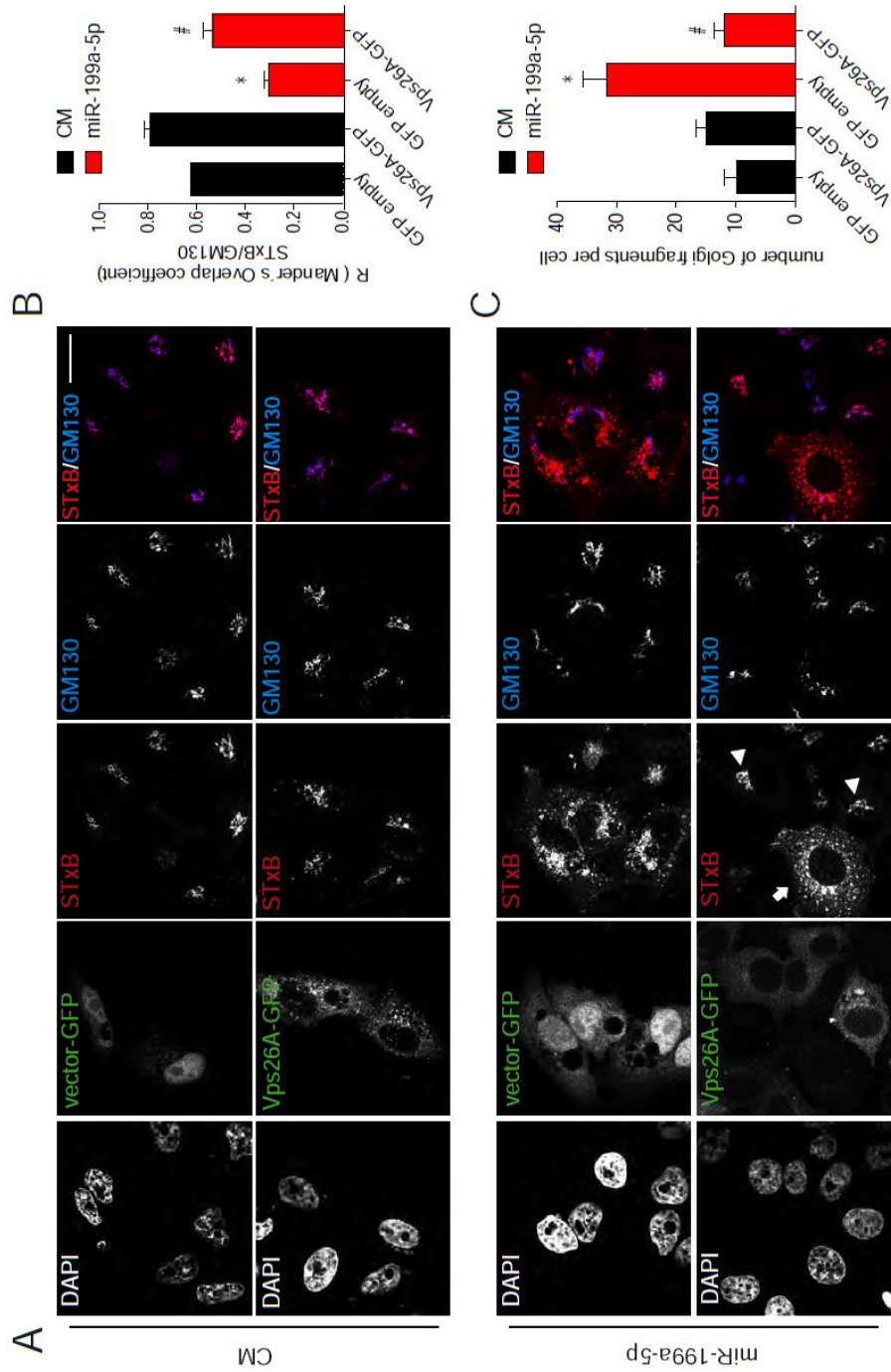


Figure 3. Vps26A is necessary for Shiga toxin internalization and Golgi maintenance structure in miR-199a-5p overexpressing HeLa cells. (A) HeLa cells co-transfected as indicated, CM and GFP or Vps26A-GFP in upper panel and miR-199a-5p with GFP or Vps26A-GFP in lower panel during 48 h. Live cells were incubated with Cy3-STxB (5 μ g/mL) on ice, which were then shifted to 37°C for 60 min; After internalization assay cells were fixed and labeled for GM130 and DAPI and Z-projections of confocal stacks are shown. Arrow indicates miR-199a-5p overexpressing cell with increased accumulation of STxB in peripheral membranes and arrowheads show Vps26A-GFP cells that efficiently accumulates StxB in Golgi area as labeled with GM130. (B) Quantification of the colocalization coefficient of Cy3-STxB and GM130 in the different observed conditions of three independent experiments are shown. (C) Quantification of Golgi fragments in the different observed conditions of three independent experiments are shown. Arrowheads show Golgi dispersed structures. Data are expressed as mean \pm SEM. *P \leq 0.05 and # P>0.05.

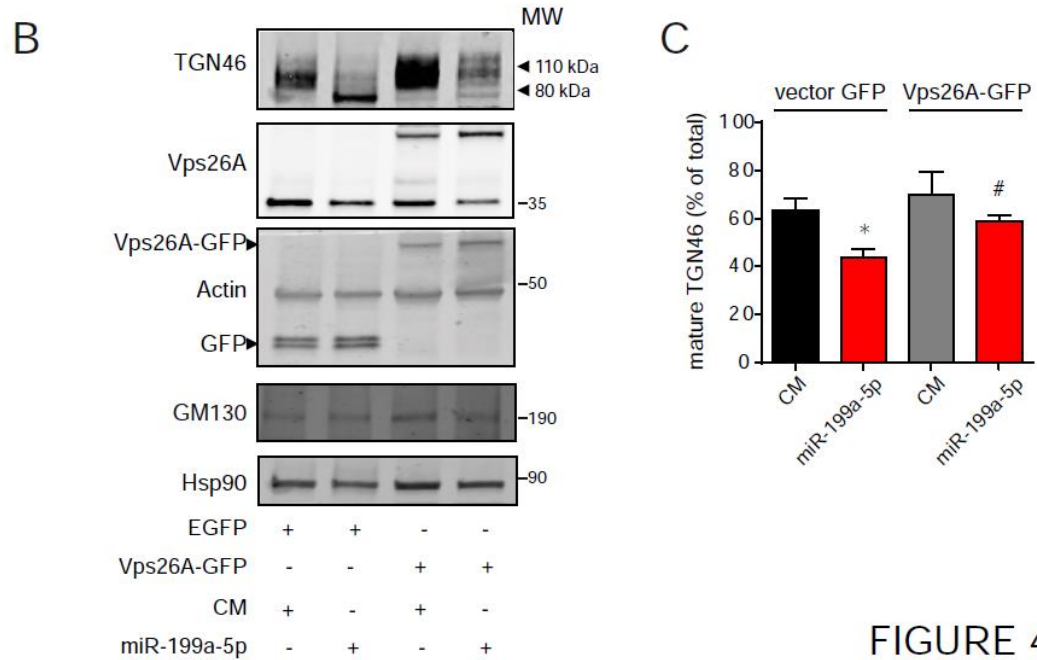
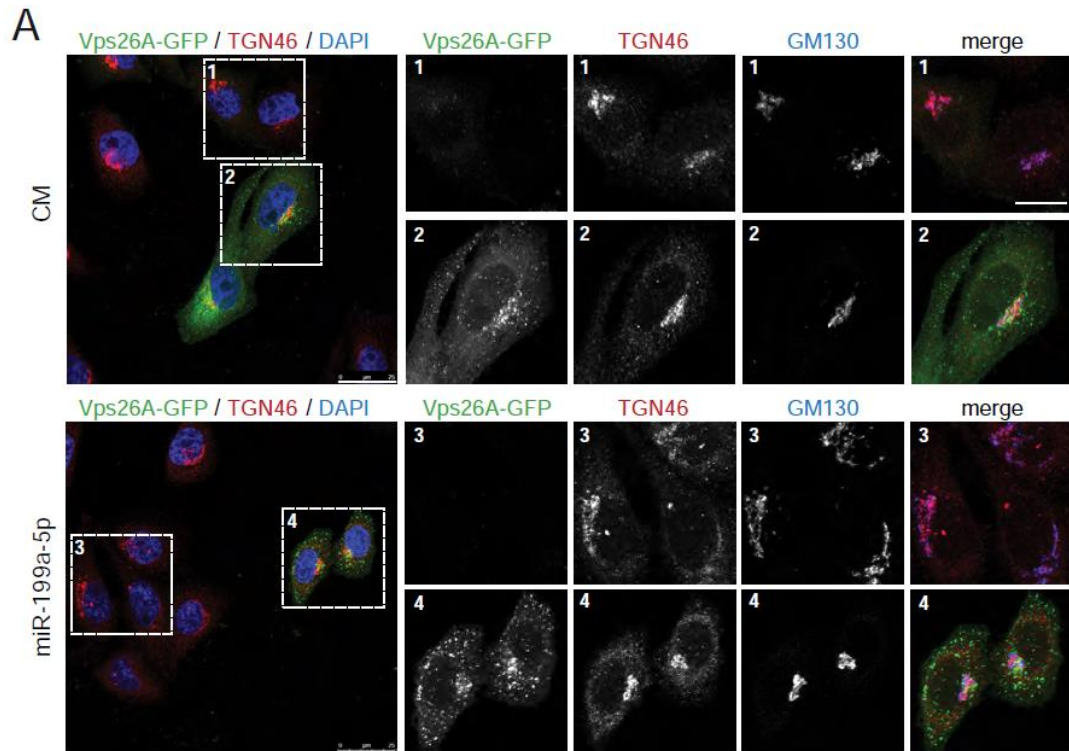


FIGURE 4

Figure 4. Vps26A is necessary for TGN46 Retrograde transport. (A) HeLa cells co-transfected as indicated, CM and Vps26A-GFP in upper panel and miR-199a-5p and Vps26A-GFP in lower panel during 48 h. Cells were fixed and labeled for GM130 and DAPI and their steady state localization were observed and shown in Z-projections of confocal stacks. (B) HeLa cells transfected as indicated (CM/EGFP, miR-199a-5p/EGFP, CM/Vps26A-GFP and miR-199a-5p/Vps26A-GFP) were analyzed by western blot for TGN46, GM130 and Vps26A expression. Actin and Hsp90 were used as loading control. (C) Quantification of mature TGN46 is as percentage of total. Data are expressed as % mean of the total TGN46 \pm SEM. * $P < 0.05$ and # $P > 0.05$.

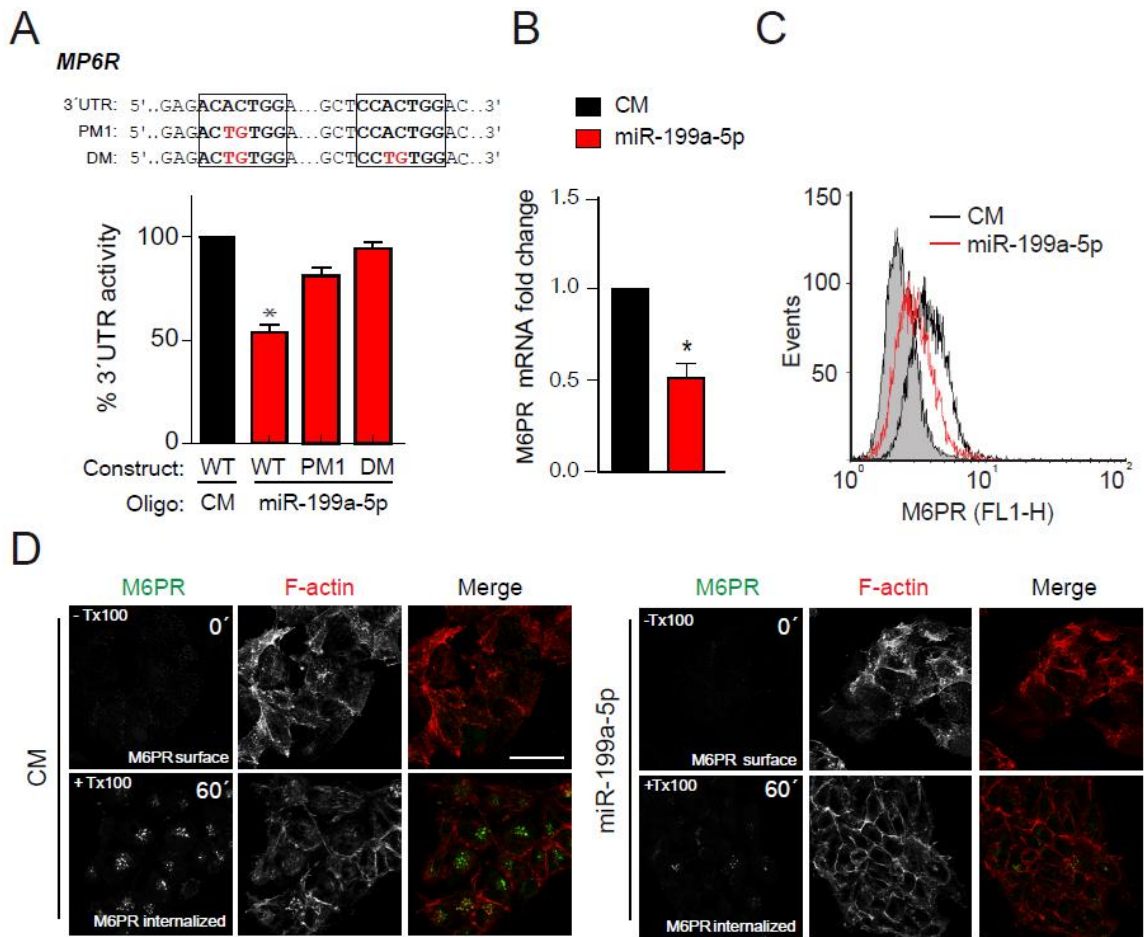


Figure 5. MiR-199a-5p regulates M6PR expression and subcellular localization. (A) Luciferase reporter activity in COS7 cells transfected with control mimic or miR-199a-5p mimic and M6PR 3' UTR containing or not (wild-type, WT) the indicated point mutation in the target miR-199a-5p-binding sites. (B). qRT-PCR expression analysis of M6PR expression in HeLa cells transfected with non-targeting control mimic (CM) and miR-199a-5p mimic. (C) Flow cytometry analysis of M6PR protein expression in HeLa cells treated as in (B). (D) Confocal microscopy immunofluorescence showing HeLa cells transfected with CM or miR-199a-5p and incubated with anti-M6PR antibody for 60 min at 4°C before fixing and then staining with anti-mouse Alexa 488 for M6PR antibody (first and third panel) or treated as above and then allowed to internalize antibody complexes for 30 min at 37°C, PFA fixed and then stained with anti-mouse Alexa 488 (second and forth panel). To visualize the F-actin fibers and nuclei, phalloidin-red and DAPI were used respectively. In A, data are expressed as a percentage of 3'UTR activity of control mimic (\pm SEM) and are representative of ≥ 3 experiments performed in triplicate. In B data are expressed as mean \pm s.e.m and representative of ≥ 3 experiments in triplicate. * $P \leq 0.05$.

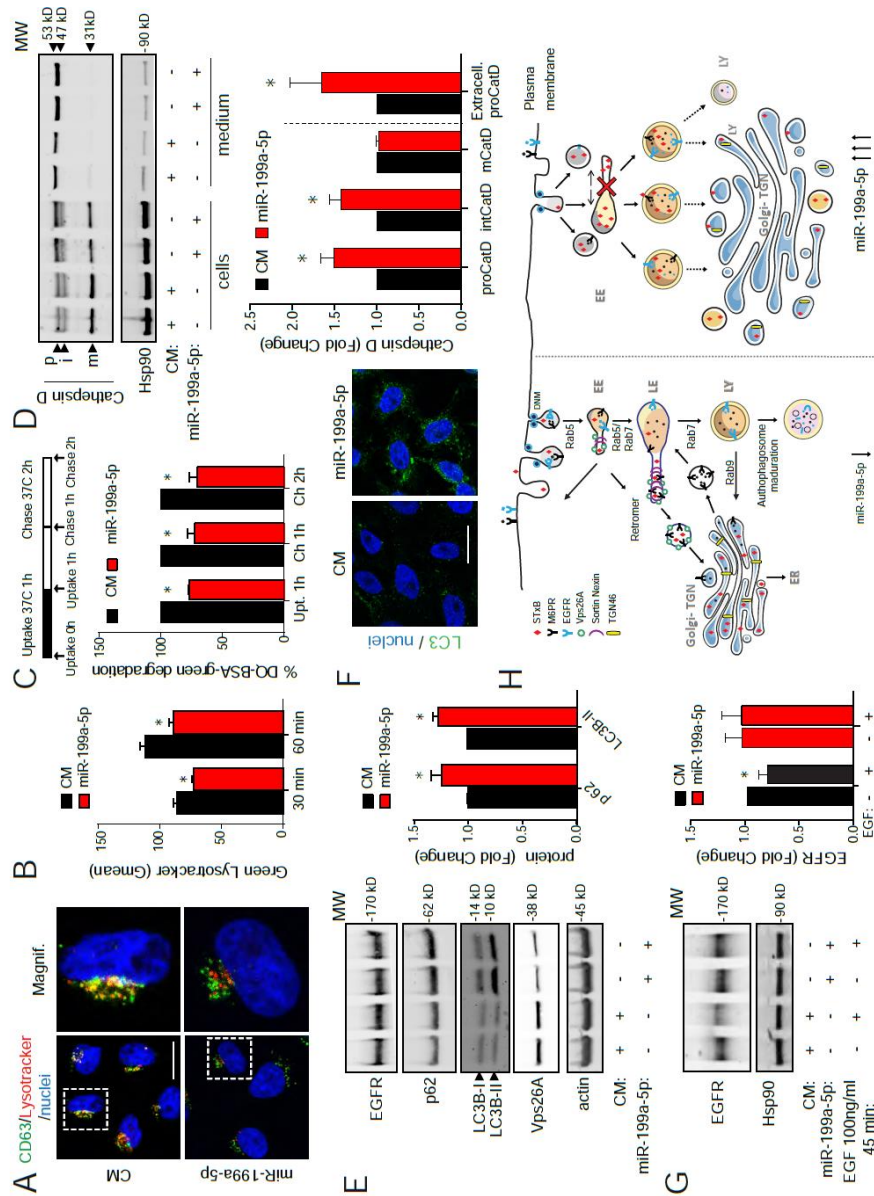


Figure 6. MiR-199a-5p regulate endolysosomal trafficking. (A) Confocal microscopy immunofluorescence images showing subcellular localization of CD63 (green) subjected to 30 min Red-LysoTracker internalization at 37°C in HeLa cells transfected as indicated. Magnification insets are shown in the right panel. (B) Flow cytometry analysis Red-LysoTracker internalization at 37°C in HeLa cells treated as in (A). Data are expressed as Gmean of three independent experiments. (C) Flow cytometry of CM or miR-199a-5p transfected HeLa cells that were cultured in presence of 200 µg/ml fluorescence DQ-BSA-green for 1 h at 37°C and incubated at 37°C for 2 h. Data are expressed as fold change of Gmean±SEM. (D) HeLa cells were treated transfected with CM and miR-199a-5p. 24 h after transfection, cells were rinsed with PBS and incubated in serum-free culture medium for 24 h. The medium was collected and precipitated with trichloroacetic acid (TCA), and the resulting pellets were analyzed by 4 – 20 % acrylamide gradient SDS-PAGE and immunoblotted with rabbit polyclonal antibody against cathepsin D. Blots were also probed with antibody to Hsp90 as a loading control. The positions of molecular mass markers (KDa) and of the precursor (pCatD), intermediate (iCatD), and mature (mCatD) forms of cathepsin D are indicated. Quantification of 3 independent experiments is shown in histograms in the lower panel. (E) Western blot analysis of EGFR, p62, LC3B-I/LC3B-II and Vps26A proteins levels in CM and miR-199a-5p transfected cells. Quantification is shown in right panel. (F) Confocal immunofluorescence analysis of LC3 in HeLa cells treated as indicated. (G) EGFR degradation assay in EGF-stimulated HeLa cells transfected with CM and miR-199a-5p. Quantification is shown in right panel. (H) Proposed model of regulation of retrograde transport by DNM/miR-199a-5p. *P<0.05

REFERENCES

- Amessou, M., Carrez, D., Patin, D., Sarr, M., Grierson, D.S., Croisy, A., Tedesco, A.C., Maillard, P., and Johannes, L. (2008). Retrograde delivery of photosensitizer (TPPp-O-beta-GluOH)₃ selectively potentiates its photodynamic activity. *Bioconjugate chemistry* 19, 532-538.
- Aranda, J.F., Canfran-Duque, A., Goedeke, L., Suarez, Y., and Fernandez-Hernando, C. (2015). The miR-199-dynamin regulatory axis controls receptor-mediated endocytosis. *Journal of cell science* 128, 3197-3209.
- Arighi, C.N., Hartnell, L.M., Aguilar, R.C., Haft, C.R., and Bonifacino, J.S. (2004). Role of the mammalian retromer in sorting of the cation-independent mannose 6-phosphate receptor. *The Journal of cell biology* 165, 123-133.
- Bolte, S., and Cordelieres, F.P. (2006). A guided tour into subcellular colocalization analysis in light microscopy. *Journal of microscopy* 224, 213-232.
- Bonifacino, J.S., and Rojas, R. (2006). Retrograde transport from endosomes to the trans-Golgi network. *Nature reviews Molecular cell biology* 7, 568-579.
- Ceresa, B.P., and Bahr, S.J. (2006). rab7 activity affects epidermal growth factor:epidermal growth factor receptor degradation by regulating endocytic trafficking from the late endosome. *The Journal of biological chemistry* 281, 1099-1106.
- Chia, P.Z., Gasnereau, I., Lieu, Z.Z., and Gleeson, P.A. (2011). Rab9-dependent retrograde transport and endosomal sorting of the endopeptidase furin. *Journal of cell science* 124, 2401-2413.
- Chia, P.Z., and Gleeson, P.A. (2011). The regulation of endosome-to-Golgi retrograde transport by tethers and scaffolds. *Traffic* 12, 939-947.
- Deinhardt, K., Salinas, S., Verastegui, C., Watson, R., Worth, D., Hanrahan, S., Bucci, C., and Schiavo, G. (2006). Rab5 and Rab7 control endocytic sorting along the axonal retrograde transport pathway. *Neuron* 52, 293-305.
- Dong, B., Kakiyama, K., Otani, T., Wada, H., and Hayashi, S. (2013). Rab9 and retromer regulate retrograde trafficking of luminal protein required for epithelial tube length control. *Nature communications* 4, 1358.
- Ganley, I.G., Espinosa, E., and Pfeffer, S.R. (2008). A syntaxin 10-SNARE complex distinguishes two distinct transport routes from endosomes to the trans-Golgi in human cells. *The Journal of cell biology* 180, 159-172.
- Hierro, A., Gershlick, D.C., Rojas, A.L., and Bonifacino, J.S. (2015). Formation of Tubulovesicular Carriers from Endosomes and Their Fusion to the trans-Golgi Network. *International review of cell and molecular biology* 318, 159-202.
- Hierro, A., Rojas, A.L., Rojas, R., Murthy, N., Effantin, G., Kajava, A.V., Steven, A.C., Bonifacino, J.S., and Hurley, J.H. (2007). Functional architecture of the retromer cargo-recognition complex. *Nature* 449, 1063-1067.
- Huang da, W., Sherman, B.T., and Lempicki, R.A. (2009). Systematic and integrative analysis of large gene lists using DAVID bioinformatics resources. *Nat Protoc* 4, 44-57.
- Huotari, J., and Helenius, A. (2011). Endosome maturation. *The EMBO journal* 30, 3481-3500.
- Jager, S., Bucci, C., Tanida, I., Ueno, T., Kominami, E., Saftig, P., and Eskelinen, E.L. (2004). Role for Rab7 in maturation of late autophagic vacuoles. *Journal of cell science* 117, 4837-4848.
- Johannes, L., and Popoff, V. (2008). Tracing the retrograde route in protein trafficking. *Cell* 135, 1175-1187.
- Kuliawat, R., Klumperman, J., Ludwig, T., and Arvan, P. (1997). Differential sorting of lysosomal enzymes out of the regulated secretory pathway in pancreatic beta-cells. *The Journal of cell biology* 137, 595-608.
- Laufman, O., Hong, W., and Lev, S. (2011). The COG complex interacts directly with Syntaxin 6 and positively regulates endosome-to-TGN retrograde transport. *The Journal of cell biology* 194, 459-472.
- Lieu, Z.Z., Derby, M.C., Teasdale, R.D., Hart, C., Gunn, P., and Gleeson, P.A. (2007). The golgin GCC88 is required for efficient retrograde transport of cargo from the early endosomes to the trans-Golgi network. *Molecular biology of the cell* 18, 4979-4991.
- Lieu, Z.Z., and Gleeson, P.A. (2010). Identification of different itineraries and retromer components for endosome-to-Golgi transport of TGN38 and Shiga toxin. *European journal of cell biology* 89, 379-393.
- Liu, T.T., Gomez, T.S., Sackey, B.K., Billadeau, D.D., and Burd, C.G. (2012). Rab GTPase regulation of retromer-mediated cargo export during endosome maturation. *Molecular biology of the cell* 23, 2505-2515.

Ludwig, T., Ovitt, C.E., Bauer, U., Hollinshead, M., Remmler, J., Lobel, P., Ruther, U., and Hoflack, B. (1993). Targeted disruption of the mouse cation-dependent mannose 6-phosphate receptor results in partial missorting of multiple lysosomal enzymes. *The EMBO journal* 12, 5225-5235.

Lytle, J.R., Yario, T.A., and Steitz, J.A. (2007). Target mRNAs are repressed as efficiently by microRNA-binding sites in the 5' UTR as in the 3' UTR. *Proceedings of the National Academy of Sciences of the United States of America* 104, 9667-9672.

Mallard, F., Antony, C., Tenza, D., Salamero, J., Goud, B., and Johannes, L. (1998). Direct pathway from early/recycling endosomes to the Golgi apparatus revealed through the study of shiga toxin B-fragment transport. *The Journal of cell biology* 143, 973-990.

McGourty, K., Thurston, T.L., Matthews, S.A., Pinaud, L., Mota, L.J., and Holden, D.W. (2012). Salmonella inhibits retrograde trafficking of mannose-6-phosphate receptors and lysosome function. *Science* 338, 963-967.

Medigeschi, G.R., and Schu, P. (2003). Characterization of the in vitro retrograde transport of MPR46. *Traffic* 4, 802-811.

Nishida, Y., Arakawa, S., Fujitani, K., Yamaguchi, H., Mizuta, T., Kanaseki, T., Komatsu, M., Otsu, K., Tsujimoto, Y., and Shimizu, S. (2009). Discovery of Atg5/Atg7-independent alternative macroautophagy. *Nature* 461, 654-658.

Perez-Victoria, F.J., Mardones, G.A., and Bonifacino, J.S. (2008). Requirement of the human GARP complex for mannose 6-phosphate-receptor-dependent sorting of cathepsin D to lysosomes. *Molecular biology of the cell* 19, 2350-2362.

Popoff, V., Mardones, G.A., Tenza, D., Rojas, R., Lamaze, C., Bonifacino, J.S., Raposo, G., and Johannes, L. (2007). The retromer complex and clathrin define an early endosomal retrograde exit site. *Journal of cell science* 120, 2022-2031.

Prescott, A.R., Lucocq, J.M., James, J., Lister, J.M., and Ponnambalam, S. (1997). Distinct compartmentalization of TGN46 and beta 1,4-galactosyltransferase in HeLa cells. *European journal of cell biology* 72, 238-246.

Ravikumar, B., Imarisio, S., Sarkar, S., O'Kane, C.J., and Rubinsztein, D.C. (2008). Rab5 modulates aggregation and toxicity of mutant huntingtin through macroautophagy in cell and fly models of Huntington disease. *Journal of cell science* 121, 1649-1660.

Rojas, R., Kametaka, S., Haft, C.R., and Bonifacino, J.S. (2007). Interchangeable but essential functions of SNX1 and SNX2 in the association of retromer with endosomes and the trafficking of mannose 6-phosphate receptors. *Molecular and cellular biology* 27, 1112-1124.

Rojas, R., van Vlijmen, T., Mardones, G.A., Prabhu, Y., Rojas, A.L., Mohammed, S., Heck, A.J., Raposo, G., van der Sluijs, P., and Bonifacino, J.S. (2008). Regulation of retromer recruitment to endosomes by sequential action of Rab5 and Rab7. *The Journal of cell biology* 183, 513-526.

Sandvig, K., Garred, O., Prydz, K., Kozlov, J.V., Hansen, S.H., and van Deurs, B. (1992). Retrograde transport of endocytosed Shiga toxin to the endoplasmic reticulum. *Nature* 358, 510-512.

Sandvig, K., Ryd, M., Garred, O., Schweda, E., Holm, P.K., and van Deurs, B. (1994). Retrograde transport from the Golgi complex to the ER of both Shiga toxin and the nontoxic Shiga B-fragment is regulated by butyric acid and cAMP. *The Journal of cell biology* 126, 53-64.

Seaman, M.N. (2004). Cargo-selective endosomal sorting for retrieval to the Golgi requires retromer. *The Journal of cell biology* 165, 111-122.

Shiba, Y., Kametaka, S., Waguri, S., Presley, J.F., and Randazzo, P.A. (2013). ArfGAP3 regulates the transport of cation-independent mannose 6-phosphate receptor in the post-Golgi compartment. *Current biology* : CB 23, 1945-1951.

Shiba, Y., Romer, W., Mardones, G.A., Burgos, P.V., Lamaze, C., and Johannes, L. (2010). AGAP2 regulates retrograde transport between early endosomes and the TGN. *Journal of cell science* 123, 2381-2390.

Sohda, M., Misumi, Y., Yamamoto, A., Nakamura, N., Ogata, S., Sakisaka, S., Hirose, S., Ikehara, Y., and Oda, K. (2010). Interaction of Golgin-84 with the COG complex mediates the intra-Golgi retrograde transport. *Traffic* 11, 1552-1566.

Thibault, P.A., Huys, A., Amador-Canizares, Y., Gailius, J.E., Pinel, D.E., and Wilson, J.A. (2015). Regulation of Hepatitis C Virus Genome Replication by Xrn1 and MicroRNA-122 Binding to Individual Sites in the 5' Untranslated Region. *Journal of virology* 89, 6294-6311.

van Rahden, V.A., Brand, K., Najm, J., Heeren, J., Pfeffer, S.R., Brulke, T., and Kutsche, K. (2012). The 5-phosphatase OCRL mediates retrograde transport of the mannose 6-phosphate receptor by regulating a Rac1-cofilin signalling module. *Human molecular genetics* 21, 5019-5038.

van Weering, J.R., Verkade, P., and Cullen, P.J. (2012). SNX-BAR-mediated endosome tubulation is co-ordinated with endosome maturation. *Traffic* 13, 94-107.

Wassmer, T., Attar, N., Bujny, M.V., Oakley, J., Traer, C.J., and Cullen, P.J. (2007). A loss-of-function screen reveals SNX5 and SNX6 as potential components of the mammalian retromer. *Journal of cell science* 120, 45-54.

Xu, N., Zhang, J., Shen, C., Luo, Y., Xia, L., Xue, F., and Xia, Q. (2012). Cisplatin-induced downregulation of miR-199a-5p increases drug resistance by activating autophagy in HCC cell. *Biochemical and biophysical research communications* 423, 826-831.

Yi, H., Liang, B., Jia, J., Liang, N., Xu, H., Ju, G., Ma, S., and Liu, X. (2013). Differential roles of miR-199a-5p in radiation-induced autophagy in breast cancer cells. *FEBS letters* 587, 436-443.

15.2 POWERPOINT PRESENTATION OF THE DEFENSE ON DECEMBER 12TH 2017


12th December 2017 1

PhD defense

Hypothesis on a non-SNARE function of syntaxin-5

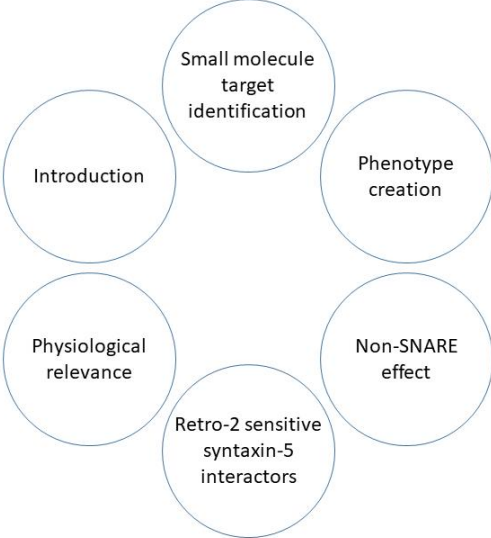
Stefan, Jan-Matthias RATHJEN, Dipl.-Biochem.
U1143 INSERM/UMR3666 CNRS: Cellular and Chemical Biology
"Chemical Biology of Membranes and Therapeutic Delivery"
E-mail: stefan.rathjen@curie.fr - rathjen.stefan@gmail.com

Thesis jury:
President: Marc le MAIRE
Reviewer: Thierry GALLI
Reviewer: Cathy JACKSON
Examiner: Anne HOUDUSSE
Examiner: Jost ENNINGA
Supervisor: Ludger JOHANNES



2

Outline

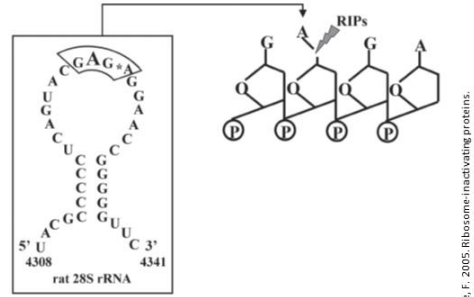


- Small molecule target identification
- Phenotype creation
- Non-SNARE effect
- Retro-2 sensitive syntaxin-5 interactors
- Physiological relevance
- Introduction

Plant and bacterial Ribosome-Inactivating Proteins

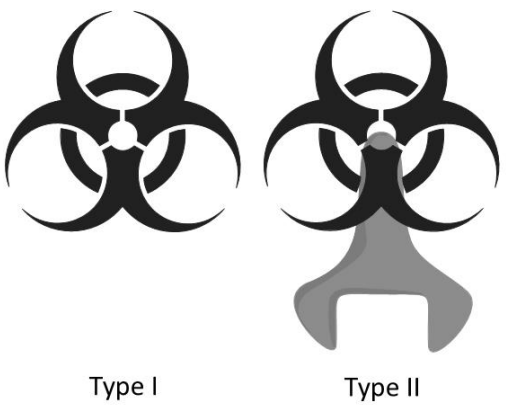
- Ribosome-Inactivating Proteins (RIPs)
- Cleave an Adenosine out of the 28S subunit
 - Protein biosynthesis inhibition
 - Cell death

ENZYMATIC MECHANISM OF ACTION OF RIPs ON 80 S RIBOSOMES



Plant and bacterial Ribosome-Inactivating Proteins

- Ribosome-Inactivating Proteins (RIPs)
 - Two types
 - Toxic subunit
- Cleave an Adenosine out of the 28S subunit
 - Protein biosynthesis inhibition
 - Cell death
 - Subunit with lectin activity



Plant and bacterial Ribosome-Inactivating Proteins

Toxic subunit

A-subunit

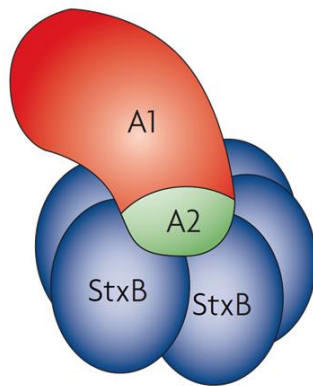
Subunit with lectin activity

B-subunit



Type II

Shiga toxin – A AB₅ RIP type II

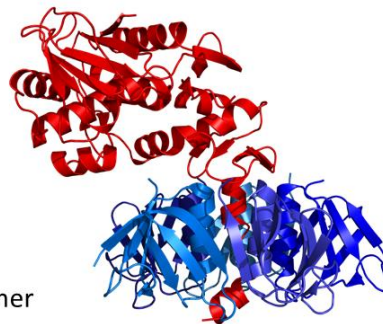


Shiga toxins

A-subunit

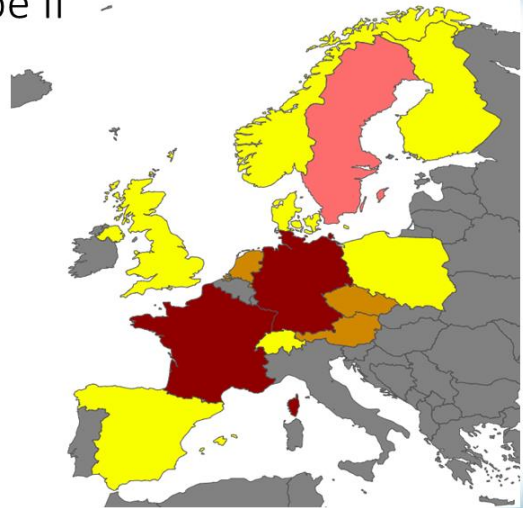
B-subunit

Homo-pentamer

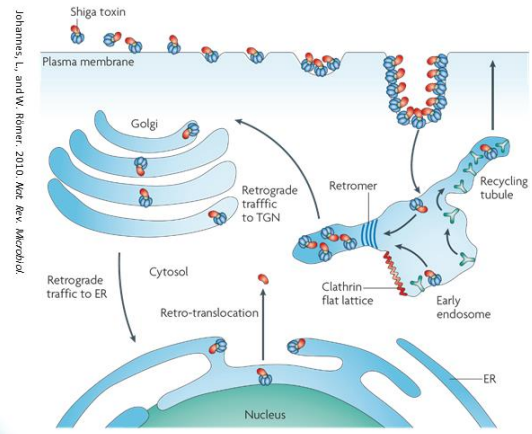


Shiga toxin – A AB₅ RIP type II

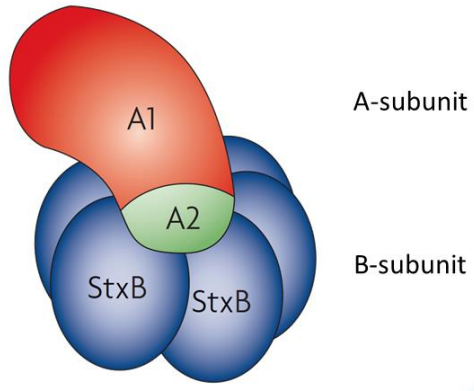
- Protein biosynthesis inhibition
- Produced by *Shigella dysenteriae*
 - Named after Kiyoshi Shiga
- Shiga-like toxins
 - Shiga toxin producing *E. coli* (STEC)
 - Enterohemorrhagic *E. coli* (EHEC)
- Outbreak in Germany in 2011
 - Potential public health risk
 - With no effective direct treatment



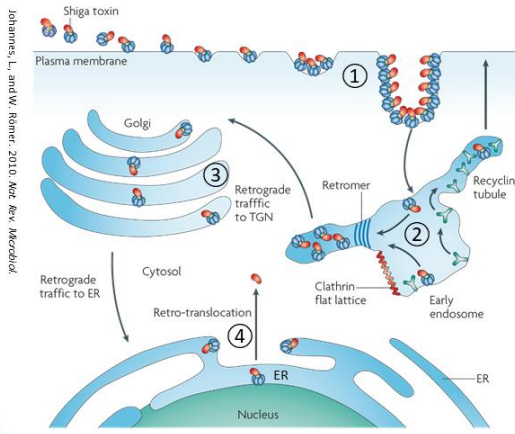
Shiga toxin – undergoes retrograde trafficking



Johannes, L., and W. Rother, 2010. *Rev. Microbiol.*



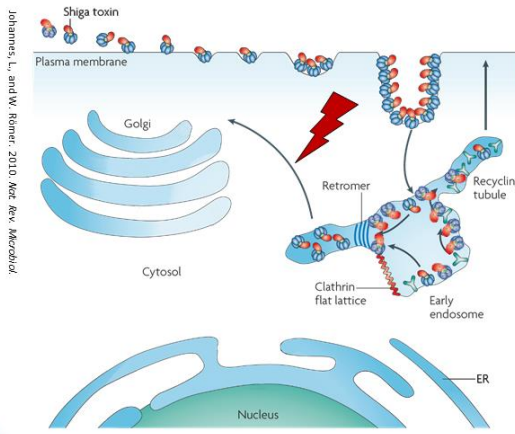
Shiga toxin – undergoes retrograde trafficking



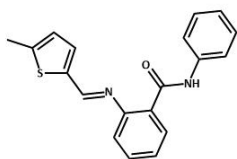
1. Binding-Clustering-Invagination
 - CLIC (clathrin independent carrier)
2. Early endosomes
3. Retrograde transport
4. ER arrival & Retro-translocation

Johannes, L., and W. Römer. 2010. *Mol. Rev. Microbiol.*

Discovery of the Retro compounds



- High throughput screening



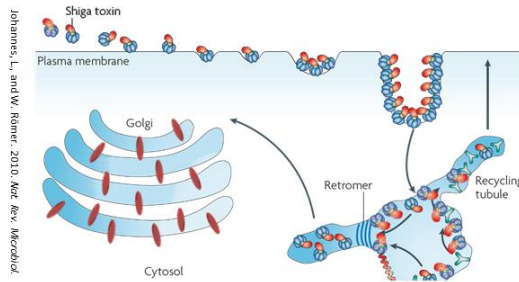
Retro-2

- Act on the level of endosomes-to Golgi trafficking
- Protected Mice against EHEC (Secher, T. 2015. *Antimicrob. Agents Chemother.*)

Johannes, L., and W. Römer. 2010. *Mol. Rev. Microbiol.*

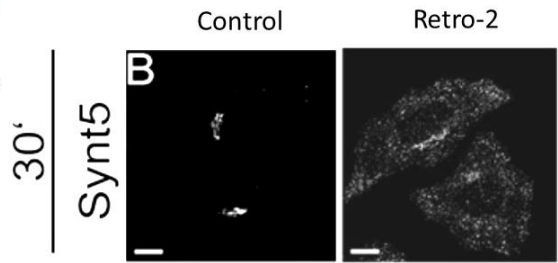


Retro compounds relocalize Syntaxin-5



Johannes, L., and W. Rother, 2010. *Mol. Rev. Microbiol.*

• Only syntaxin-5 affected

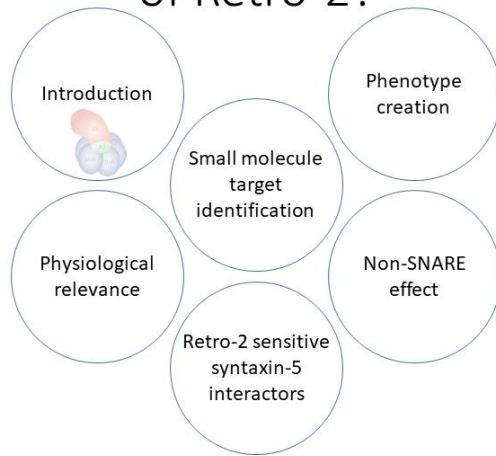


Stechmann, B. 2010. *Cell*.

1. What is the cellular target of Retro-2?
2. What is the link between:
 - Shiga toxin trafficking inhibition
 - Syntaxin-5 relocalization?

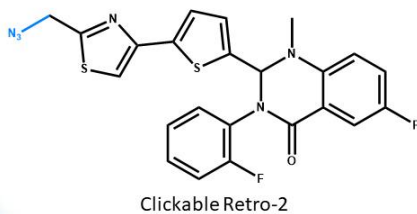
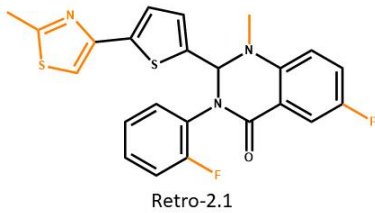
Outline

What is the cellular target of Retro-2?





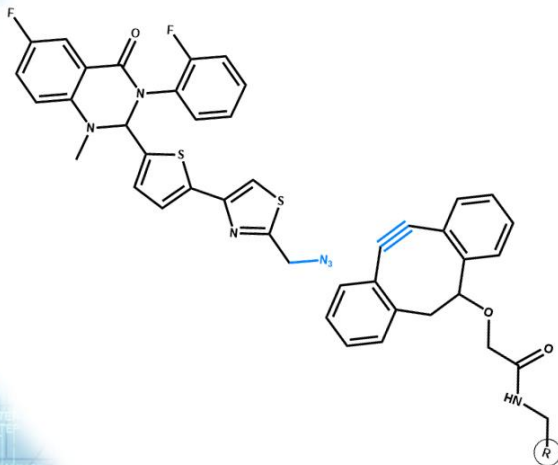
The evolution of Retro-2



- Cyclisation (Park, J.G. 2012. *Sci. Rep.*)
- Structure-Activity Relationship (SAR) study (Noel, R. 2013. *J. Med. Chem.*)
 - 500-fold more potent
- Chemical functionalization
Bioorthogonal click-chemistry



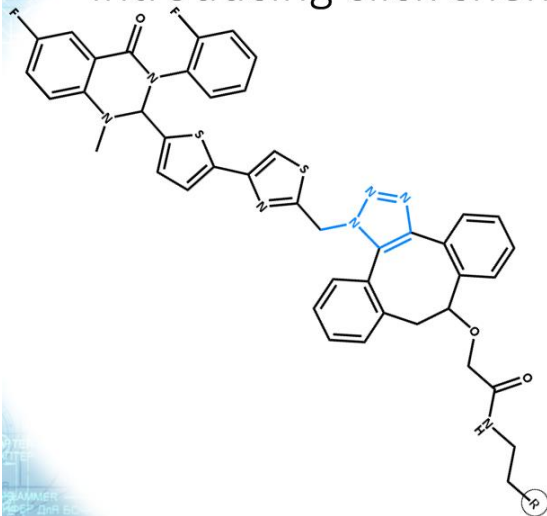
Introducing click chemistry



- Cyclisation (Park, J.G. 2012. *Sci. Rep.*)
- Structure-Activity Relationship (SAR) study (Noel, R. 2013. *J. Med. Chem.*)
 - 500-fold more potent
- Chemical functionalization
Bioorthogonal click-chemistry

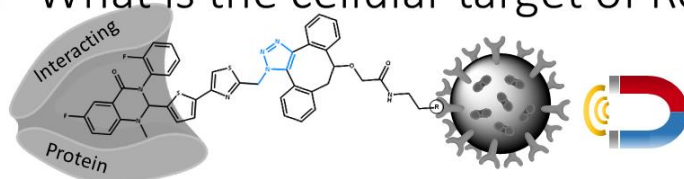


Introducing click chemistry



- Chemical functionalization
 - Bioorthogonal click-chemistry
- Covalent bonds between a small molecule and a probe
 - Biotin
 - Fluorophore

What is the cellular target of Retro-2?

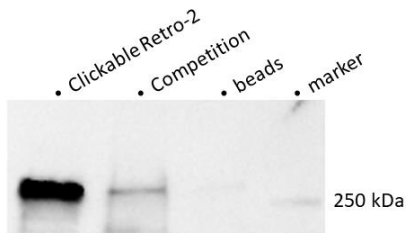


Selected proteins	Peptides, Analyses, Distribution						MW (kDa)	Description
	beads		Clickable Retro-2	5-fold un-clickable Retro-2 competition				
GCN1L_HUMAN	-	-	33	3	-	-	292,8	Translational activator GCN1
SC16A_HUMAN	-	-	17	3	-	-	233,5	Protein transport protein Sec16A
GEM14_HUMAN	-	-	13	4	-	-	120,0	Gem-associated protein 4

Peptide rule: At least 3 peptides in best Analysis – MGDC and the group of Damarys Loew

What is the cellular target of Retro-2?

- Is it syntrophin-5? ~~X~~
- Sec16A is pulled-down
- Verified by Western blotting



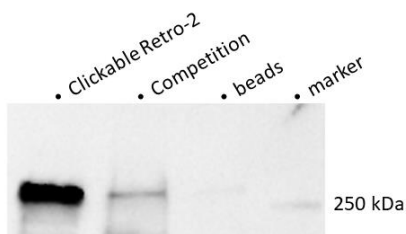
Peptide rule: At least 3 peptides in best Analysis

Is this a direct interaction with Sec16A?

Is this a direct interaction with Sec16A?

- Is it syntrophin-5? ~~X~~
- Sec16A is pulled-down
- Verified by Western blotting

Selected proteins	Peptides, Analyses, Distribution				MW (kDa)	Description
	beads	Clickable Retro-2	5-fold un-clickable Retro-2 competition			
GCN1L_HUMAN	-	33	3	-	292,8	Translational activator GCN1
SEC16A_HUMAN	-	17	3	-	233,5	Protein transport protein Sec16A
GEM14_HUMAN	-	13	4	-	120,0	Gem-associated protein 4



Anti-Sec16A-Western bot

Is this a direct interaction with Sec16A?

Verify Sec16A as a target of Retro-2

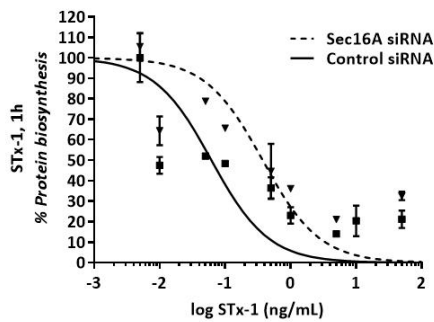
- If Retro-2 binds and inhibits Sec16A
- Sec16A depletion = Retro-2 treatment?

1. Protection against protein biosynthesis inhibition
2. Inhibition of STxB Golgi arrival
3. Relocalization of syntaxin-5

1. Protection against protein biosynthesis inhibition

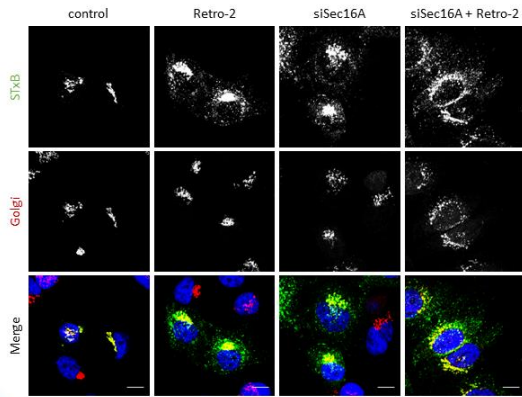
- If Retro-2 binds and inhibits Sec16A
- Sec16A depletion = Retro-2 treatment?

- If Retro-2 binds and inhibits Sec16A
- Sec16A depletion = Retro-2 treatment?



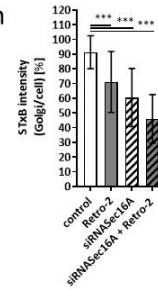
✓6-fold protection in intoxication

2. Inhibition of STxB Golgi arrival

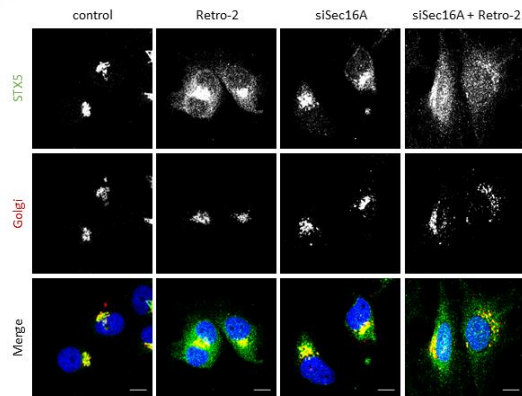


- If Retro-2 binds and inhibits Sec16A
- Sec16A depletion = Retro-2 treatment?

- ✓ 6-fold protection in intoxication
- ✓ Trafficking inhibition



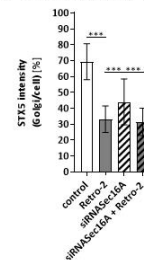
3. Syntaxin-5 relocalization



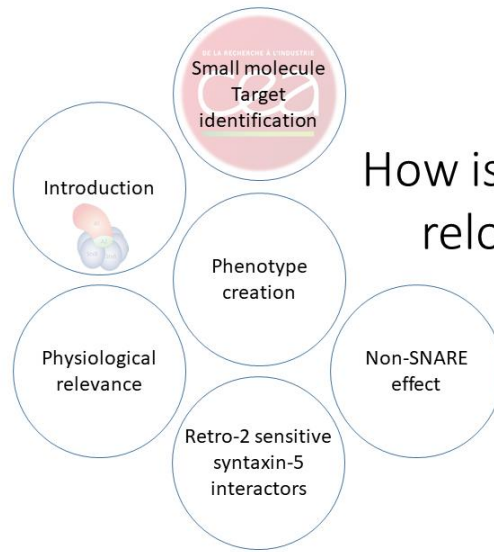
- If Retro-2 binds and inhibits Sec16A
- Sec16A depletion = Retro-2 treatment?

- ✓ 6-fold protection in intoxication
- ✓ Trafficking inhibition
- ✓ Syntaxin-5 relocalization

! Confirmation of Sec16A as a target of Retro-2

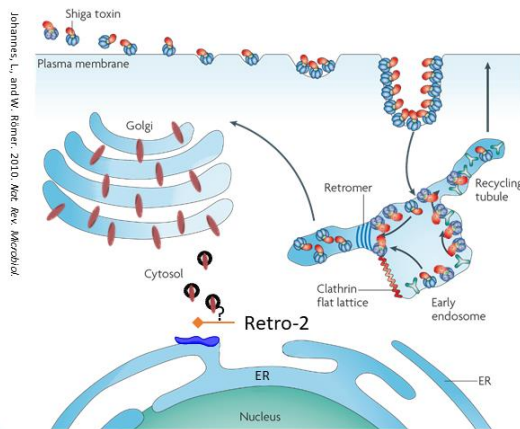


Outline



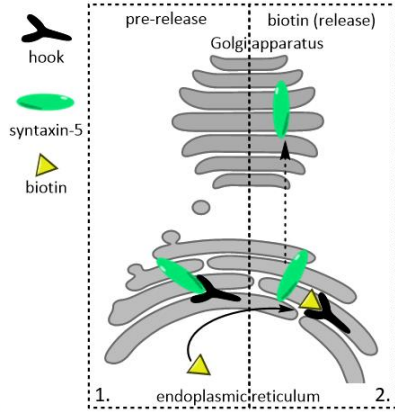
How is syntaxin-5 relocalized?

Retro-2 and siSec16A relocalize Syntaxin-5



- Syntaxin-5 cycles to the ER
- Sec16A involved in COPII vesicle formation
- Syntaxin-5 putative COPII binding site
- Does Retro-2 interfere with the syntaxin-5 cycling?

Retention Using Selective Hooks - RUSH



NATURE METHODS | ARTICLE



Synchronization of secretory protein traffic in populations of cells

Gaëlle Boncompain, Severine Divoux, Nelly Gareil, Helene de Forges, Aurianno Lescure, Lynda Latreche, Valentina Mercanti, Florence Jollivet, Graça Raposo & Franck Perez

Affiliations | Contributions | Corresponding author

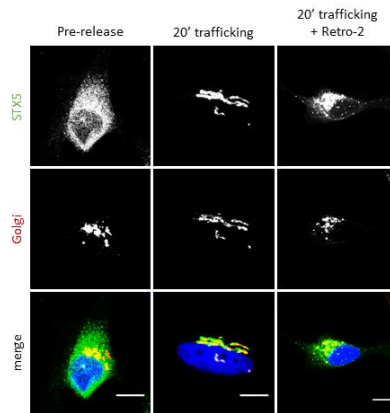
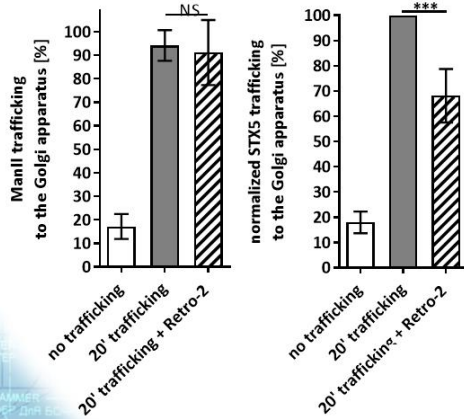
Nature Methods 9, 493–498 (2012) | doi:10.1038/nmeth.1928

Received 02 August 2011 | Accepted 24 January 2012 | Published online 11 March 2012

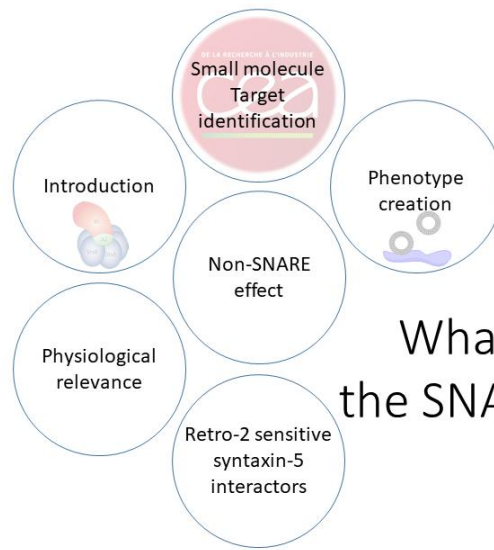
Two-state assay:

1. Fluorescent labeled syntaxin-5 is trapped in the ER
2. Trafficking to the Golgi induced upon biotin treatment

Retro-2 effect on syntaxin-5 anterograde trafficking

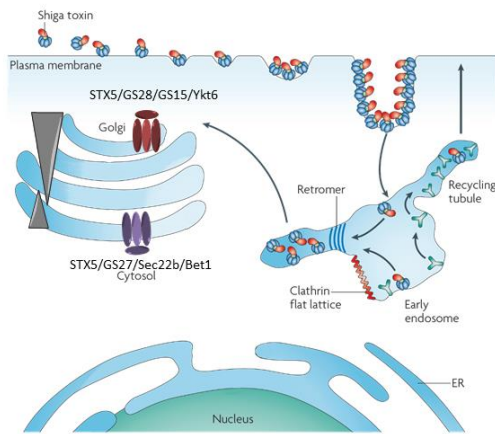


Outline

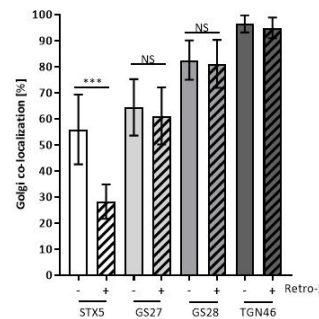


What happens to the SNARE complexes?

Syntaxin-5's SNARE function in Shiga toxin trafficking

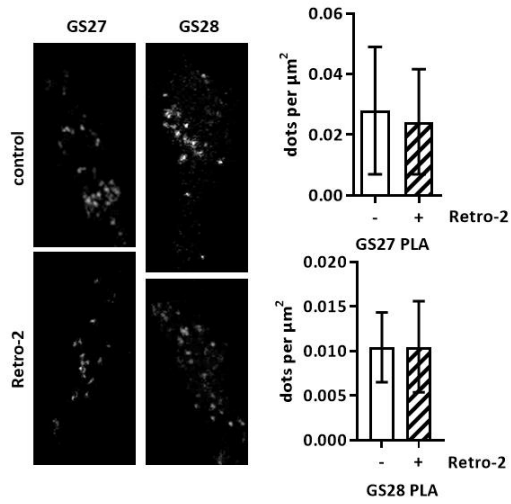


- SNARE complex is involved in Shiga toxin trafficking
- Do not relocate!

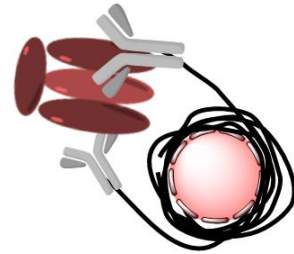


Maria Daniela Garcia-Castillo, Christine Viaris de Lesegno & the group of Damarys Loew

Syntaxin-5's SNARE function in Shiga toxin trafficking



- SNARE complex is involved in Shiga toxin trafficking
- Do not relocalize!
- Remain in close proximity



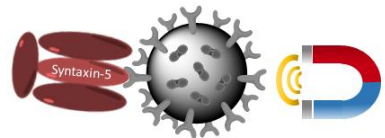
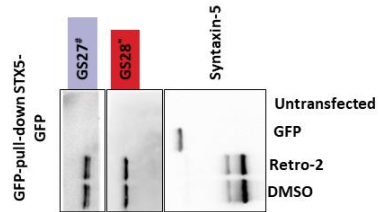
Christine Viaris de Lesegno

Syntaxin-5's SNARE function in Shiga toxin trafficking

Selected proteins	Peptides		MW [kDa]	Description
	Control	+Retro-2		
STX5 [#]	18	28	39,7	Syntaxin-5
GOSR1	5	8	28,6	GS28 (Golgi SNAP receptor complex member 1)
VTI1B	4	3	26,7	Vesicle transport through interaction with t-SNAREs homolog 1B
LG3BP	3	3	65,3	Galectin-3-binding protein
GOSR2	3	2	24,8	GS27 (Golgi SNAP receptor complex member 2)
BET1 [#]	2	2	13,3	BET1 homolog
VTI1A	2	2	25,2	Vesicle transport through interaction with t-SNAREs homolog 1A
SC24A	1	1	119,8	Protein transport protein Sec24A
STX6	1	1	29,2	Syntaxin-6
YKT6	1	1	22,4	Synaptobrevin homolog YKT6
VAMP8	1	3	11,4	Vesicle-associated membrane protein 8

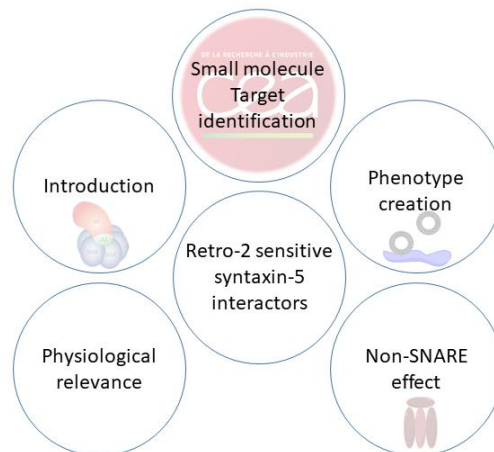
- SNARE complex is involved in Shiga toxin trafficking
- Do not relocalize!
- Remain in close proximity
- Still interact with each other

Retro-2 does not affect the formation of syntaxin-5 SNARE complexes



Maria Daniela Garcia-Castillo & the group of Damarys Loew

Outline



What is the explanation of the Shiga toxin trafficking inhibition?

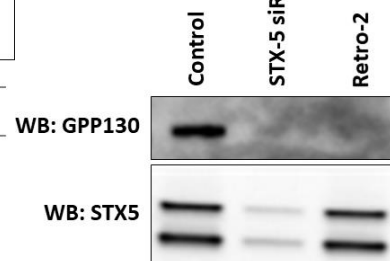
Are there Retro-2-sensitive interactors?



GPP130 is a new and Retro-2 sensitive interacting partner of syntaxin-5

Selected proteins	Peptides		MW [kDa]	Description
	Control	+Retro-2		
GOLI4	4	-	81,9	Golgi integral membrane protein 4 (GPP130)
BAG6	3	-	119,4	Large proline rich protein BAG6
TGN2	2	-	51,1	TGN-integral membrane protein 2 (TGN46)
AP1G1	1	-	91,4	AP-1 complex subunit gamma-1
BET1L	1	-	12,4	BET1-like protein
GOLM1	1	-	45,3	Golgi membrane protein 1 (GP73)
SC16A	1	-	233,5	Protein transport protein Sec16A

GFP-pull-down STX5-GFP

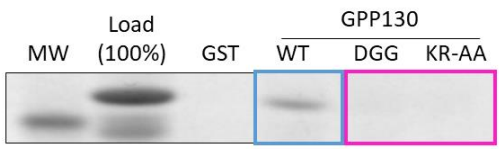
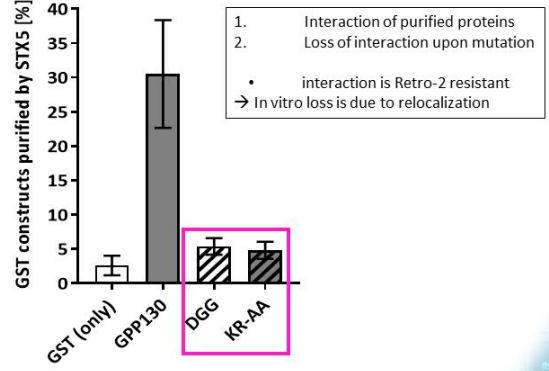
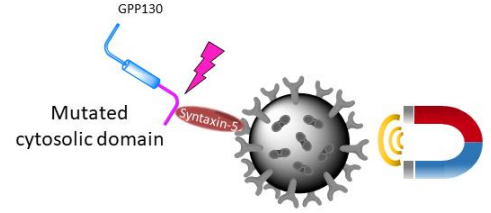


Exciting!
GPP130 involved in Shiga toxin trafficking

Mukhopadhyay, S., and A.D. Linstedt. 2012. Science



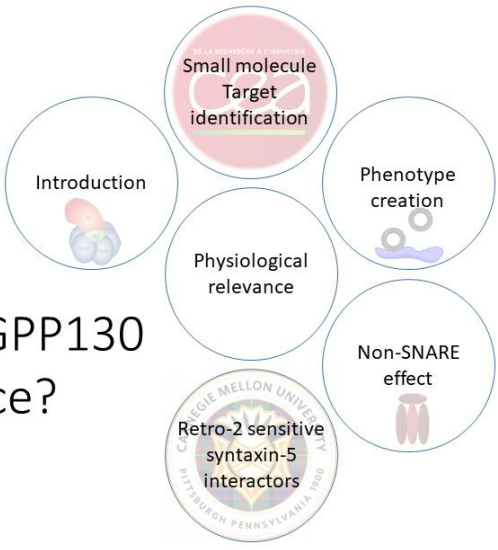
Do GPP130 and syntaxin-5 interact directly?



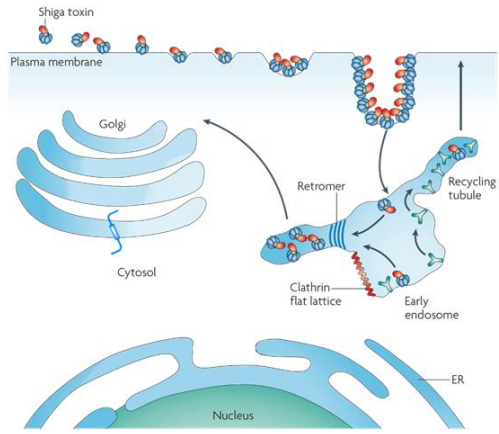
Collin Bachert & Adam Linstedt

Outline

Syntaxin-5-GPP130 relevance?

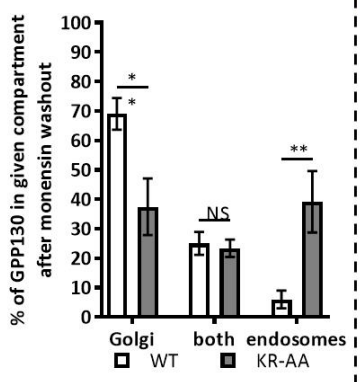
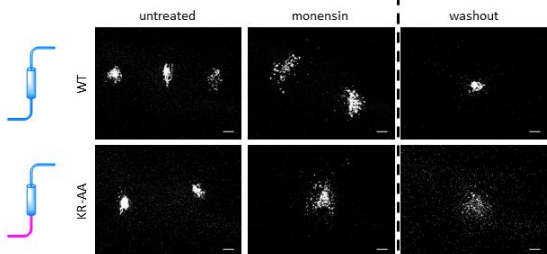


GPP130



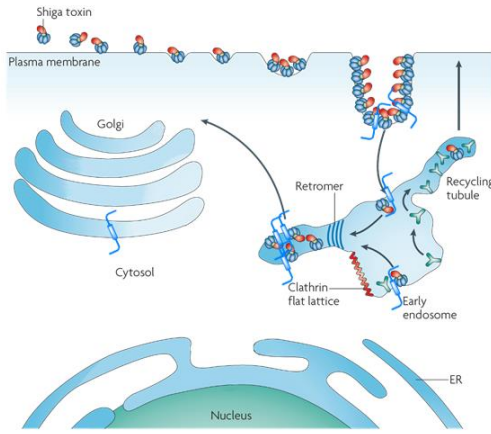
- GPP130 cycles between cis-Golgi and plasma membrane (2004. *Mol. Biol. Cell.*)

GPP130 cycling



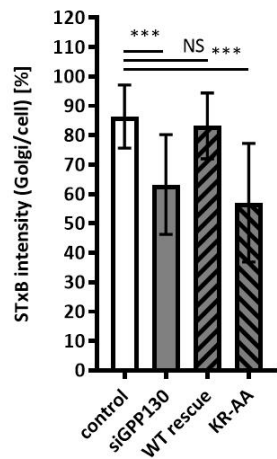
- Syntaxin-5-GPP130 interaction is involved in cycling

GPP130



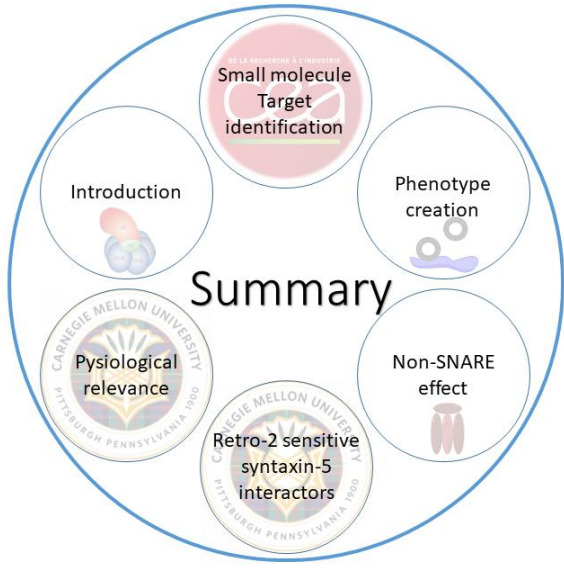
- ✓ GPP130 cycles between cis-Golgi and plasma membrane (2004. *Mol. Biol. Cell.*)
- GPP130 is involved in Shiga toxin intoxication (2012. *Science*)

Syntaxin-5-GPP130 interaction in Shiga toxin trafficking

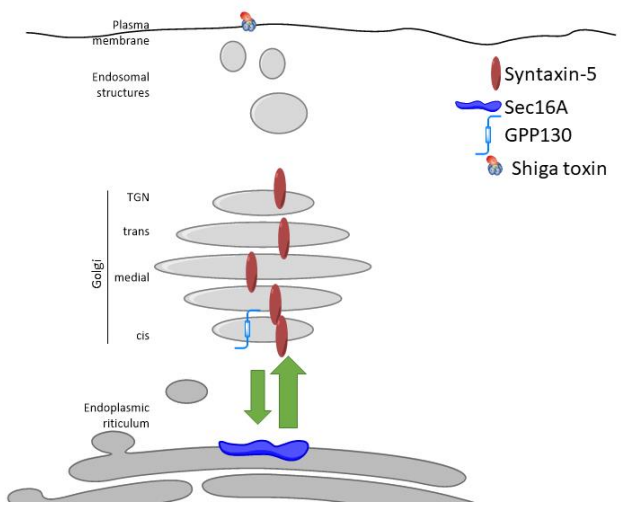


- GPP130-syntaxin-5 interaction**
- ✓ The cycling process of GPP130
 - ✓ Golgi arrival of Shiga toxin

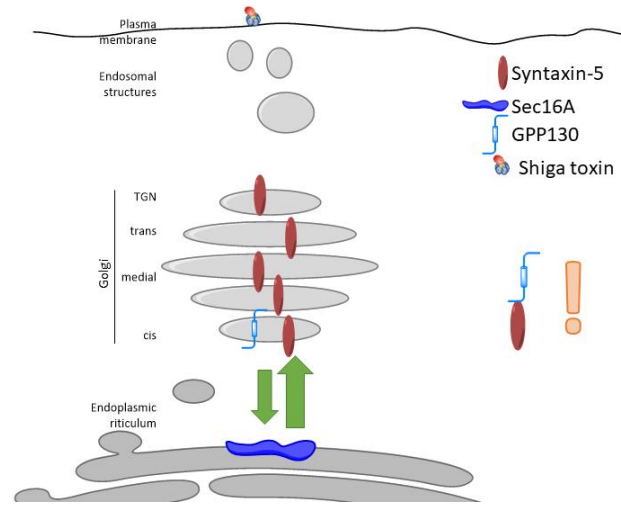
Outline



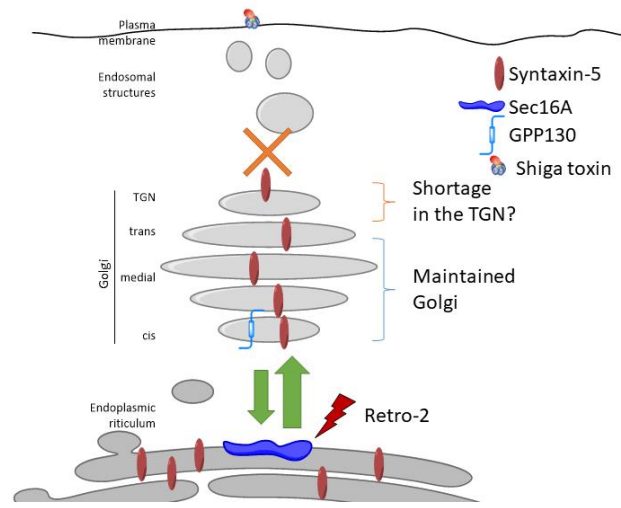
Summary

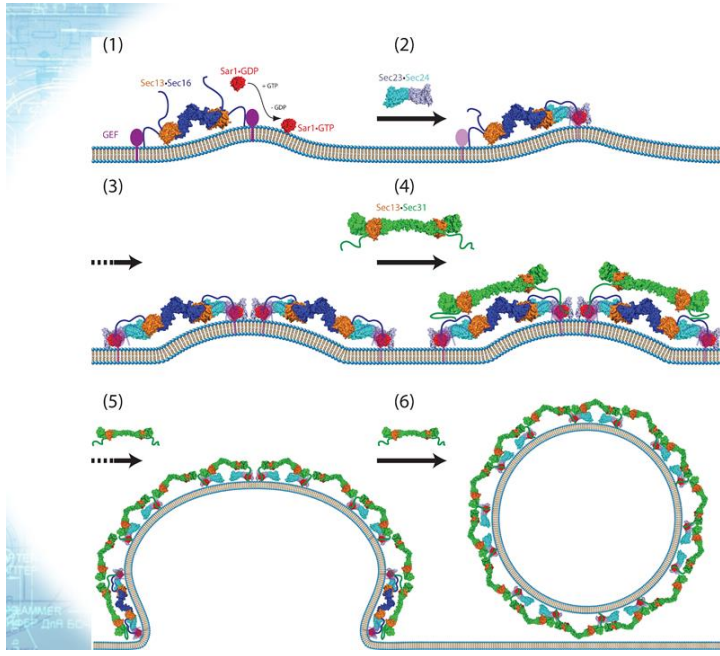
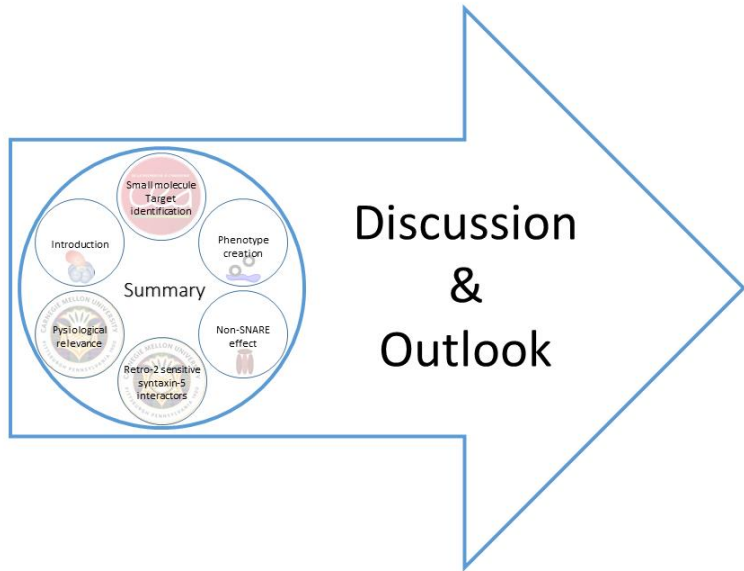


Summary



Summary

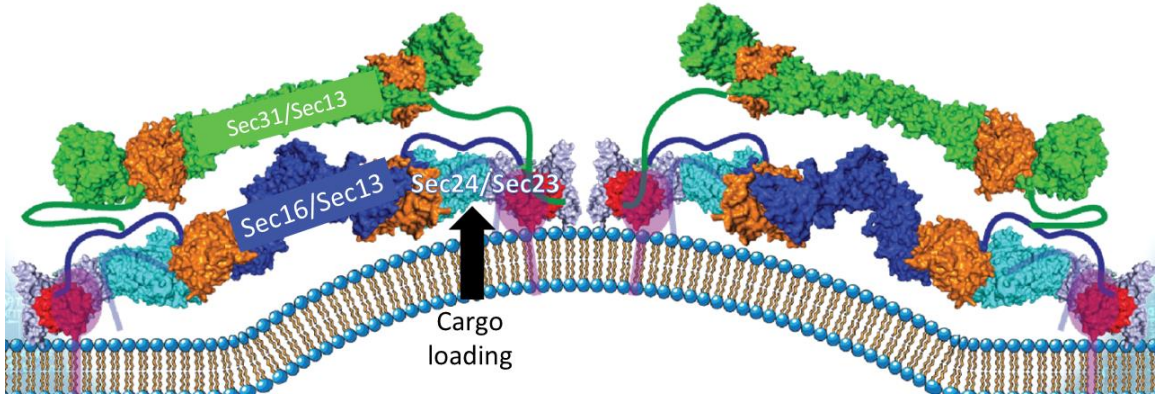




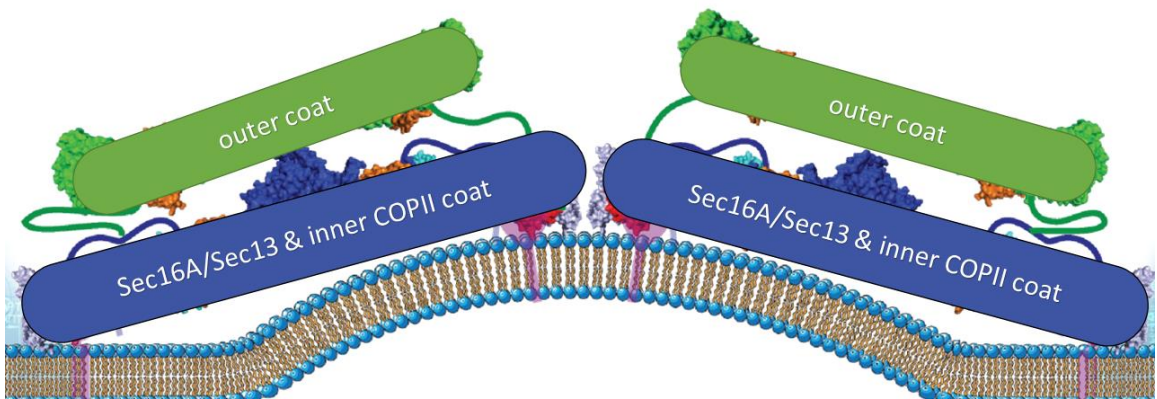
COPII vesicle formation

1. Sec16/13 association with the ER → Sar1 → membrane bending
2. Sec16/13/Sar1 recruit Sec23/24
3. self-association into oligomers.
4. Sec13/31 recruitment; assembling near and/or in place of Sec16
5. Sec13/31 replaces Sec16/13 → GTP hydrolysis by Sar1 → initiation release
6. COPII coat carrier leaves ER - Sec16/13 remains in the ER.

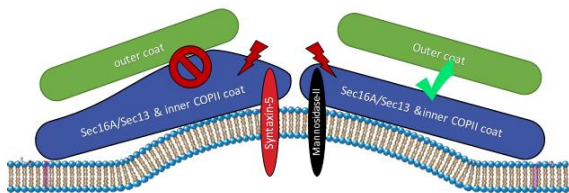
Discussion: hypothetical Retro-2 effect



Discussion: hypothetical Retro-2 effect



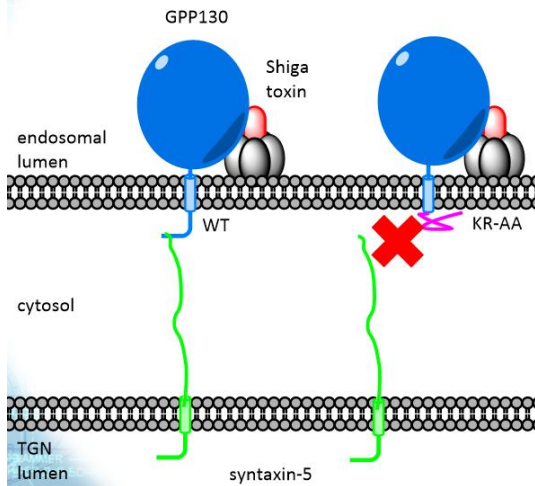
Discussion: hypothetical Retro-2 effect



Outlook

- Crystal structures of Retro-2 with the Sec16A_{frag}/Sec13
- Extent by Sec23/Sec24 ± cargos
- High resolution cryo EM on membranes
- Ultimately illustrating the full cargospecific COPII vesicle ±Retro-2

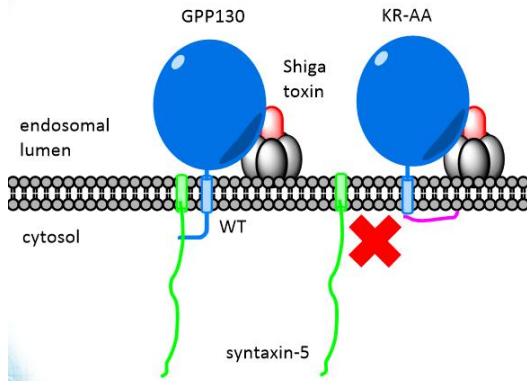
Discussion: GPP130-syntaxin-5 interaction



Trans-interaction

- Short GPP130's cytosolic domain
 - No tethering
- Could be a contact site
 - Never seen before between endosomes and the Golgi

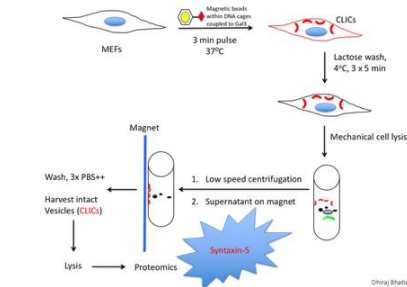
Discussion: GPP130-syntaxin-5 interaction



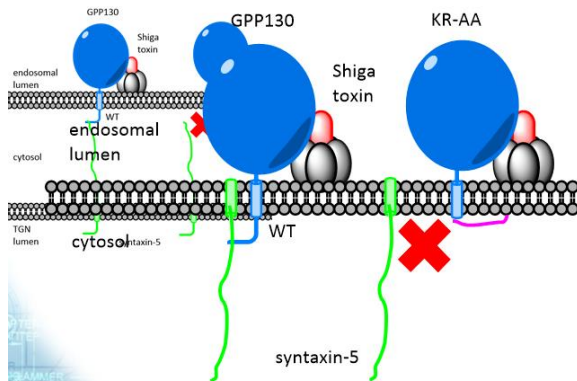
cis-interaction

- Syntaxin-5 on endosomes?
 - cis-interaction on endosomes?
- Sorting function of syntaxin-5

Highly speculative



Discussion: GPP130-syntaxin-5 interaction



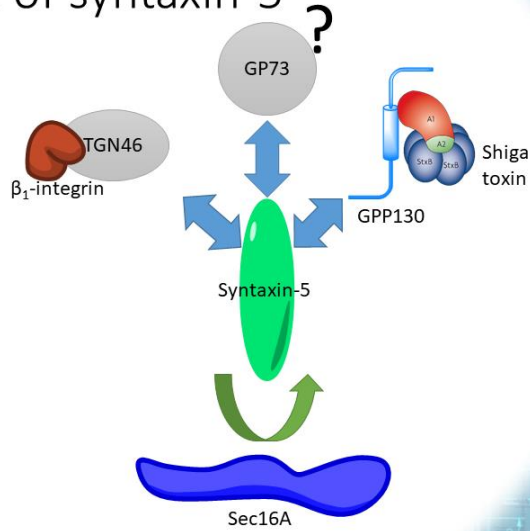
Outlook

- Co-crystal: GPP130 & syntaxin-5
 - Idea: of binding region and cytosolic domain

- | | |
|--|--|
| <ul style="list-style-type: none"> • Syntaxin-5-HRP in EM <ul style="list-style-type: none"> • Is there endosomal syntaxin-5? • Syntaxin-5-SNAPtag <ul style="list-style-type: none"> • Fluid phase uptake of BG-Fluorophore | <ul style="list-style-type: none"> • Show interaction on liposomes <ul style="list-style-type: none"> • Fluorescence clustering |
|--|--|

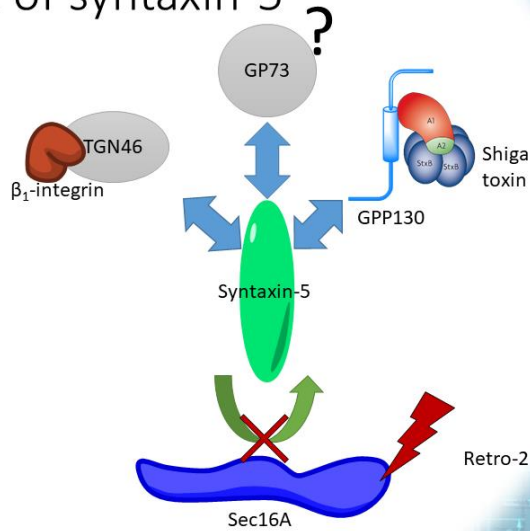
Discussion: Sorting role of syntaxin-5

Selected proteins	Peptides		MW [kDa]	Description
	Control	+Retro-2		
GOLI4	4	-	81,9	Golgi integral membrane protein 4 (GPP130)
BAG6	3	-	119,4	Large proline rich protein BAG6
TGON2	2	-	51,1	TGN-integral membrane protein 2 (TGN46)
AP1G1	1	-	91,4	AP-1 complex subunit gamma-1
BET1L	1	-	12,4	BET1-like protein
GOLM1	1	-	45,3	Golgi membrane protein 1 (GP73)
SC16A	1	-	233,5	Protein transport protein Sec16A



Discussion: Sorting role of syntaxin-5

Selected proteins	Peptides		MW [kDa]	Description
	Control	+Retro-2		
GOLI4	4	-	81,9	Golgi integral membrane protein 4 (GPP130)
BAG6	3	-	119,4	Large proline rich protein BAG6
TGON2	2	-	51,1	TGN-integral membrane protein 2 (TGN46)
AP1G1	1	-	91,4	AP-1 complex subunit gamma-1
BET1L	1	-	12,4	BET1-like protein
GOLM1	1	-	45,3	Golgi membrane protein 1 (GP73)
SC16A	1	-	233,5	Protein transport protein Sec16A



- Find endogenous cargos
- Find interacting regions
- Mutating binding regions
- Studying cycling

Thank you all for all the years!



PhD defense
 Hypothesis of a non-SNARE
 function of syntaxin-5

Thank you for
your attention!

Thesis jury:
 President: Marc le MAIRE
 Reviewer: Thierry GALLI
 Reviewer: Cathy JACKSON
 Examiner: Anne HOUDUSSE
 Examiner: Jost ENNINGA
 Supervisor: Ludger JOHANNES

